NASA SP-218

ANALYSIS OF A JET IN A SUBSONIC CROSSWIND

A symposium held at
LANGLEY RESEARCH CENTER
Hampton, Virginia
September 9–10, 1969

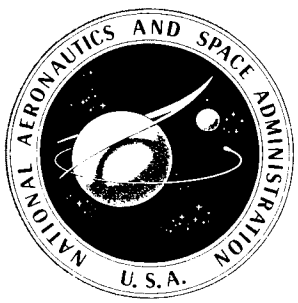

NATIONAL AERONAUTICS AND SPACE ADMINISTRATION

NASA SP–218

ANALYSIS OF A JET IN A SUBSONIC CROSSWIND

A symposium held at
Langley Research Center
Hampton, Virginia
September 9–10, 1969

Scientific and Technical Information Division
OFFICE OF TECHNOLOGY UTILIZATION
NATIONAL AERONAUTICS AND SPACE ADMINISTRATION
1969
Washington, D.C.

FOREWORD

An important aspect of estimating the aerodynamic characteristics of V/STOL aircraft in transition between hover and wingborne flight is an understanding of the flow field induced by the efflux of the lifting-propulsive device. The influence of this efflux dominates the aerodynamic interference effects for aircraft that use high-disk-loading devices such as turbofan or turbojet lift engines. At the present time, approximately a dozen organizations are working independently on this problem. Several fundamentally different approaches are being applied toward understanding and solving the problem. Recognizing this activity, NASA decided to hold a Symposium on the Analysis of a Jet in a Subsonic Crosswind on September 9 and 10, 1969, at the Langley Research Center to present the currently available results.

The objective of this meeting was to provide an opportunity for persons working in the area to present and discuss their work and, in many cases, their opinions. The presentations were made in two sessions:

Session I - Experimental Results

Session II - Empirical and Analytical Descriptions of the Jet and Induced Flow

This publication includes 15 papers presented at the symposium. The attendees are listed at the end.

It should be emphasized that this publication essentially represents a compilation of papers presented by authorities from various governmental and private organizations. In order to expedite publication, this document has been printed from copy provided by the authors.

The Langley Research Center wishes to express its appreciation to all authors and to the organizations they represent, for their substantial contributions to this program and for the timeliness of their responses both to the program activities and to the symposium.

CONTENTS

SESSION I - EXPERIMENTAL RESULTS

SESSION II - EMPIRICAL AND ANALYTICAL DESCRIPTIONS OF THE JET AND INDUCED FLOW

*This paper was presented, but it is not included in this volume because it had been submitted prior to the symposium for publication in the Journal of Fluid Mechanics.

JET-WAKE CHARACTERISTICS AND THEIR INDUCED AERODYNAMIC EFFECTS ON V/STOL AIRCRAFT IN TRANSITION FLIGHT

By Richard J. Margason
NASA Langley Research Center

and

Richard Fearn
University of Florida

SUMMARY

A summary indicating the general trends of jet-wake-induced aerodynamic effects on V/STOL aircraft in transition flight is given. The jet wake including the adjacent flow field is described qualitatively, and a quantitative measurement of the circulation in the wake is presented. These measurements indicate that the circulation may be somewhat greater than that generated by potential flow around a circular cylinder. Finally, an extensive list of related reports has been included.

INTRODUCTION

The purpose of this paper is to summarize results of previous experimental investigations of the aerodynamic interference effects experienced by V/STOL aircraft in the transition speed range. (Additional summary papers are presented in refs. 1 to 6.) These effects have been the subject of a large number of experimental investigations (refs. 7 to 18). Most of this research effort has been directed toward the investigation of the forces and moments induced on the aircraft by the interaction of the vertical jets with the free-stream air. In addition, a description of the character of the jet wake is presented.

SYMBOLS

A	area, ft^2 (m^2)
b	wing span, ft (m)
c	wing chord, ft (m)
D	jet diameter, ft (m)
L	lift, lb (N)

ΔL	increment of lift interference caused by the flow from a jet, lb (N)
ΔM	increment of pitching-moment interference caused by the flow from a jet, ft-lb (m-N)
q_∞	free-stream dynamic pressure, lb/ft^2 (N/m^2)
q_j	jet dynamic pressure, lb/ft^2 (N/m^2)
T	thrust, lb (N)
V_∞	free-stream velocity, fps (mps)
V_j	jet velocity, fps (mps)
V_∞/V_j	effective velocity ratio
X,Y,Z	coordinate axes
x,y,z	Cartesian coordinates, ft (m)
γ	nondimensional circulation strength, $\Gamma/2DV$
Γ	circulation strength, ft^2/sec (m^2/sec)
Γ_{max}	maximum circulation strength for potential flow around half of a circular cylinder, $2DV_\infty$, ft^2/sec (m^2/sec)
Γ_o	total circulation for a wing with an elliptic lift distribution, $4L/\rho V_\infty b$, ft^2/sec (m^2/sec)
δ_f	flap deflection, deg
δ_j	jet deflection from free-stream direction, deg
ζ	natural jet coordinate normal to ξ-η plane, ft (m)
η	natural jet coordinate in the lateral direction, measured parallel to Y-axis, ft (m)
θ	angular cylindrical coordinate, rad
ξ	natural jet coordinate along the axis of the jet, ft (m)
ρ	density, $slugs/ft^3$ (kg/m^3)

AERODYNAMIC INTERFERENCE EFFECTS

During transition flight of V/STOL aircraft, the jets issuing from the aircraft are swept rearward by the free-stream flow and are rapidly rolled up into a pair of vortices (fig. 1). The wakes induce suction pressures on the fuselage and a distribution of downwash over the aircraft. This downwash is in effect an induced twist on the wing and tail and an induced camber over the length of the airplane.

The general trend of these jet-induced effects is illustrated in figure 2. There is usually a loss in lift which tends to increase with increasing forward velocity. The loss in lift is about the same with the tail off the aircraft and with the tail on. There is an increment of pitching moment in transition flight which tends to increase nose-up with increasing velocity. Because of the change in downwash in the vicinity of the tail, there is an additional increment of pitching moment induced when the tail is on.

Recently, an investigation (ref. 18) was undertaken to determine the effect of the jet-exit location on the interference on a wing. This investigation used a model with a simple fuselage and an unswept, untapered wing with an aspect ratio of 6 and a 30-percent-chord slotted Fowler-type flap. This model was mounted on a sting-supported strain-gage balance. Two jets, one on each side of the fuselage, were mounted independently of the wing at about the 25-percent semispan station. The jet exits were positioned at each of the various longitudinal and vertical locations shown by the plus marks in figure 3. Results of this investigation show that negative lift interference was experienced when the jet exits were located ahead of the wing. Favorable interference effects, however, are encountered with the jets below the wing and aft of the wing midchord. The fact that the interference effects are most favorable for locations closest to the flap indicates that the jet is probably helping the wing and flap achieve their full lift potential.

VISUALIZATION OF FLOW PHENOMENA

OF A JET IN A CROSS WIND

The following description of the flow phenomena involved in the transition problem is based primarily on flow visualization. The shape of the jet wake when influenced by the free stream is presented in figure 4. These data are from an experimental investigation (ref. 19) in which the wake exits from the nozzle at a deflection angle δ_j to the free stream. (See refs. 20 to 32 for other investigations and refs. 33 to 52 for analyses of the jet in a cross wind.) The free stream deflects the wake back until it tends toward the free-stream flow. As a result of this investigation, the empirical equation given in figure 4 was obtained. It describes the path of the jet as a function of the effective velocity ratio (the square root of the ratio of the free-stream dynamic pressure to jet dynamic pressure) and the deflection angle of the jet.

A more detailed look at the jet in a cross wind is shown in figure 5 where the flows induced in and around the jet are shown. This photograph, which was obtained by using water-tunnel flow visualization at the Office National D'Études et de Recherches Aérospatiale (O.N.E.R.A.), shows a flat plate with a jet exhausting from it. Near the leading edge of the plate are orifices through which colored milk is emitted. When the colored filament on the center line approaches the jet exit, it divides and is swept around the jet. This indicates that there is a stagnation point near the front of the jet. The visible portion of the jet wake indicates that some of the flow from the free stream is sucked into the jet. The filament adjacent to the jet passes beside the jet and is then induced upward into the turbulent wake region behind the jet. Even the filaments farthest from the center line of the exit are sucked toward the jet and into the wake region. In the wake region, a considerable amount of entrainment by the jet can be seen.

In figure 6, two photographs of oil flow on the surface of the plate are presented. The lower one is a closeup near the jet exit. A line trails diagonally downstream from the jet and bounds the wake region. A careful inspection of the stream lines on the surface shows that the free-stream flow is deflected around the periphery of the jet and into the wake boundary. In the wake region, the flow near the jet is entrained forward by the jet. Farther downstream of the jet exit, the wake flow is deflected away and carried off with the boundary of the wake on the surface of the plate. This wake boundary appears to be a second pair of vortices which are similar to a Kármán vortex street. This vortex street is probably formed around the potential core of the jet.

The pressure distribution which is induced on the surface of the plate is presented in figure 7. For these particular data, which are from reference 34, the effective velocity ratio was 0.25. The region of positive pressure ahead of the jet indicates a force augmenting the jet thrust. The region of negative pressure adjacent to and aft of the jet indicates a force opposing the jet thrust behind the jet. This pressure distribution accounts for the nose-up interference pitching moment described earlier. The area covered by the negative pressure is noticeably larger than the area covered by the positive pressure. As a result there is the lift loss.

Figure 8 is a photograph of the cross section of the jet wake in a water tunnel. The air bubbles are flowing around the jet wake; the white region is the jet. The primary features are the swirl of the two elements of vorticity in this jet cross section and the fact that the cross section is kidney shaped.

STRENGTH OF THE VORTICES IN A JET WAKE

An investigation was conducted recently in the Langley 300-MPH 7- by 10-foot wind tunnel to determine experimentally the strength of the contrarotating vortices in the wake of a jet in a cross flow by use of a vortex meter. The meter consisted of a 1/2-inch-diameter paddle wheel which spins in a rotational flow field.

The first phase of the investigation was calibration of revolutions of the vortex meter against circulation strength of the flow field. This was accomplished by measuring the strength of the trailing vortex sheet from a rectangular-planform wing with an aspect ratio of 6. (See ref. 18 for a description of the wing.) The vortex meter was placed about 1/2 inch aft of the trailing edge of the wing at several spanwise locations, and the revolutions were measured. In addition, the lift of the wing was measured with a six-component strain-gage balance. Then, this measured lift and a calculated lift distribution for the wing were used to determine the magnitude and distribution of the circulation in the wake of the wing as a function of spanwise location. The measured values are superimposed on the calculated distribution of vortex strength in figure 9 where the circulation ratio is presented as a function of spanwise location. Inboard of the 30 percent location, the measurements were too low to be accurate, and outboard of the 95 percent spanwise location, the meter was measuring the change in circulation distribution caused by the rolling up of the wing-tip vortex. However, the correlation is good for the portion of the span between these two locations, and the measurements over this portion were used to establish the vortex-meter calibration.

Next, the circulation in a jet was measured. For these measurements a 1-inch-diameter nozzle was mounted through a ground board normal to the free stream. The measurements were made in planes normal to the jet axis as shown in figure 10. The most complete data were obtained for an effective velocity ratio of 0.25 at a distance of 6 jet diameters along the jet path.

These results, which are presented in figure 11, indicate a nondimensional circulation of approximately 2 for each vortex. The form of the nondimensional circulation is obtained from analyses of the jet which use the circulation obtained in potential flow around a circular cylinder (ref. 37). This is done because the cross-sectional shapes predicted by this model are similar to the observed shapes. In this model the strength of the vortex sheet describing the flow around a circle is

$$\Gamma(\theta) = -2V_\infty \sin\theta$$

Integrating this circulation around a semicircle gives the maximum strength of each vortex as

$$\Gamma_{max} = \left| \int_0^\pi \Gamma(\theta) \frac{D}{2} d\theta \right| = 2DV_\infty$$

The nondimensional circulation is defined as

$$\gamma = \frac{\Gamma}{2DV_\infty}$$

The experimental results indicate that the circulation is approximately twice the value predicted by the potential-flow model.

It should be indicated that these results are not precise, and the preliminary nature of the experiment should be emphasized. There was difficulty in measuring small amounts of circulation because the meter was calibrated over a wide range of rpm. Hence, the sensitivity of the measurement was too coarse at low rpm. This led to error in determining the total circulation because the regions of low levels of circulation were large in area, and as a result, their contribution to the total vortex strength was more than expected. Further, since the vortex meter was rigidly mounted on a wand, there was some difficulty in alining it to the local flow. It was noted that when the meter was out of alinement by about 10° or greater, it tended to oscillate about an equilibrium position in the absence of vorticity. This oscillation showed up as revolutions on the meter. These results describe only a single test condition and will require additional verification before extrapolating to other conditions.

CONCLUDING REMARKS

The general trends of the effects of lifting jets on the aerodynamics of V/STOL aircraft in the transition speed range have been indicated. The character of the fluid flow in the jet and the adjacent flow field has been described qualitatively, and finally, a quantitative measurement of the circulation in the wake has been presented. These measurements indicate that the circulation may be somewhat greater than that generated by potential flow around a circular cylinder. An extensive list of related reports has been included.

REFERENCES

1. Williams, John; and Wood, Maurice N.: Aerodynamic Interference Effects With Jet-Lift V/STOL Aircraft Under Static and Forward-Speed Conditions. Tech. Rep. No. 66403, Brit. R.A.E., Dec. 1966.

2. Wood, M. N.: Jet V/STOL Aircraft Aerodynamics. Ann. N.Y. Acad. Sci., vol. 154, art. 2, Nov. 22, 1968, pp. 893-920.

3. Seidel, M.: Der Einfluss eines geneigten Strahles auf das Strömungsfeld in der Umgebung eines Leitwerks sowie auf dessen Luftkraftbeiwerte - Teil II: Literaturübersicht. DFL-Ber. Nr. 0532, 1969.

4. Skifstad, J. G.: Aerodynamics of Jets Pertinent to VTOL Aircraft. AFAPL-TR-69-28, U.S. Air Force, Mar. 1969.

5. Lee, C. C.: A Review of Research on the Interaction of a Jet With an External Stream. Tech. Note R-184 (Contract No. DA-01-021-AMC-11528(Z)), Res. Lab., Brown Eng. Co., Inc., Mar. 1966. (Available from DDC as AD 630 294.)

6. Garner, Jack E.: A Review of Jet Efflux Studies Applicable to V/STOL Aircraft. AEDC-TR-67-163, U.S. Air Force, Sept. 1967. (Available from DDC as AD 658 432.)

7. Otis, James H., Jr.: Induced Interference Effects on a Four-Jet VTOL Configuration With Various Wind Planforms in the Transition Speed Range. NASA TN D-1400, 1962.

8. Vogler, Raymond D.: Interference Effects of Single and Multiple Round or Slotted Jets on a VTOL Model in Transition. NASA TN D-2380, 1964.

9. Vogler, Raymond D.; and Kuhn, Richard E.: Longitudinal and Lateral Stability Characteristics of Two Four-Jet VTOL Models in the Transition Speed Range. NASA TM X-1092, 1965.

10. Davenport, Edwin E.; and Kuhn, Richard E.: Wind-Tunnel-Wall Effects and Scale Effects on a VTOL Configuration With a Fan Mounted in the Fuselage. NASA TN D-2560, 1965.

11. Hickey, David H.; Kirk, Jerry V.; and Hall, Leo P.: Aerodynamic Characteristics of a V/STOL Transport Model With Lift and Lift-Cruise Fan Power Plants. Conference on V/STOL and STOL Aircraft, NASA SP-116, 1966, pp. 81-96.

12. Margason, Richard J.: Jet-Induced Effects in Transition Flight. Conference on V/STOL and STOL Aircraft, NASA SP-116, 1966, pp. 177-189.

13. Spreemann, Kenneth P.: Free-Stream Interference Effects on Effectiveness of Control Jets Near the Wing Tip of a VTOL Aircraft Model. NASA TN D-4084, 1967.

14. Margason, Richard J.; and Gentry, Garl L., Jr.: Aerodynamic Characteristics of a Five-Jet VTOL Configuration in the Transition Speed Range. NASA TN D-4812, 1968.

15. Barrack, Jerry P.; and Kirk, Jerry V.: Low-Speed Characteristics of High-Performance Lift-Engine V/STOL Aircraft. [Preprint] 680644, Soc. Automot. Eng., Oct. 1968.

16. Seidel, M.: Der Einfluss eines geneigten Strahles auf das Strömungsfeld in der Umgebung eines Leitwerks sowie auf dessen Luftkfraftbeiwerte - Teil I: Versuchseinrichtung, Vorversuche und Kraftmessungen mit horizontalem und vertikalem Strahl. DFL-Ber. Nr. 0487, 1968.

17. Winston, Matthew M.: Wind-Tunnel Data From a 0.16-Scale V/STOL Model With Direct-Lift and Lift-Cruise Jets. NASA TM X-1758, 1969.

18. Carter, Arthur W.: Effects of Jet-Exhaust Location on the Longitudinal Aerodynamic Characteristics of a Jet V/STOL Model. NASA TN D-5333, 1969.

19. Margason, Richard J.: The Path of a Jet Directed at Large Angles to a Subsonic Free Stream. NASA TN D-4919, 1968.

20. Callaghan, Edmund E.; and Ruggeri, Robert S.: Investigation of the Penetration of an Air Jet Directed Perpendicularly to an Air Stream. NACA TN 1615, 1948.

21. Ruggeri, Robert S.; Callaghan, Edmund E.; and Bowden, Dean T.: Penertration of Air Jets Issuing from Circular, Square, and Elliptical Orifices Directed Perpendicularly to an Air Stream. NACA TN 2019, 1950.

22. Jordinson, R.: Flow in a Jet Directed Normal to the Wind. R. & M. No. 3074, Brit. A.R.C., 1958.

23. Keffer, J. F.; and Baines, W. D.: The Round Turbulent Jet in a Cross-Wind. J. Fluid Mech., vol. 15, pt. 4, Apr. 1963, pp. 481-497.

24. Abramovich, G. N.: The Theory of Turbulent Jets. M.I.T. Press, c.1963, pp. 541-552.

25. Vakhlamov, S. V.: Computation of the Trajectory of a Jet in a Drifting Flow. FTD-TT-65-1977, U.S. Air Force, June 13, 1966. (Available from DDC as AD 639159.)

26. Storms, Kenneth R.: Low-Speed Wind Tunnel Investigation of a Jet Directed Normal to the Wind. Rep. 885, Aeronaut. Lab., Univ. of Washington, Nov. 1965.

27. Epshtein, A. M.: Shape of Turbulent Jet Axis in an Unbounded Horizontal Cross Flow. J. Eng. Phys., vol. 9, no. 4, Oct. 1965, pp. 303-306.

28. Shandorov, G. S.: Calculation of a Jet Axis in a Drifting Flow. NASA TT F-10,638, 1966.

29. Albertson, M. L.; Dai, Y. B.; Jensen, R. A.; and Rouse, Hunter: Diffusion of Submerged Jets. Paper No. 2409, Trans. Amer. Soc. Civil Eng., vol. 115, 1950, pp. 639-697.

30. Ricou, F. P.; and Spalding, D. B.: Measurements of Entrainment by Axisymmetrical Turbulent Jets. J. Fluid Mech., vol. II, pt. 1, Aug. 1961, pp. 21-32.

31. Pratte, Bruce D.; and Baines, W. Douglas: Profiles of the Round Turbulent Jet in a Cross Flow. J. Hydraulics Div., Amer. Soc. Civil Eng., vol. 92, no. HY6, Nov. 1967.

32. Nayar, B. M.; Siddon, T. E.; and Chu, W. T.: Properties of the Turbulence in the Transition Region of a Round Jet. Tech. Note No. 131 (AFOSR-68-2880), Inst. Aerosp. Studies, Univ. of Toronto, Jan. 1969.

33. Vogler, Raymond D.: Surface Pressure Distributions Induced on a Flat Plate by a Cold Air Jet Issuing Perpendicularly From the Plate and Normal to a Low-Speed Free-Stream Flow. NASA TN D-1629, 1963.

34. Bradbury, L. J. S.; and Wood, M. N.: The Static Pressure Distribution Around a Circular Jet Exhausting Normally From a Plane Wall Into an Air-Airstream. C.P. No. 822, Brit. A.R.C., 1965.

35. Gelb, G. H.; and Martin, W. A.: An Experimental Investigation of the Flow Field About a Subsonic Jet Exhausting Into a Quiescent and a Low Velocity Airstream. Can. Aeronaut. Space J., vol. 12, no. 8, Oct. 1966, pp. 333-342.

36. Spring, Donald J.; and Street, Troy A.: Experimental Investigation of the Pressure Distributions Induced Upon a Body of Revolution by Several Transverse Jets at Low Speeds. Rep. No. RD-TM-68-7, U.S. Army Missile Command, Aug. 1, 1968.

37. Chang-Lu, Hsiu-Chen: Aufrollung eines zylindrischen Strahles durch Querwind. (Rollup of a Cylindrical Jet in a Crosswind.) Doctorial Dissertation, Univ. of Göttingen, 1942.

38. Fraser, J. P.: Three-Dimensional Study of a Jet Penetrating a Stream at Right Angles. J. Aeronaut. Sci. (Readers' Forum), vol. 21, no. 1, Jan. 1954, pp. 59-61.

39. Gordier, Robert L.: Studies on Fluid Jets Discharging Normally Into Moving Liquid. Tech. Paper No. 28, Ser. B (Contract Nonr 710(26)), St. Anthony Falls Hydraulic Lab., Univ. of Minnesota, Aug. 1959.

40. Kirkpatrick, David L. I.: Wind-Tunnel Corrections for V/STOL Model Testing. M.A.E. Thesis, Univ. of Virginia, 1962.

41. Monical, Richard E.: A Method of Representing Fan-Wing Combinations for Three-Dimensional Potential Flow Solutions. J. Aircraft, vol. 2, no. 6, Nov.-Dec. 1965, pp. 527-530.

42. Wooler, P. T.; Burghart, G. H.; and Gallagher, J. T.: Pressure Distribution on a Rectangular Wing With a Jet Exhausting Normally Into an Airstream. J. Aircraft, vol. 4, no. 6, Nov.-Dec. 1967, pp. 537-543.

43. Wooler, P. T.: On the Flow Past a Circular Jet Exhausting at Right Angles From a Flat Plate or Wing. J. Roy. Aeronaut. Soc., vol. 71, Mar. 1967, pp. 216-218.

44. Rubbert, P. E.; Saaris, G. R.; Scholey, M. B.; Standen, N. M.; and Wallace, R. E.: A General Method for Determining the Aerodynamic Characteristics of Fan-in-Wing Configurations. Vol. 1 - Theory and Application. USAAVLABS Tech. Rep. 67-61A, U.S. Army, Dec. 1967.

45. Rubbert, P. E.; and Saaris, G. R.: A General Three-Dimensional Potential-Flow Method Applied to V/STOL Aerodynamics. [Preprint] 680304, Soc. Automot. Eng., Apr.-May 1968.

46. Hardy, William G. S.: Non-Parallel Flow Interactions. M.A.E. Thesis, Univ. of Virginia, June 1967.

47. Matthews, G. B.; and Hardy, William G. S.: Wind Tunnel Wall Effects in V/STOL Model Testing. NASA CR-66721, 1968.

48. McAllister, Jack Donald: A Momentum Theory for the Effects of Cross Flow on Incompressible Turbulent Jets. Ph. D. Thesis, Univ. of Tennessee, Aug. 1968.

49. Soukup, Stephen M.: Potential Flow Aspects of the Cross-Sectional Deformation of Jet Configurations in Cross-Flow. M.S. Thesis, Univ. of Tennessee, Dec. 1968.

50. Wooler, P. T.: Flow of a Circular Jet Into a Cross Flow. J. Aircraft (Eng. Notes), vol. 6, no. 3, May-June 1969, pp. 283-284.

51. Vizel, Ya. M.; and Mostinskii, I. L.: Deflection of a Jet Injected Into a Stream. J. Eng. Phys., vol. 8, no. 2, Feb. 1965, pp. 160-163.

52. Gerend, Robert Paul: Penetration of a Jet Into a Nonuniform Stream. M.S. Thesis, Seattle Univ., June 1968.

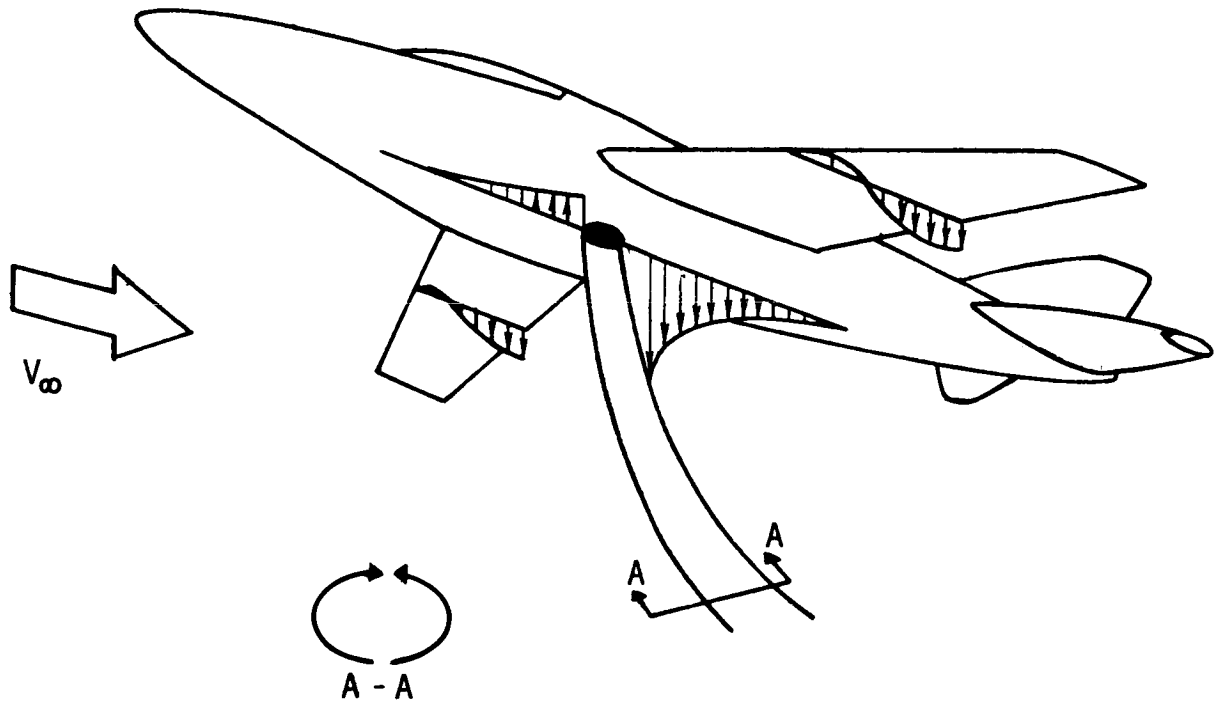

Figure 1.- Jet wake from a V/STOL aircraft in transition flight rolls up into a pair of contrarotating vortices.

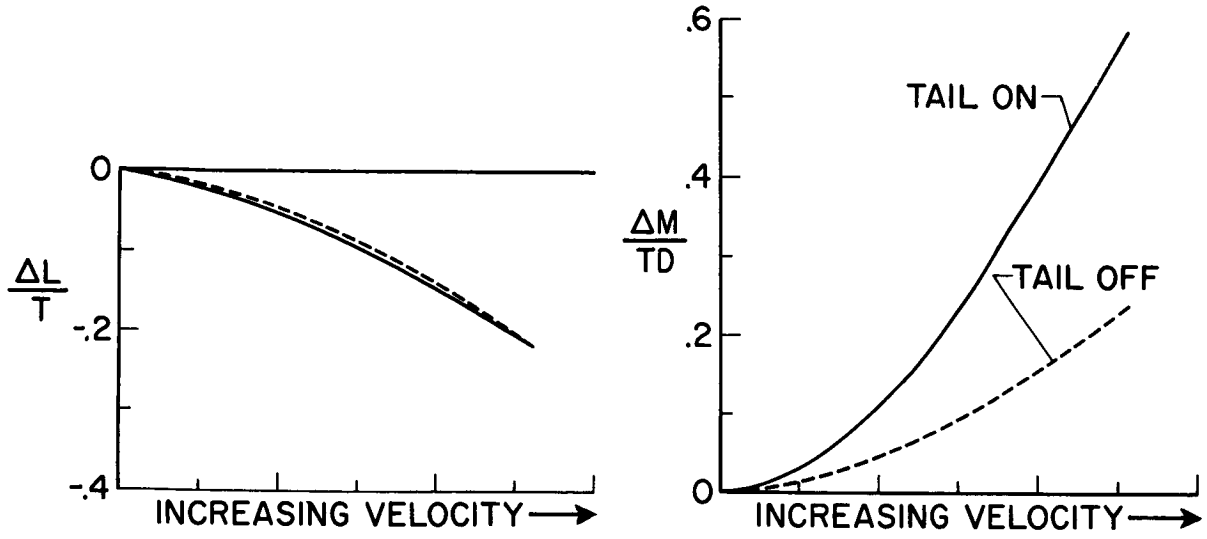

Figure 2.- General trend of jet-induced lift loss and pitching moment in transition flight.

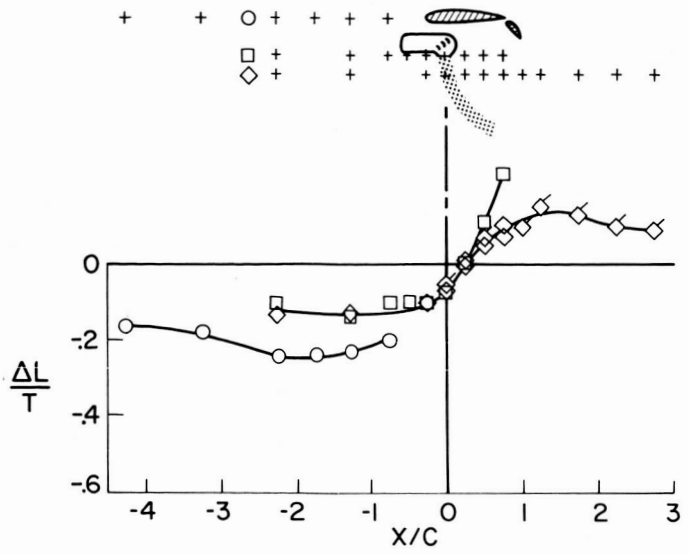

Figure 3.- Increments of interference lift during transition flight for varying chordwise locations of the jets. $\delta_f = 40^\circ$; $\delta_j = 90^\circ$; $V_\infty/V_j = 0.18$. Flagged symbols indicate jet support assembly was located downstream of the wing.

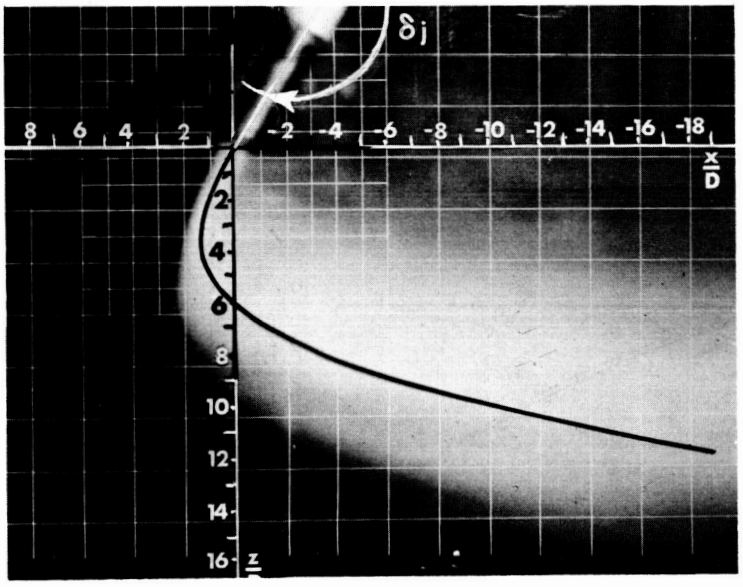

Figure 4.- The center-line path of jet wakes obtained from flow visualization studies. Empirical equation describing path of jet is

$$\frac{x}{D} = -\frac{q_\infty/q_j}{4 \sin^2\delta_j}\left(\frac{z}{D}\right)^3 - \frac{z}{D}\cos\delta_j.$$

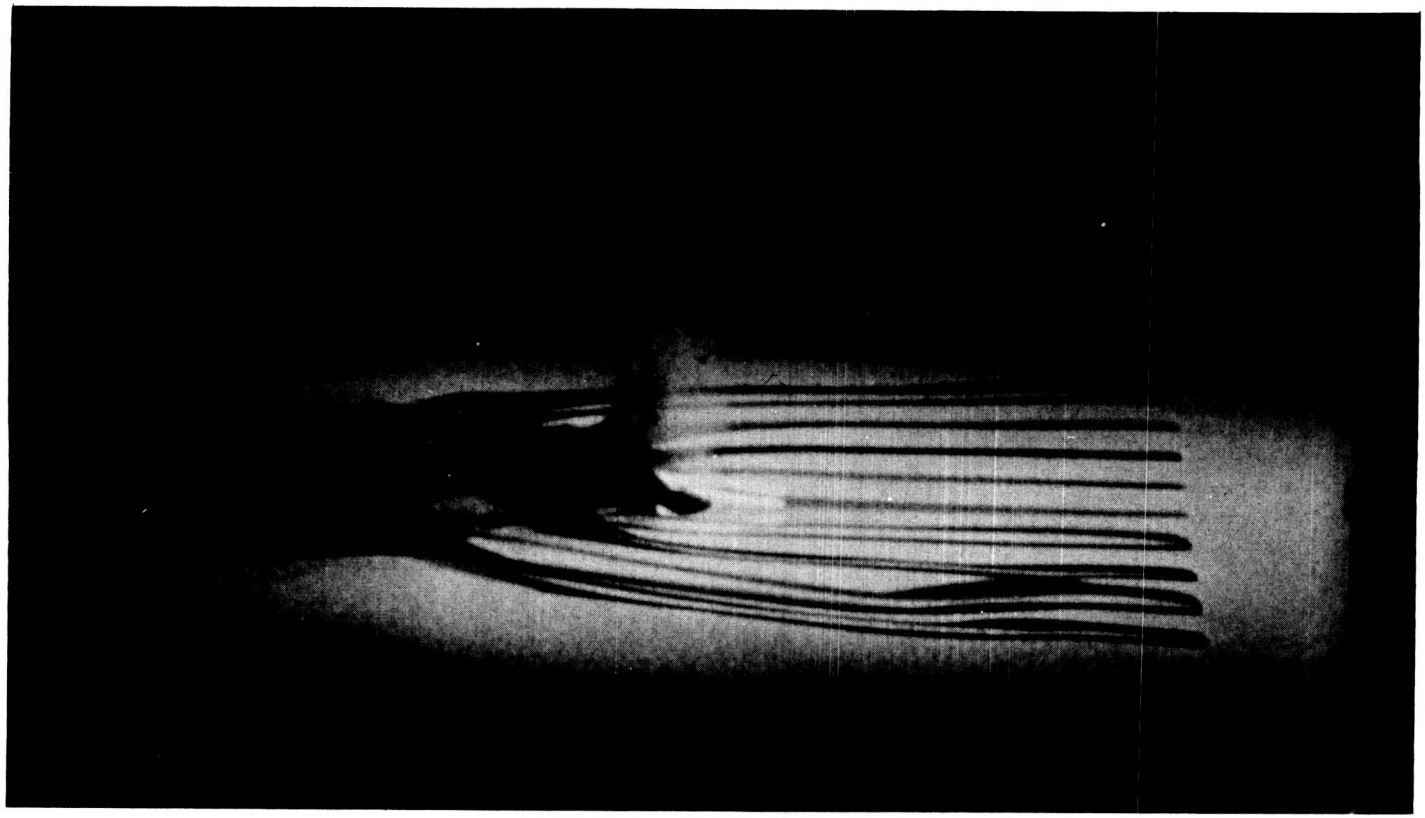

Figure 5.- Photograph of the flow induced around and into a jet exhausting normal to the free stream. (Photograph from O.N.E.R.A. motion-picture film no. 575 entitled "Flows With Large Velocity Fluctuations.")

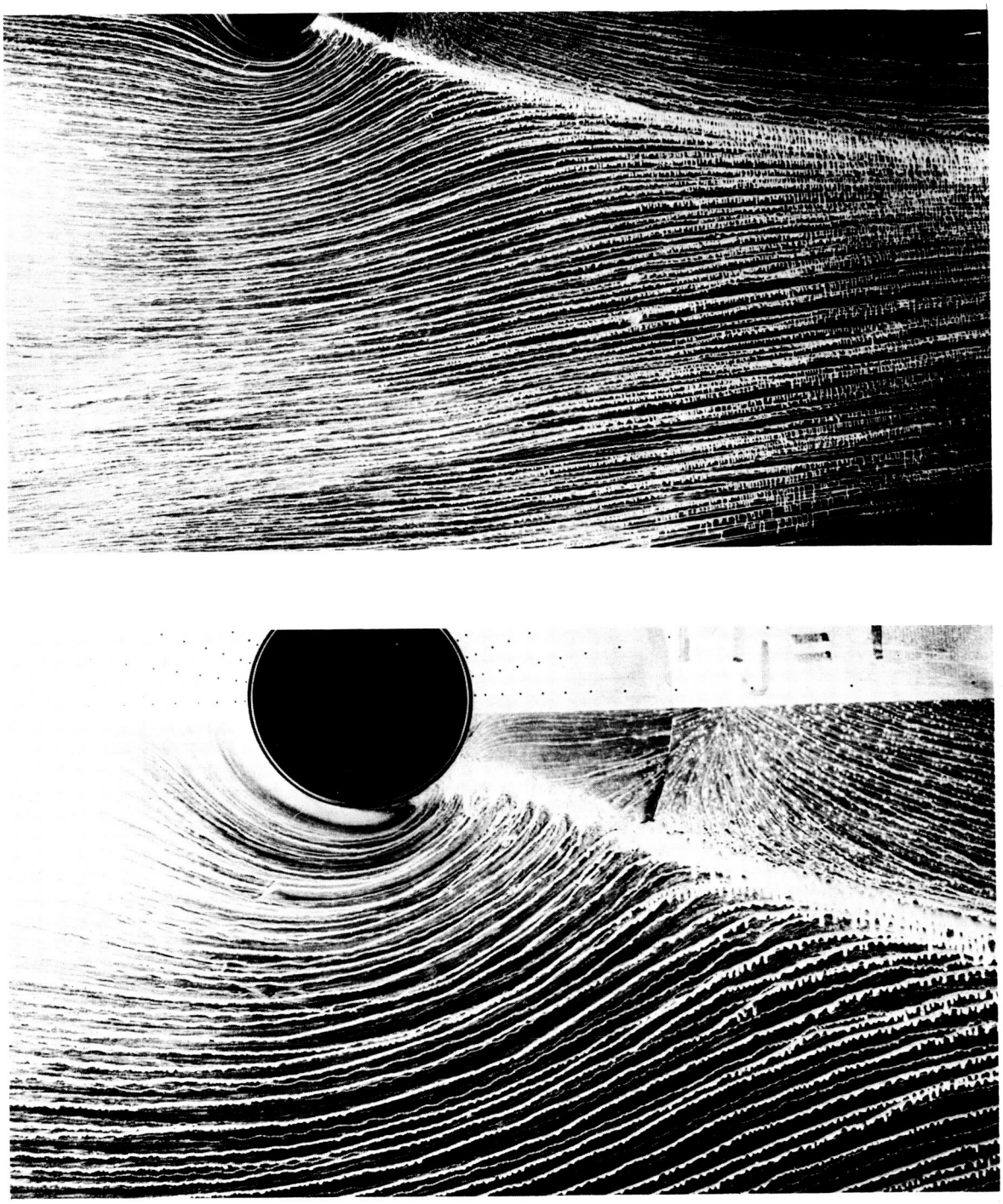

Figure 6.- Photograph of oil flow on the surface of a plate which has a jet exhausting normal to the plate and to a free stream (O.N.E.R.A. photograph). Lower photograph is closeup of upper.

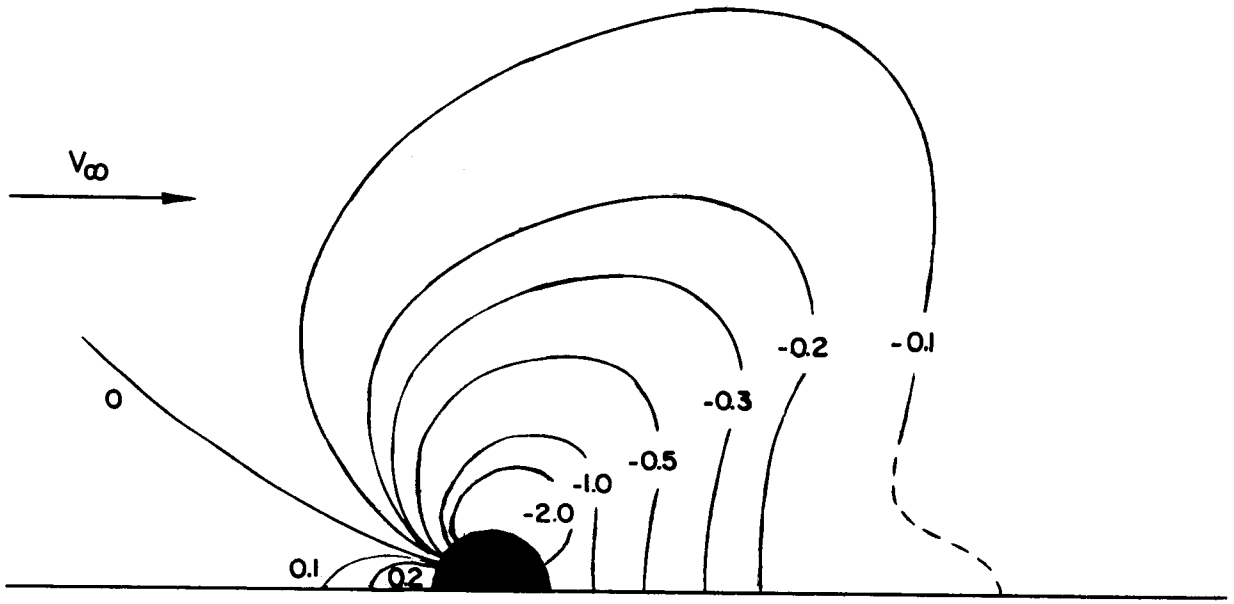

Figure 7.- Pressure distribution on the surface of a plate which has a jet exhausting normal to the plate and to a free stream. $V_\infty/V_j = 0.25$.

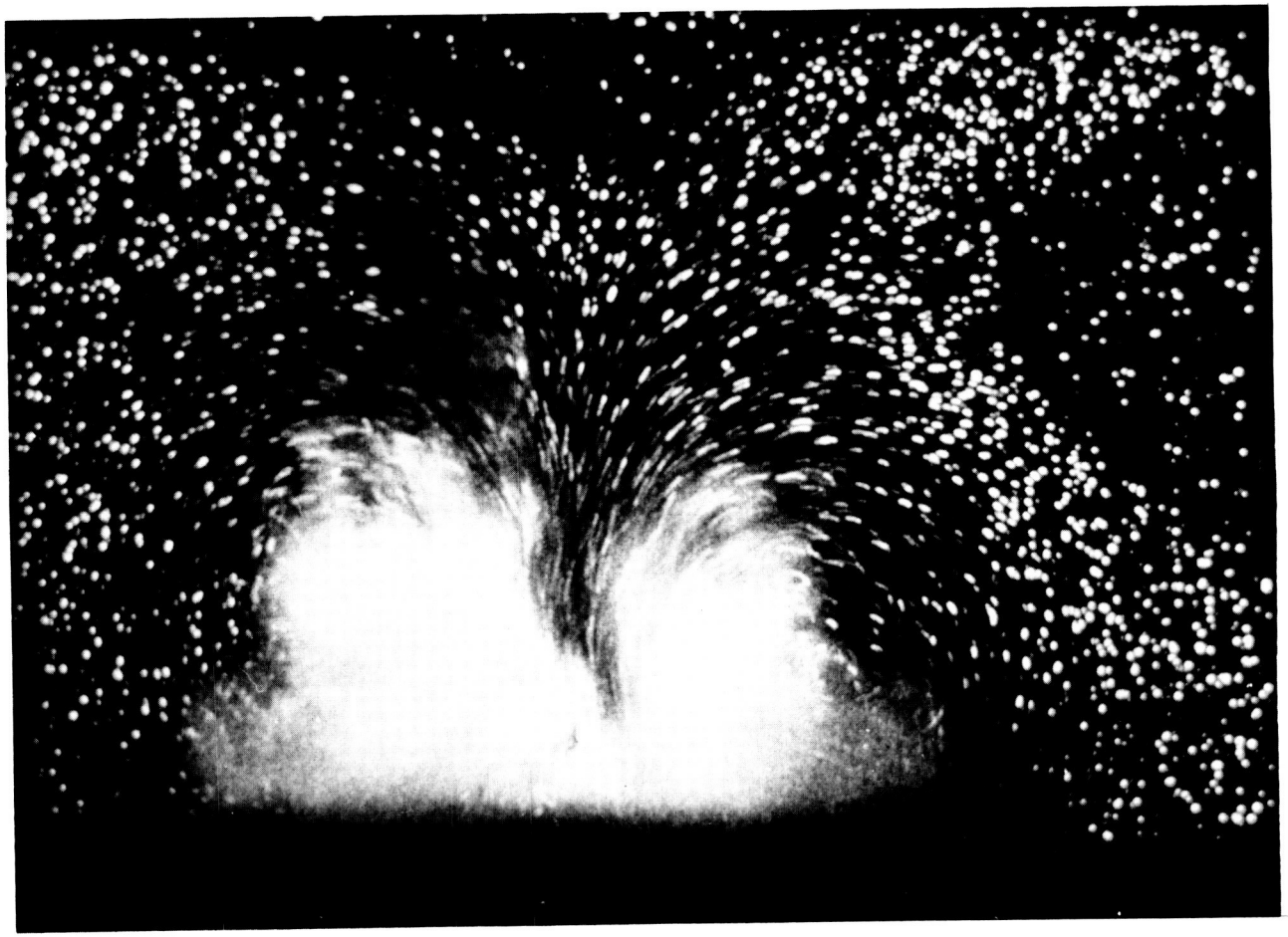

Figure 8.- Cross section of the wake of a jet exiting perpendicular to the free stream in a water tunnel. This cross section is approximately 6 nozzle diameters downstream of the nozzle exit along the jet path. (Photograph from O.N.E.R.A. motion-picture film no. 575 entitled "Flows with Large Velocity Fluctuations.")

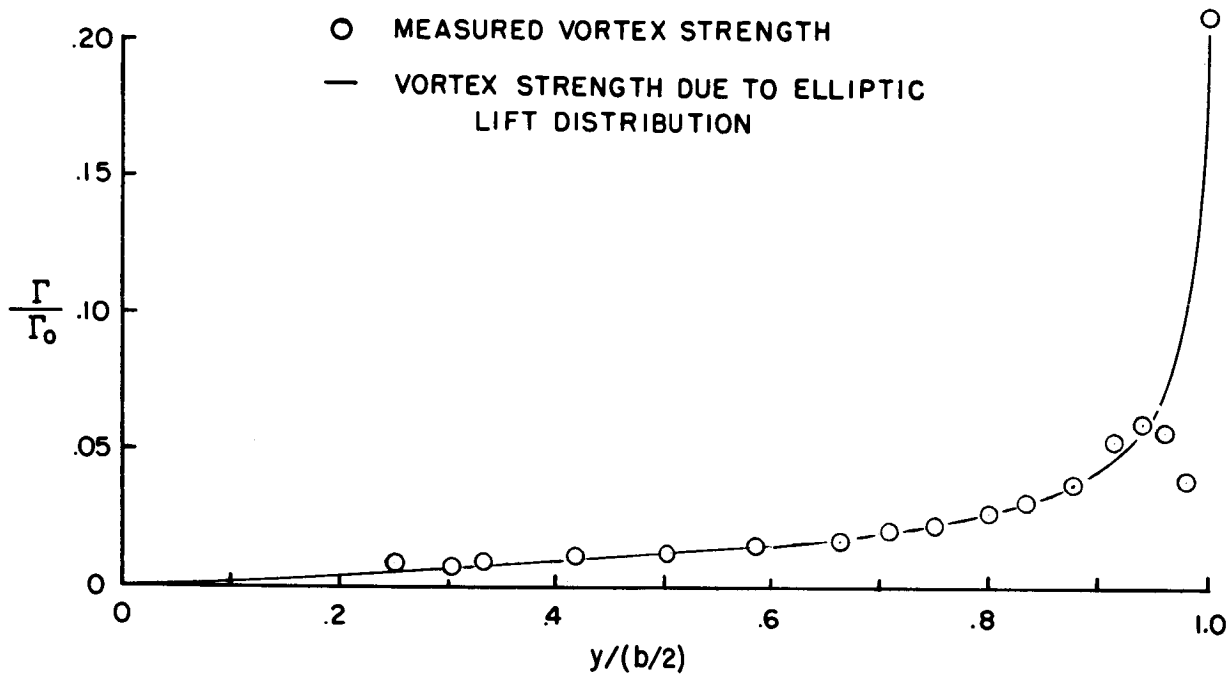

Figure 9.- Vortex meter calibration using wing trailing vortex sheet.

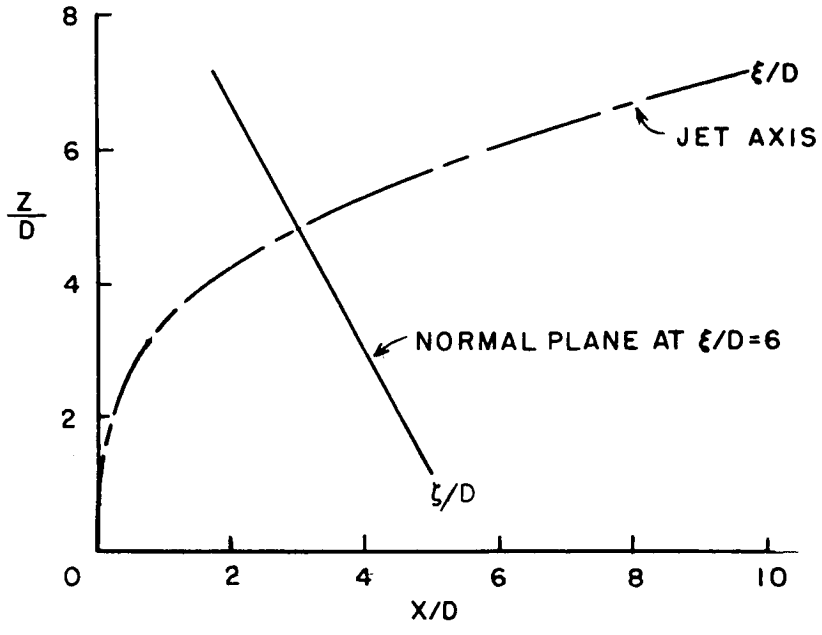

Figure 10.- Location of normal plane where circulation contours were measured. $V_\infty/V_j = 0.250$.

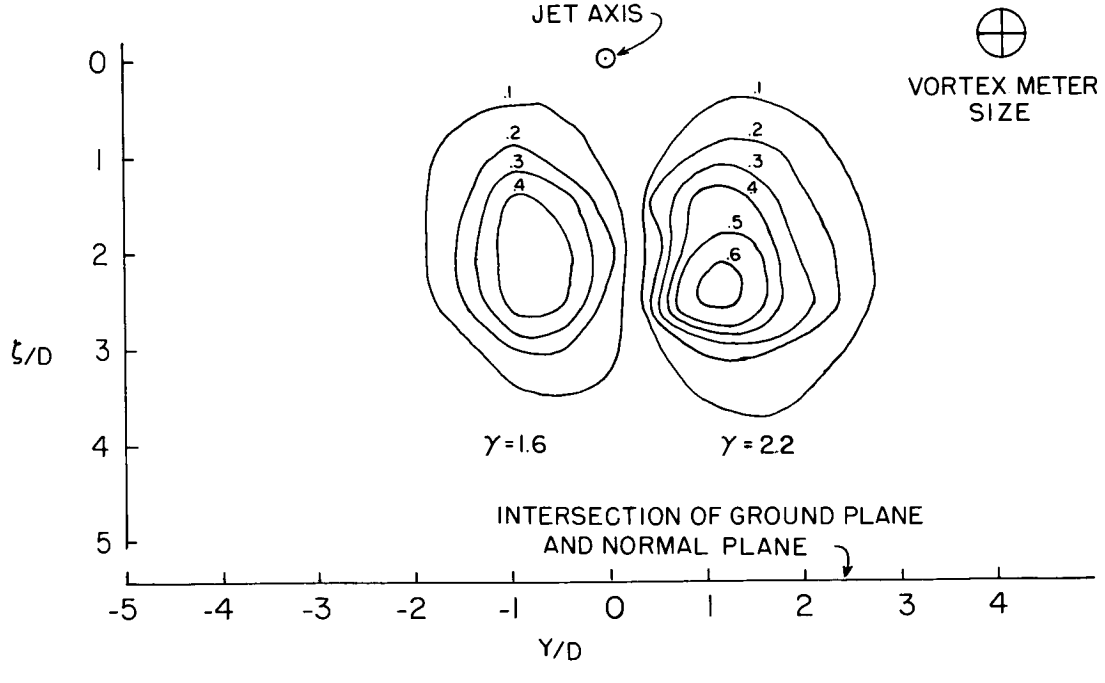

Figure 11.- Jet circulation contours at the $\xi/D = 6$ location. The position of the jet center line is indicated. In addition, a schematic sketch of the circle swept out by the 1/2-inch vortex-meter paddle blades is shown.

THE PHYSICAL NATURE OF THE SUBSONIC JET IN A CROSS-STREAM

By James F. Keffer,

University of Toronto

2

SUMMARY

A description of the physical characteristics of the subsonic jet entering a stream with a non-zero, cross-component is presented. Three zones, in which the dynamics of the flow are significantly different, are defined. The structure of the mean and turbulent motion is discussed with reference to the various entrainment processes.

INTRODUCTION

Probably the first stimulus for an understanding of the mixing which arises in a jet of fluid discharging into a cross-flowing stream occurred because of its application to the emission of effluents from a chimney stack. Only a cursory observation of a plume is needed to show the remarkably rapid diffusion which can take place in the natural wind with adiabatic or nearly adiabatic thermal lapse rates. It is clear from this that the momentum fluxes of the opposing streams create an efficient mechanism of entrainment of free-stream fluid. Indeed, the principle is so basic that it is used to promote fluid mixing in a large number of mechanical systems.

Lately there has been a resurgence of interest in the detailed features of the fundamental problem. This is partly because of the increasing awareness of the public and government about our need to understand the role of turbulent dispersion of waste effluent. But there has been stimulation, as well, because of the application to jet thrust systems in some aircraft. The deflected jetsof a V/STOL plane for example, interfere with the aerodynamic performance. This aspect has received some attention recently by Williams and Wood (ref. 1) and Margason (ref. 2). It should perhaps be noted that a much earlier paper by Ribner (ref. 3) anticipated this interest with an examination of the effect of a jet upon the stability of a

jet aircraft.

Considering the basic problem of a jet in a cross-wind, Ruggeri et al (refs. 4,5,6 and 7), in a series of early papers, explored the effect of the addition of heat and change of orifice shape upon the flow. The significance of their work to the present discussion is limited, however, since the wind tunnel used to contain the cross-stream, was narrow. This essential two-dimensionality would be expected to limit the lateral spread of the jet and, as will be seen later, the effect of the flow around the jet edges is important to the entrainment. The first relevant experimental work on the problem was due to Jordinson (ref. 8), who made some simple measurements of the trajectory of the round jet. He defined the centreline as the point of maximum velocity measured with a pitot-tube and pitch meter at successive vertical stations. As well, Jordinson surveyed the cross-section of the jet. The resulting contours were very revealing in that they showed the edges of the jet to be sheared by the cross-stream and distorted in the down-stream direction. The distinctive kidney-shape was indicative of a secondary mode of entrainment as will be discussed in some detail in subsequent sections.

A second experimental study by Gordier (ref. 9) carried out a series of tests over the same general range of velocity ratios as Jordinson but used a jet discharging into a water tunnel. The results defining the trajectory were consistent with previous work and this was the first indication that a Reynolds number similarity existed. The examination of the structure of the turbulence within the deflected jet system was undertaken by Keffer and Baines (ref. 10). Using hot wire anemometer techniques the mean of the turbulent intensities as well as the mean velocity quantities were taken. The results showed that within the range of velocity ratios used by Jordinson and Gordier, a self-similarity of the mean flow field could be defined if one chose to scale the velocity terms by a reference velocity difference along a natural system of co-ordinates intrinsic to the jet flow (see figure 1). The success of this scaling was only limited for the mean turbulent intensities, however. The rather high level of turbulence intensity precludes us from considering the data to be more than a qualitative specification of magnitude.

The problem has been extended further by a number of investigators both experimentally and by phenomenological model equations. No attempt is made here to be comprehensive but a few examples are mentioned to show the present trend of the research. Pratte and Baines (ref. 11) examined the far field behaviour of the jet, that is, the region well beyond the zone of maximum curvature. Somewhat surprisingly, it appears that the proper scaling function which one should use to collapse

the trajectories on a single functional curve depends upon the velocity ratio rather than the momentum ratio. Fan (ref. 12) has introduced the effect of a stratified environment upon the growth and trajectory of what should be termed a plume. Analytically, he has suggested a mathematical model based upon the drag of the plume in the cross-stream. Margason (ref. 13), in a series of wind tunnel tests considered the effects of large variation of the angle of entry of the jet to the main stream, as did Platten and Keffer (ref. 14). In the former study empirical fits were made to the trajectories found by a number of workers with rather uniform results. Platten and Keffer proposed a model equation to account for the two basic modes of entrainment which exist in the deflected jet. A solution of the equations gave good fits to the experimental trajectories over a limited range of injection angles.

As a result of the work briefly outlined above, a distinct picture of the physical nature of the jet is beginning to emerge. There are some important areas of disagreement, not, happily, in the experimental results, but in the mathematical models which are used to interpret them. Most significant perhaps, is the controversy about the mechanism of entrainment of ambient fluid by which the jet grows. This paper will inevitably incorporate a personal bias into the argument and the emphasis will be placed upon the structure of the turbulence within the flow rather than the phenomenological replacement of the turbulence. It would appear that while the salient features are reasonably well understood, most of the intimate and therefore interesting details still command our intensive and enlightened interpretation.

SYMBOLS

d - orifice diameter

R - velocity ratio

U - axial jet velocity

U_c - maximum U at any cross-section

U_j - initial jet velocity

U_o - free stream velocity

U_v - vortex entrainment velocity

u - turbulent velocity

x,y,z - Cartesian co-ordinates

ξ,η,ζ - curvilinear co-ordinates

ξ^*,x^* - distances measured from virtual source

θ - local jet angle

θ_j - angle of jet injection

PHYSICAL DESCRIPTION

In the discussion which follows we reduce the problem to its simplest form. This becomes an examination of a round jet of fluid discharging from an infinite plane into an ambient, miscible fluid of the same density, which has a non-zero, cross-stream component of velocity. The influence of the surrounding geometry, such as the presence of a chimney stack or the fuselage of an aircraft, will be ignored. The significant parameter will thus be the velocity ratio R defined as the exit jet velocity U_j divided by the constant and uniform cross-stream velocity U_o. It will further be assumed that the initial absolute velocity in the jet is large enough that the developed flow, which takes place upon the mixing of the streams, will be turbulent. A second parameter is introduced, the angle of injection θ_j. Clearly, a complete variation of θ_j through 180° would include the special cases of a jet in an opposing stream and the jet in a co-flowing stream. Generally, however, we shall restrict our interest to moderate deviations of θ_j from the 90° direction. A schematic of the jet is shown in figure 1.

It is convenient to think of the jet as arbitrarily separated into three regions:

(1) the source flow, where the effect of orifice geometry, plate and/or tunnel boundary layer and potential core may be important,

(2) the curvilinear zone, where the jet flow is fully developed from the standpoint of the turbulence structure and the entrainment mechanisms proceed in a relatively straightforward manner and

(3) the far region, where the jet flow, having approached its asymptotic state, is almost entirely dissipated and, on a mean flow basis, indistinguishable from the main stream.

The Source Flow

Relatively little work has been done in this region. Essentially the flow at exit bears a close resemblence to the free jet in that it possesses a core of potential fluid. The term potential is relative. The fluid emerging from the orifice

is considered to have a negligible amount of turbulence compared to that which subsequently develops in the fully mixed region of the jet. It is probable that the flow in this zone is Reynolds number dependent, as was found by Baines (ref. 15) for the free jet, although not enough experimental data are available to make a definitive statement. It has been shown (refs. 10, 11, and 14) that the length of the potential core varies directly with R, but again the specific functional trend has not been reported in the literature for a large range of velocity ratios.

Keffer and Baines (ref. 10) indicated that if substitution is made for the core region and a virtual origin or point source defined by extrapolating the developed jet flow back through the plane of emission, the decay of centreline velocity will plot universally on a single functional plot. This implies a kinematic or Reynolds number similarity for all deflected jets, at least for the range of flows tested. At very low velocity ratios, however, of the order of 4 or less, the flow loses this characteristic. A premature deflection of the core region by the pressure field occurs and the trajectory centreline, extrapolated back to the virtual origin, does not go through the physical origin for the flow. For a jet discharging at right angles to the stream this means that the trajectory at the source is not tangent to the x-axis. This can lead to difficulties in the mathematical modelling of the flow.

In addition to the displacement or shift effect it was found that, at these very low velocity ratios, the jet momentum relative to the free stream is not sufficient to allow the flow to escape the boundary layer of the exit plane. This introduces a complication for, unless particular care is taken to eliminate the boundary layer, the results from different laboratories will be influenced by the different magnitude of boundary layer entrainment. Since this introduces an additional and relatively uncontrolled parameter into the system and we will not consider these low values of R further. It will be assumed that the velocity ratio is sufficiently high that the jet flow can escape the influence region of the surface. It should perhaps be noted that a related problem is of some significance. The performance of the jet when deflected by a gradient wind is certainly relevant. For reasons of simplicity, however, most studies to date have been concerned with the uniform wind profile.

The previously mentioned experiments of Ruggeri et al considered the effect of shape change of the discharge opening. This can be expected to affect the nature of the source flow. Its significance must be negligibly small in the developed region of the flow, however, where it is possible to replace the initial conditions by a virtual origin. For an orifice flow, a contraction co-efficient is generally necessary to reduce the data to a convenient base, compatible say with a sharply con-

verging nozzle. If a length of tube is used to eject the jet fluid, the exit profile will be markedly non-uniform, the exact shape depending upon the length of tube or the stage of development of the tube flow. It will thus be necessary to define an appropriate momentum flux for the jet by means of a correction co-efficient multiplying the square of the average velocity.

The Curvilinear Region

As the jet issues from the exit plane the relative velocity between the jet and stream fluid creates a turbulent mixing layer around the periphery. This mixing layer grows in the direction of the jet flow, eroding the potential zone of fluid in a manner similar to the free jet. In the present case, the growth is more rapid and the potential core length much shorter. For velocity ratios of 4, 6 and 8 the core length is of the order 1, 2 and 3 orifice diameters respectively. For the free jet, the core length is about 6. At the end of the core, the jet fluid is fully turbulent and the lateral velocity profile, taken typically in a streamwise traverse, is more or less Gaussian. We define this as the beginning of the curvilinear zone and the flow is said to be fully developed at this point.

At present, the behaviour of the flow in the lee of the jet, conveniently termed the 'wake', is not well understood. It is possible that the analogy of Jordinson has some validity. He suggests that the jet can be considered to act as a porous cylinder with suction, the sink effect being necessary to account for the entrainment of free-stream fluid. Although offering some convenience this model cannot be expected to tell us much about the true nature of the entrainment processes. Clearly the mechanisms must be different in the stagnation region at the front of the jet and in the 'wake'.

The cross-sectional profiles of Jordinson and Keffer and Baines (for example see figure 2) have shown the strong lateral deflection of the jet sides by the shearing of the cross-stream. Turbulent entrainment of free stream fluid will occur at the sides because of the relative motion. As it is swept around into the wake region, the fluid will be incorporated into the main jet system. The result is a helical circulation pattern. The generation of the circulation will continue as long as the jet has a component of velocity normal to the free stream. Appropriately this helicity has been interpreted as a counter-rotating, vortex pair and it can be shown from analytical arguments (ref. 14) that the vorticity generation will reach a maximum within this curvilinear region. A plot of the rate of change of circulation velocity is shown in figure 3 as a function of deflection angle. It might be suspected that the helicity would play a major role in the entrainment of free-

stream fluid and the analytical model of Platten and Keffer together with the experimental results, appears to bear this out.

In the frontal regions of the jet, the flow is partially stagnated. As the jet deflects, there will be a component of motion of the free-stream fluid parallel to the mean direction of the jet flow. This situation is just that required for a free jet type of entrainment. Although the details of how a turbulent front expands into a non-turbulent region of fluid are not at all well understood at present, heuristically we may argue in terms of a phenomenological model. A requirement for entrainment is simply the existence of relative motion between streams of fluid. An instability develops which breaks up into turbulent mixing and the high velocity fluid, or jet flow, diffuses into or entrains the outer stream. We would thus use, in lieu of the precise location of the turbulent-non-turbulent interface, a simple specification of the jet boundary. Conveniently this could be the point where the jet velocity excess has decreased to an arbitrary level, say 10%.

From a physical point of view we thus have two mechanisms of entrainment, the ordinary free-jet flow type which can be handled by the conventional phenomenological approach and the entrainment supplied by the helicity in the 'wake region' of the jet. Clearly a successful analytical model must in some way incorporate these two processes.

The developed jet flow in this zone displays some of the characteristics associated with the simple free-jet. The measurements of Keffer and Baines of the mean flow distribution show a self-similarity of the axial velocity vector when taken along a curvilinear lateral co-ordinate, η. The scaling was achieved by using the excess velocity, $(U-U_o)$ and dividing by the local centreline velocity excess, (U_c-U_o). The collapsed data shown in figure 4, resembles the conventional Gaussian distribution plot although the scatter is marked. The functional shape is not really surprising. With this technique of stretching the data small differences tend to be obscured. Nevertheless, the results show no unexpected anomalies.

The variation of centreline velocity, i.e. along the jet trajectory, shows a universality which again tends to resemble the free jet (figure 5). The decay of mean velocity is more intense, however, as would be expected with the higher rates of entrainment and the variation of mean velocity at the centreline of the jet does not have the simple inverse linear relationship with distance characteristic of the free jet. It is significant that when the differences of the source as a function of velocity ratio are accounted for by allowing the position of the virtual origin to vary, the mean flow characteristics are strongly self-similar for this curvilinear region.

The turbulence measurements display less self-similarity when the same method of plotting is used (figure 6). As with all simple free turbulent shear flows, the structure of the turbulence requires a longer period than the mean flow to reach an equilibrium state. In the present situation, the intense mixing and decay prevents this and an equilibrium situation is not reached. In fact, since the region is really an interim state for the whole of the deflected jet flow, it is probably incorrect to speak in terms of an equilibrium or asymptotic state for the curvilinear zone.

From the above remarks we can summarize the main features of the flow in this second region. The curvilinear zone clearly has most of the characteristics of simple jet flows, for example, entrainment, axial velocity decay, self-similarity and turbulence structure. We can choose to interpret the flow as a special case of the simple jet if an appropriate system of curvilinear co-ordinates is defined. The most distinguishing feature is the presence of the 'wake' region and the attendent circulatory flow which exists within it. Although it is possible to exclude this 'wake' from the basic jet flow analysis, the consequences of the extra entrainment cannot be ignored.

Far Field Region

Beyond the zone of maximum curvature, entrainment has reduced the jet velocity excess to a point where it cannot be measured by conventional techniques and it becomes necessary to define the jet boundary for these conditions by the use of a tracer such as low level heat or smoke. We may think of this as the onset of the final region of the deflected jet flow. Pratte and Baines (ref. 11) were able to observe the far field behaviour visually and it showed a double-valued power law variation for the centreline trajectory when scaled in terms of the velocity ratio. Their functions took the form,

$$\frac{x}{dR} \sim \left(\frac{\xi}{dR}\right)^n$$

where the exponent 'n' was 1.0 up to an ξ/dR of 2 and 0.33 beyond that. Their range of velocity ratios extended from 5 to 35. The earlier results of Keffer and Baines, which accounted for the variation of the virtual origin, suggested the relation

$$\frac{x^*}{dR^2} \sim \left[\frac{(\xi^*)}{dR^2}\right]^n$$

with 'n' = 1.0 in the first portion of the flow but falling off as the limit of observation ($\xi^*/dR^2 = 2.0$) was reached. These results are consistent in that they imply that the zone of curvilinear flow is significantly different than the far field.

Although the axial component of mean velocity is virtually zero, this region of the flow should still show the effect of the swirl generated in the curvilinear zone since vorticity is remarkably long-lived. The jet in this final phase contains its original vertical momentum. It will therefore continue to rise, but at an ever-decreasing rate as the momentum is diffused over the steadily increasing area of each horizontal plane. Because of this, additional vorticity will continue to be generated all along the trajectory of the jet. But the rate of generation will decrease as we travel further along the jet path and the processes of ordinary viscous dissipation will cause the absolute magnitude of the vorticity to decrease. The limit state of this flow will thus be a pair of weak, counter-rotating line vortices, being carried along by the main stream.

The structure of the turbulence in this final phase must also be dominated by the viscous decay. The smaller eddies will be dissipated most rapidly and as is found with grid-produced turbulence, the largest eddies, which are characteristic of the generating grid, remain. They tend to retain their identity while the smaller scales disappear. In a sense the counter-rotating vortex pair in this present system is analogous to the large eddy of the grid flow. It is probably more accurate to view these vortices, at least in the final phase, as general patterns of circulation rather than discrete and perhaps measureable line vortices.

The entrainment mechanism in this final phase must depend almost entirely upon the vortex flow since there no longer is an effective component of relative axial motion between the jet and the free stream. We would expect, therefore that the absolute entrainment would decrease and the rate of jet spread would fall off. The measurements of Pratte and Baines support this. A plot of the width of the jet with respect to the axial path gives

$$\frac{\Delta\zeta}{dR} \sim \left(\frac{\xi}{dR}\right)^n$$

where 'n' is 1.35 in the curvilinear region. This changes abruptly to 0.33 for the far field.

DISCUSSION

For meteorological applications, the far field region would be of most importance. Interest for aerodynamic study, however, would centre upon the first two regions of the flow. Within the zone of maximum curvature, where the flow has reached a developed state of turbulence and where the dynamic effects are strong, attempts have been made to formulate model equations for the flow. For example, in the work of Fan (ref. 12), the presence of entrainment, additional to that supplied by free jet theory, is attributed to a pressure difference around the jet flow. By employing a suitable drag co-efficient, Fan's model appears to predict the trajectories of both buoyant and non-buoyant plumes reasonably well. On physical grounds, however, this concept is not attractive, since in regions away from the source, the processes involved in jet entrainment are most likely to result from free stream effects not depending upon pressure gradients.

In contrast, Platten and Keffer (ref. 14) have suggested that the extra entrainment must result from the observed circulatory flow, i.e. the so-called vortex pair. As discussed above, it may be more reasonable to think of these motions as large turbulent eddies within the jet system, rather than a pair of strong line vortices such as would be observed from a delta wing. This would not affect the analysis, however. The work of Pratte and Keffer (ref. 16) on turbulent swirling jets has verified that a marked increase in entrainment results when swirl is added to a simple jet flow, the spread rate increasing by a factor of two for a swirl velocity of the same order initially as the axial velocity. Although it is not yet clear whether the free jet and vortex contributions to entrainment are interactive, the simple additive model of Platten and Keffer, predicts the experimental results well.

Aside from obvious practical applications, the study of the deflected jet is of considerable fundamental interest in that it represents a particular example of a free turbulent shear flow. As an exercise in basic research, the problem may be expected to tell us something about the structure of turbulence generally. Although the simplest of free turbulent shear flows (jets and mixing layers) are self-preserving, (ref. 17) enabling spread and decay rates to be predicted from the equations of motion, the present flow is not. The presence of the co-flowing component of the external stream precludes this particular analysis even when use is made of the intrinsic co-ordinate system. As mentioned above, however, the results show the flow to be roughly self-similar in the zone of curvature. This does enable some simplification to be made in the analysis of the problem. Much more experimental work is required in this region

to establish the more subtle characteristics of the turbulence, however.

REFERENCES

1. Williams, J. and Wood, M.N.: Aerodynamic Interference Effects with Jet-Lift V/STOL Aircraft under Static and Forward-Speed Conditions. Tech. Rep. No. 66403, Brit. R.A.E., Dec. 1966.

2. Margason, R.J.: Jet-Included Effects in Transition Flight. Conference on V/STOL and STOL Aircraft, NASA SP-116, 1966, pp. 177-189.

3. Ribner, H.S.: Field of Flow About a Jet and Effects of Jets on Stability of Jet-Propelled Airplanes. NACA War. Rep. L 213, 1946.

4. Callaghan, E.E. and Ruggeri, R.S.: Investigation of the Penetration of an Air Jet Directed Perpendicularly to an Air Stream. NACA TN 1615, June 1948.

5. Ruggeri, R.S., Callaghan, E.E. and Bowden, D.T.: Penetration of Air Jets Issuing from Circular, Square and Elliptical Orifices Directed Perpendicularly to an Air Stream. NACA TN 2019, Feb. 1950.

6. Callaghan, E.E. and Ruggeri, R.S.: A General Correlation of Temperature Profiles of a Heated Air Jet Directed Perpendicularly to an Air Stream. NACA TN 2466, Sept. 1951.

7. Ruggeri, R.S.: General Correlation of Temperature Profiles Downstream of a Heated Air Jet Directed at Various Angles to the Air Stream. NACA TN 2855, Dec. 1952.

8. Jordinson, R.: Flow in a Jet Directed Normal to the Wind. R. and M. No. 3074, Aero. Res. Comm. (Great Britain), Oct. 1956.

9. Gordier, R.L.: Studies on Fluid Jets Discharging Normally into Moving Liquid. St. Anthony Falls Hyd. Lab., Tech. Paper, No. 28, Series B, Aug. 1959.

10. Keffer, J.F. and Baines, W.D.: The Round Turbulent Jet in a Cross-Wind. J. Fluid Mech., Vol. 15, Pt. 4, 1963, pp. 481-496.

11. Pratte, B.D. and Baines, W.D.: Profiles of the Round Turbulent Jet in a Cross Flow. J. Hyd. Div., Proc. A.S.C.E., Nov. 1967, pp. 53-64.

12. Fan, L.N.: Turbulent Buoyant Jets into Stratified or Flowing Ambient Fluids. Rep. No. KH-R-15, Keck Hyd. Lab., California Inst. Technology, June 1967.

13. Margason, R.J.: The Path of a Jet Directed at Large Angles to a Subsonic Free Stream. NASA TN D-4919.

14. Platten, J.L. and Keffer, J.F.: Entrainment in Deflected Axisymmetric Jets at Various Angles to the Stream. Univ. of Toronto, Mech. Eng. TP-6808, June 1968.

15. Baines, W.D.: Discussion of 'Diffusion of Submerged Jets'. Trans. A.S.C.E., Vol. 115, 1950.

16. Pratte, B.D. and Keffer, J.F.: Swirling Turbulent Jet Flows. Part I: The Single Swirling Jet. Univ. of Toronto, Mech. Eng., TP-6901, March 1969.

17. Townsend, A.A.: The Structure of Turbulent Shear Flow. Cambridge University Press, 1956.

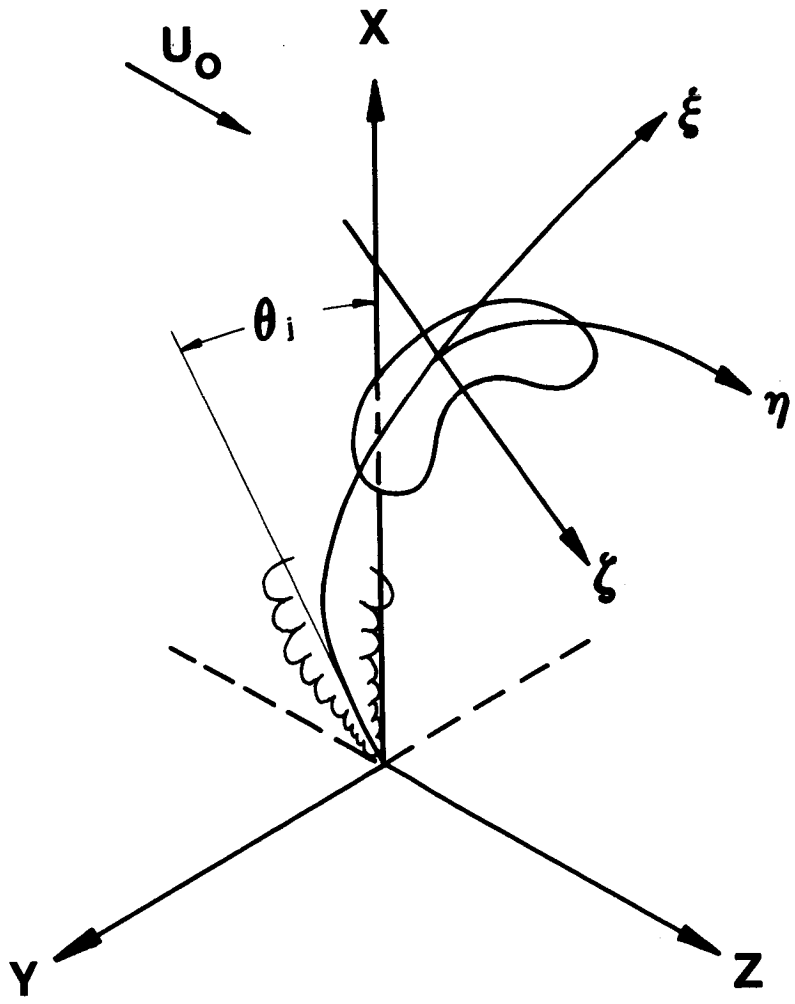

Figure 1.- Intrinsic co-ordinate system for the deflected jet.

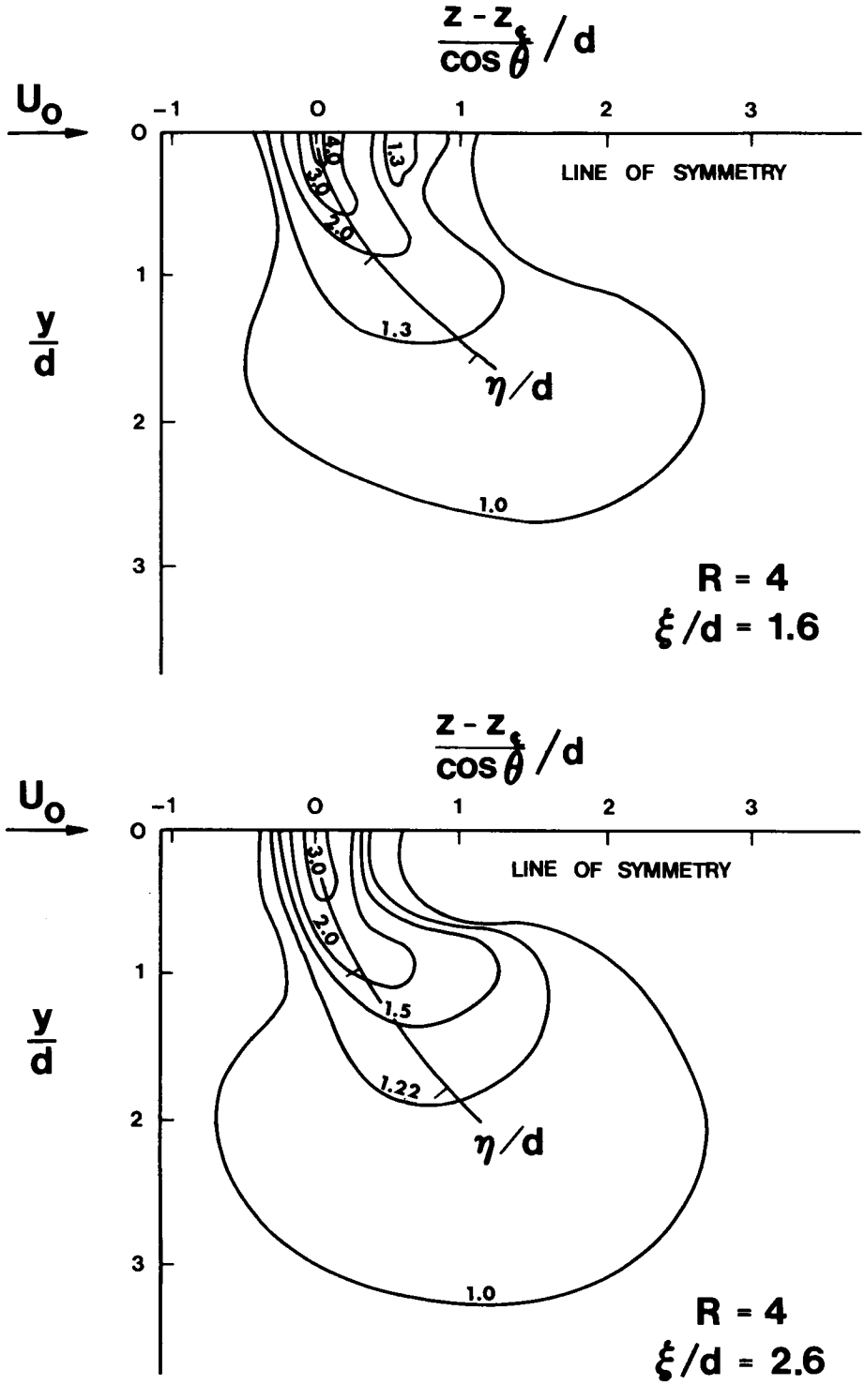

Figure 2.- Typical velocity contours.

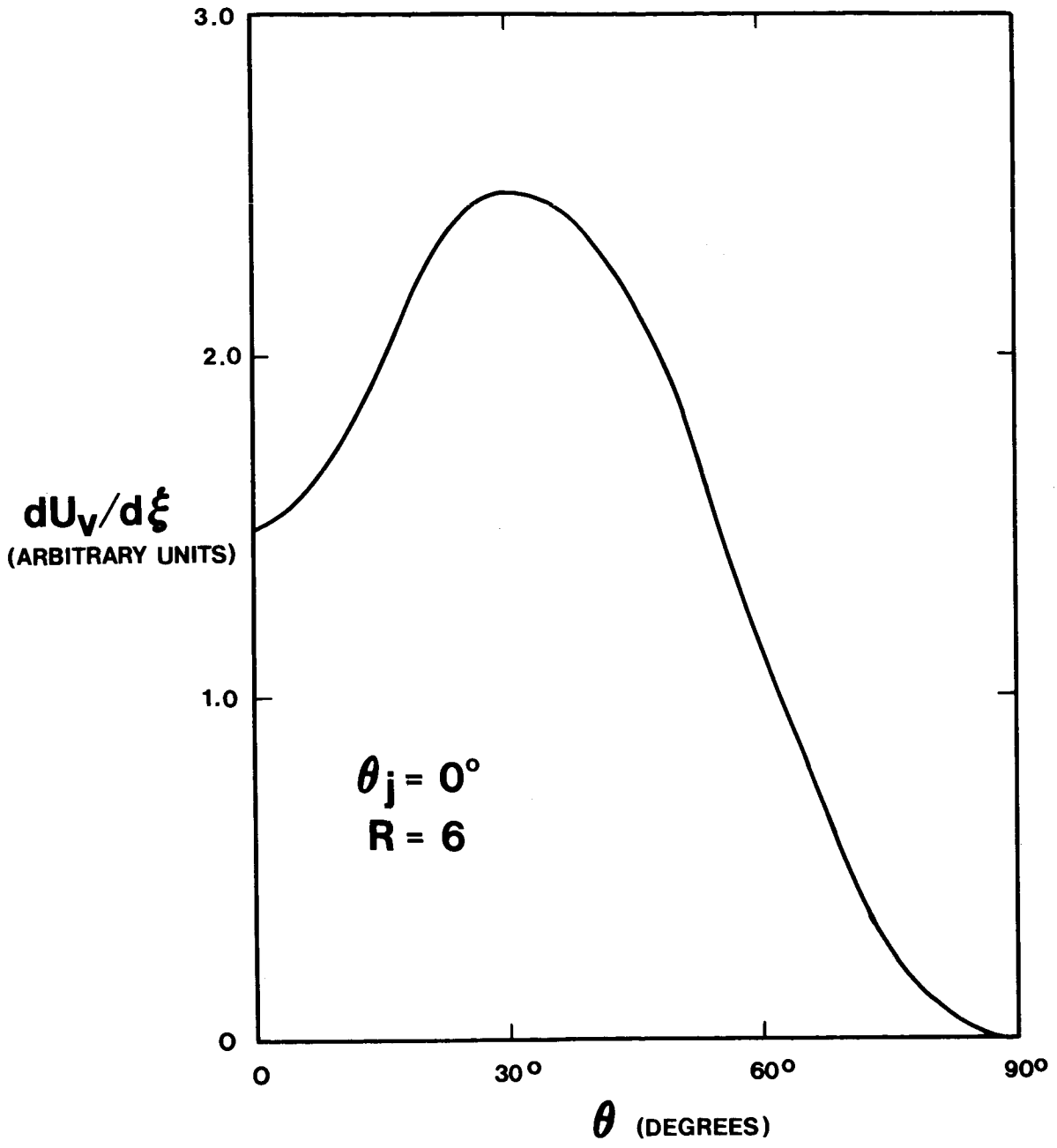

Figure 3.- Typical variation of vortex entrainment velocity.

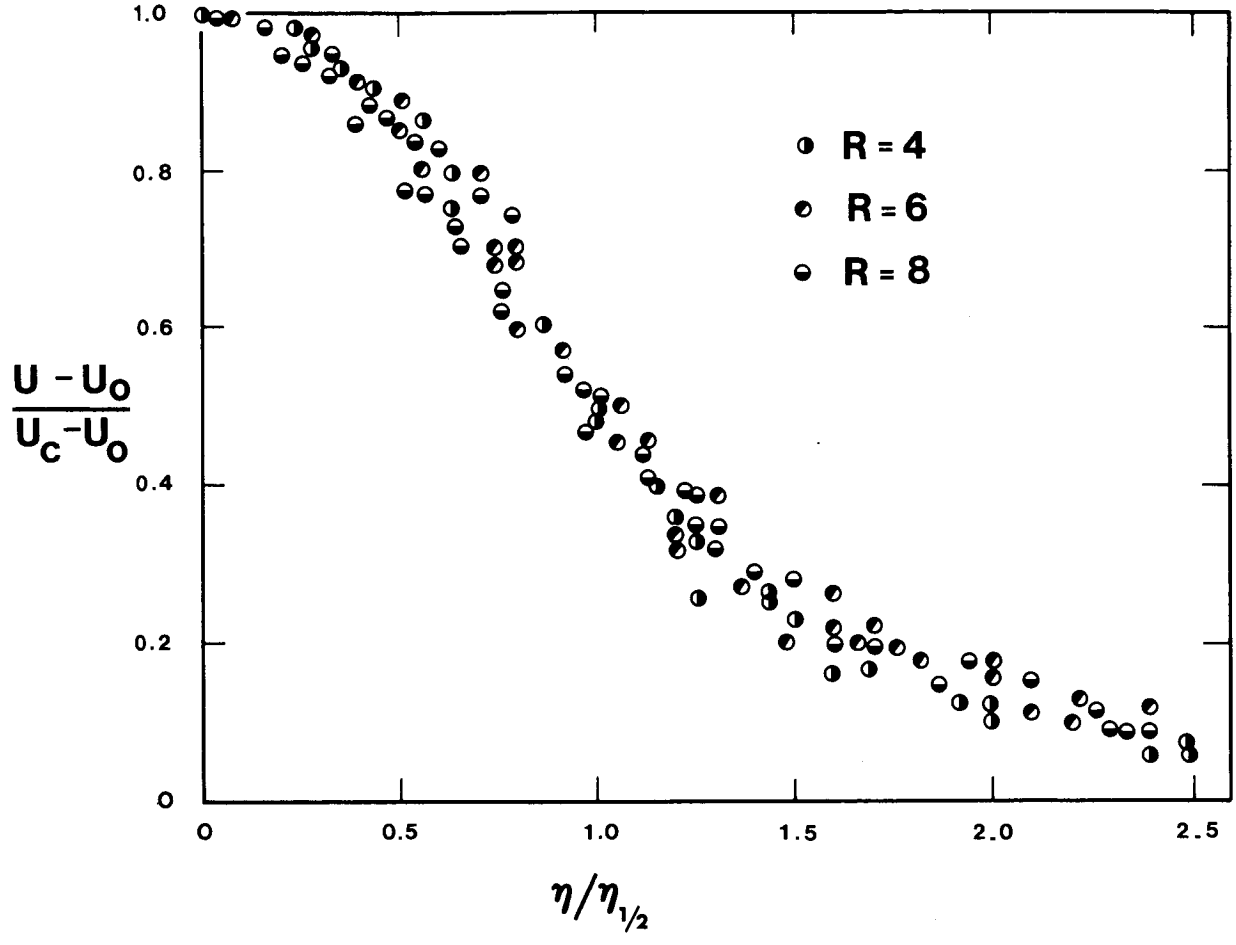

Figure 4.- Self-similarity of mean velocity.

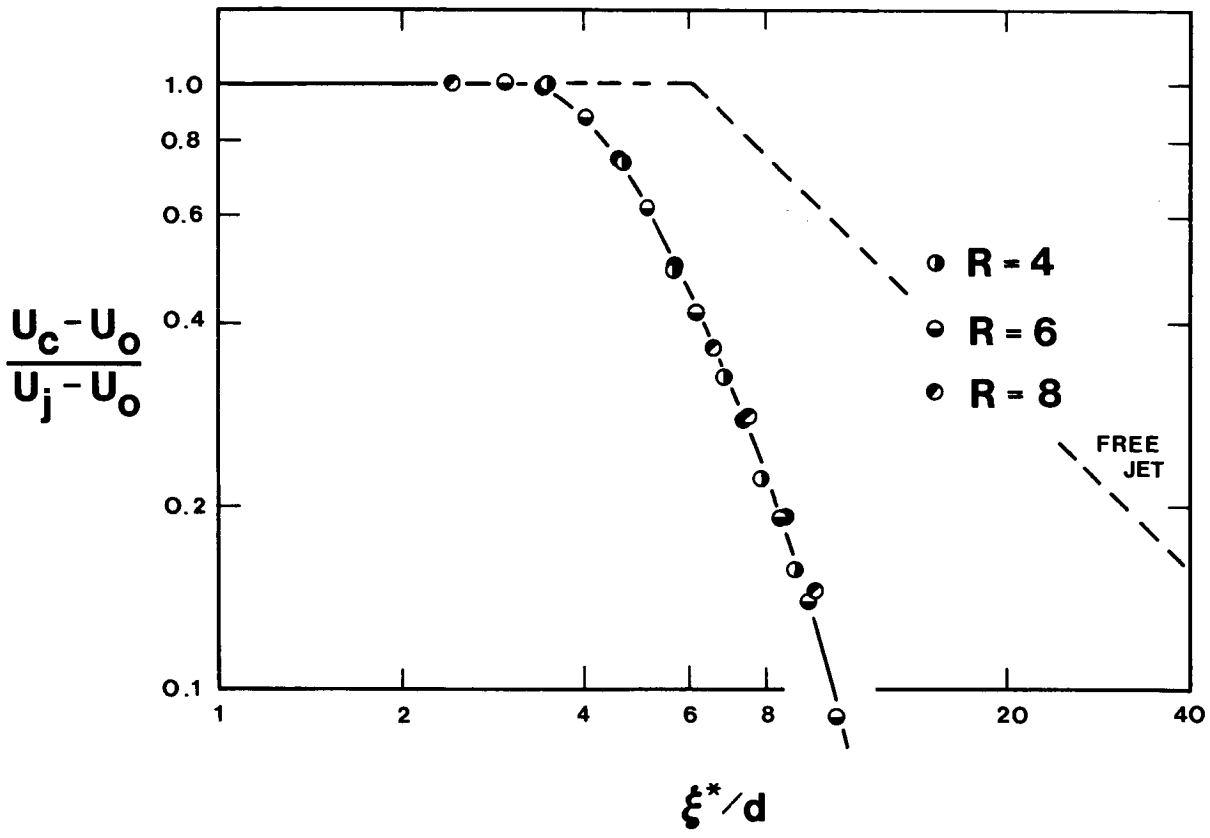

Figure 5.- Decay of mean velocity.

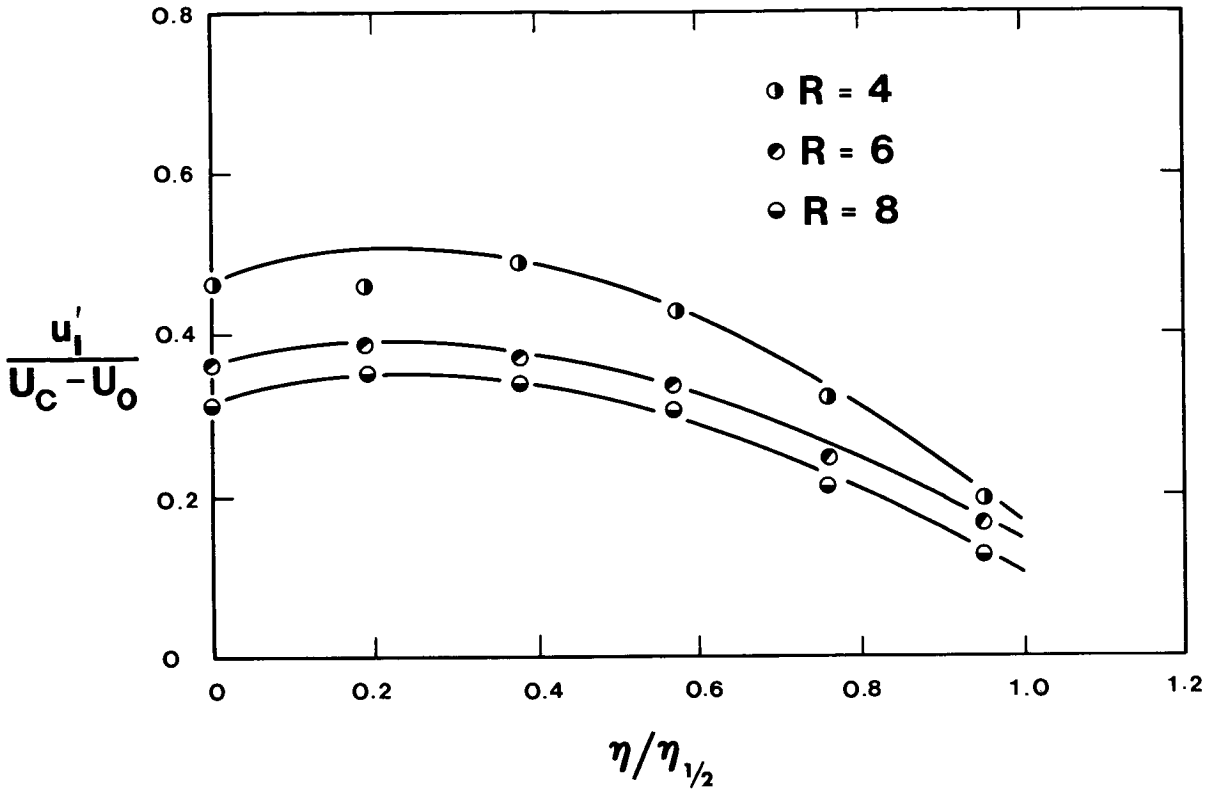

Figure 6.- Turbulent intensity.

THE AERODYNAMICS OF THE LIFTING JET IN A CROSS FLOWING STREAM

By J. E. Hackett and H. R. Miller

Lockheed-Georgia Aerospace Research Laboratory

For many methods of treating the problem of the lifting jet in a cross flowing stream theoretically, it is necessary to know, in advance, the mean path of the jet, which is usually determined experimentally. For the general design problem, and particularly where novel configurations are being investigated, this can prove awkward. The long-term aim of the work currently in progress at the Lockheed-Georgia Research Laboratory is therefore to predict the path of the lifting jet plume or plumes with sufficient details of the flow structure to allow pressures to be calculated on nearby surfaces.

Like many other investigators in this area, we started our theoretical approach by repeating H. C. Chang's (née Lu, ref. 1) calculation of the self-induced distortion of a two-dimensional circular cylinder immersed in a mainstream, with the aim of extending the work into a genuine three-dimensional approach, rather than using her time analogue for jet direction. Before launching into a three-dimensional perturbation study, however, we felt a need to understand more about the validity of any potential-flow type of approach and also more about the topology of this particular example of vortex roll-up.

In 1961 experiments were conducted on a wind-tunnel model of a lifting-fan nacelle which generated a 6.4-inch-diameter jet at 200 ft/sec. (See ref. 2.) In part of that study, smoke was introduced upstream of the intake to form a round jet emerging below the model. The familiar vortex roll-up could be seen using the light screen technique and a flow structure was deduced which has been confirmed more recently at a very much lower Reynolds number. The mean flow seen then strongly resembles the much smaller scale laminar flow shown in figure 1. There is therefore some expectation that viscous effects will be superposable.

Figure 2 picks out certain streamlines inside the jet and shows how jet fluid becomes part of the trailing vortex. It was pointed out to us by Dr. Kroeger of ARO Inc., that the jet (almost) splits into two parts down its fore and aft centerline to form one spiral of each trailing vortex. We also see in figure 2 that the trailing vortices contain adjacent spirals of jet and mainstream fluid. This is further illustrated in figures 3 and 4. Smoke spirals of jet fluid in figure 1 and of mainstream air in figure 4 illustrate that, even for these essentially laminar flows, mixing is quite efficient. The jet in figure 4 is emitted from a representative aircraft model; very similar effects were seen using small tubes as for figure 1.

It is fortunate that the experimentally-found variation of lift interference force with radius has a maximum value some distance from the cylinder surface. This gives some hope that a meaningful finite vortex representation can be accomplished without the need for an excessive number of vortex elements. Nevertheless, we have felt it desirable to study local effects near vortices.

In figure 5(a), we see a streamline path for a circle represented by 48 vortices. Small perturbations, not visible at the scale of the figure, are encountered as vortices are passed. If constant length steps are used for tracking, the process is quite stable. It is interesting to note that, on starting a streamline inside the circle, we find the fluid there is virtually at rest (just as Prandtl said it would be). There is slight drift, however, due to the fact that the number of vortices is finite, and this allows the streamline to penetrate the cylinder surface from inside and join the stable "pseudo boundary layer" on the outside.

Figure 5(b) illustrates how the pressure coefficient C_p varies along the streamline shown in figure 5(a). The waves in the potential flow curve are due to the waviness of the streamline as it passes individual vortices. In figure 6 more local errors in the pressure coefficient are examined. It seems that a band of about $1\frac{1}{2}$ pitches thick should be avoided.

We have also looked at local kinematic effects to answer the question "what happens to the joining line between vortices?" Figure 7 identifies the area we have studied in this regard, which is shown at enlarged scale in figure 8. Clearly the thickness of the convoluted layer will decrease as the mesh size decreases. One is also tempted to speculate that some sort of mixing process is being implied which may be capable of later reinterpretation in viscous terms. Even for a two-dimensional model, these convolutions become very complex; in three dimensions they will be almost unimaginable.

Much of the work just described was carried out more than a year ago. In the interim, we have studied vortex roll-up behind heavily loaded wings, using similar techniques (see ref. 3). Recently we have resumed work on jet plumes; a three-dimensional perturbation scheme is being programed in which elements with circulation components in the vortex ring direction are used in addition to the vertical ones of the two-dimensions-plus-time method. We anticipate considerable difficulties in monitoring and understanding the progress of transient three-dimensional geometries and have prepared for this by getting involved with computer graphics. We are indebted to Dave Smith of our Systems Sciences Laboratory, who has been instrumental in the development of our computer graphics capabilities. Figure 9 shows the familiar H. C. Chang type of calculation, using 48 points. In practice, motion is added and the viewpoint may be changed almost arbitarily. We believe this will be invaluable when interpreting three-dimensional perturbation studies.

REFERENCES

1. Lu, Hsih-Chia: On the Surface of Discontinuity Between Two Flows Perpendicular to Each Other. Eng. Rep. 4, Nat. Tsing Hua Univ., Oct. 1948.

2. Hackett, J. E.: Wind Tunnel Tests on a Streamlined Fan-Lift Nacelle. R. & M. No. 3470, Brit. A.R.C., 1967.

3. Hackett, J. E.; and Evans, M. R.: Vortex Wakes Behind High-Lift Wings. AIAA Paper No. 69-740, July 1969.

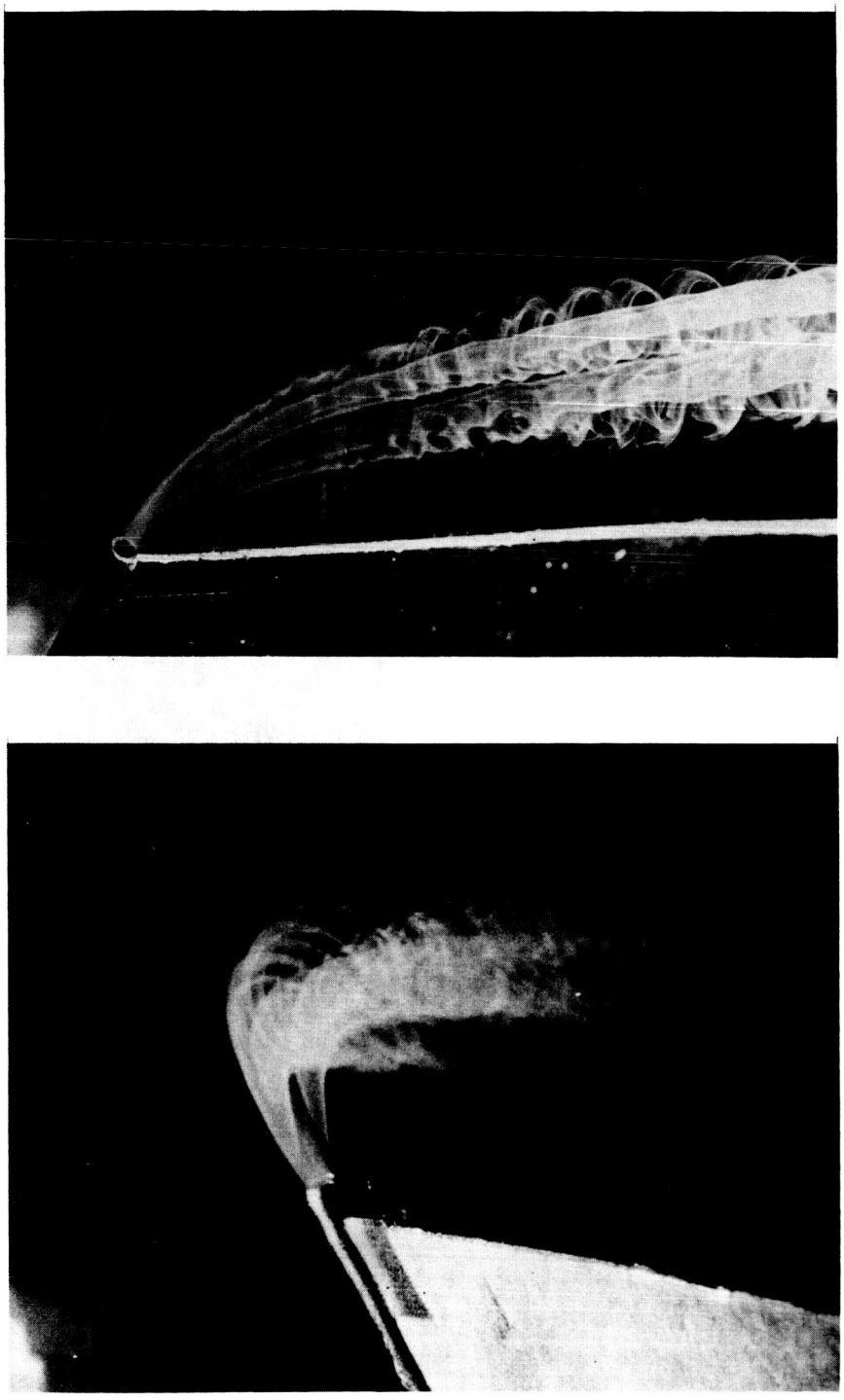

Figure 1.- A low Reynolds number smoke jet.

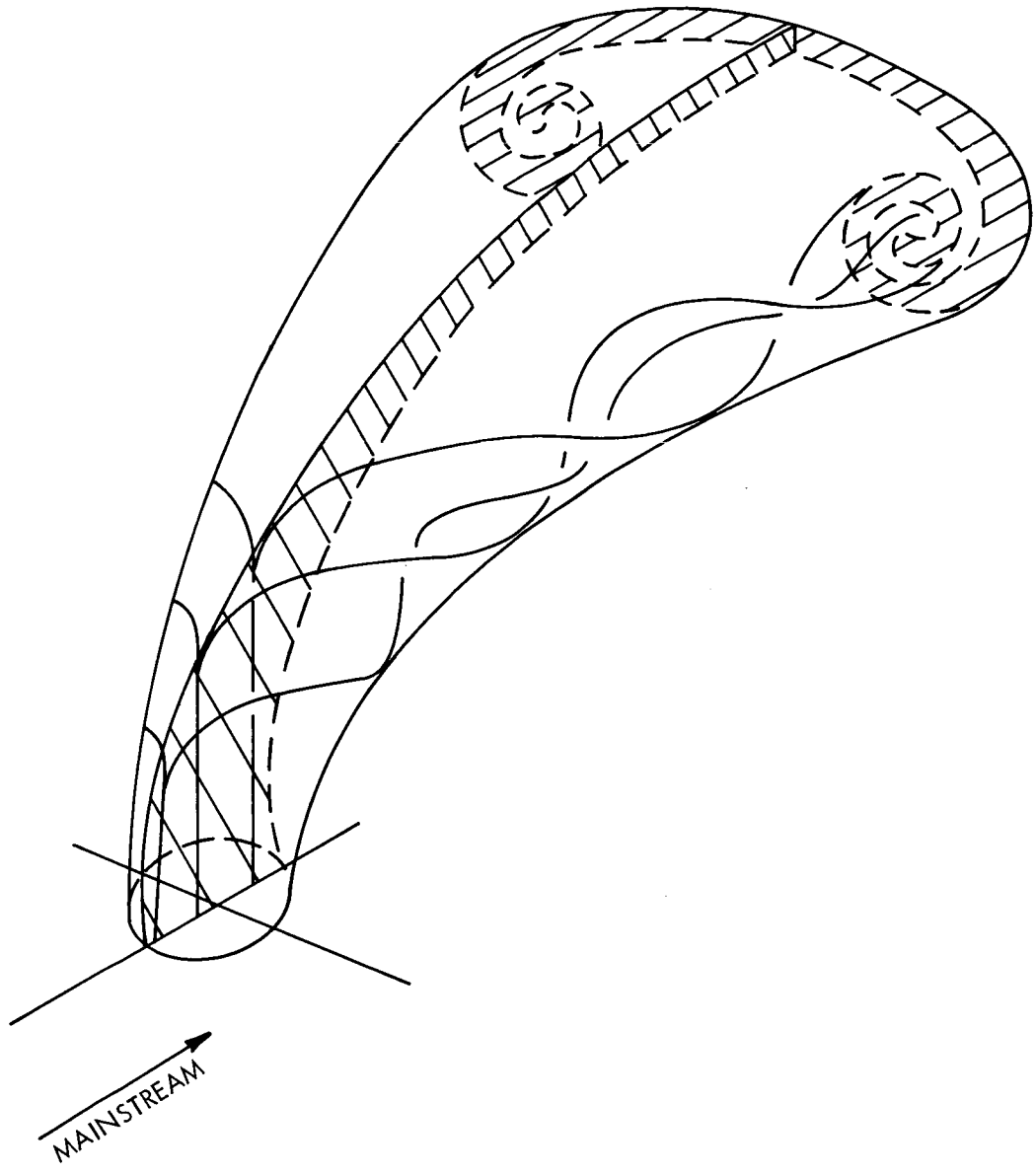

Figure 2.- Formation of trailing vortices showing distortion of jet fluid.

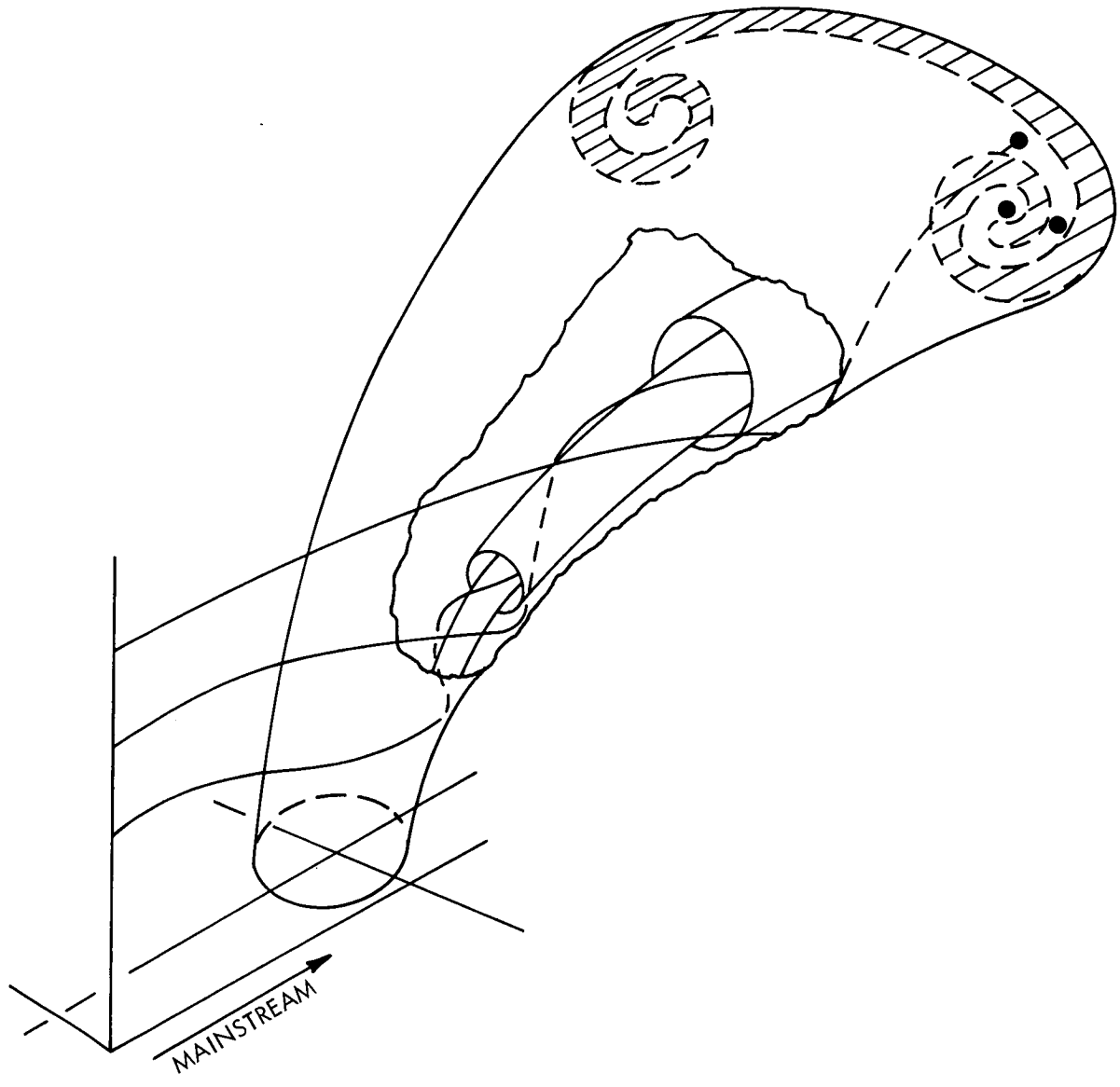

Figure 3.- Formation of trailing vortices showing entrainment of mainstream fluid into trailing vortices.

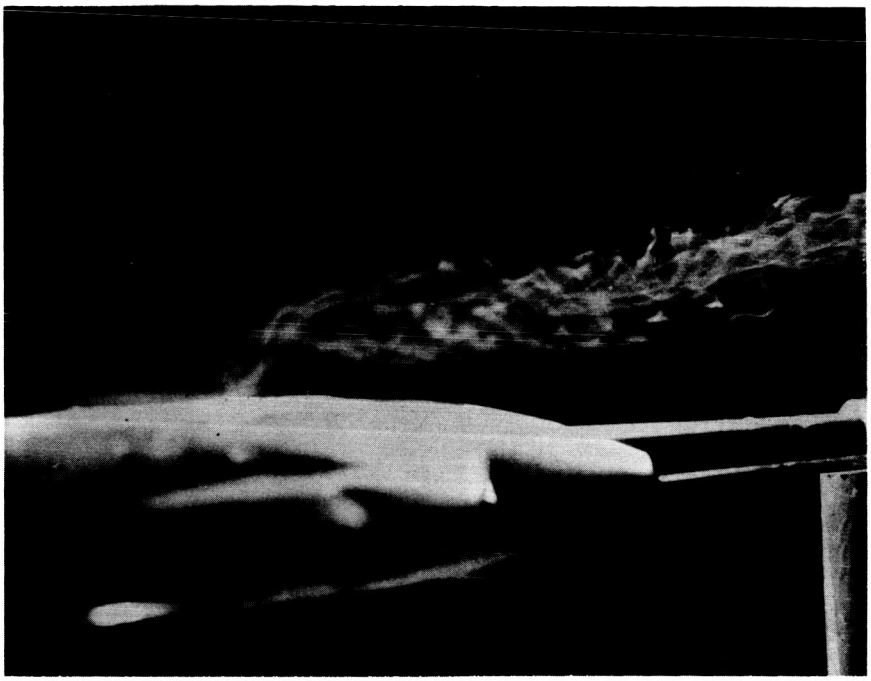

Figure 4.- Smoke visualization of entrainment of mainstream fluid into trailing vortices.

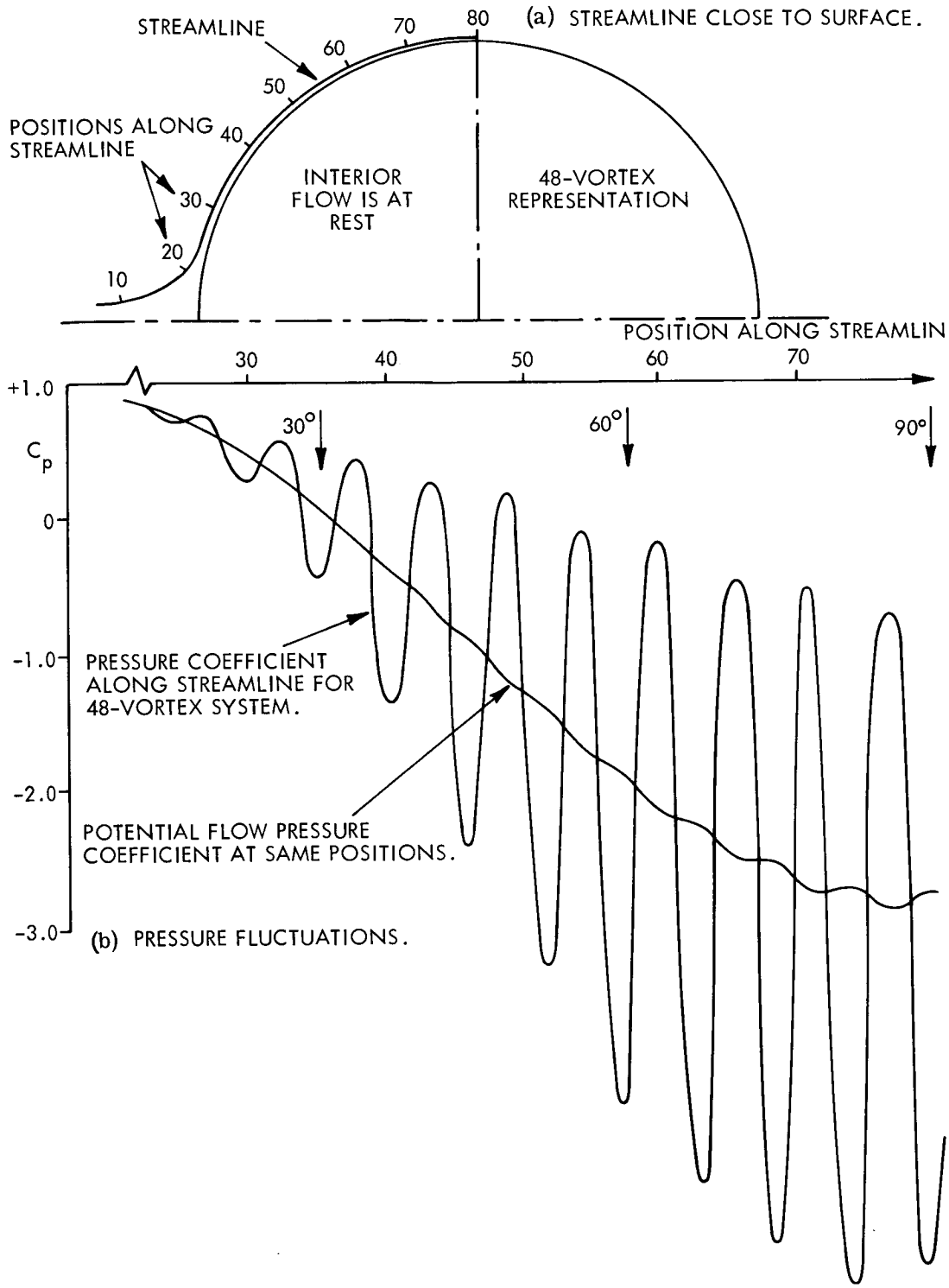

Figure 5.- Streamlines and pressure fluctuations near a cylinder represented by point vortices.

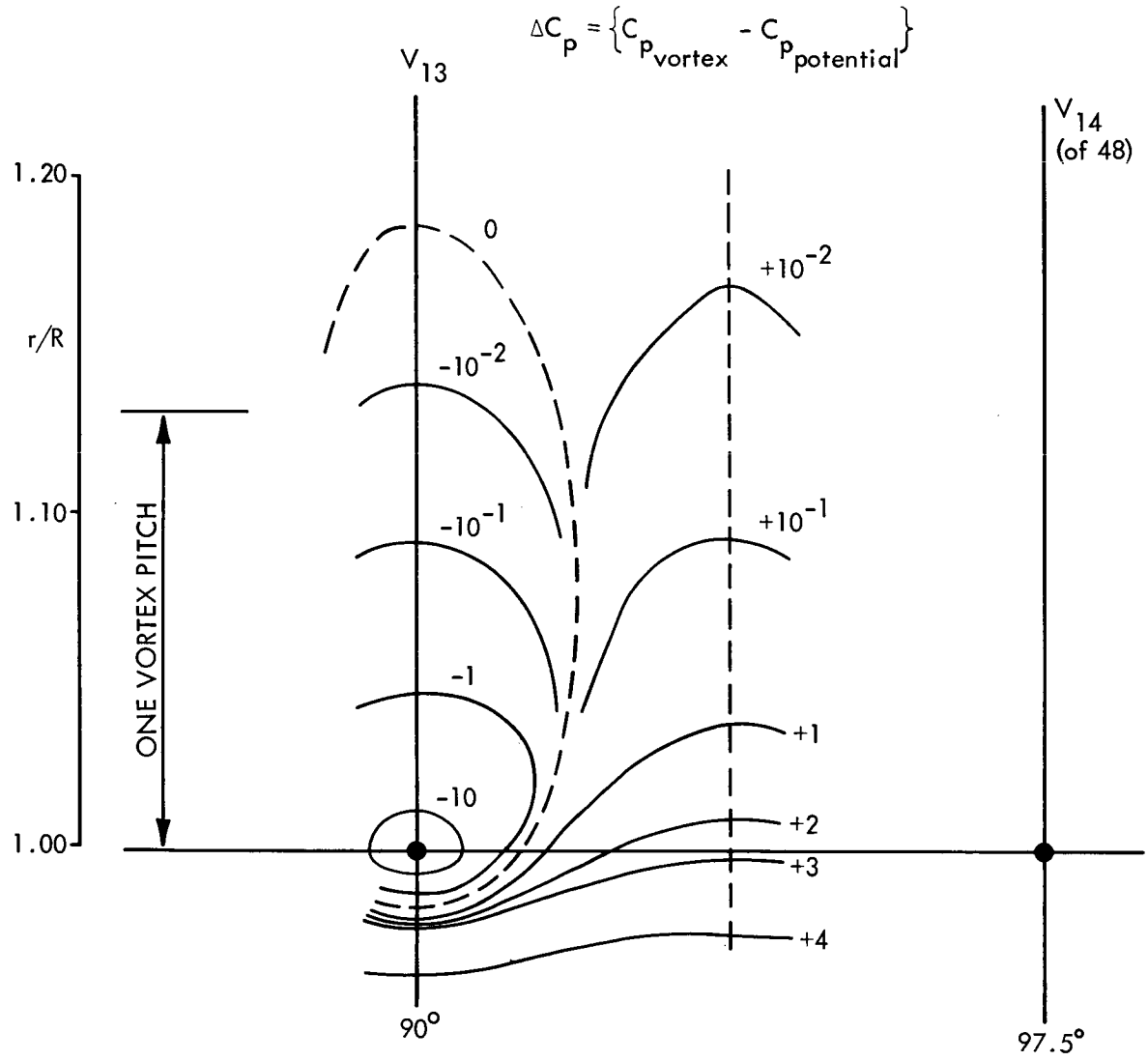

Figure 6.- Pressure errors near to point vortices used to represent a cylinder.

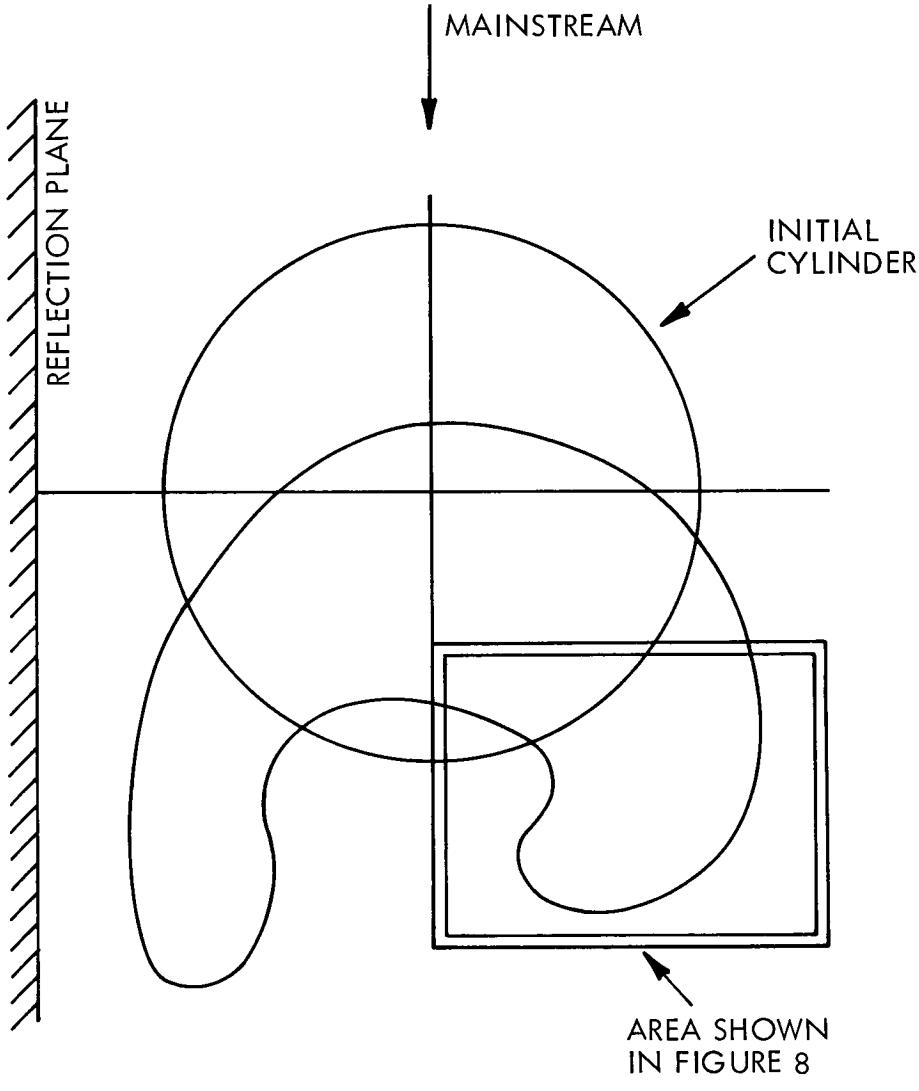

Figure 7.- Distortion of twin cylinders.

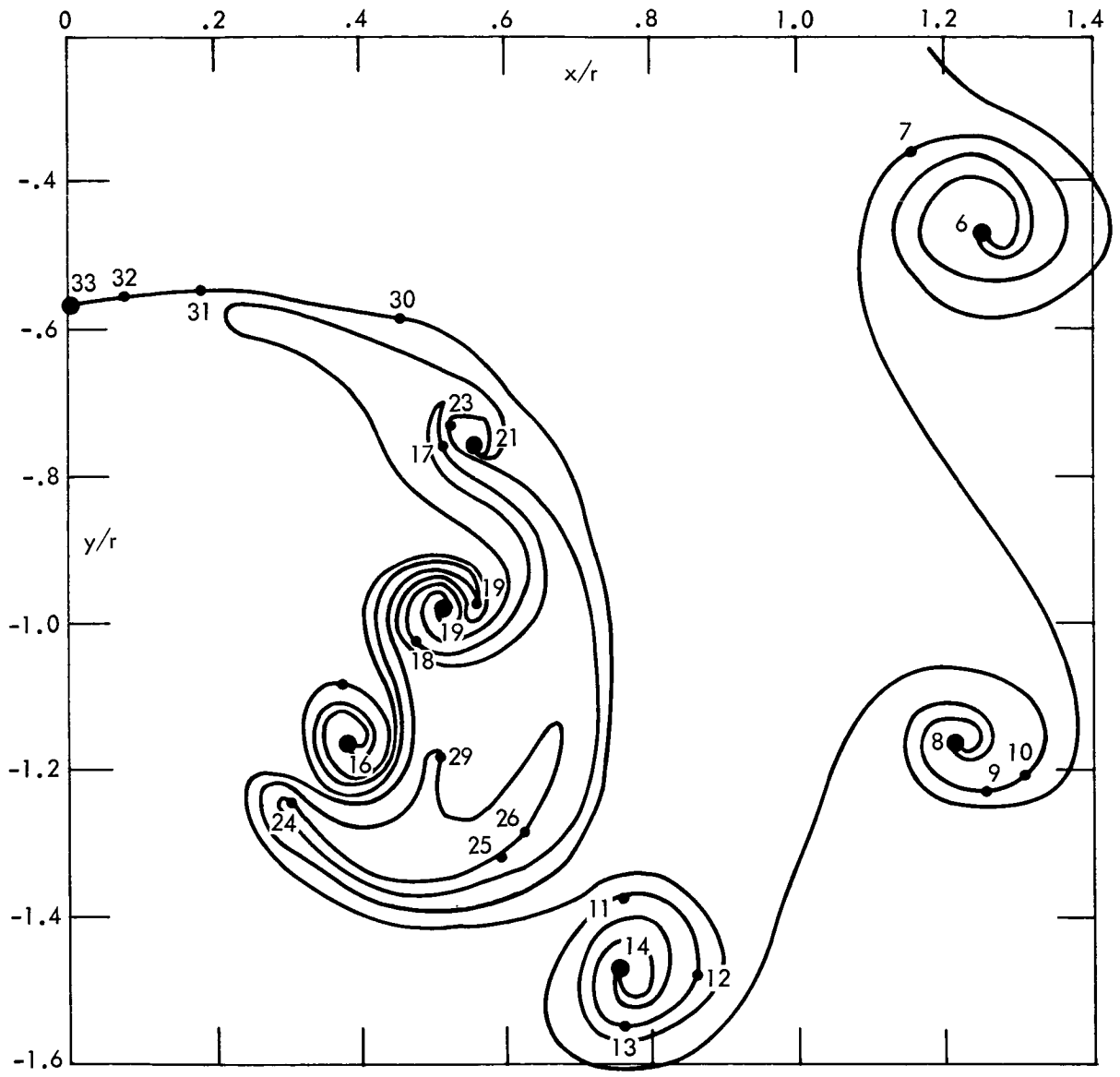

Figure 8.- Convolutions.

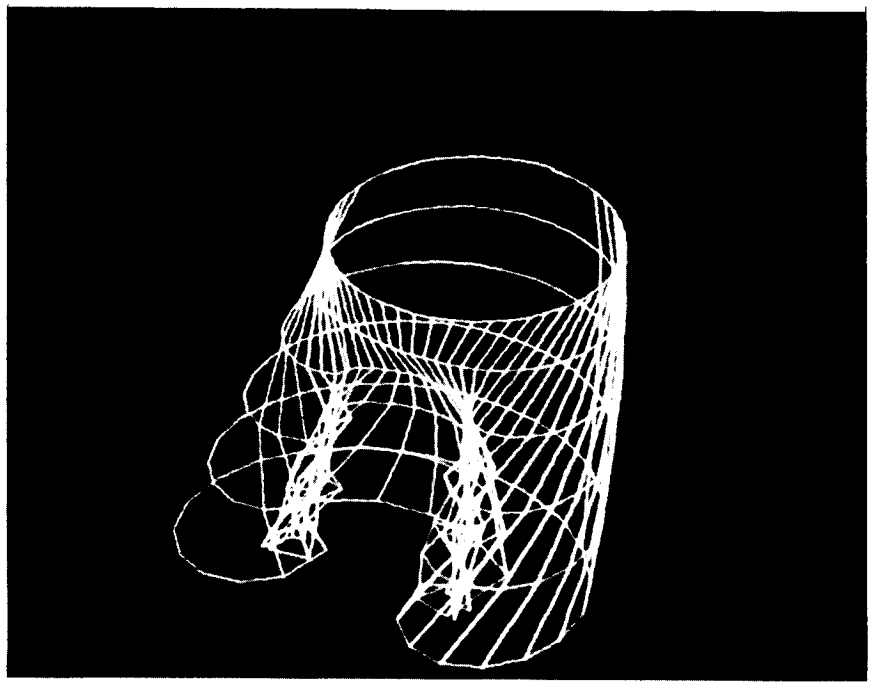

Figure 9.- Computer-graphic display of the results of an H. C. Chang type of calculation.

EXPERIMENTAL INVESTIGATION OF PRESSURES INDUCED ON A FLAT PLATE BY A JET ISSUING INTO A SUBSONIC CROSSWIND*

By Howard M. McMahon and David K. Mosher

Georgia Institute of Technology

SUMMARY

Measurements of static pressure distributions on a flat plate are presented for circular and non-circular jets issuing normal to the plate surface at various jet exit velocities. Certain trends concerning the pressure distribution patterns were noted. It was observed that the pattern for a given exit shape and jet velocity is similar to that for a smaller length-to-width ratio exit shape at a higher jet velocity. A check was made to see if this could be related to the jet plume path. The results indicate that the pressure distribution on the plate depends upon the character of the jet as well as upon the path of the jet plume relative to the plate.

4

INTRODUCTION

Increasing interest in V/STOL aircraft during recent years has been reflected in the reporting of a number of experiments concerned with the interaction of a turbulent jet and a subsonic deflecting stream. The interaction of the exhaust from a lift-fan or a lift-jet with the air flowing over an aircraft in forward motion can cause large lift losses and moment changes during the critical transition phase from vertical to conventional horizontal flight.

Experimental results can be grouped into four categories:

1) Gross lift and moment measurements on aircraft configurations with various jet exit geometries and locations. (See, for example, refs. 1 and 2.)
2) Penetration of the jet into the deflecting stream. (See, for example, refs. 3 and 4.)
3) Measurements of the flow field in and around the jet plume. (See, for example, refs. 5 and 6.)
4) Pressure distribution measurements on the surface from which the jet is issuing. (See, for example, refs. 7 and 8.)

---

* This work is supported by the U. S. Army Research Office-Durham- under contract No. DAHC04 68 C0004.

An experimental program is underway at Georgia Tech covering areas 2, 3 and 4. Some results have been reported in reference 9. Further surface-pressure distribution results are presented here.

The interaction between the jet and the deflecting stream is characterized by a combination of phenomena - the jet displaces the deflecting stream ("blockage"), captures some of the deflecting-stream fluid ("entrainment"), and causes a low-energy region to form downstream of the jet plume ("wake"). Three different jet exit configurations were used in the present study with the aim of achieving large changes in these interaction phenomena, thus leading to a better insight into the interference problem. Previously reported data on other than circular jets have been confined to penetration or gross lift and moment results. The only exception known to the authors is reference 10, where pressure distributions on the underside of a wing containing a rectangular jet orifice were reported. However, true flat plate conditions were not present in this test and no measurements were made away from the surface. Thus, a comprehensive study of different exit configurations was felt to be in order.

SYMBOLS

a	radius of the circular jet orifice
$\dot{m}$	ratio of jet exit momentum flux to free-stream momentum flux, $\sqrt{\frac{\rho_j V_j^2}{\rho_\infty V_\infty^2}}$
V_j	jet exit velocity
V_∞	free-stream velocity
x	coordinate in the free-stream direction
z	coordinate normal to the plate
ρ_j	jet exit density
ρ_∞	free-stream density

EQUIPMENT AND PROCEDURES

Experiments were conducted in the Georgia Tech 9-foot subsonic wind tunnel. Figure 1 is a view of the test section looking upstream and shows the plate mounted 12 inches above the bottom of the tunnel on thin support struts. The nozzle supply pipe and all of the pressure leads were enclosed in a streamlined fairing located under the center of the plate.

Figure 2 shows the details of the plate construction. The plate is 3/8-inch-thick aluminum, 48 inches in chord and 66 inches in span, with a rounded leading edge. A disc, 32 inches outside diameter and 7 inches inside

diameter, contains twelve 0.040-inch-diameter pressure taps along a radius. This disc can be rotated remotely to obtain a complete picture of the pressure distribution. Inside the disc and bolted to the top of the nozzle supply pipe is a replaceable nozzle block. Two nozzle geometries having the same exit area were used. The nozzle block containing the 2-inch-diameter circular nozzle is shown installed in the plate. The exit geometry of the second nozzle (exhibited on the plate surface in figure 2) was a slot 1.0 inches by 2.36 inches, rounded by a semi-circle of 0.5 inch radius at either end. As shown in figure 3, when the longer dimension of this jet exit was aligned perpendicular to the free-stream flow direction the exit configuration is termed "blunt". When the nozzle block was rotated ninety degrees such that the longer dimension was parallel to the free-stream direction the configuration is termed "streamwise". Surface pressures near the jet exit were measured by pressure taps in the top of the nozzle block. The components making up the plate surface were assembled and aligned within ± 0.010 inches. The velocity profile of the boundary layer on the plate was measured on the centerline 15 inches from the leading edge with the jet off and was found to follow the 1/7 (turbulent) power law, with a boundary layer thickness of about 1 inch.

Air for the jet was supplied by a 100 H.P. centrifugal compressor through a 6-inch line. The jet exit velocity was set using the total pressure as measured in the supply pipe just before the jet nozzle contraction, assuming the static pressure at the jet exit to be free-stream static and the nozzle discharge coefficient to be 100%. The uniformity of the jet exit flow was checked by making total and static pressure surveys in the jet exit plane with the tunnel off. Results showed a velocity variation of less than 2% over the exit cross sections. Further details of the test equipment are given in reference 9.

Oil-film flow visualization was done by covering the plate with white contact paper and applying a mixture of lamp-black, oleic acid, and diesel oil. When a pattern of the oil film became established, the jet and tunnel flows were stopped and the result photographed. The main features of the oil pattern were found to be repeatable but the intensity of some of the features was found to depend on oil mixture and the time allowed for development of the pattern.

All pressures were measured with a variable-capacitance electric manometer calibrated against an alcohol micro-manometer. In general, the plate pressure measurements were accurate to within ± 1% of the free-stream dynamic pressure and were repeatable within ± 1%. In regions very near the jet and also in the near wake behind the jet the pressure readings were fluctuating. The time-averaged readings were recorded and were repeatable to within ± 5% of the free-stream dynamic pressure.

Previous investigators (ref. 7) have shown that for a circular jet the primary parameter in the interference problem is the ratio of jet exit momentum flux to the undisturbed free-stream momentum flux, $\sqrt{\frac{\rho_j V_j^2}{\rho_\infty V_\infty^2}} = \dot{m}$. In order to establish the Reynolds number dependence for the blunt jet, plate pressures

for this jet were compared at V_∞ = 25 and 50 feet per second while holding $\dot{m}$ = 8. The differences were not significant. All data reported here are for a free-stream velocity of 50 feet per second.

RESULTS AND DISCUSSION

Two sets of oil-film photographs were taken, one for the jet in the crosswind and the other for a long solid body of the same shape as the jet exit placed normal to the plate and replacing the jet. The two sets of photographs are compared to one another in figures 4, 5, and 6. The free-stream velocity in all cases is directed from the top to the bottom of the photographs. The oil pattern associated with the jet indicates strong entrainment of deflecting-stream air into the jet and also into the wake region behind the jet. Similar results were observed at $\dot{m}$ = 4 and $\dot{m}$ = 12, with the wake becoming broader in all cases as $\dot{m}$ was increased. The oil flow pattern is, of course, not necessarily indicative of the flow field off the plate because of the presence of the plate boundary layer.

Figures 7 and 8 show static pressure distributions on the plate surface at $\dot{m}$ = 8 plotted in coefficient form. The static pressure coefficients were obtained by measuring the difference in static pressure at a point on the plate with and without jet flow and dividing the difference by the free-stream dynamic pressure. The static pressure coefficient with the jet off was very uniform over the entire plate, the measured values deviating from the average value of 0.01 by less than 0.003. Only the pressure distribution over half the plate is presented in the figures and is plotted so as to contrast the results from the streamwise and blunt configurations with those obtained for the more familiar circular jet. The pressure distribution for several cases was checked across the span of the plate and the symmetry of the flow with respect to the centerline was found to be excellent.

Figures 7 and 8 show that there is a rearward shift of the low-pressure region as the jet exit becomes more blunt. Similar trends were noted at $\dot{m}$ = 4 and $\dot{m}$ = 12 and the corresponding pressure distributions are shown in reference 9. Additional measurements of plate static pressure have also been made at $\dot{m}$ = 10 for all three jet configurations and at $\dot{m}$ = 20 for the blunt jet configuration.

When all of the pressure distribution data were assembled in an array of contour plots with rows of the array representing increasing $\dot{m}$ and columns representing increasing jet bluntness, a roughly "diagonal" trend was noted in the shape of the pressure contour patterns. That is, the shape of the pressure contours for the streamwise jet at $\dot{m}$ = 8 is similar to that for the circular jet at $\dot{m}$ = 12 and also similar to that for the blunt jet at $\dot{m}$ = 20. A comparison is made in figure 9 to illustrate this trend. It should be noted that the observed "diagonal" trend represents a correspondence more in pressure contour pattern than in pressure magnitude.

Some investigators have suggested that the primary factor determining the magnitude and distribution of the surface pressures resulting from the interference of a jet with a deflecting stream is the rolling up of the wake into a vortex pair downstream of the jet exit. This in turn suggests that the position of the vorticity is important in evaluating the interference effect, that is, the proximity of the jet plume path to the plate surface may be a major factor in the interference as displayed by the surface pressures. One possible explanation, then, of the "diagonal" trend noted above is that the similar pressure contour patterns for the various jets are a result of similar jet plume paths, since it is known (ref. 4) that jets of different initial shapes penetrate different distances into the deflecting stream. Measurements were made of jet plume centerline paths, here defined as the locus of points of maximum total pressure as measured in the jet plume in the vertical plane of symmetry. The results are shown in figure 10. It is seen that there is no correlation between the similar pressure patterns in figure 9 and the corresponding jet plume paths. To verify this, the jet plume path prediction of reference 11 was used to select a value of $\dot{m}$ for the circular jet which would give approximately the same plume path as that for the blunt jet at $\dot{m} = 8$. The required value was $\dot{m} = 6.8$. The two plume paths are shown in figure 10 and the plate pressure distributions are compared in figure 11. The result confirms that the proximity of the jet plume is not in itself a measure of the interference pressure distribution on the plate surface. Thus, the combination of blockage, entrainment, and wake effects which, in some proportion, specifies the character of a given jet plays a major role in the interference problem in addition to the role played by the path of the jet plume relative to the surface. The character of the jet cannot be well defined nor understood from surface measurements alone. Considerable experimental data giving the flow field details off the plate are required before a better understanding will be achieved.

CONCLUDING REMARKS

Oil flow traces and pressure distributions on the plate surface indicate large changes in the interference between the jet and the deflecting stream when the jet exit configuration is varied. These changes are indicative of a complex interplay between blockage, entrainment, and wake phenomena which is not as yet well understood. Detailed measurements of the flow field off the surface are needed to aid in the understanding. A certain similarity between plate pressure contours for the different jets was noted which cannot be attributed solely to the proximity of the jet plume to the plate surface but which must also depend upon the character of the jet. It would appear that a mathematical model must incorporate the features of blockage, entrainment, and wake if it is to describe successfully the jet interference problem for various jet exit configurations.

REFERENCES

1. Vogler, R. D.: Interference Effects of Single and Multiple Round or Slotted Jets on a VTOL Model In Transition. TN D-2380, Aug. 1964, NASA.

2. Margason, R. J., and Gentry, G. L.: Aerodynamic Characteristics of a Five-Jet VTOL Configuration in the Transition Speed Range. TN D-4812, Oct. 1968, NASA.

3. Margason, R. J.: The Path of a Jet Directed at Large Angles to a Subsonic Free Stream. TN D-4919, Nov. 1968, NASA.

4. Ruggeri, R., Callaghan, E., and Bowden, D.: Penetration of Air Jets Issuing from Circular, Square, and Elliptical Orifices Directed Perpendicularly to an Air Stream. TN 2019, Feb. 1950, NACA.

5. Keffer, J. F., and Baines, W. D.: The Round Turbulent Jet in a Cross Wind. Journal of Fluid Mechanics, Vol. 15, Part 4, April 1963, pp. 481-497.

6. Jordinson, R.: Flow in a Jet Directed Normal to the Wind. R & M 3074, October 1956, British Aero. Res. Council.

7. Bradbury, L. J. S., and Wood, M. N.: The Static Pressure Distribution Around a Circular Jet Exhausting Normally from a Plane Wall into an Airstream. C.P. No. 822, 1965, British Aero. Res. Council.

8. Gelb, G. H., and Martin, W. A.: An Experimental Investigation of the Flow Field about a Subsonic Jet Exhausting into a Quiescent and a Low Velocity Air Stream. Canadian Aeronautics and Space Journal, Vol. 12, No. 8, October 1966, pp. 333-342.

9. Wu, J. C., McMahon, H. M., Mosher, D. K., and Wright, M. A.: Experimental and Analytical Investigations of Jets Exhausting into a Deflecting Stream. AIAA Paper No. 69-223, February 1969.

10. Peake, D. J.: The Pressures on a Surface Surrounding a Jet Issuing Normal to a Mainstream. Report LR-410 (NRC-8275), Nov. 1964, National Research Council of Canada, Ottawa, Can. (Available from DDC as AD 463295.)

11. Williams, J., and Wood, M. N.: Aerodynamic Interference Effects with Jet-Lift V/STOL Aircraft under Static and Forward-Speed Conditions. Zeitschrift für Flugwissenshaften, Vol. 15, No. 7, July 1967, pp. 237-256.

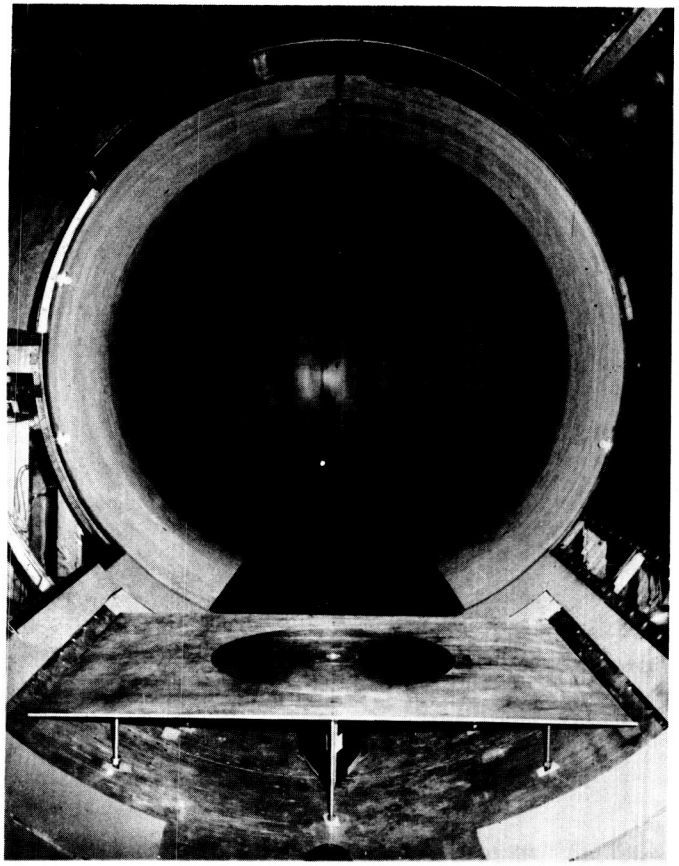

Figure 1.- Plate installed in test section.

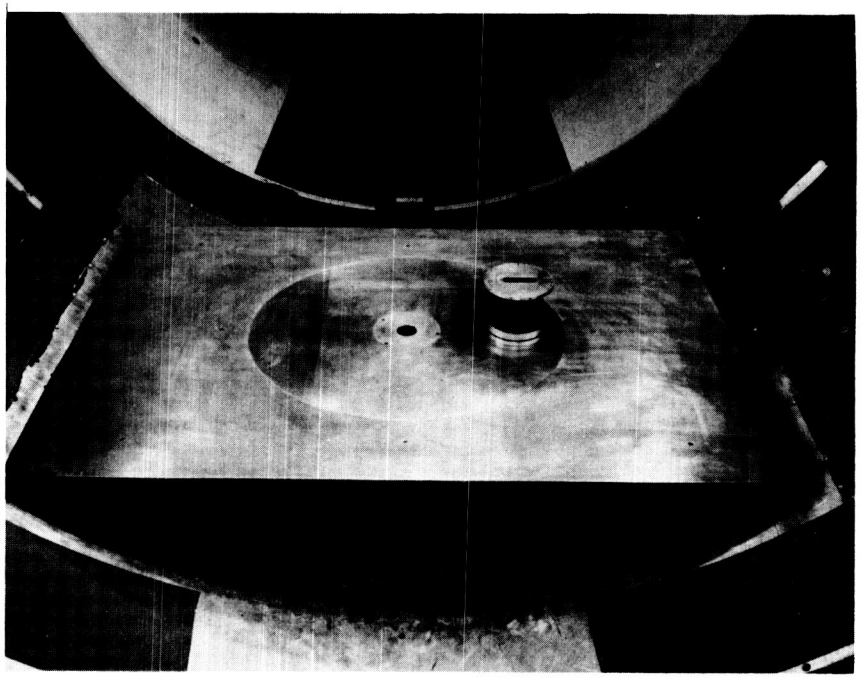

Figure 2.- Plate and nozzle block details.

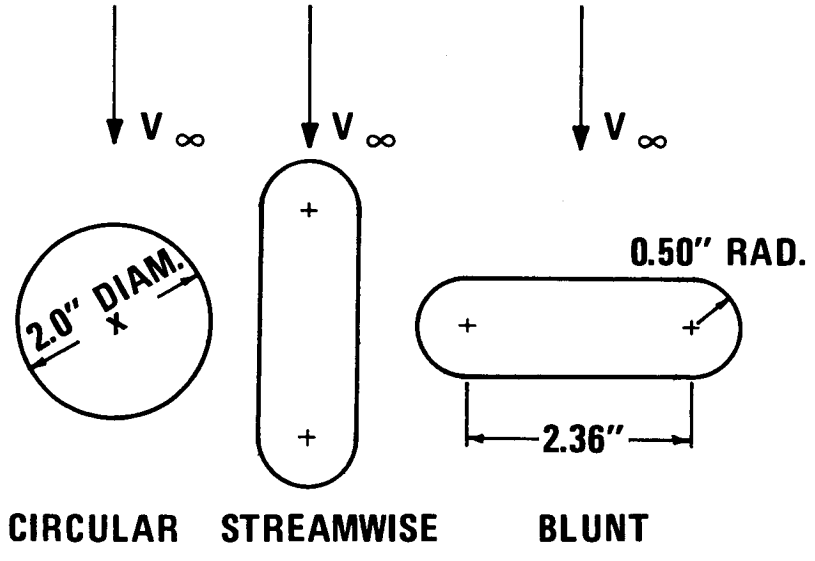

Figure 3.- Jet exit configurations.

(a) Solid blockage.

(b) $\sqrt{\frac{\rho_j V_j^2}{\rho_\infty V_\infty^2}} = 8.$

Figure 4.- Flow patterns on the plate, circular nozzle.

(a) Solid blockage.

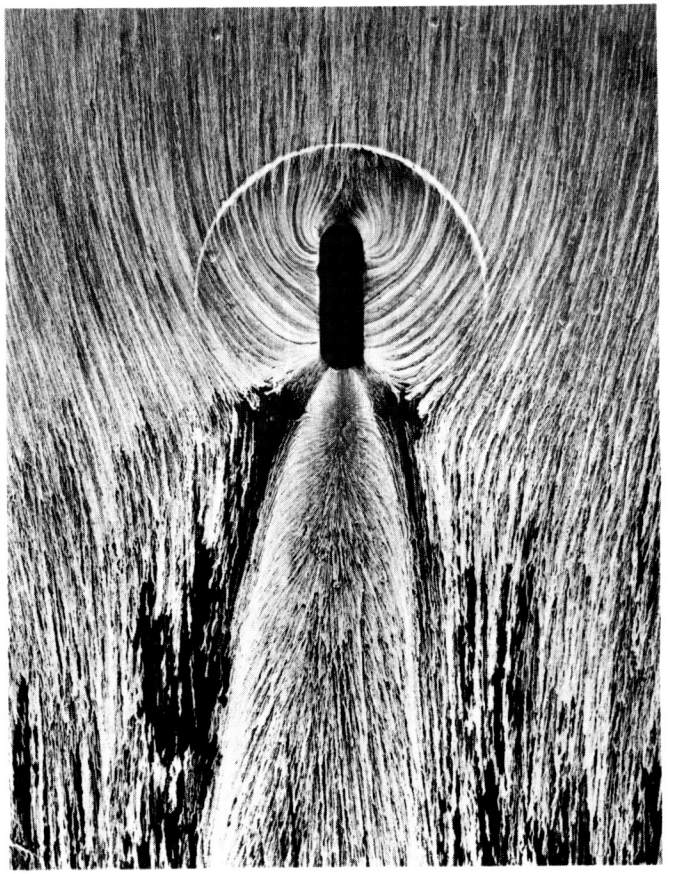

(b) $\sqrt{\frac{\rho_j V_j^2}{\rho_\infty V_\infty^2}} = 8.$

Figure 5.- Flow patterns on the plate, streamwise nozzle.

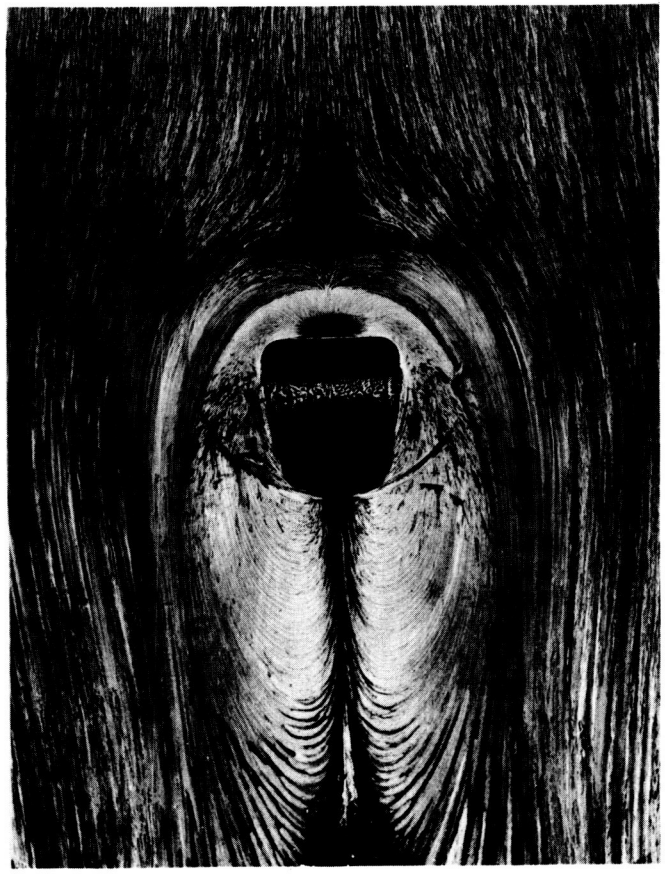

(a) Solid blockage.

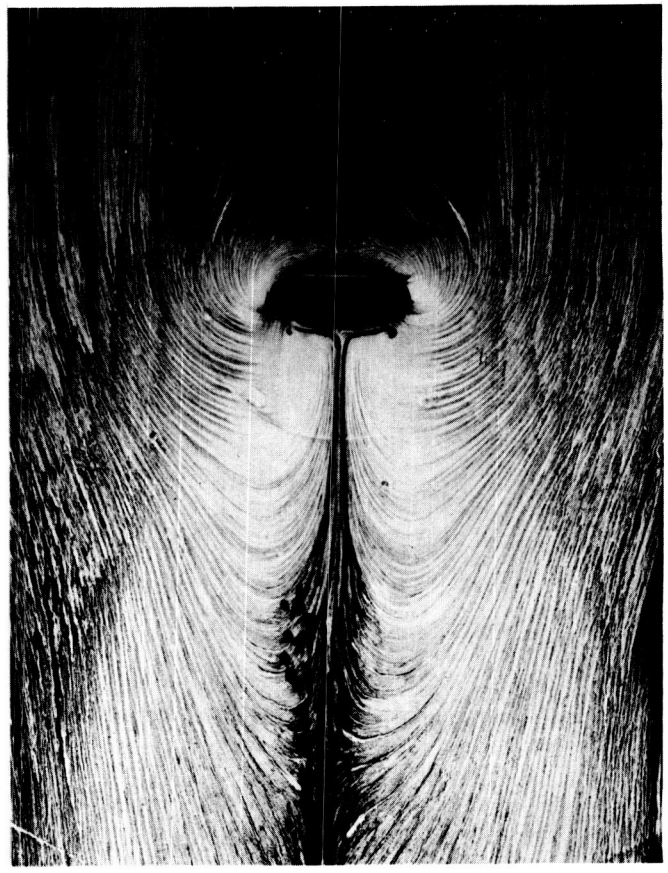

(b) $\sqrt{\frac{\rho_j V_j^2}{\rho_\infty V_\infty^2}} = 8.$

Figure 6.- Flow patterns on the plate, blunt nozzle.

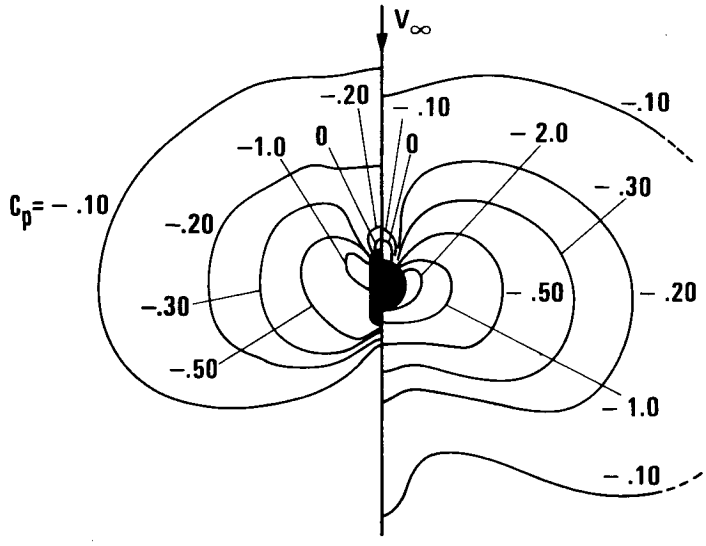

Figure 7.- Plate pressure coefficients C_p around a streamwise and circular jet at $\sqrt{\frac{\rho_j V_j^2}{\rho_\infty V_\infty^2}} = 8.$

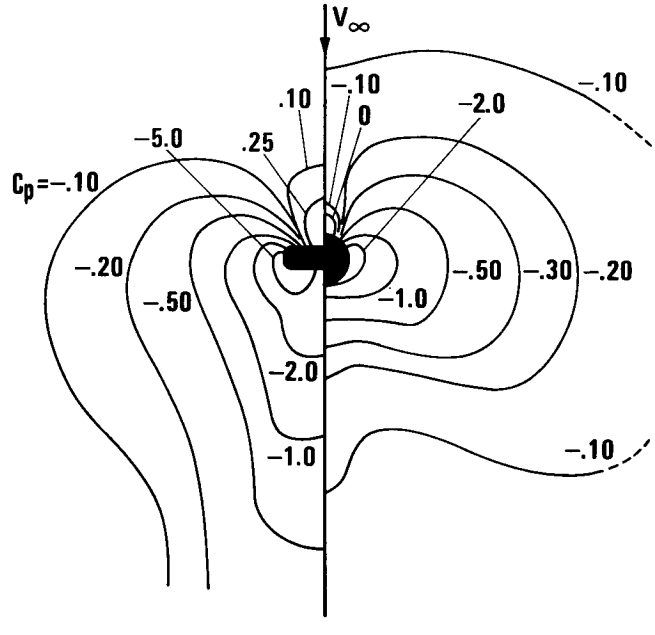

Figure 8.- Plate pressure coefficients C_p around a blunt and circular jet at $\sqrt{\frac{\rho_j V_j^2}{\rho_\infty V_\infty^2}} = 8.$

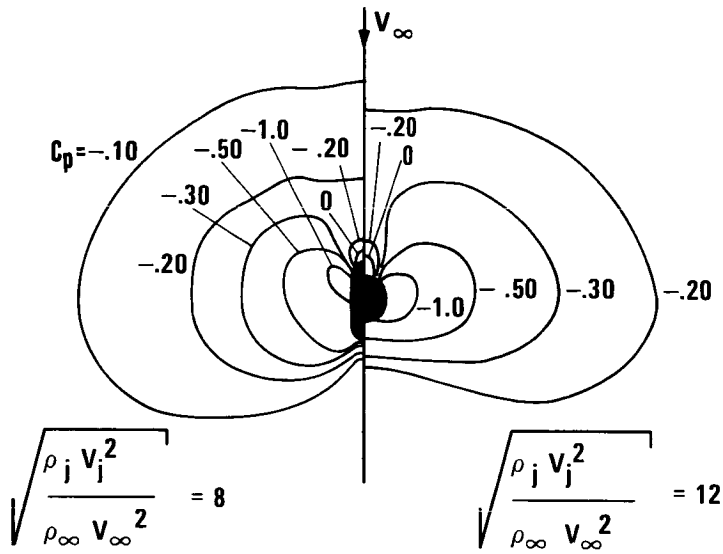

Figure 9.- Plate pressure coefficients C_p around a streamwise and circular jet.

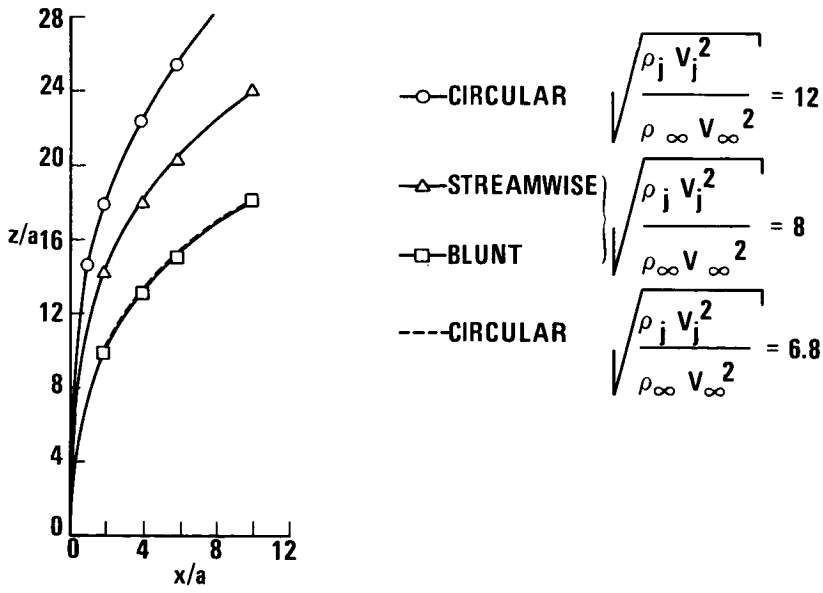

Figure 10.- Measured jet plume centerline paths.

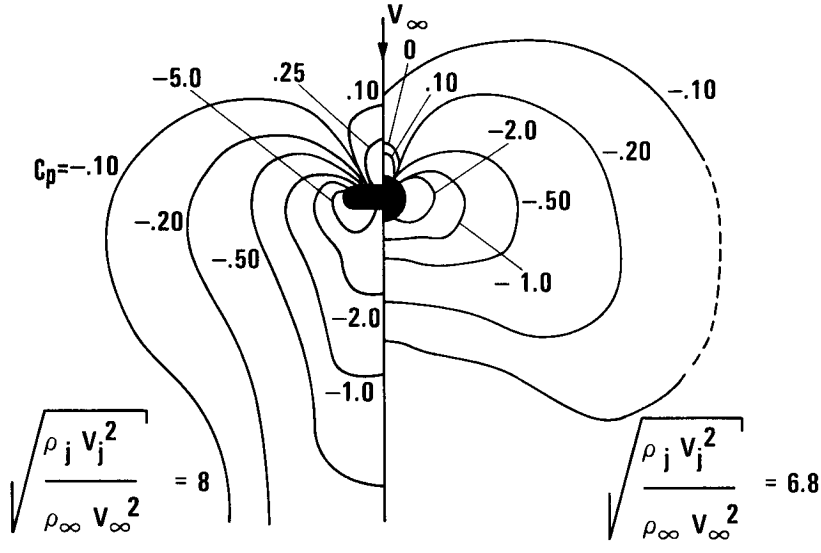

Figure 11.- Plate pressure coefficients C_p around a blunt and circular jet with matching plume centerline paths.

EXPERIMENTAL REACTION JET EFFECTS AT SUBSONIC SPEEDS

By Troy A. Street and Donald J. Spring

Advanced Systems Laboratory
of the U. S. Army Missile Command

SUMMARY

A brief description of the total overall reaction jet program of the Advanced Systems Laboratory is given as well as a brief review of the work done to date. A more thorough presentation of the subsonic experimental data is made.

INTRODUCTION

The purpose of this paper is to give a very brief synopsis of the trends in the aerodynamic data that the U.S. Army Missile Command has accumulated experimentally in the subsonic regime. Predominately, the data collected to date in the subsonic regime has been for the sonic jet with underexpanded flow injecting into a subsonic freestream. The data presented herein is a collection from a test of an axisymmetric body of revolution with a sonic jet injecting into a freestream Mach number of 0.285 and a sonic jet injecting from a flat plate into freestream Mach numbers of 0.1, 0.2, 0.4, and 0.6.

SYMBOLS

b	fin span or slot width, inches
c	fin chord, inches
C_N	normal force coefficient
C_p	pressure coefficient
D	body diameter, inches
d	jet diameter, inches

e	base of natural logarithm
F_{ni}	normal interference force, lbs
F_T	force due to thrust of the jet, lbs
K	empirical constant
M	freestream Mach number
$\dot{m}$	mass rate of flow, lb/sec
N	empirical constant
P	freestream static pressure, psia
P_c	total pressure in the jet chamber, psia
Q	jet-to-freestream momentum ratio
R	radius, inches
V	velocity, ft/sec
α	angle of attack, degrees
Δ	increment
δ_t	slot length, inches
θ	angle from upstream freestream, degrees

Subscripts:

j	jet
∞	freestream

HISTORICAL BACKGROUND

The U.S. Army Missile Command is currently endeavoring to develop those techniques required to predict the aerodynamic coefficients necessary for design of reaction jets as control devices. This stimulates research activities in the dual areas of bringing to bear those techniques from other disciplines as well as advancing the state-of-art in the solution of fluid mechanics problems.

The current research program of the Advanced Systems Laboratory

of the U.S. Army Missile Command fundamentally draws upon past and present analytical and experimental efforts to obtain design parameters and prepares for the future to utilize the forthcoming generation of computers. Throughout the program the range of interest addresses itself to the ultimate objective of developing the capability to predict the aerodynamic characteristics of axisymmetric bodies of revolution using multiple reaction jets anywhere on the body with any jet orientation, jet condition or injectant, and a wide speed range from low subsonic deep into hypersonic. Of course, the ultimate objective is so broad that only small segments are being examined in logical sequence.

The current approaches are as follows:

A. Theoretical Approach

B. Analytical or Semi-Empirical Approach

C. Empirical Correlation Approach

D. Experimental Approach

The first three approaches will be very briefly described with the Experimental Approach in the subsonic regime receiving the majority of attention for the interest of this symposium, although considerably more experimental data has been collected in the supersonic regime by the Advanced Systems Laboratory than has been accumulated in the subsonic regime. This is not to de-emphasize the Army's interest in the subsonic regime but merely to state that the Army, historically, has had more pressing needs in the transonic and supersonic regimes.

APPROACHES

(a) Theoretical Approach

In this effort a numerical solution to the Navier Stokes equations is being sought for a slot ejecting normally into a supersonic approach flow. Finite difference approximations are used to replace the derivatives in the unsteady Navier Stokes equations. An initial flow field is assumed and the flow allowed to develop with time. The steady state solution is desired and results as the limit of the unsteady solution. At present the method is progress-

ing normally but steady state has not been reached. An inherent drawback in the technique has limited the present effort to extremely low Reynolds number and to laminar flow. Future efforts will strive to overcome these drawbacks.

(b) Analytical or Semi-Empirical Approach

The supersonic analytical approach, as reported previously in the literature[1] is based upon the "equivalent body analogy" concept. This concept is for a sonic, normal, underexpanded jet. The jet is assumed to be replaceable by an equivalent solid body that will produce a similar effect on the body of revolution. The equivalent body is determined by relating the change in the longitudinal component of momentum of the jet to the drag of an equivalent body. The equivalent body is assumed to be a sphere-cylinder body with the origin of the sphere placed on the jet centerline at the sphere radius above the jet exit as shown in Figure 1. The method of characteristics is then run for the equivalent body. The intersection of the characteristics net with the missile body provides a surface for the integration of pressure to determine the interference forces and moments. A comparison of the data obtained by this technique with the experimental data for the incremental normal force coefficient variation with Mach number for various pressure ratios is shown in Figure 2. The trends obtained by this equivalent body analogy are correct while the magnitude appears to be in error from 11 to 16%.

The subsonic analytical approach is described in another paper at this symposium by Robert Rosen, Norbert A. Durando, and Louis A. Cassel of the McDonnell Douglas Corporation, which is under contract to the Advanced Systems Laboratory to develop this subsonic approach.

(c) Empirical Correlation Approach

The empirical correlation approach used the force data obtained during the experimental tests for Mach numbers 0.8 to 4.5 for various pressure ratios and axial jet locations on a body of revolution.

The augmentation ratio, K_n, was selected as a pertinent parameter to measure the control force. The augmentation ratio is defined as

$$K_n = 1 + F_{ni}/F_T$$

where F_{ni} is the normal interference force and F_T is the jet thrust.

The procedure for developing the empirical technique was to plot the augmentation ratio, K_n, as a function of jet momentum-to-freestream momentum, Q. The curves were linearized by multiplying the augmentation ratio by the momentum ratio. The results were then curve fit. The curves were then rotated to a common slope and shifted to a common origin.

Two empirical constants, K and N, are required at this point. K is the empirical constant required to rotate the curves and N is the empirical constant required to translate the curves to a common origin. These two empirical constants are functions only of the type of jet, slot or circular, and the body axial location. Figure 3 shows the calculated values of the empirical technique compared with the corresponding experimental data to be within an accuracy of $\pm$ 10%.

(d) Experimental Approaches

The models used for the experimental reaction jet programs consisted of a 4-caliber tangent ogive nose with a cylindrical afterbody, Figures 4 and 15, for tests at Mach numbers of 4.5 to 0.8 and 0.285 and a flat plate at Mach numbers of 0.6,0.4,0.2,and 0.1. Force and moment tests were conducted for the Mach number range 4.5 to 0.8 and a flow field survey conducted for the Mach number range 1.2 to 0.9; the flat plate was used in a pressure test.

The force and moment tests were for angle of attack of $\pm$ 4° using the model shown in Figure 4. Either air or nitrogen was used as the secondary gas and was injected normal to the surface at a sonic exit Mach number. Artificial boundary layer trips were included in all tests to assure a turbulent boundary layer.

Figure 5 shows a typical variation of the normal force coefficient with angle of attack for various jet total-to-freestream static pressure ratios as a variable. Two features should be noted concerning these figures:

(1) Over the angle of attack range $\pm$ 4 degrees, these data vary linearly with no discontinuities.
(2) These data at the zero angle-of-attack intercepts represent the augmentation or degradation of the control force.

These data are in the transonic region where information is sorely

needed.

Another significant program investigated the jet on stabilizing surfaces located aft of the control jets[2], with the testing performed at Mach numbers of 0.9 and 1.2 for several jet pressure ratios. An example of the changes due to jet momentum ratio is shown in Fig. 6. A small (¼-inch dia.) flow probe and pitot-static tube was used to map the flow fields in the immediate vicinity of the fin, and the resulting data were reduced in terms of velocity components in the X,Y,Z plane. Figure 7 shows a representative survey. The data from this series of tests are being used to determine the flow field properties downstream of a control jet, and are being applied in the efforts to develop a prediction technique.

Recently the NASA Langley Research Center and the U.S. Army Missile Command's Advanced Systems Laboratory began a joint effort to study the effects of a predominantly sonic jet injecting from a flat plate into a subsonic freestream. The joint study consists of an initial test phase that was completed in August 1969, a final test phase to be completed later in 1969, and an analysis of the data collected. The initial test phase was a flat plate pressure test, while the final test phase will consist of a rake survey of the jet wake.

The subsonic flat plate test data recently collected at Langley Research Center has not been fully analyzed. However, a presentation of some of the significant aspects so far unveiled is presented in Figures 8 through 14. The flat plate was oriented at zero angle of attack for the tests and each test point was repeated twice. Figure 8 shows the effect of pressure coefficient, C_p, variation with radial length, R, for a 0.33-inch diameter sonic nozzle on the upstream ray ($\theta = 0$) as well as the variation of C_p at each orifice with the number of times the data was repeated. A slight positive C_p immediately in front of the jet exists at this very low freestream Mach number, 0.1, and momentum ratio (jet-to-freestream ratio,Q) of 2.0. When comparing Figures 8 and 9 for the same momentum ratio but different Mach numbers (0.1 and 0.6, respectively), it becomes apparent that the scatter in the upstream ray of Figure 8 is that due to Mach number. At the lower Mach number the freestream flow around the jet fluctuates considerably. Most likely the fluctuations exist at the higher Mach numbers but at a sufficiently high frequency that their effect is damped in the length of tubing from the static orifice to the pressure transducer located outside the tunnel.

Additional pressure distribution on rays $\theta = 90^{o}$ and 150^{o} for the Mach number 0.6 and the momentum ratio 2.0 conditions are shown in Figures 10 and 11. The $\theta = 90^{o}$ ray shows only a small increase in C_p near the nozzle. The $\theta = 150^{o}$ ray shows a negative C_p near the nozzle that is caused by either entrainment or blockage or both.

Figures 12 through 14 show the effect of higher jet pressure which is reflected in the momentum ratio increase to 100. Figure 12 shows a typical upstream pressure distribution with a significant increase in C_p near the nozzle. This is because of the blockage effect at the higher Mach number for this condition.

Figures 13 and 14 show the pressure distribution for the 90^{o} and 150^{o} rays, respectively. For this Mach number, 0.6, the lowest value of pressure coefficient exists at the 90^{o} ray at the pressure orifice nearest the nozzle. Next examine the 150^{o} ray and note the lowest pressure exists an inch from the nozzle and some pressure recovery near the jet has been manifested between the 90^{o} ray and the 150^{o}; also the magnitude of pressure coefficient is less on the 150^{o} ray.

Comparing Figures 9 through 11 with Figures 12 through 14, respectively, shows that increasing the momentum ratio effectively moves the lowest pressure (originally behind the jet) forward. The lowest pressure remains near the jet. As this lowest pressure moves forward, a recovery process apparently originates near the jet and moves outward along the rays.

The above comparison suggests that a tremendous viscous interaction process is displayed in these adjacent areas as the high pressure region in front of the jet attempts to rush into low pressure regions downstream of the jet. This in turn would suggest that considerable mixing occurs not only in the freestream itself but between the freestream and the nozzle injectant.

The subsonic experimental data[3] was accumulated on the axisymmetric body, shown in Figure 15, with the pressure orifices. The model is 2.25 inches in diameter, with rows of orifices 30^{o} around the body from the jet. Both circular nozzles and radial slot nozzles were used. The effects of a sonic, circular jet on the longitudinal pressure distribution is shown in Figures 16 through 19. Figure 16 shows a typical pressure distribution on the axisymmetric body. (The rows of pressure coefficient distribution with longitudinal length X measured from the jet correspond

to the rows shown in Figure 15. The row through the jet centerline is the middle row with the discontinuous distribution at the jet location.) There exists a small pressure rise upstream of the jet on the jet centerline. However, the dominating factor is the low pressure in back of the jet and on the adjacent rows of orifices. As shown in Figures 16 and 17 the pressure profile changes very little with angle of attack. An increase in momentum ratio failed to change the pressure distribution; it only succeeded in reducing the upstream positive pressure and reducing the value of negative pressure as shown in Figure 18.

The effect of a sonic, slot nozzle was to increase the positive C_p ahead of the jet and reduce the negative C_p behind and on the sides of the jets, Figure 19. The reduction on the adjacent rows is because the slots are much closer to the rows than when the jet was circular. The same throat area existed for the slot as for the circular nozzle. The injectant is spread over a large region thereby causing a slightly greater disturbance to the flow field. This, in turn, manifests a slightly greater change in aerodynamic coefficients.

It was not felt that these various changes in chamber pressure, angle of attack, or slot configurations changed the aerodynamics of the body by a significant amount. The conclusion was that, for the range of parameters tested, the sonic jet dominated the Mach number 0.285 freestream so overwhelmingly that no other test variable emerged except in a very weak manner. Logically, it would appear that, because of curvature effects, the jet would dominate the flow over an axisymmetric body more than it would for a flat plate.

CONCLUSIONS

The following conclusions are drawn:

1. The Army Missile Command has been successful in the supersonic regime with a pure blockage model replacing the jet.

2. In the subsonic regime, based on the axisymmetric body and the flat plate tests, the dominating factors appear to be (a) the jet in the low subsonic regime and (b) viscous interaction in the higher subsonic regimes.

REFERENCES

1. Cassel, L. A.; Davis, J. G.; and Engh, D. P.: Lateral Jet Control Effectiveness Prediction for Axisymmetric Missile Configurations. Rep. No. RD-TR-68-5, U.S. Army Missile Command, June 1968.

2. Dahlke, C. W.: An Experimental Investigation of Downstream Flow-Field Properties Behind a Sonic Jet Injected into Transonic Freestream From A Body of Revolution (Series II). Rep. No. RD-TM-69-2, U.S. Army Missile Command, Feb. 1969.

3. Spring, Donald J.; and Street, Troy A.: Experimental Investigation of the Pressure Distributions Induced Upon a Body of Revolution by Several Transverse Jets at Low Speeds. Rep. No. RD-TM-68-7, U.S. Army Missile Command, Aug. 1, 1968.

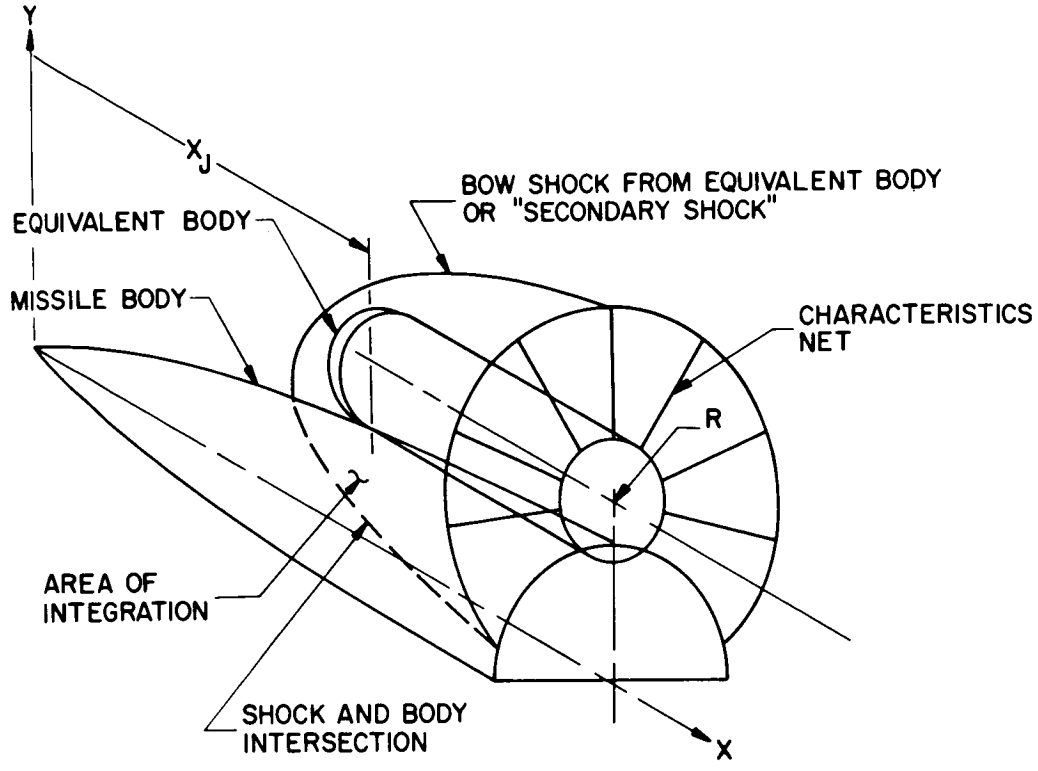

Figure 1.- Model for equivalent body analogy.

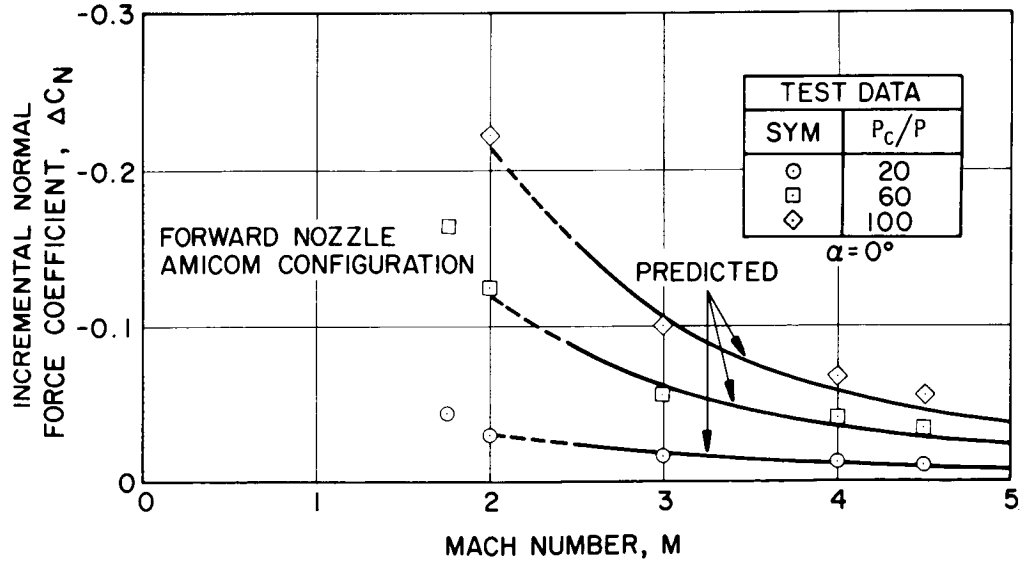

Figure 2.- Comparison of predicted and experimental normal force coefficients.

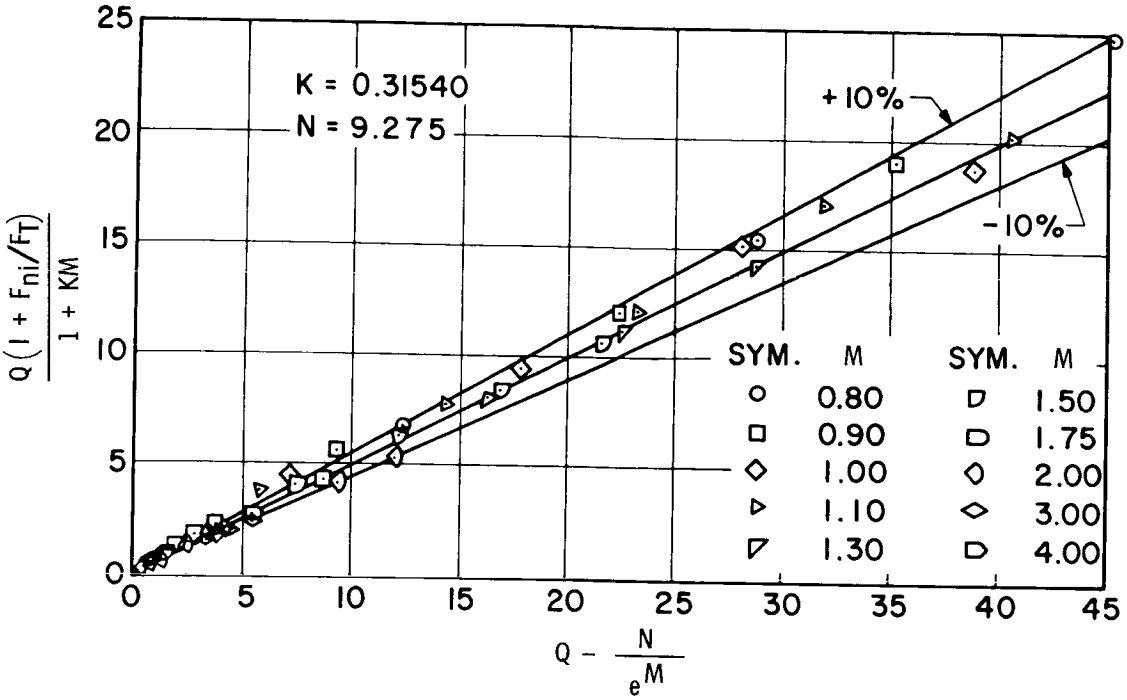

Figure 3.- Empirical-correlation-technique comparison.

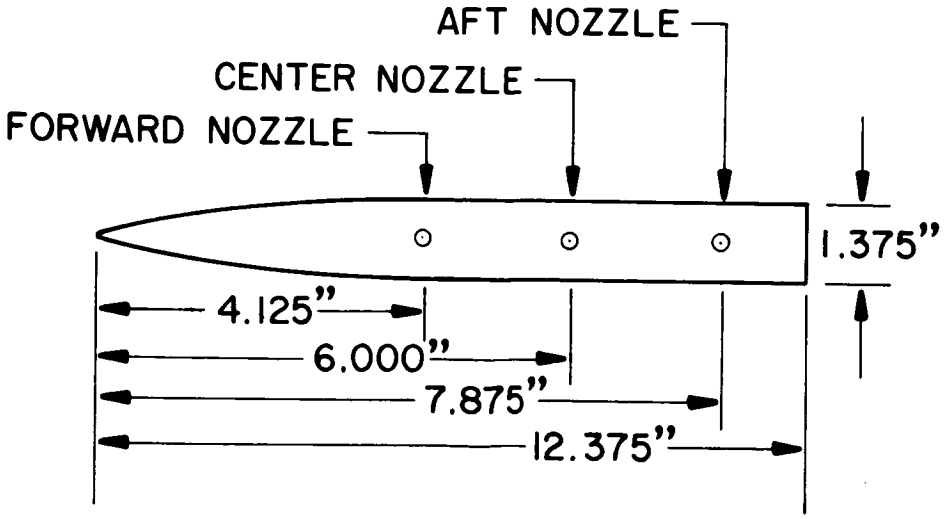

Figure 4.- Schematic drawing of experimental model.

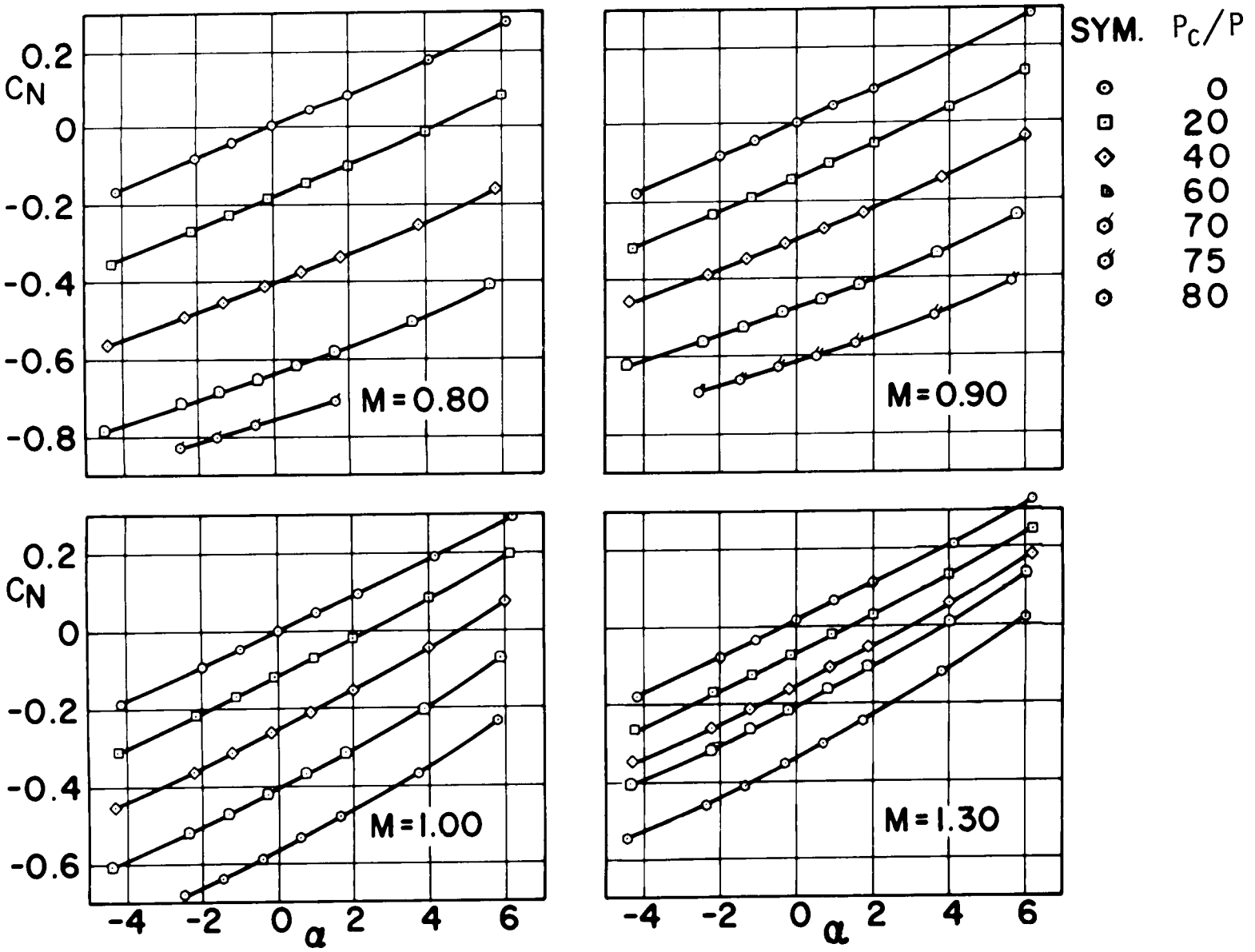

Figure 5.- Variation of experimental normal force coefficient with angle of attack.

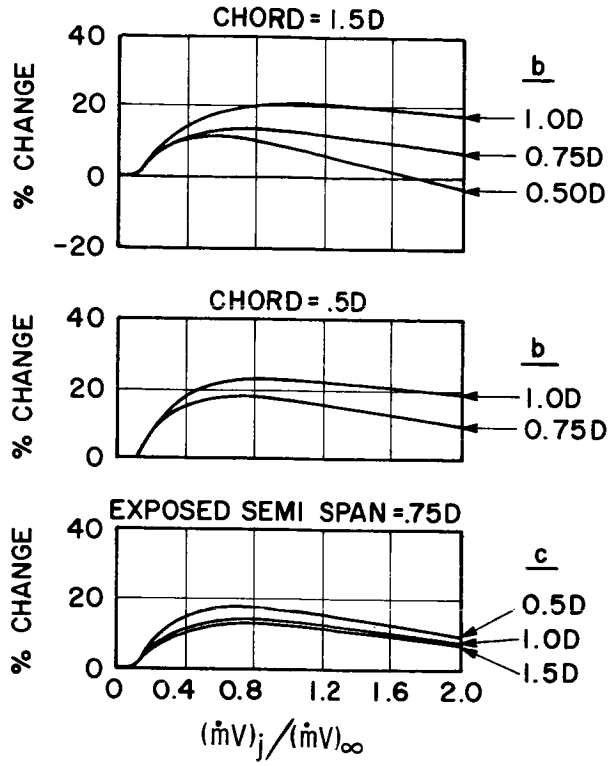

Figure 6.- Percent change in fin pitching moment due to jet momentum ratio for several rectangular downstream fins.

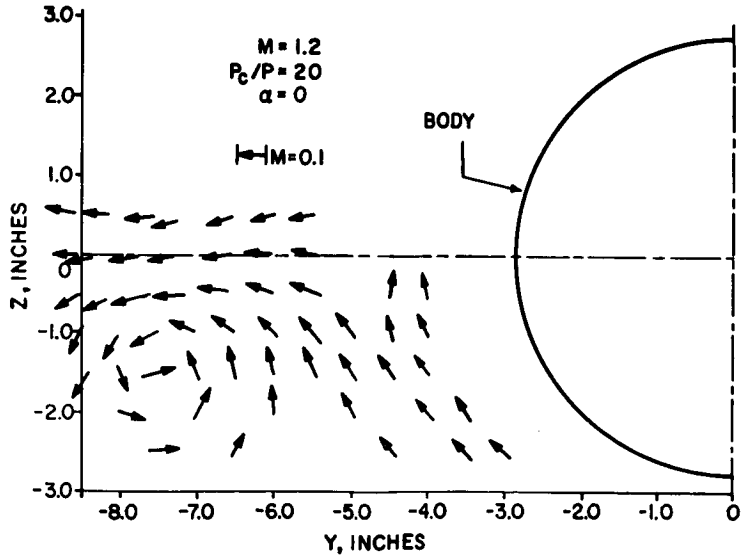

Figure 7.- Velocity components at downstream fin location obtained in flow-field survey.

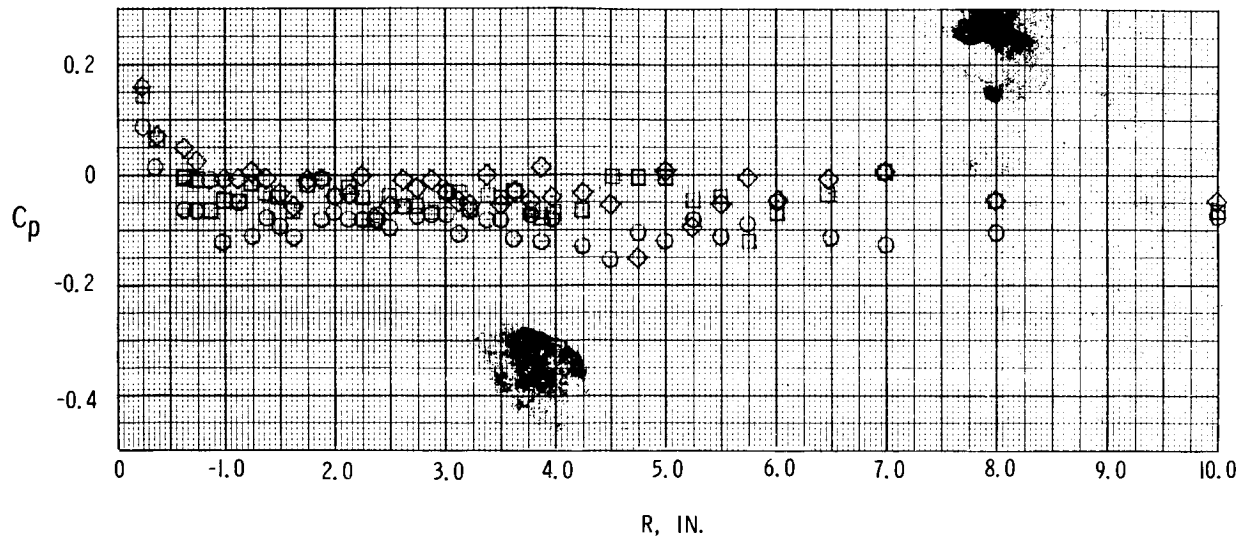

Figure 8.- Flat-plate pressure distribution at M = 0.1 for 0^0 ray. Q = 2.

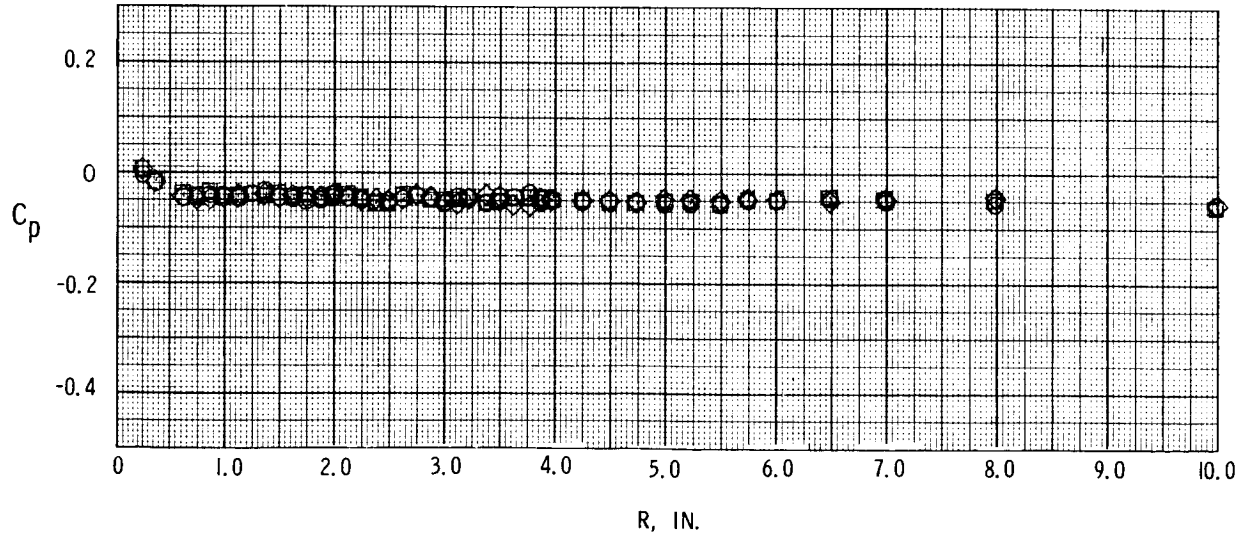

Figure 9.- Flat-plate pressure distribution at M = 0.6 for 0^0 ray. Q = 2.

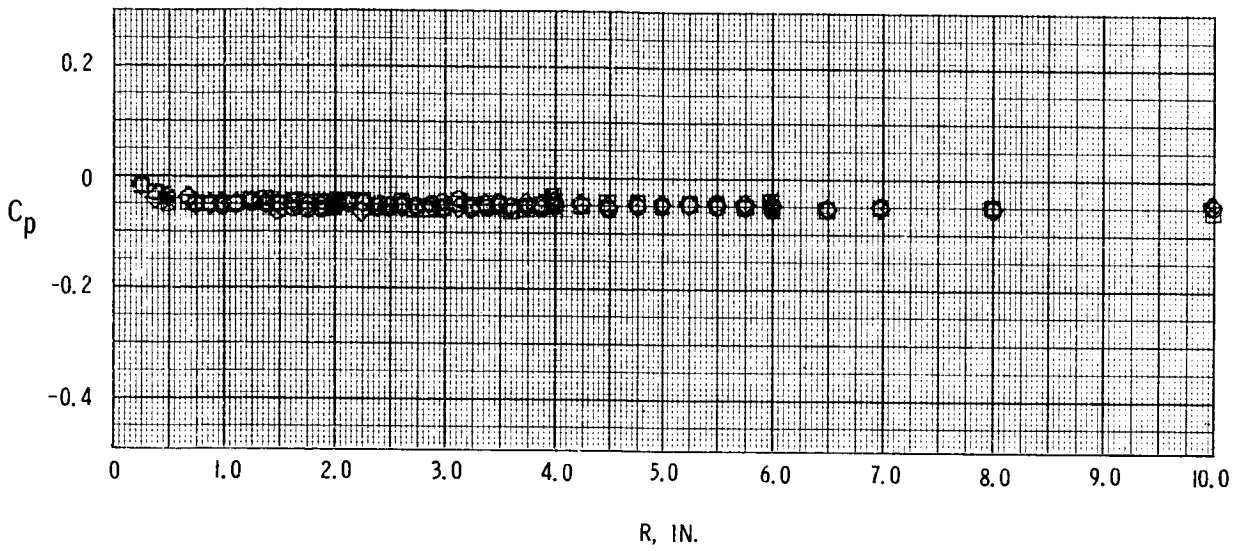

Figure 10.- Flat-plate pressure distribution at M = 0.6 for 90° ray. Q = 2.

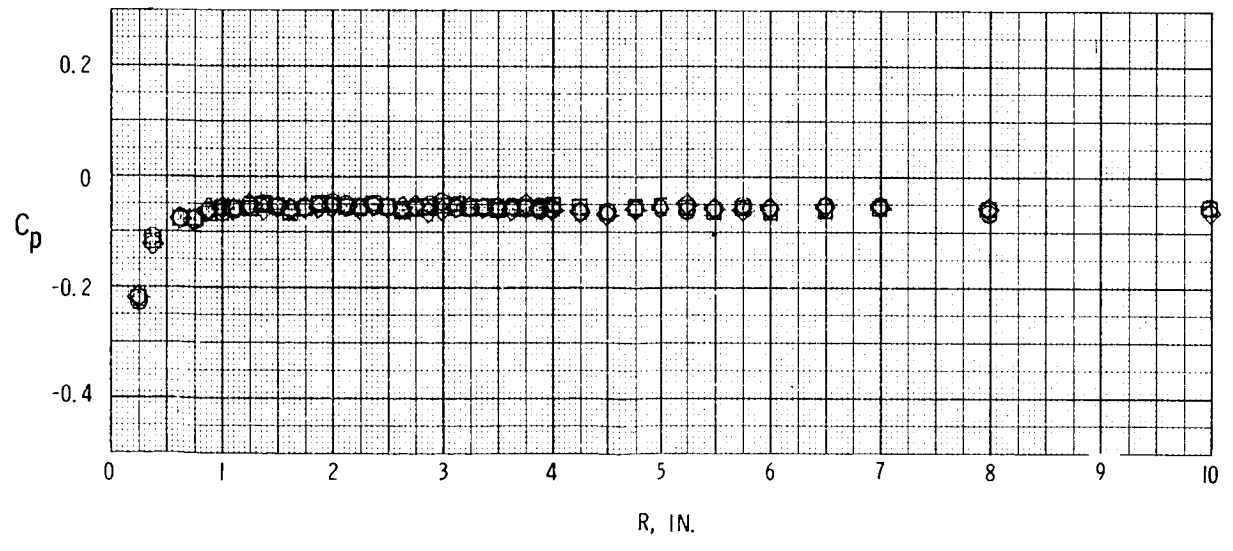

Figure 11.- Flat-plate pressure distribution at M = 0.6 for 150° ray. Q = 2.

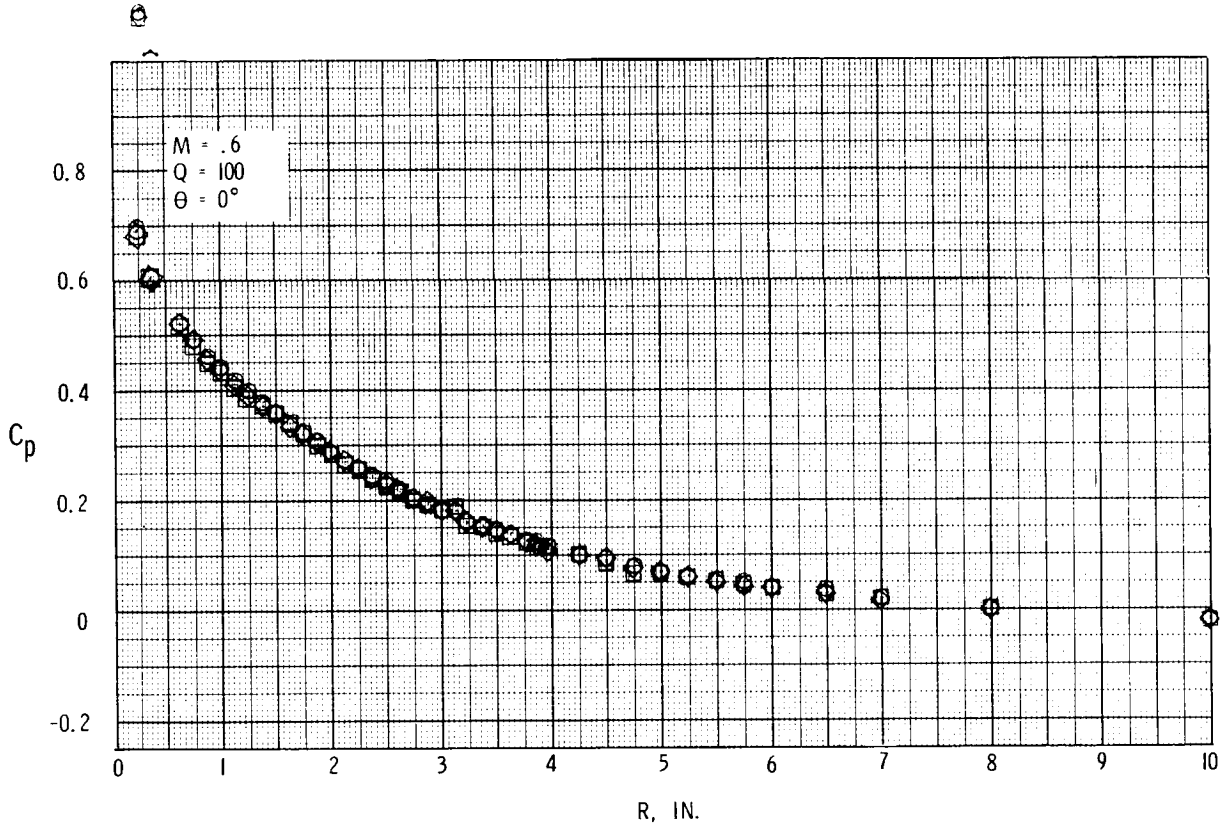

Figure 12.- Flat-plate pressure distribution at M = 0.6 for 0^0 ray with increased momentum ratio.

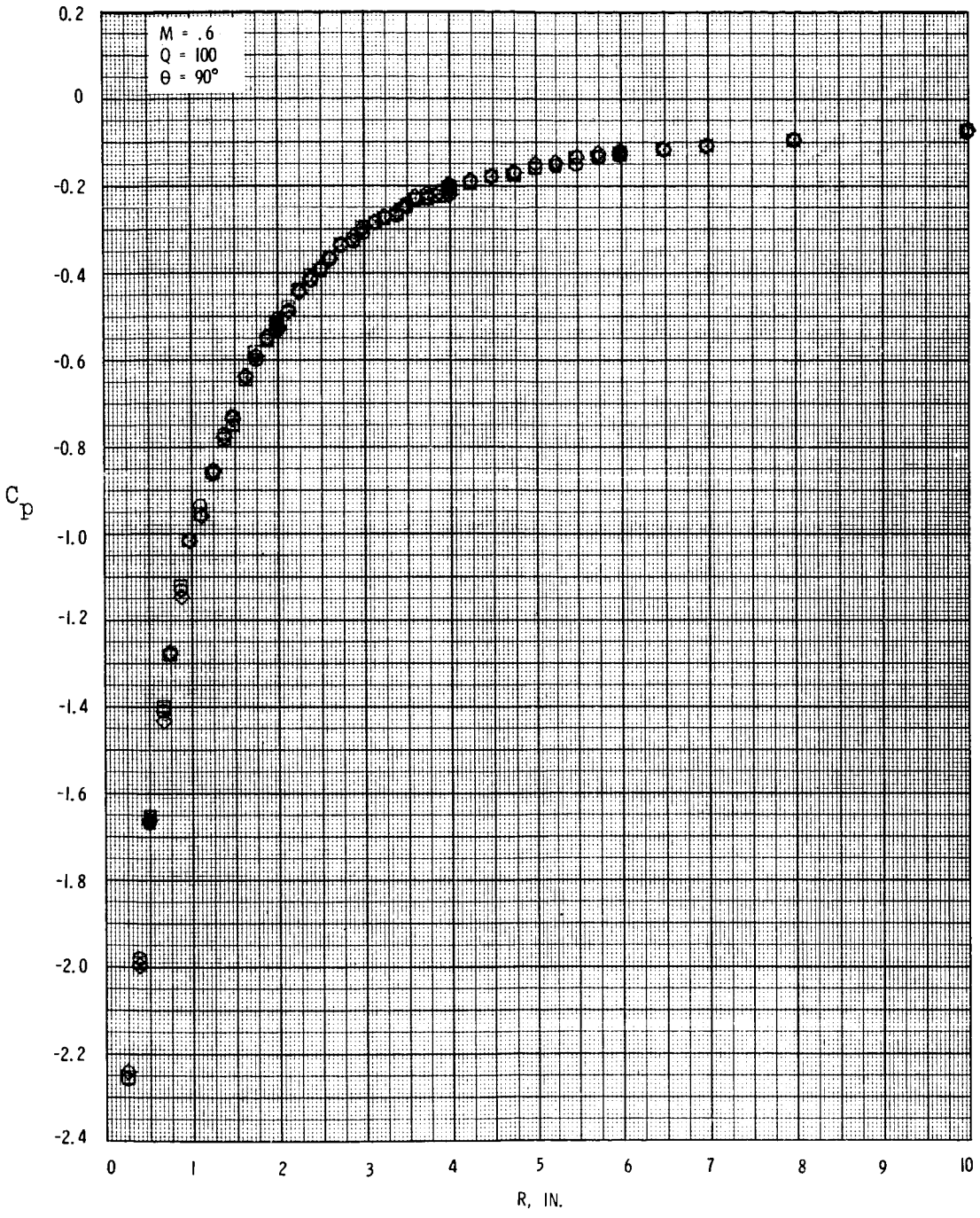

Figure 13.- Flat-plate pressure distribution at M = 0.6 for 90° ray with increased momentum ratio.

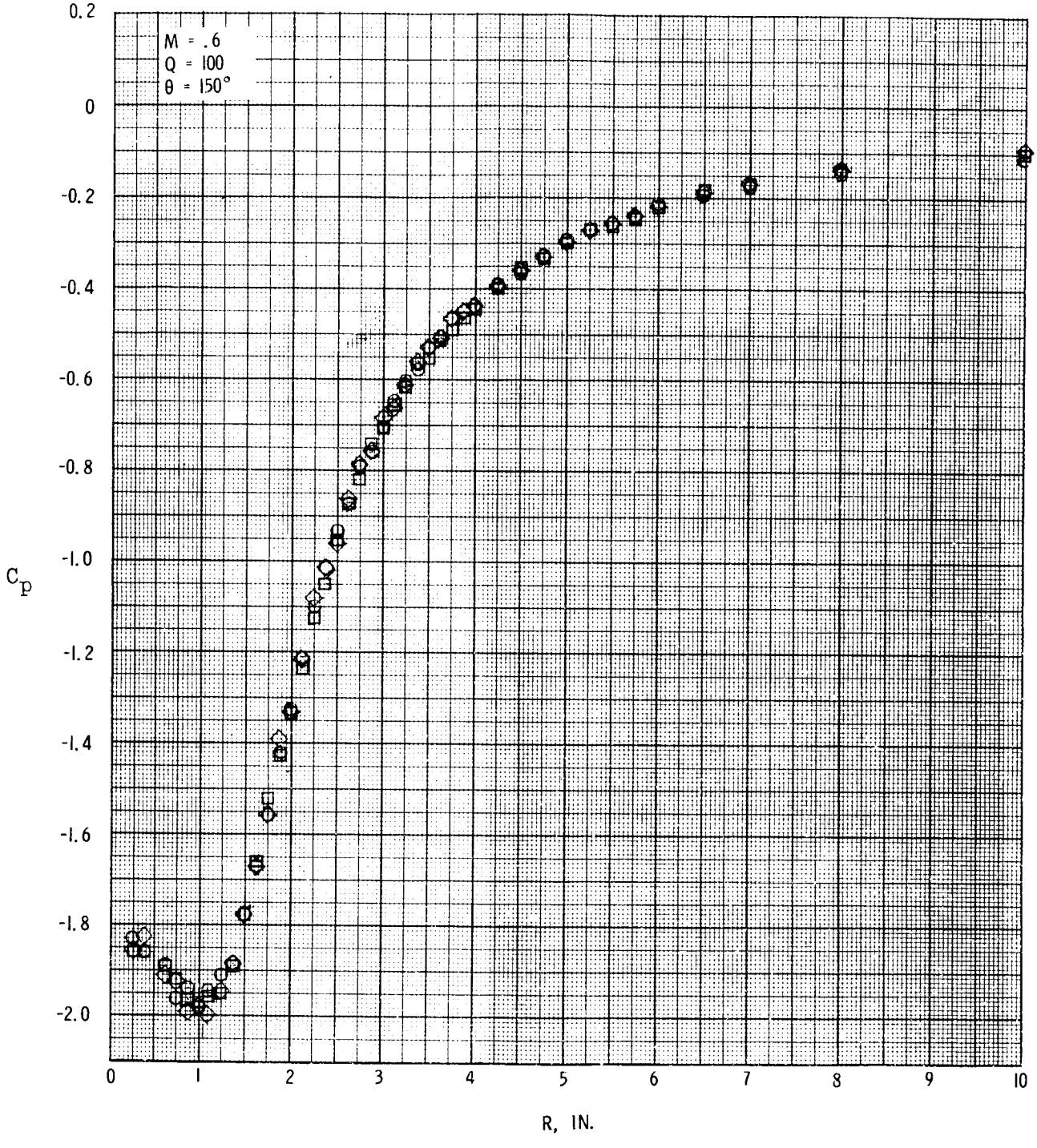

Figure 14.- Flat-plate pressure distribution at M = 0.6 for 150° ray with increased momentum ratio.

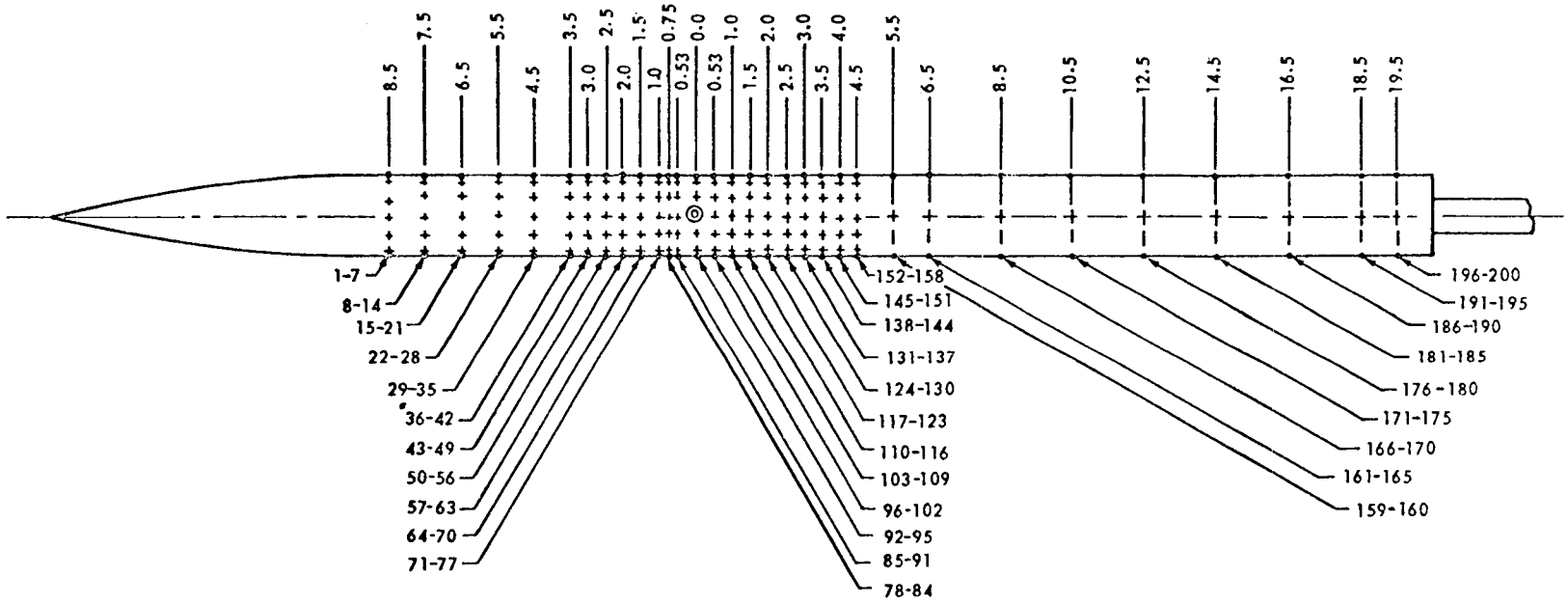

Figure 15.- Pressure-orifice locations.

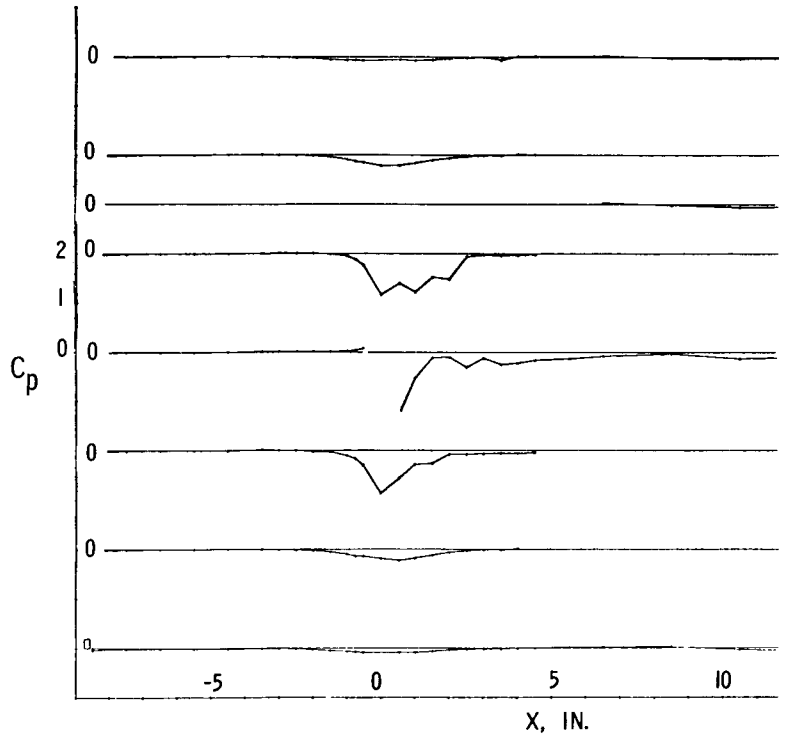

Figure 16.- Three-dimensional body pressure distribution for circular nozzle. d = 0.27 in.; Q = 1.75; P_c = 250 psia; $\alpha = 0^o$.

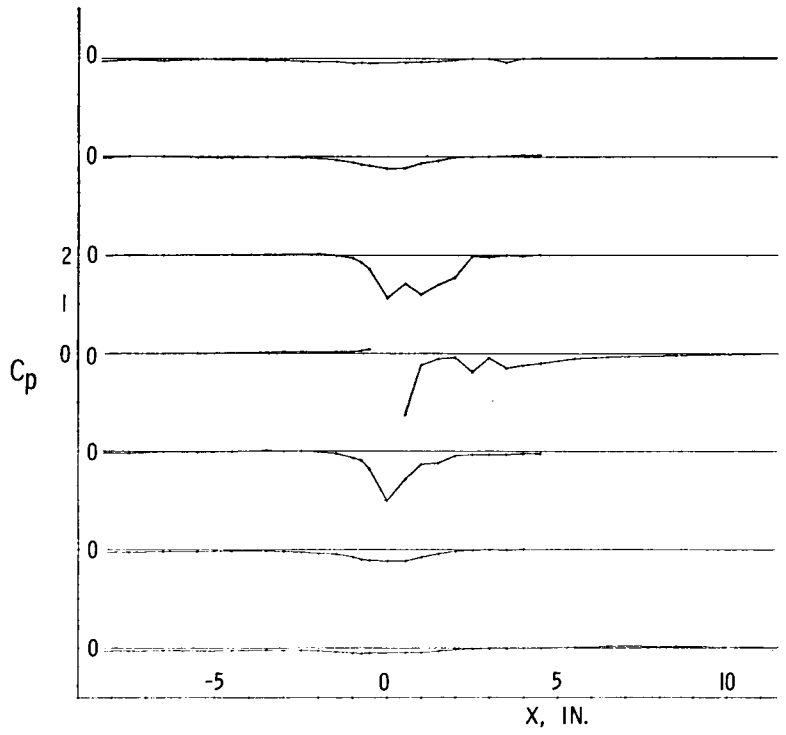

Figure 17.- Three-dimensional body pressure distribution for circular nozzle. d = 0.27 in.; Q = 1.75; P_c = 250 psia; $\alpha = -5^o$.

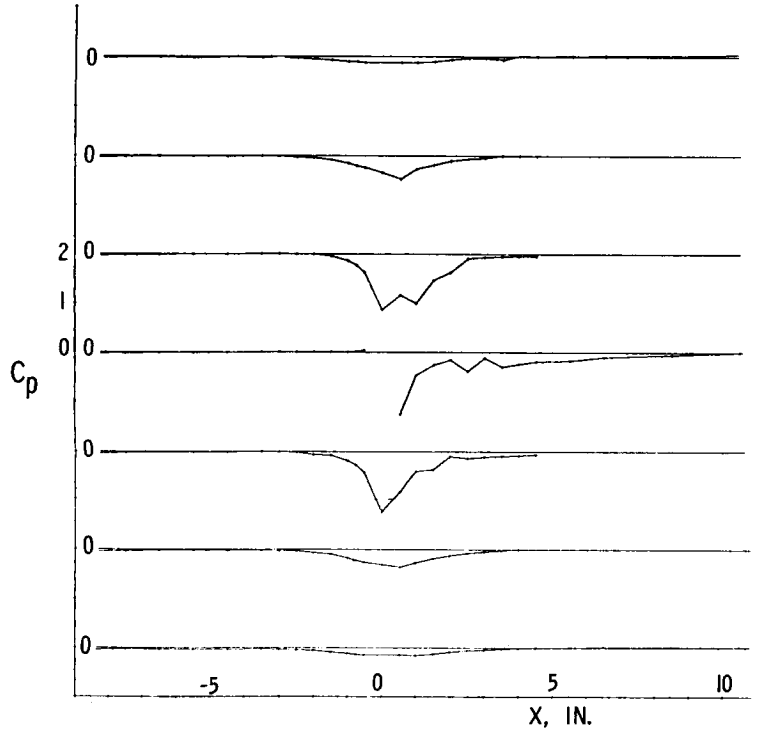

Figure 18.- Three-dimensional body pressure distribution for circular nozzle. d = 0.27 in.; Q = 3.00; P_c = 450 psia; $\alpha = 0^o$.

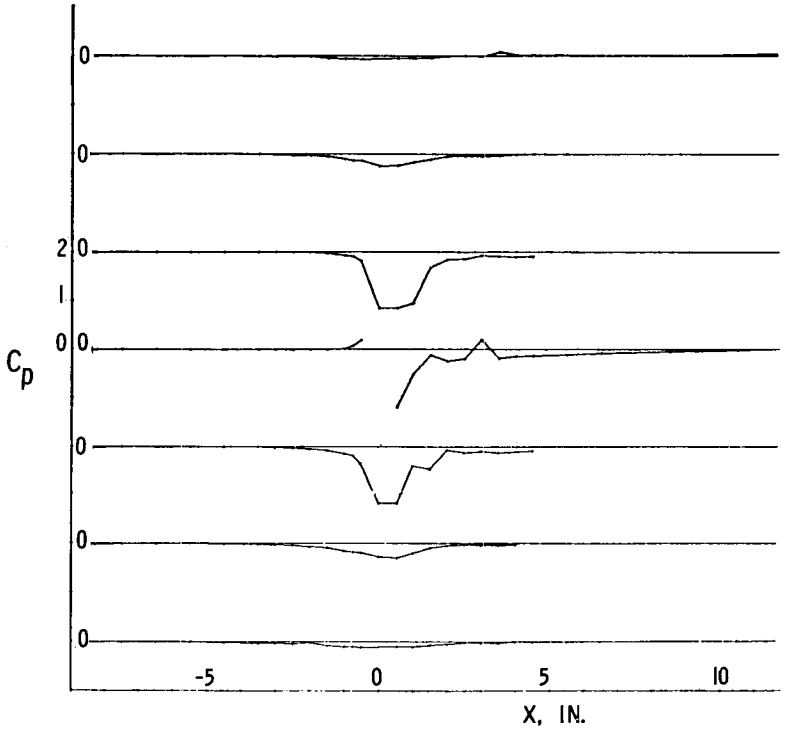

Figure 19.- Three-dimensional body pressure distribution for slot nozzle. b = 0.45 in.; δ_t = 0.131 in.; Q = 3.19; P_c = 450 psia; $\alpha = 0^o$.

A BLOCKAGE-SINK REPRESENTATION OF JET INTERFERENCE EFFECTS FOR NONCIRCULAR JET ORIFICES

By J. C. Wu and M. A. Wright

Georgia Institute of Technology

SUMMARY

A study of the subsonic jet-in-crosswind problem is made by using a two-dimensional potential-flow representation of jet interference effects. Analyses are made for two different jet exit configurations: an ellipse with its major axis alined with the free stream flow direction, and an ellipse with its minor axis in the free-stream direction. In each of the configurations the jet issues normally from the surface of an infinite plate into the crosswind. The model uses a blockage-sink representation of the jet interference effects on the crosswind. The blockage element consists of a jet-exit-shaped cylinder with an attached afterbody and is used to simulate the effect of the jet-wake combination in displacing the crossflow. The sink element is placed in the afterbody to simulate the combined effect of entrainment by the jet as well as by the wake. Calculated pressure distributions on the plate are compared with experimental data obtained with similar jet exit configurations. The results show that the two-dimensional representation is useful for the case of high jet-to-crosswind speed ratio.

6

INTRODUCTION

This paper treats the problem of a single subsonic turbulent jet issuing normally from the surface of an infinite plate into a subsonic crosswind. It has been observed that the presence of the jet in the crosswind leads to a separation of the crosswind behind the jet. The combined effects of aerodynamic forces acting on the jet and the entrainment of the crossflow fluid into the jet, which carries momentum with it, causes the jet to spread, deform, and deflect after leaving the plate. In turn, the jet interferes with the flow of the crosswind by displacing it, entraining it, and causing the separation region to form; these three factors are usually referred to as the blockage effect, the entrainment effect, and the wake effect, respectively. Because of the complexity of the jet interference phenomena, there is presently no complete theory treating the detailed flow in this problem. In lift-jet or lift-fan powered V/STOL applications, the change in surface pressure due to the jet interference is of primary concern. During the past few years, several analytical flow models (refs. 1, 2, 3) have been proposed as means of representing the jet interference effects,

Work supported by the U.S. Army Research Office, Durham, North Carolina, under contract No. DAHC04 68 C0004.

and from these representations, the interference surface pressure can be calculated. The models have the common feature of requiring the use of either empirical or semiempirical information concerning the path of the jet in the crosswind. Potential flow elements, that is, vortices or a combination of doublets and sinks, are placed on or near the center line of the jet plume. The velocity induced by the potential elements on the surface is used to calculate the interference pressure. The models differ in the factors that are accounted for (or neglected) and in the manner in which these factors are represented. In two of the proposed models the effect of entrainment is ignored. To the authors' knowledge, no numerical results have been reported that use these models for other than a circular jet exit configuration. Other models may result from the extension of the work of Lu Chang (ref. 4) concerning the time-dependent deformation of a circular column of fluid in a crossflow. This extension is being considered at the Georgia Institute of Technology as well as other places, but results are at present inconclusive.

The principal objective of this paper is to demonstrate that for the case of high jet-to-crosswind speed ratio, it is possible to use a two-dimensional approximation with a blockage-sink representation to study the jet interference effects with noncircular as well as circular jet exit configurations. The case of high-speed ratio is of particular importance for lift-jet or lift-fan powered V/STOL aircraft in the transition phase of a flight. Results presented are for elliptical jet exit configurations, the major axis of the ellipse being either alined with or perpendicular to the free-stream direction.

SYMBOLS

A, B	constants in conformal transformation, eq. (8)
C_f	integrated pressure coefficient
C_p	pressure coefficient, eq. (1)
d	diameter of a circular jet exit
k	half-width of Rankine oval
m	sink strength for entrainment
n	half-length of Rankine oval
p	local static pressure
p_∞	free stream static pressure
r	plate radial coordinate
R, R_o	radial limits of integration, eq. (18)
S	strength of source-sink pair in Rankine oval

u	local velocity in direction of free stream
v	local velocity normal to free stream
U_∞	free-stream velocity
U_j	jet velocity
x_s	sink location for entrainment
$z = x+iy$,	plate complex coordinates
β	plate angular coordinate
$\zeta = \xi+i\eta$,	Rankine oval complex coordinates
ρ	density
ω	complex potential

Subscripts:

b	blockage-induced velocity components
s	sink-induced velocity components

Superscript:

$( )'$	ζ-plane velocity components

ANALYSIS

The blockage-sink representation has the advantage of being relatively simple and easily interpretable. In reference 1 an analytical model based on this representation was developed. A doublet distribution along the jet center line was used to simulate the blockage effect due to the jet plume, and a sink distribution was used to simulate the entrainment of crosswind fluid into the jet. The authors of reference 1 stated that because of the manner in which the blockage effect was simulated, the representation of the flow near the jet was not expected to be good. They showed that with a suitable choice of entrainment coefficients, the model gives a calculated surface pressure field in good agreement with experimental data for a circular jet issuing normally from the center of a large rectangular wing placed at zero lift and with a jet-to-crosswind speed ratio of 10. Neither theoretical nor experimental results were presented in reference 1 for a midspan of the wing covering a distance of 10 jet radii. Experimental data from other sources (refs. 5 and 6), however, have shown that the interference pressure on this portion of the surface contributes substantially to the overall interference effects of lift loss and nose-up pitching moment.

In the present approximation the effect of variation of flow between planes parallel to the plate is considered unimportant and ignored as far as the calculation of surface pressure is concerned. It is noted that the jet interference problem is basically three-dimensional. Nevertheless, the simplifications and versatility resultant from its use makes the two-dimensional approach attractive. For example, the representation of noncircular jet exit shapes with the use of a three-dimensional model involves considerable complications. To the authors' knowledge, no analytical results using a three-dimensional model for other than the circular jet exit configuration have been reported. As shall be shown, with a two-dimensional model the generalization to noncircular jet exit shapes is very straightforward. The question remains as to what is the region of validity of the approximation. In reference 5 the authors presented some results using a two-dimensional model for a circular jet. Many of the observations presented in reference 5 are also pertinent to noncircular jets. These results are not repeated here, but the major conclusions are summarized below.

Experimental observations indicate that if the jet-to-crosswind speed ratio is sufficiently high, the jet deforms and deflects significantly only after it has penetrated several jet radii into the crosswind. Since the velocity induced by a three-dimensional blockage or sink element at a given point in the flow field is inversely proportional to the square of the distance between the element and the point, three-dimensional effects on the interference surface pressure are expected to be small for the high-speed-ratio case, particularly in regions close to the jet exit. A surface pressure distribution was calculated by using a large number of three-dimensional doublets and sinks placed along an empirical jet-center-line path for a speed ratio of 8. The result was shown to agree very well with that obtained with an equivalent two-dimensional representation. Thus, for the circular-jet case, the effect of jet deflection was considered to be unimportant for speed ratios in excess of 8. The same conclusion is expected to be valid for noncircular jets, as long as the jet penetration is not much less than that for a circular jet at a speed ratio of 8.

Two other questions were also discussed in reference 5. The first concerns the justification of using a potential model to represent the jet interference effect on the crosswind, and the second concerns the relative importance of the entrainment effect. It was felt that, outside of the jet plume and its wake, the crossflow is essentially inviscid and the use of a potential flow representation is justified. However, inasmuch as there exists an extensive wake region of low total pressure, the representation of the entire crossflow by a constant-total-pressure potential-flow model is too strong a requirement on the model. Accordingly, a region downstream of the jet covering a total angle of 90° was excluded from the surface pressure calculations. With the exclusion of this wake region, it was shown that the entrainment effect, contrary to some previous conclusions, contributes significantly to the jet interference.

It should be noted that the two-dimensional approximation used here is not related to the two-dimensional slotted jet problem which is also of current interest.

Aside from the simplifications resulting from the use of the two-dimensional approach and the subsequent extension to noncircular jet exit shapes, the present

model differs from the blockage-sink model used in reference 1 in that, in addition to representing the effect of jet plume blockage, an attempt is made to simulate the effect of the wake blockage by attaching an afterbody to the cylinder. It has been shown in reference 6 that the pressure distribution around a solid circular cylinder calculated from potential theory accounting for only the cylinder blockage differs greatly from experimentally observed pressure distribution on a plate to which a solid circular cylinder is attached perpendicularly. Figure 1 presents a comparison of the calculated and experimentally obtained constant-pressure contours shown in terms of the pressure coefficient C_p defined by

$$C_p = \frac{p - p_\infty}{\frac{1}{2}\rho U_\infty^2} \tag{1}$$

The dashed curves are calculated contours and the solid curves are experimental. Since the effect of plate boundary layer on the plate pressure is of secondary importance (ref. 6), it is suspected that the effect of blockage of the crosswind by the wake is of considerable importance. Accordingly, constant-pressure contours on the plate were calculated by use of a solid cylinder-afterbody representation and compared with the experimentally measured pressure distribution around a circular cylinder in figure 2. Again, the dashed curves are calculated contours and the solid curves are experimental. The shape of the afterbody used in the calculation is also shown in figure 2. The manner in which this particular afterbody shape is obtained will be discussed later. The agreement between the two sets of contours is satisfactory outside the excluded wake-flow region. It is noted that the solid circular cylinder case, aside from the plate boundary-layer effect, is truly two-dimensional. A comparison of figure 1 with figure 2 shows that the addition of the afterbody significantly improved the blockage representation.

In addition, the present analysis considers the entrainment of crosswind fluid to take place mainly through the wake rather than along the jet periphery, as was assumed in reference 1. There is some evidence supporting this approach (ref. 7), although detailed information concerning the detailed entrainment mechanism involving nonparallel streams is still lacking. It is recognized that the entrainment effect is better represented by a distribution of sinks along the jet and wake periphery, but in the absence of empirical information, a single sink placed in the afterbody is used to simulate the lumped entrainment effect. Preliminary studies using a distribution of sinks along the line of symmetry were made. It was found that the resulting interference pressure did not differ greatly from that obtained by using an equivalent single sink. As in reference 5, no attempt is made here to simulate the flow in the wake or to calculate the interference pressure in a region where viscous effects are thought to be highly important. Because of the present uncertainty concerning the character of the wake, the development of an analytical model representing the wake flow must await further detailed experimentation.

With the potential-flow model, the blockage-induced velocity and the entrainment-induced velocity are superpositioned to give the total interference velocity. The simulation of the blockage effect of the jet-wake combination is obtained from the flow around a transformed Rankine oval. The oval, formed by

placing a source of strength S at the point $(\xi_1,0)$ in the ζ-plane (ξ,η) and a sink also of strength S at $(\xi_2,0)$, with $\xi_2 > \xi_1$, in a uniform stream U_∞ in the positive ξ-direction, is shown in figure 3. The complex potential for this flow is

$$\omega = -U_\infty \zeta - S \ln (\zeta - \xi_1) + S \ln (\zeta - \xi_2) \tag{2}$$

and the complex velocity is

$$-u_b' + iv_b' = \frac{d\omega}{d\zeta} = -\frac{U_\infty - S}{\zeta - \xi_1} + \frac{S}{\zeta - \xi_2} \tag{3}$$

where u_b' and v_b' are, respectively, the ξ- and η-components of the flow velocity, the prime denoting that these quantities are the components in the ζ-plane and the subscript b denoting that the velocity results from blockage.

It is straightforward to show that the oval is symmetrical about both the ξ-axis and the line $\xi = (\xi_1 + \xi_2)/2$. The half-length of the oval is

$$n = \frac{1}{2}\left[(\xi_2 - \xi_1)^2 + 4(\xi_2 - \xi_1)S/U_\infty\right]^{1/2} \tag{4}$$

and thus the upstream stagnation point is $(\xi_3,0)$, ξ_3 being given by

$$\xi_3 = \frac{\xi_1 + \xi_2}{2 - n} \tag{5}$$

The shape of the oval is given by the equation

$$\frac{(\xi_2 - \xi_1)\eta}{\xi^2 + \eta^2 - \xi_1 - \xi_2 + \xi_1\xi_2} = \tan \frac{U_\infty \eta}{S} \tag{6}$$

and k, the half-width of the oval, is given by

$$4k^2 - (\xi_2 - \xi_1)^2 = 4k(\xi_2 - \xi_1) \operatorname{ctn}\left[\frac{4k(\xi_2 - \xi_1)}{4n^2 - (\xi_2 - \xi_1)^2}\right] \tag{7}$$

If any two of the four parameters, $\xi_2 - \xi_1$, S/U_∞, n, and k, are given, the shape of the oval is determined.

Consider now a solid line segment extending from the point $(\xi_4,0)$ to the upstream stagnation point of the oval $(\xi_3,0)$ and coinciding with the ξ-axis, with $\xi_4 < 0$ and $|\xi_4| > |\xi_3|$ as shown in figure 3. The line is taken to be attached to the oval. Since the flow past the oval is symmetrical about the ξ-axis, the presence of the solid line does not disturb the flow. The transformation

$$z = A\zeta + B\sqrt{\zeta^2 - \xi_4^2} \tag{8}$$

maps the solid line segment in the ζ-plane into a portion of an ellipse in the z-plane as shown in figure 4. The semiaxes of the ellipse, which has its center coinciding with the origin of the z-coordinates, are $\xi_4 A$ and $\xi_4 B$. The semiaxis $\xi_4 A$ coincides with the x-axis and may be either major or minor. The flow past the line segment plus the Rankine oval in the ζ-plane corresponds to the flow past the ellipse with an afterbody in the z-plane, the shape of the afterbody being that of the Rankine oval transformed in accordance with equation (8). The size of the ellipse is determined by the value of ξ_4. By varying the parameters k and n, a variety of afterbody shapes are obtained. The points of attachment where the afterbody is joined to the ellipse are given by

$$x = A\xi_3 \tag{9}$$

$$y = \pm B\sqrt{\xi_4^2 - \xi_3^2} \tag{10}$$

The complex velocity in the z-plane is given by

$$-u_b + iv_b = \frac{d\omega}{dz} = \frac{d\omega}{d\zeta}\Big/\frac{dz}{d\zeta} \tag{11}$$

where $\frac{d\omega}{d\zeta}$ is given by equation (3) and

$$\frac{dz}{d\zeta} = A + \frac{B\zeta}{\sqrt{\zeta^2 - \xi_4^2}} \tag{12}$$

The computation of u_b and v_b in the z-plane from equation (11) is easily performed by first finding the values in terms of a given value of ζ, and then determining the value of z corresponding to that value of ζ obtained by use of equation (8).

The entrainment effect is simulated by placing a point sink of strength m in the z-plane at the point $(x_s, 0)$ with $x_s > \xi_4 A$. The complex velocity due to the sink in the z-plane is simply

$$-u_s + iv_s = \frac{m}{z - x_s} \tag{13}$$

where the subscript s denotes sink- or entrainment-induced velocity components.

The total velocity components due to the cylinder-afterbody blockage and the sink are given by

$$u = u_b + u_s \tag{14}$$

$$v = v_b + v_s \tag{15}$$

For a constant-total-pressure potential flow, the pressure coefficient C_p, with U_∞ assigned the value of unity for simplicity in computations, is

$$C_p = 1 - u^2 - v^2 \tag{16}$$

It is noted that the case of a circular-shaped jet exit is a special case of the above. The transformation (8) for this special case becomes, with $A = 1/2$, $B = 1/2$, and $\xi_4 = d$, the diameter of the circle,

$$z = \frac{1}{2}\left(\zeta + \sqrt{\zeta^2 - d^2}\right) \tag{17}$$

Results for a circular-shaped jet have been presented in reference 5. In the present paper, interference surface pressure fields are calculated by using the two-dimensional blockage-sink model for an elliptically shaped jet exit with a major to minor axis ratio of 3.36. This ratio is selected so that the calculated results may be compared with experimental results using jet exit configurations approximating the elliptical shapes. The experimental data were obtained in the Georgia Institute of Technology 9-foot low-speed wind tunnel. A description of the experiments is given as a part of this Proceedings, in a paper authored by H. M. McMahon and D. K. Mosher. It is noted that the experimental jet exits are not elliptical, but are slotted with a total length of 3.36 inches and a width of 1.00 inches, as shown in figure 5. In the calculations, ξ_4 is selected so that the major and minor axes of the ellipse have, respectively, the values 3.36 inches and 1.00 inches. The area of the ellipse, however, is approximately 16 percent smaller than that of the jet exit in the experiments.

Calculated pressure contours for the elliptically shaped jet with the major axis of the ellipse alined with the free-stream direction are compared with experimental results for a speed ratio of 12 using the slotted jet exit with the length of the slot oriented streamwise. Figure 6 shows this comparison, with the calculated contours shown as dashed curves and the experimental contours shown as solid curves. It is seen that, with the choice of the parameters as given on figure 6, the two sets of contours agree well with each other over a large region on the plate. The calculated surface force distribution around the jet, represented by the integrated pressure coefficient

$$C_f = \int_{R_o}^{R} C_p r \, dr \tag{18}$$

where R_o is the contour of the jet exit, is compared with experimental data in figure 7. Again, good agreement is observed.

Similar comparisons are given in figures 8 and 9 for a jet with its longer dimension perpendicular to the free-stream direction. The calculated results are for the elliptically shaped jet and the experimental data are for the slotted jet at the speed ratio of 12. Again, good agreement is observed. Results for speed ratios other than 12 were also obtained, although not presented here. In general, the calculated results, with a suitable choice of parameters, agreed reasonably with the experimental data over a large region on the plate.

In selecting numerical values for the parameters used in the calculations, available experimental contours are used as a guide. Thus the present model, like previously proposed models, requires empiricism. The calculation procedure required in the two-dimensional model, however, is sufficiently simple to permit a parametric study from which the dependence of these parameters on the jet-to-crosswind speed ratio and on the jet exit shape may be obtained. This work is presently in progress.

CONCLUDING REMARKS

The present work is motivated by a need to establish a better basic understanding of the jet interference phenomena. Attempts are therefore made to select a simple and yet physically interpretable model to represent the jet interference effects. In this regard, the two-dimensional blockage-sink representation appears to be successful. In view of the perhaps drastic simplifications introduced, the observed agreement between the calculated interference pressure field and the experimental data for noncircular as well as for circular jet exits is encouraging. Some dependence on empiricism is presently unavoidable in developing any analytical model with the hope of representing the very complex interference flow. In the present analysis, this dependence leads to the selection of the parameters n and k, which are, respectively, related to the length and width of the wake, and to the selection of m and x_s, which are related to the entrainment effects. In the calculation of the interference pressure outside of the wake-flow region, the effect of the wake blockage length does not appear to be important. This has been verified by computational results. The most pertinent parameters are therefore k, x_s, and m. The dependence of these three parameters on the jet-to-crosswind speed ratio and on the jet exit shape needs to be obtained experimentally. Preliminary results based on the parametric study using the two-dimensional model, however, lead to certain conclusions which appear to be physically reasonable. For example, the trend concerning the entrainment rate is that, with the crosswind speed held constant, the amount of crosswind fluid entrained increases with increasing jet speed. The conclusion that the entrainment takes place mainly through the

wake (ref. 7) is substantiated by the analysis in that the results with the point sink placed inside the afterbody led to better agreement with experimental data than the results with the sink placed at the center of the jet. It was also found, contrary to the indication of oil film photographs (ref. 5), that the use of a narrower wake, that is, afterbody, at higher speed ratios gives calculated results in better agreement with experimental data. This may be explained by the fact that the jet entrains a greater amount of low-energy crosswind fluid at higher speed ratios and hence delays the separation. Additional parametric studies using the two-dimensional model are in progress. It is hoped that these studies will lead to additional information enabling better predictions of interference effects and perhaps areas of experimental emphasis as well as possibilities of alleviating the adverse interference effects.

For a jet with a speed ratio significantly less than 8, three-dimensional effects are expected to be important because of the rapid deflection of the jet. The two-dimensional model described here provides a basis for the development of a more refined three-dimensional model. The extension will require the specification of a number of additional parameters, such as the variation of the entrainment rate along the jet path, the deformation of the jet, and the wake geometry along the jet path. Furthermore, experiments indicate that far downstream of the jet exit, the jet plume deforms to a kidney shape containing a pair of vortices. It is uncertain at the present time whether the effect of this vortex pair is of primary importance to the interference pressure. This question as well as the formation of and detailed flow in the wake region appear to be areas requiring further investigation.

REFERENCES

1. Wooler, P. T., Burghard, G. H., and Gallagher, J. T.: Pressure Distribution on a Rectangular Wing With a Jet Exhausting Normally Into an Airstream. J. Aircraft, vol. 4, no. 6, Nov.-Dec. 1967, pp. 537-543.

2. Wooler, P. T.: On the Flow Past a Circular Jet Exhausting at Right Angles From a Flat Plate or Wing. J. Roy. Aeronaut. Soc., vol. 71, Mar. 1967, pp. 216-218.

3. Monical, Richard E.: A Method of Representing Fan-Wing Combinations for Three-Dimensional Potential Flow Solutions. J. Aircraft, vol. 2, no. 6, Nov.-Dec. 1965, pp. 527-530.

4. Lu, Hsih-Chia: On the Surface of Discontinuity Between Two Flows Perpendicular to Each Other. Eng. Rep. 4, Nat. Tsing Hua Univ., Oct. 1948.

5. Wu, J. C., McMahon, H. M., Mosher, D. K., and Wright, M. A.: Experimental and Analytical Investigations of Jets Exhausting Into a Deflecting Stream. AIAA Paper No. 69-223, Feb. 1969.

6. Bradbury, L. J. S., and Wood, M. N.: The Static Pressure Distribution Around a Circular Jet Exhausting Normally From a Plane Wall Into an Airstream, C.P. No. 822, Brit. A.R.C., 1965.

7. McAllister, Jack Donald: A Momentum Theory for the Effects of Cross Flow on Incompressible Turbulent Jets. Ph.D. Diss., Univ. Tenn., 1968.

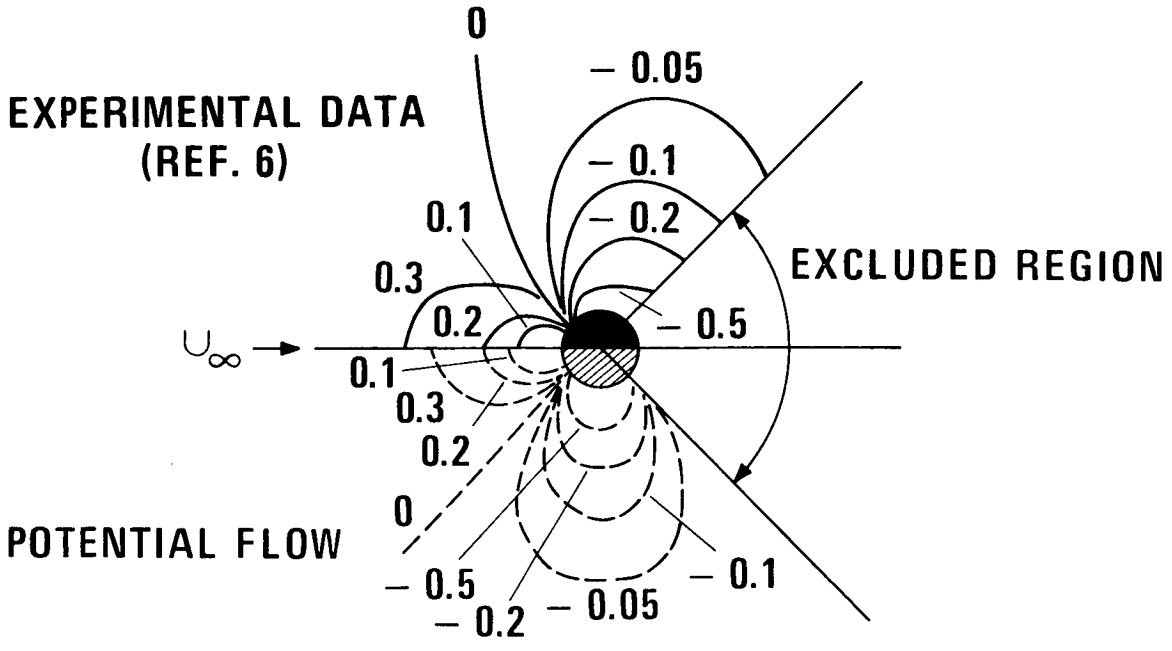

Figure 1.- Constant C_p contours around a circular cylinder.
Potential flow – circular cylinder only.

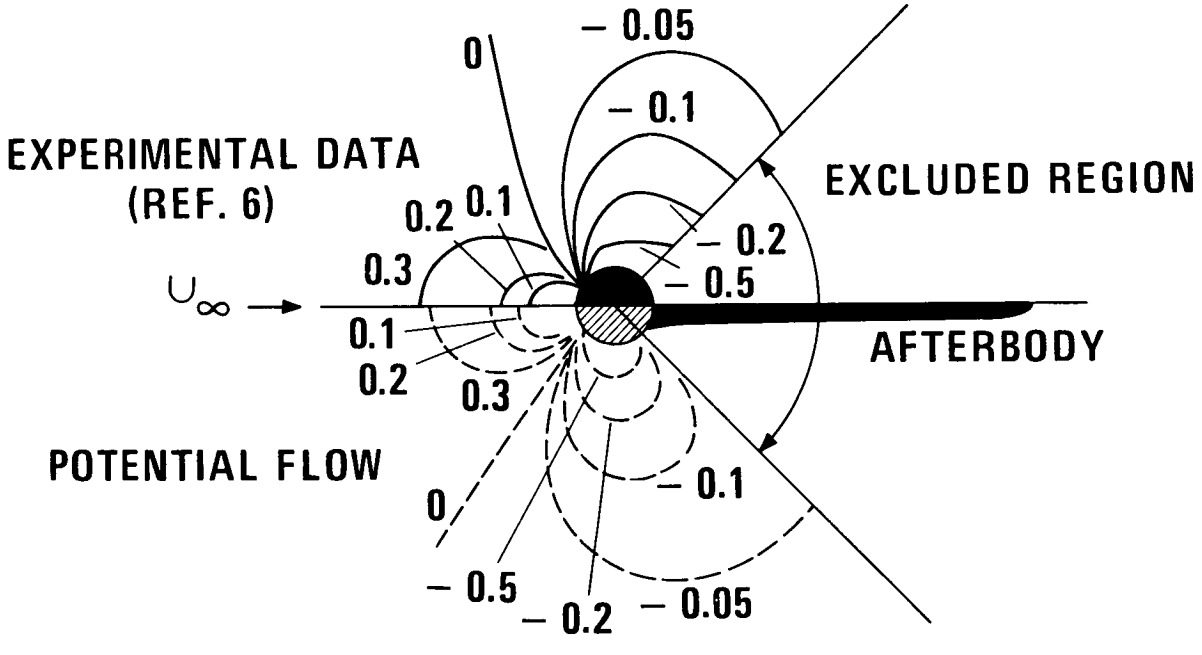

Figure 2.- Constant C_p contours around a circular cylinder.
Potential flow – circular cylinder with afterbody.

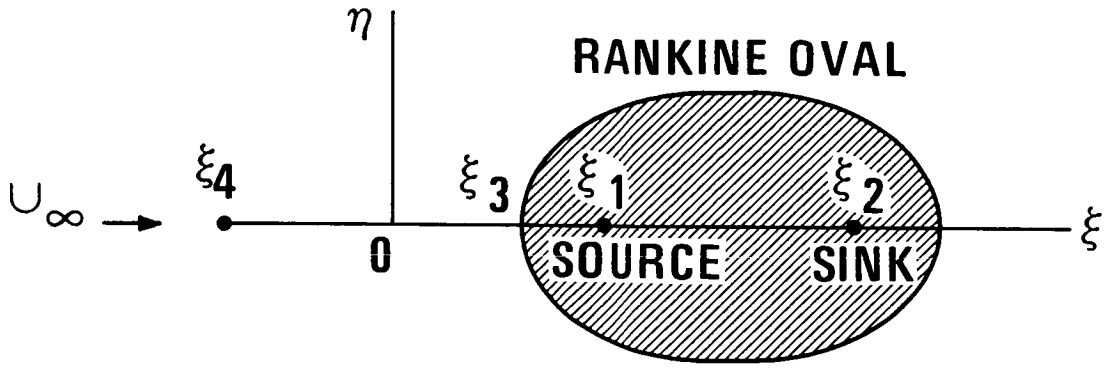

Figure 3.- The ζ-plane.

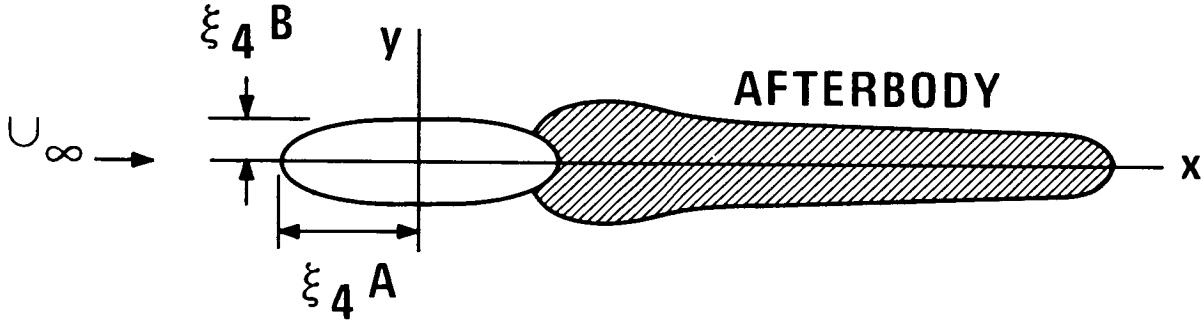

Figure 4.- The z-plane.

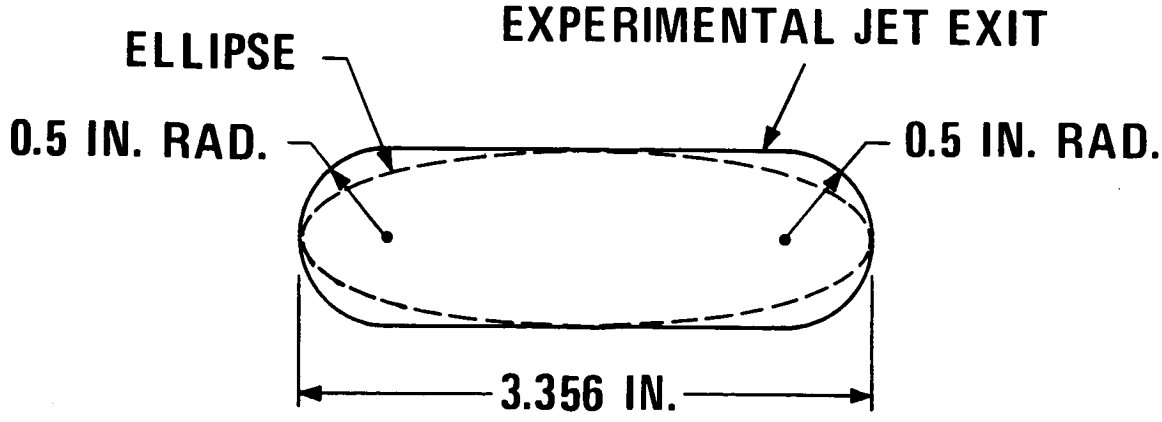

Figure 5.- Shapes of jet exit.

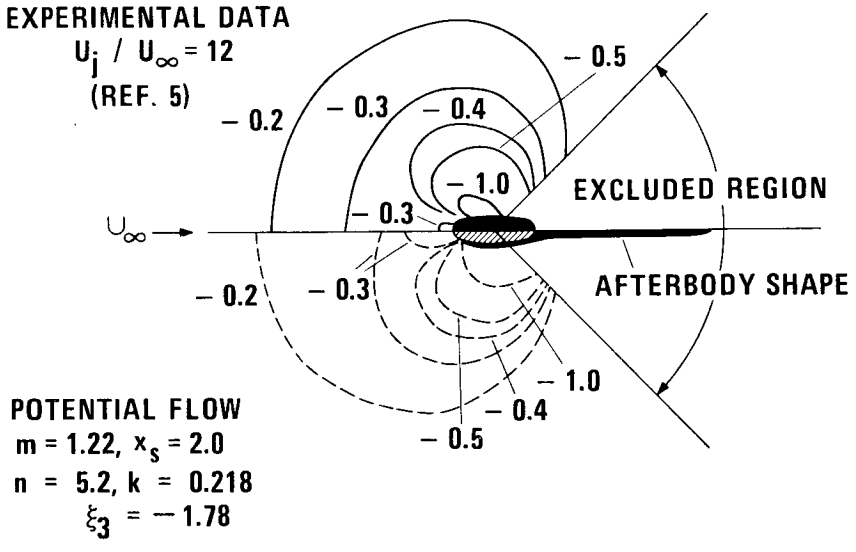

Figure 6.- Constant C_p contours around streamwise jet exit.

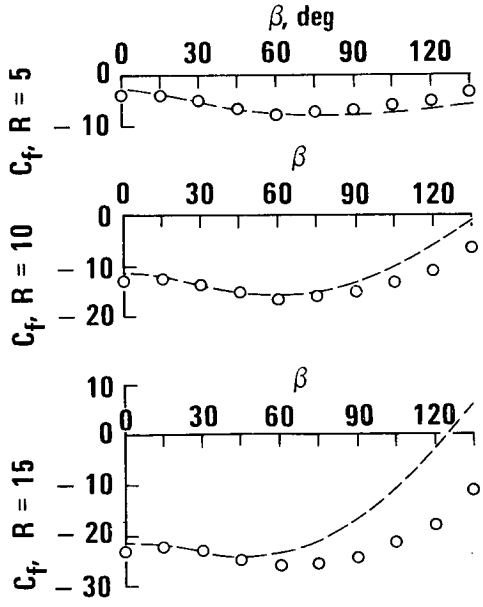

○ EXPERIMENTAL DATA, $U_j / U_\infty = 12$ (REF. 5)

– – – POTENTIAL FLOW, m = 1.22, x_s = 2.0

η = 5.2, k = 0.218, ξ_3 = – 1.78

Figure 7.- Surface force distribution around streamwise jet.

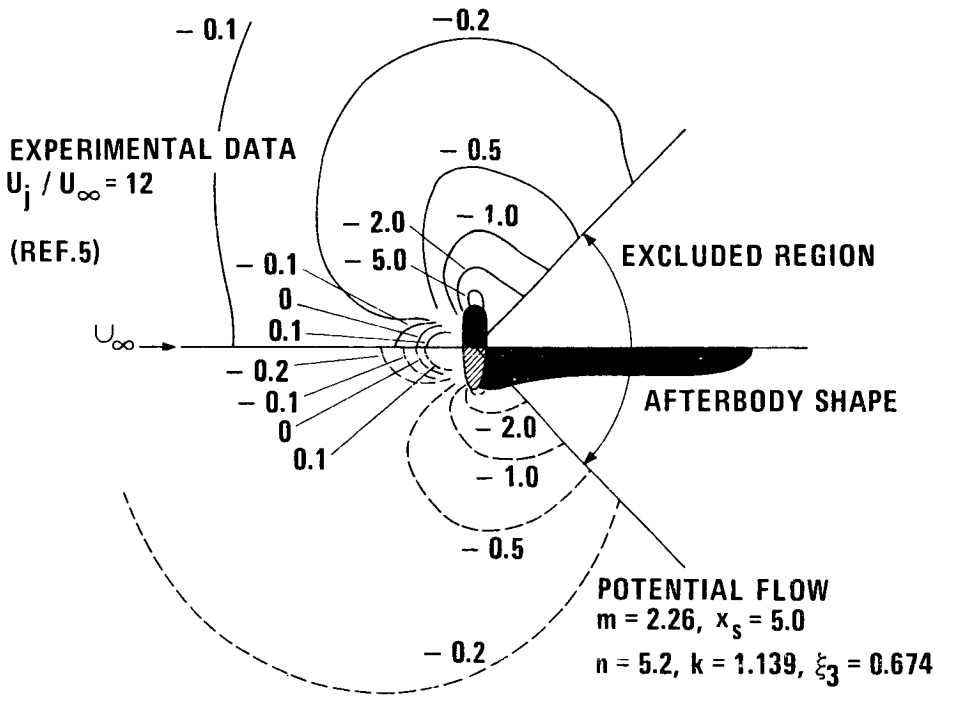

Figure 8.- Constant C_p contours around blunt jet exit.

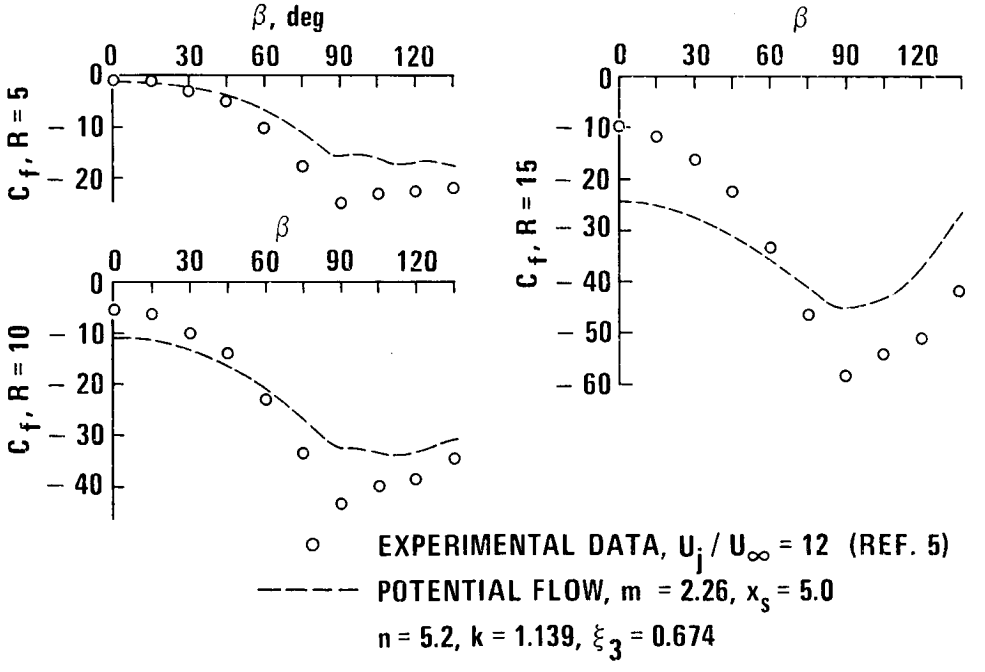

Figure 9.- Surface force distribution around blunt jet exit.

DEVELOPMENT OF AN ANALYTICAL MODEL FOR THE FLOW OF A JET INTO A SUBSONIC CROSSWIND

By P. T. Wooler

Northrop Corporation
Aircraft Division

SUMMARY

The interaction between a jet exhausting at a large angle from a surface into a subsonic crosswind is discussed. The problem of determining the position of the jet centerline is considered first. An analytical model is discussed which represents the deflecting mechanism by mainstream entrainment and a pressure force. Two methods for obtaining the jet induced velocity field are explored. The first, a vorticity model, is shown to be useful for V/STOL preliminary design. The second method, a sink-doublet model, describes the flow in more detail and is shown to predict wing surface pressure distributions which agree very well with test data.

INTRODUCTION

There is considerable interest in airplanes with the capability of taking off and landing in a short distance. One method of achieving such performance is to use lifting jets or fans, installed in the wing or fuselage of the airplane and exhausting at right angles to the direction of flight.

In the transition phase of such flight, important jet on airstream interference problems arise. It has been demonstrated experimentally that in the transition phase the jet induces an asymmetric pressure loading on the surface from which it is exhausting. The pressure loading can adversely affect the lift and pitching moment on the airplane, usually in the form of significant losses in the lift and an appreciable increase in the nose-up pitching moment. The development of a satisfactory theoretical model of this type of flow field is therefore desirable to assist in the design of V/STOL airplanes and to enable a satisfactory wind-tunnel correction method to be developed for powered-lift wind-tunnel testing.

In this paper the development of an analytical model for the flow of a jet into a subsonic crosswind is discussed. The development of a method for calculating jet centerlines is considered first and then the problem of determining the jet crossflow interference velocity field is investigated.

SYMBOLS

A_j	Jet cross-sectional area
b	Wing span
C	Circumference of jet cross section
C_D	Crossflow drag coefficient of jet
c	Wing chord (root chord for delta wing)
C_p	Pressure coefficient
d	Length of major axis in elliptical representation of jet cross section
E	Mass entrainment of mainstream fluid into jet per unit length of jet
E_1, E_2, E_3	Entrainment coefficients
K	Jet area factor, $A_j = Kd^2$
L_i, M_i	Interference lift and moment (value with jet on - value with jet off)
m	Velocity ratio, U_{jo}/U
$\bar{m}$	Sink strength of jet element
R	Local jet radius of curvature
s	Coordinate along jet centerline
S	Wing surface area
T	Thrust of jet
U	Mainstream speed
U_j	Jet speed
W	Complex velocity potential for ellipse
x, y, z	Coordinate system defined in Figure 1
x_j	x-coordinate of center of exhausting jet
ζ	Coordinate in complex plane
θ	Angle defined in Figure 1

μ Doublet strength

ρ Jet and mainstream density

Γ Jet circulation per unit length

Subscripts:

o Refers to conditions at the jet exit

i Refers to interference value (value with jet on - value with jet off)

THE JET CENTERLINE

When a jet exhausts at an angle into a crossflow, it is deflected into the crossflow direction due to the effects of viscous entrainment of the crossflow by the jet and also due to crossflow induced pressure forces on the jet boundary (Figure 1). A method for calculating jet centerlines and the jet induced velocity field has been presented in Reference 1. It is assumed in this model that the mass entrainment E of the crossflow into unit length of the jet is given by

$$E = \rho E_1 \, Ud \cos \quad + \frac{\rho E_2 (U_j - U \sin \theta) C}{1 + E_3 U \cos \theta / U_j} \tag{1}$$

It is also assumed that the pressure force on a jet element of unit length is

$$C_D \frac{1}{2} \rho U^2 \cos^2 \theta \, d \tag{2}$$

The equations of continuity and tangential momentum for the jet may then be deduced by taking U_j to be the mean jet velocity. The centrifugal force is equal to the mass of air entrained times the normal free stream velocity component plus a drag term given by equation (2). This force is equal to the rate of change of the jet momentum in a direction normal to the jet centerline.

The equations of motion for the jet development are then

$$\rho \frac{d}{ds} (A_j U_j) = E \tag{3}$$

$$\rho \frac{d}{ds} (A_j U_j^2) = EU \sin \theta \tag{4}$$

$$\frac{\rho A_j U_j^2 \frac{d^2x}{dz^2}}{\left[1 + \left(\frac{dx}{dz}\right)^2\right]^{3/2}} = \left(E + \frac{1}{2} C_D \rho U d \cos\theta\right) U \cos\theta \qquad (5)$$

To solve these equations, it is necessary to postulate the cross-sectional shape of the jet. It is assumed that the jet changes linearly from the circular cross section to an elliptical section of 4 to 1 major to minor axis ratio in a predetermined distance proportional to the initial jet diameter and to the initial jet velocity and retains this section thereafter. This assumption permits A_j to be written as a function of d, the jet major axis.

Equations (3), (4), and (5) are then a set of differential equations for the variables x, U_j, d as functions of the variable z and the parameters E_1, E_2, E_3, and C_D.

C_D is taken to be 1.8, a representative value for the drag coefficient of an ellipse. E_2 is set equal to .08 to give correlation with the data of Reference 2 for the free jet case.

The entrainment coefficients E_1, E_3 are chosen to give correlation with available test data for jet centerlines. This correlation is demonstrated in Figure 2.[1] Although the comparison in Figure 2 is for jets exhausting normally to a wall, equations (3) through (5) may be solved for other values of the angle between the jet and crossflow. A change in angle simply involves a change in the boundary conditions for the differential equations.

The differential equations (3) through (5) may be solved in closed form in the special case when $\theta \sim 0$ and the velocity ratio is not too large. For, in this case equation (1) may then be written

$$E = \rho E_1 U d \qquad (6)$$

and equations (3) through (5) reduce to

$$\rho \frac{d}{dz} (A_j U_j) = E \qquad (7)$$

$$\rho \frac{d}{dz} (A_j U_j^2) = 0 \qquad (8)$$

[1] References 3 and 4.

$$\rho A_j U_j^2 \frac{d^2x}{dz^2} = \left(E + \frac{1}{2} C_D \rho U d\right) U \tag{9}$$

If we now assume that A_j is proportional to d^2 and write

$$A_j = Kd^2 \tag{10}$$

K being a constant, then equations (7) through (9) may be integrated.

For the case in which the jet is exhausting normally into the crossflow, the following expression follows for the jet centerline

$$\frac{x}{d_o} = \frac{(2E_1 + C_D) K}{2E_1^2} \left[\exp\left(\frac{E_1}{K} \cdot \frac{z}{md_o}\right) - \frac{E_1}{K} \cdot \frac{z}{md_o} - 1 \right] \tag{11}$$

This expression has the interesting property that it implies that x/d_o is a function of z/md_o. This functional relationship is verified in Table 1 using data obtained from Reference 3.

This functional relationship has been shown to be valid for large values of m in Reference 5 where the formula

$$(x/d_o)^2 = 7 (z/md_o)^5 \tag{12}$$

was obtained for the jet centerline.

TABLE 1. TABULATION OF EXPERIMENTAL DATA (REFERENCE 3)

x/d_o	m		
	4.3	6.2	8.1
	z/md_o		
1	0.66	0.65	0.67
1.5	0.79	0.79	0.80
2	0.89	0.88	0.91
2.5	0.98	0.99	0.99
3	1.06	1.06	1.07
4	1.17	1.18	1.19
6	1.36	1.39	1.38
10	1.63	1.64	1.60

JET INDUCED VELOCITY FIELD

Jet induced interference forces and moments can be significant in a V/STOL concept and it is desirable to be able to estimate these effects. Two methods will be discussed in this paper. The first is a vorticity model which replaces the jet by a series of horseshoe vortices. The strength of the vortices are determined from the jet momentum flow and the curvature of the jet centerline.

The second model is a sink-doublet model. The sinks represent the entrainment of the crossflow fluid by the jet and the doublet represents the blockage effect of the jet on the mainstream.

VORTICITY MODEL

When the jet leaves the nozzle it is deflected into the crossflow direction and its cross section changes from its initial circular section into a kidney-type shape as illustrated in Figure 1. Two contra-rotating vortices are observed in tests involving jets in a crossflow. These vortices are observed to grow in strength as the jet is deflected further into the crossflow direction and it would appear that they ought to make an important contribution to the jet induced velocity field.

Consequently, in the vorticity model presented in Reference 6, the jet is replaced by a system of horseshoe vortices (see Figure 3). An empirical equation

$$x/d_o = .19\ m^2 \left[\cosh\left(z/.19\ m^2 d_o\right)\right] - 1 \qquad (13)$$

is used for the jet centerline. It is assumed that:

(1) The jet momentum flow $\rho A_j U_j^2$ is constant along the jet path.

(2) The force on a jet element of length δs, normal to the centerline, is equal to $\rho A_j U_j^2 \delta s/R$ where R is the local radius of curvature derived from equation (13).

(3) The mainstream flow near the jet is assumed to be along the jet path direction and to have a mean velocity equal to the undisturbed mainstream velocity U.

With these assumptions the circulation, Γ, per unit length of the jet is given by

$$\frac{\Gamma}{U} = \frac{\pi}{4} \frac{d_o}{R} \left(\frac{U_{jo}}{U} \right)^2 \tag{14}$$

Together with this jet "bound" vorticity there is a trailing vorticity which is a consequence of this "bound" vorticity. This trailing vorticity, which increases in strength as it moves from the jet exit, accounts for the eventual breaking up of the jet into a vortex pair discussed earlier.

The velocity field due to the interference of the jet on the mainstream is obtained by dividing the jet into a number of elements, the vorticity of each element being calculated from equation (14). Each element is replaced by a horseshoe vortex, the trailing arms of the horseshoe vortex being one jet diameter apart.

Calculations of the velocity field enable the jet induced velocity field on any neighboring surface to be obtained. Using a lifting surface theory for a finite wing and an image system for an infinite flat plate enables wing loadings and pressure coefficients to be derived. Figure 4 shows calculations of the pressure coefficient on a flat plate.[1] Calculations of the interference lift and moment for a delta wing are shown in Figures 5 and 6.

The vorticity model is very easy to use and is useful for obtaining the significance of the parameters involved. For example, Figure 7 shows how m and x_j/c affect the interference lift and moment for a 60 degree delta wing. Figure 8 shows the importance of the area ratio S/A_{jo}. This figure shows the variation of the interference lift with area ratio for a given jet static thrust and free stream velocity when either the jet area or wing area is kept constant.

[1] Reference 7.

SINK-DOUBLET MODEL

The sink-doublet model is a natural extension of the method for obtaining the jet centerline discussed earlier. The interference effects of the jet are accounted for by distributing sinks and doublets along the jet, as illustrated in Figure 9. The sink strengths $\bar{m}$ are made proportional to the mass of air entrained by the jet. That is

$$\bar{m} = \frac{E \delta s}{\rho d} \tag{15}$$

The doublets represent the blockage effect of the jet, and their strengths, μ, are obtained from the coefficient of the $1/\zeta$ term in the complex velocity potential expansion $W(\zeta)$ for the two-dimensional flow past an ellipse.

Thus

$$\mu = \frac{\pi U d^2}{4} \left[1 - \frac{5}{4} \frac{z}{m d_o} \right] \tag{16}$$

in the region where the jet is deforming from a circular to an elliptic section, and

$$\mu = \frac{\pi U d^2}{4} (5/8) \tag{17}$$

after the jet has achieved its final elliptic section.

The jet induced velocity field can be calculated and wing loadings can be obtained by making use of a lifting surface theory. Calculations of wing loadings using this model are shown in Figure 10 and show good correlation with test data.

The normal procedure for calculating surface pressure distributions has to be modified in the case of a wing containing a jet exhausting at an angle into a mainstream. The reason for this is that besides inducing a velocity normal to the wing, the jet also induces a velocity tangential to the wing surface which may be of the same order of magnitude as the induced velocity due to the lifting effect of the wing. Thus, although this jet induced tangential velocity has only a minor effect on the wing loading, it may cause a significant change in the surface pressure field. That there is a significant effect is illustrated in Figure 11. Figure 11 demonstrates that the loading is not distributed equally on the upper and lower surfaces, which would be the case without the effect of the jet.

Figure 12 shows the theoretical and experimental interference spanwise loading for the wing of Figure 10. The theoretical predictions are quite good although it is noticed that the tendency is to smooth out the loading which suggests that an improvement in the numerical procedure employed in the lifting surface program would improve the correlation.

CONCLUDING REMARKS

An analytical method has been developed for predicting jet centerlines for jets exhausting at right angles into a subsonic crossflow. The method calculates centerlines which are in good agreement with wind-tunnel test results. This method can be extended to include cases when the jet is exhausting into a crossflow at angles other than 90 degrees.

A vorticity method for calculating the jet interference velocity field has been discussed. Calculations for the lift and pitching moment demonstrate the usefulness of the method for undertaking a parametric study.

An alternative model which replaces the jet by a distribution of sinks and doublets is also discussed. Calculations of wing surface pressure distributions for a single jet exhausting at right angles into a crossflow indicate that this approach will also be a useful method for design purposes. This second method has the advantage that it can be extended to include jet deflection angles other than 90 degrees, multiple jets, changes in power and changes in crossflow velocity.

REFERENCES

1. Wooler, P. T., Burghart, G. H., and Gallagher, J. T., "Pressure Distribution on a Rectangular Wing With a Jet Exhausting Normally into an Airstream," Journal of Aircraft, Vol. 4, No. 6, Nov-Dec., 1967.

2. Ricou, F. P. and Spalding, D. B., "Measurement of Entrainment by Axisymmetrical Turbulent Jets," Journal of Fluid Mechanics, Vol. 11, 1961.

3. Jordinson, R., "Flow in a Jet Directed Normal to the Wind," British Aeronautical Research Council R&M 3074, 1958.

4. Keffer, J. F. and Baines, W. D., "The Round Turbulent Jet in a Cross-Wind," Journal of Fluid Mechanics, Vol. 15, 1963.

5. Wooler, P. T., "Flow of a Circular Jet Into a Cross Flow," Journal of Aircraft, Vol. 6, No. 3, May-June, 1969.

6. Wooler, P. T., "On the Flow Past a Circular Jet Exhausting at Right Angles From a Flat Plate or Wing," Journal of the Royal Aeronautical Society, Vol. 71, March 1967.

7. Bradbury, L. J. S. and Wood, M. N., "The Static Pressure Distribution Around a Circular Jet Exhausting Normally from a Plane Wall Into an Airstream," C. P. No. 822, British Aeronautical Research Council, 1965.

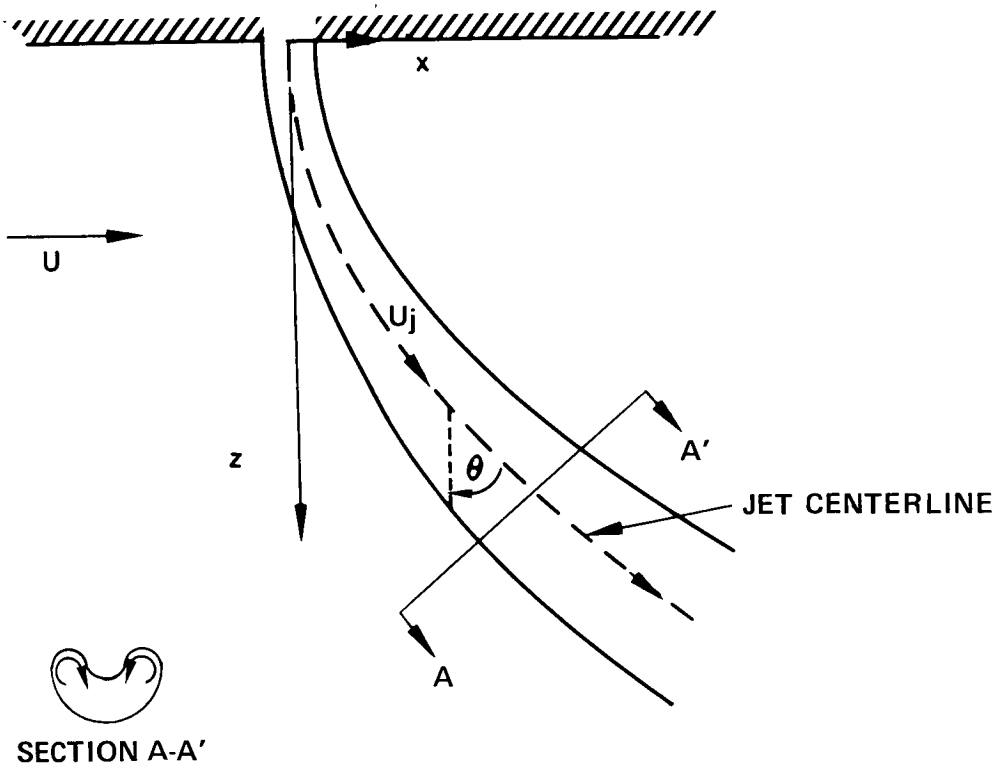

Figure 1.- Diagram of jet exhausting into a crossflow.

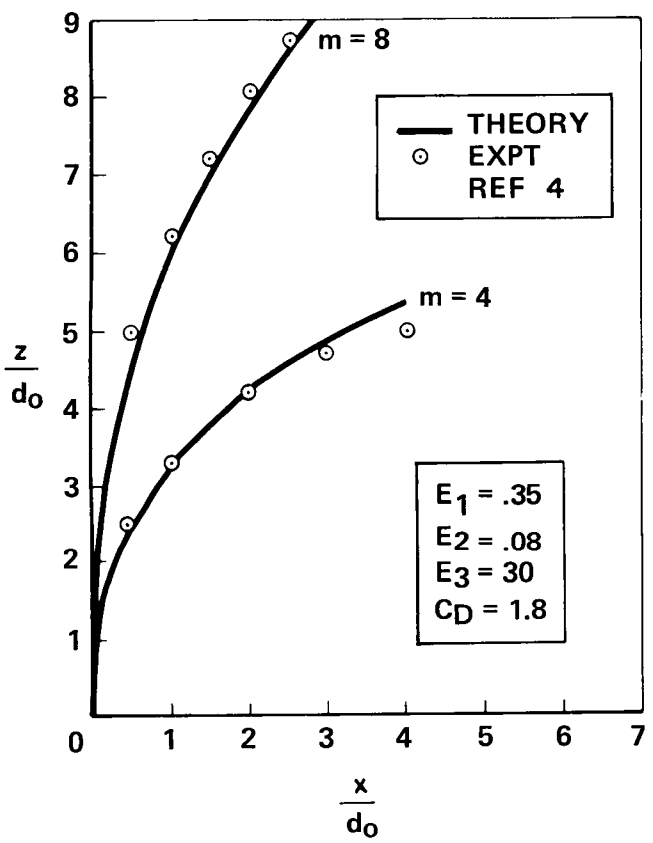

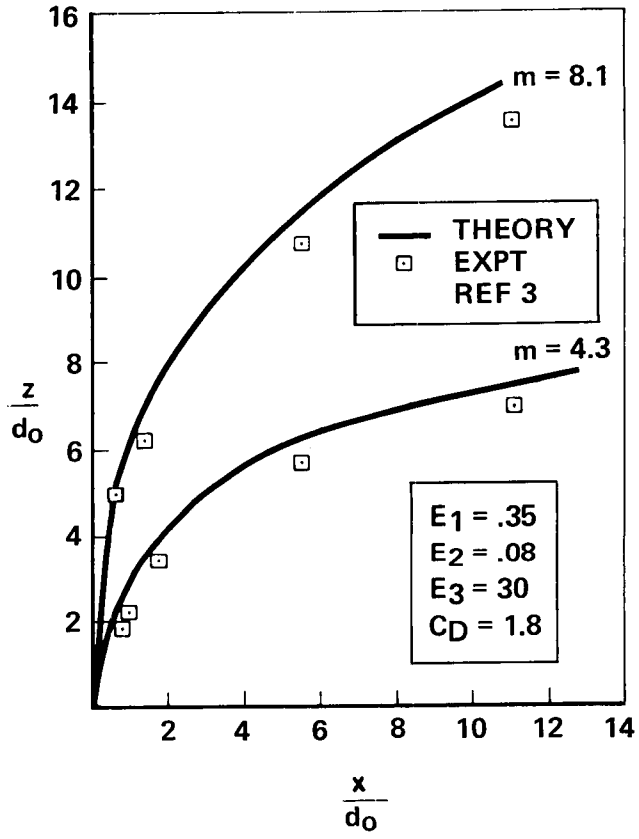

Figure 2.- Correlation of entrainment coefficients with test data for jet centerlines.

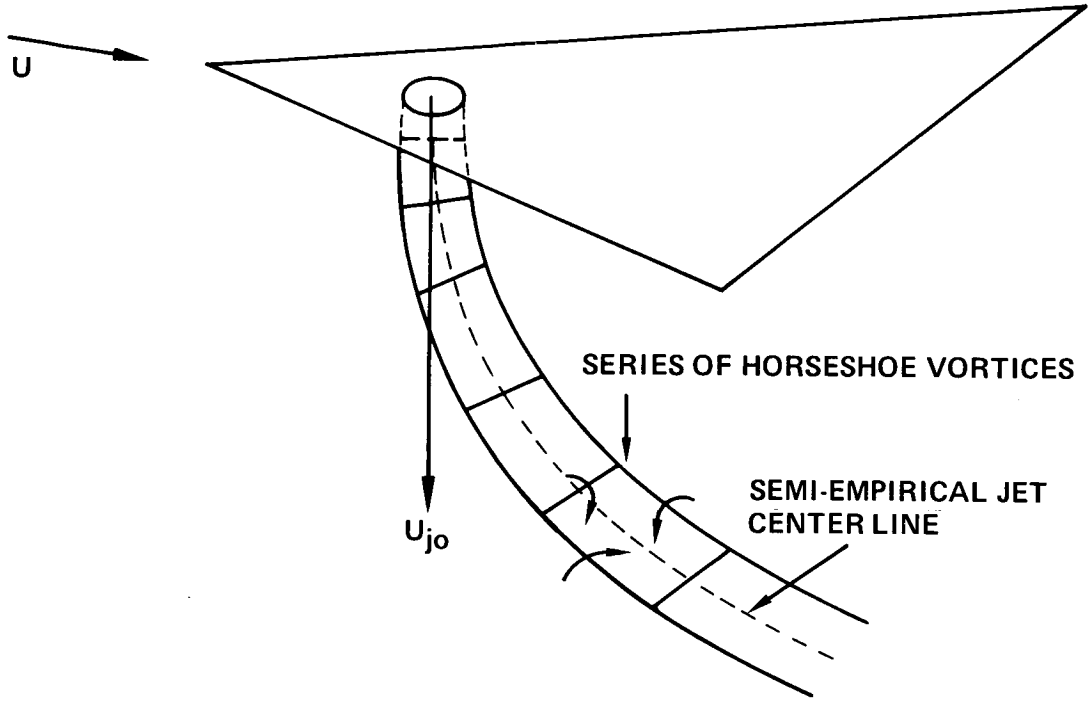

Figure 3.- Diagram of vortex sheet model.

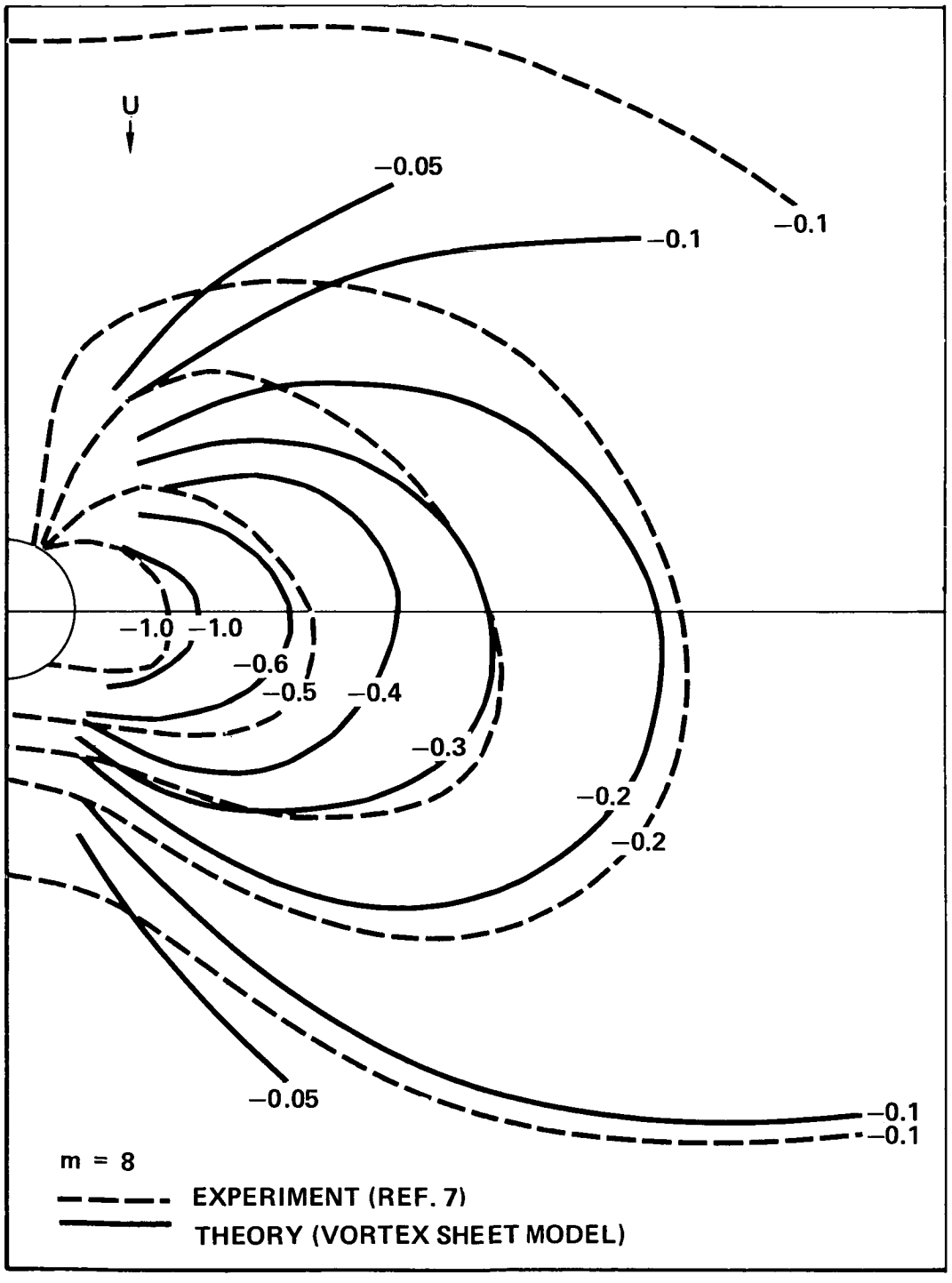

Figure 4.- Pressure coefficient on a flat plate.

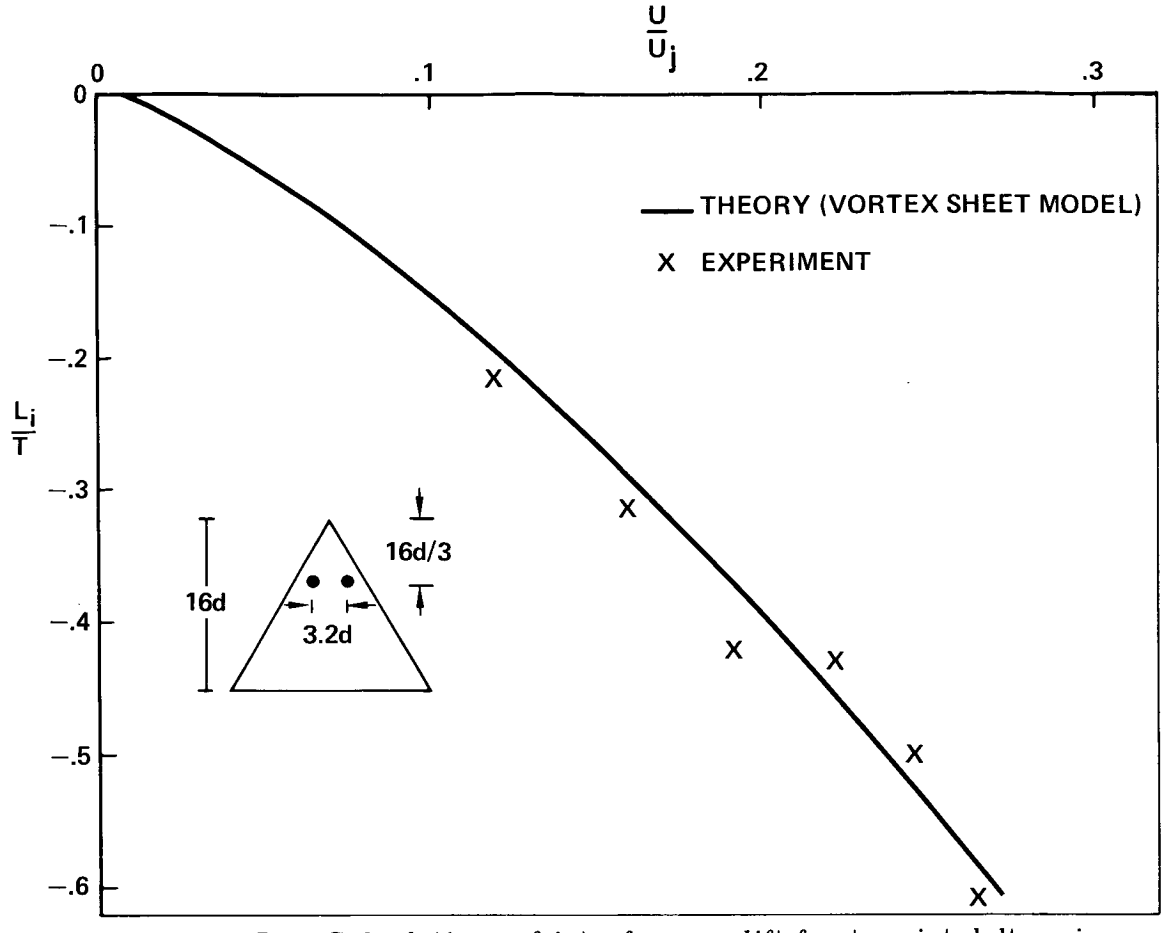

Figure 5.- Calculations of interference lift for two-jet delta-wing configuration.

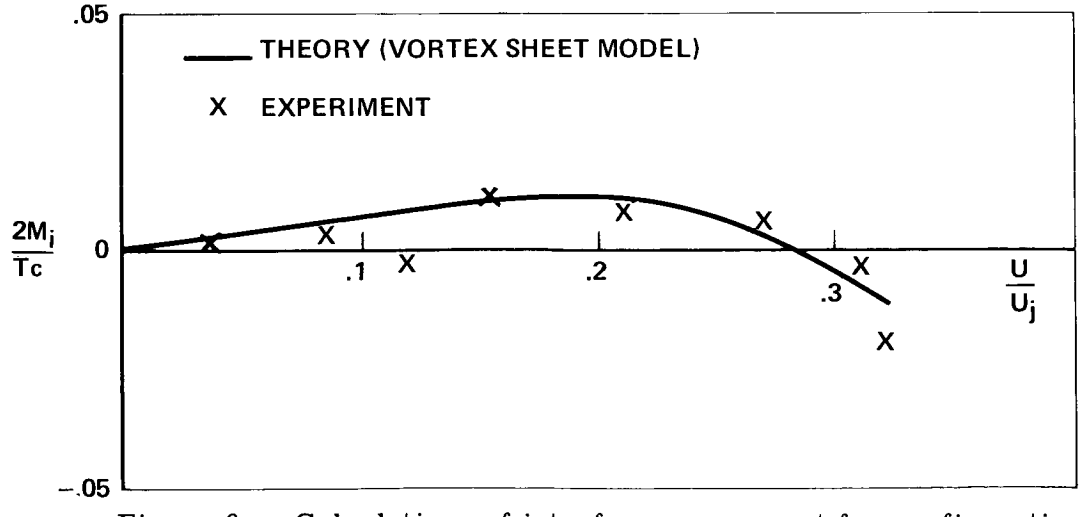

Figure 6.- Calculations of interference moment for configuration in Figure 5.

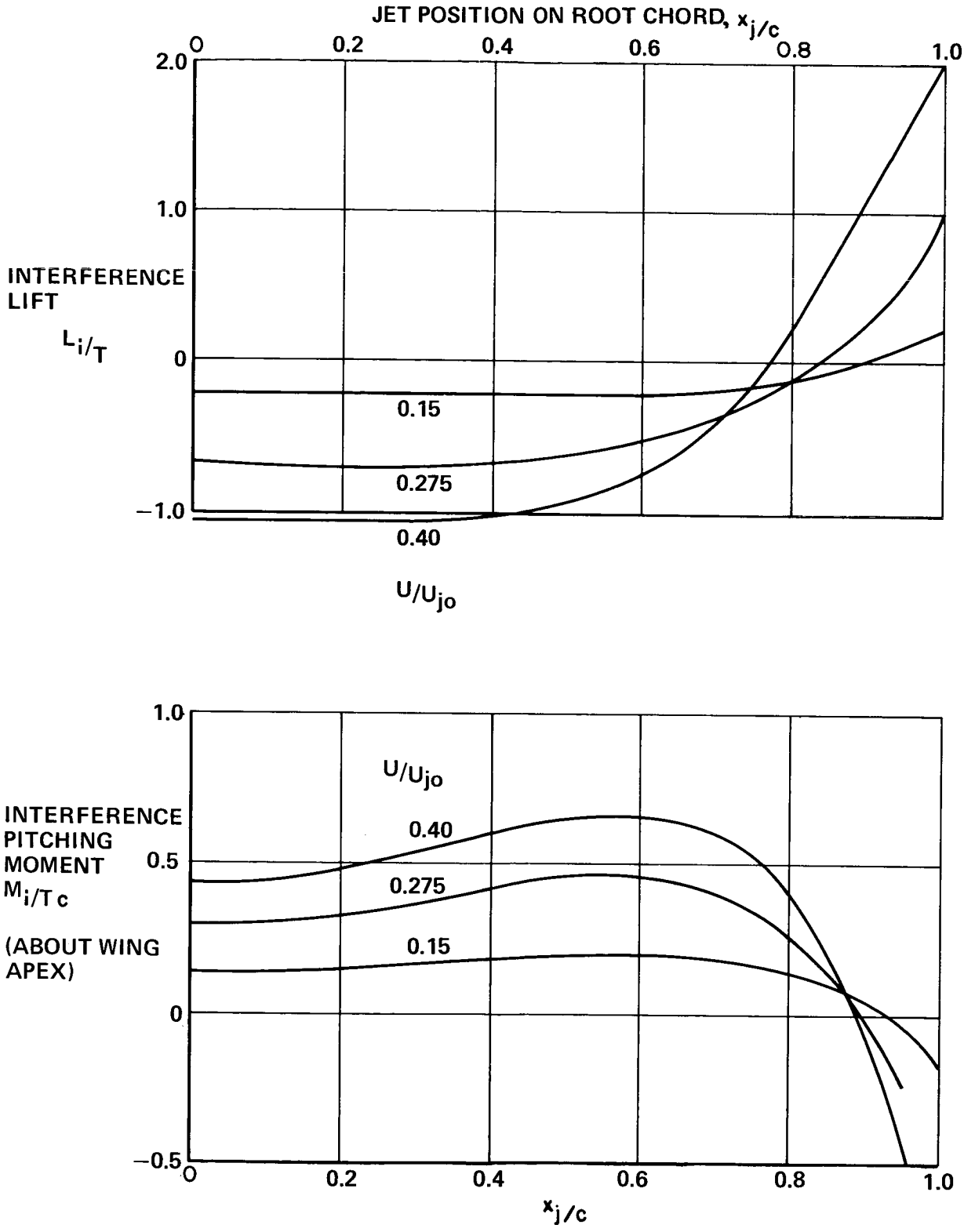

Figure 7.- Effect of velocity ratio and jet position on interference lift and moment for a 60 degree delta wing.

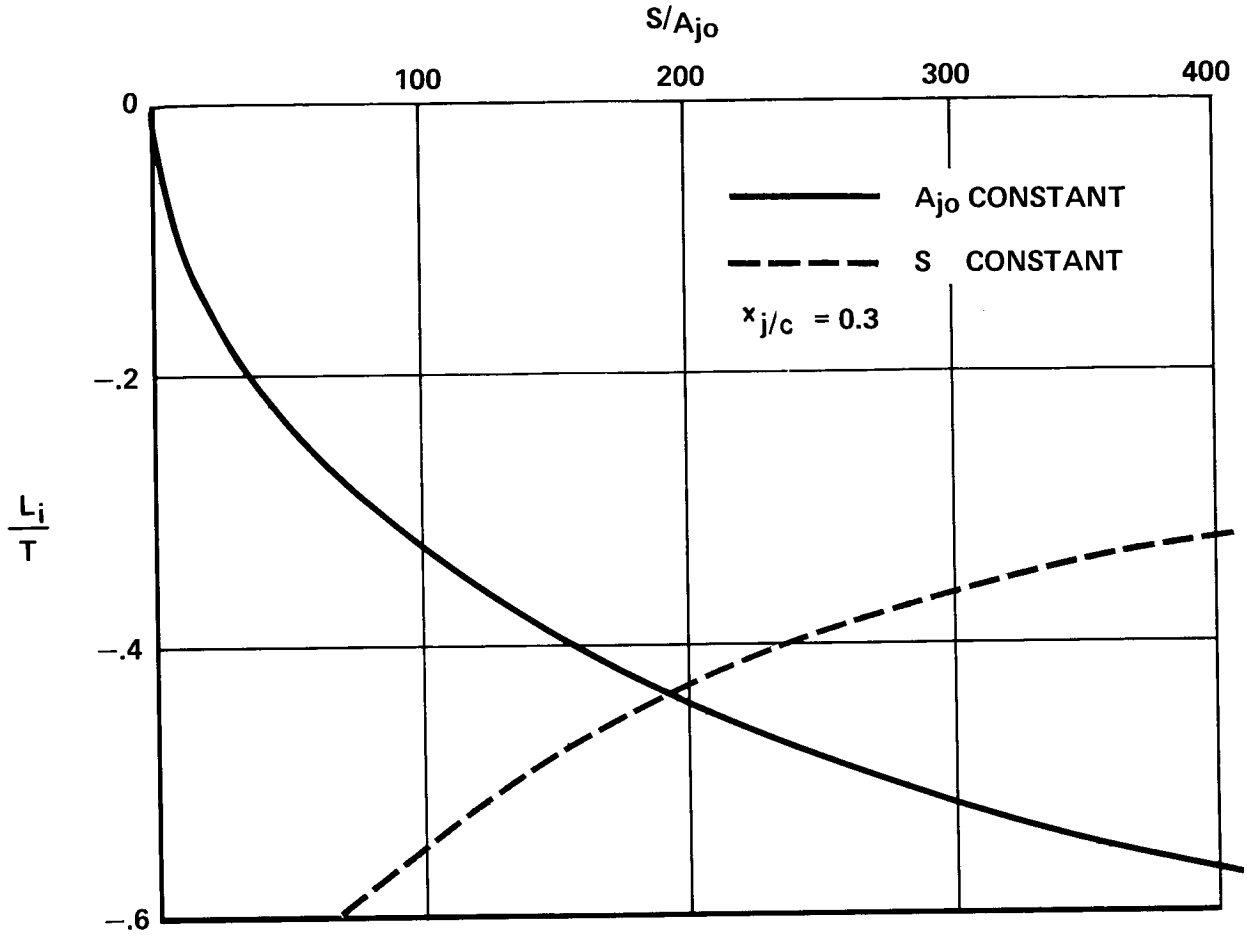

Figure 8.- Effect of area ratio on interference lift.

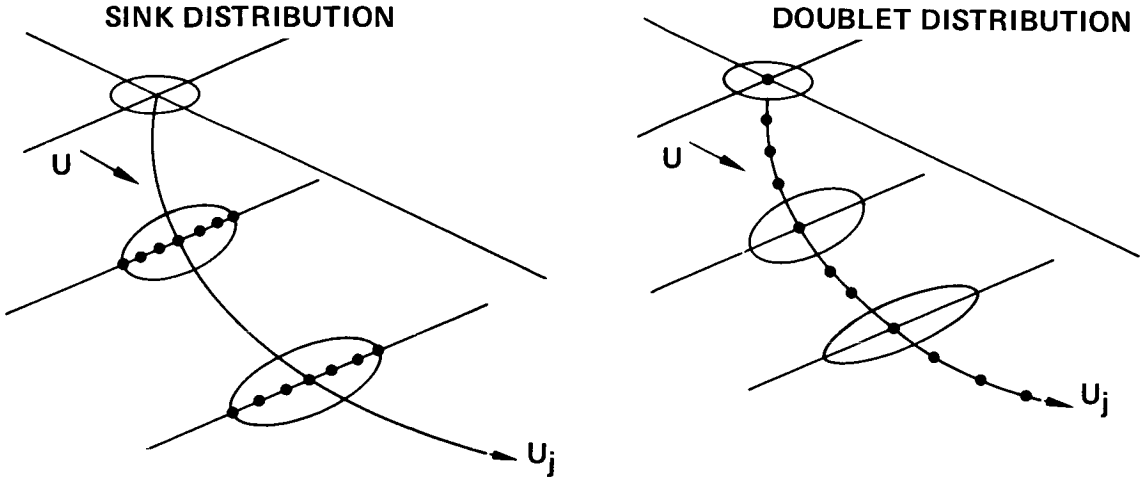

Figure 9.- Distribution of sinks and doublets along jet path.

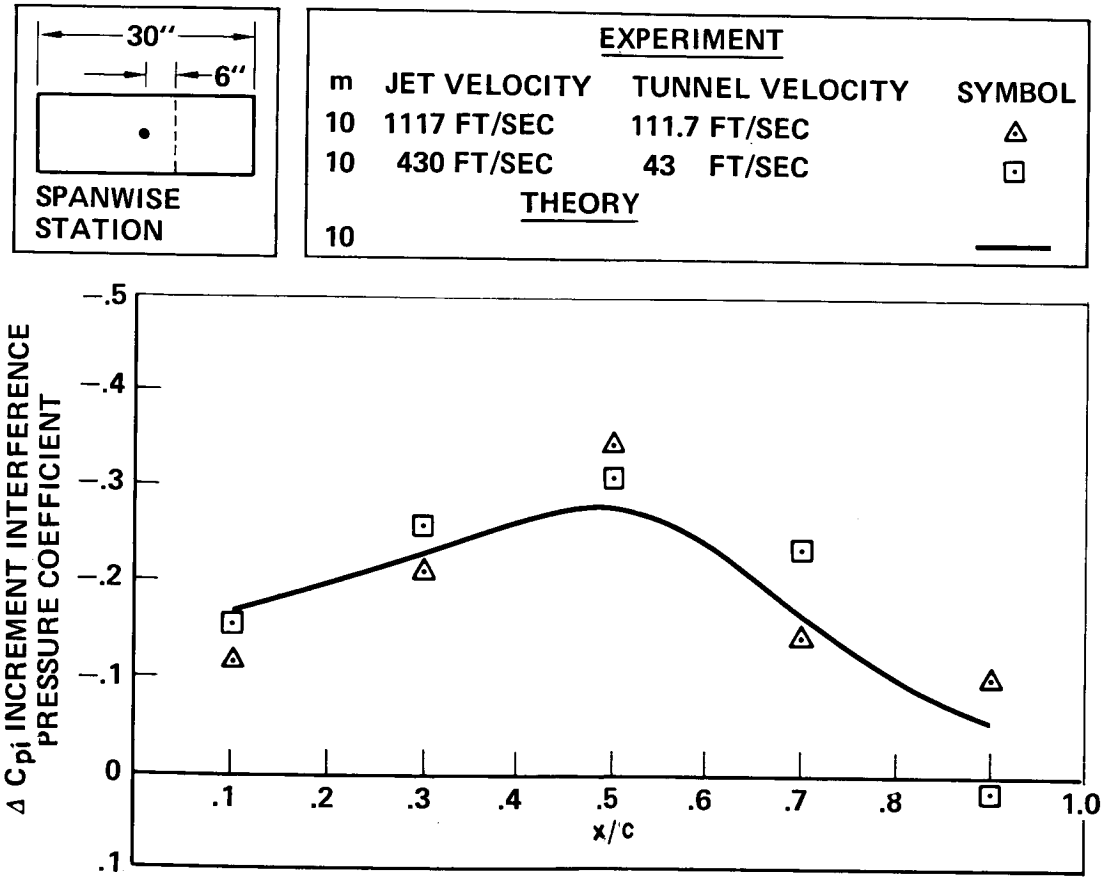

Figure 10.- Correlation of theoretical and experimental data for wing loading.

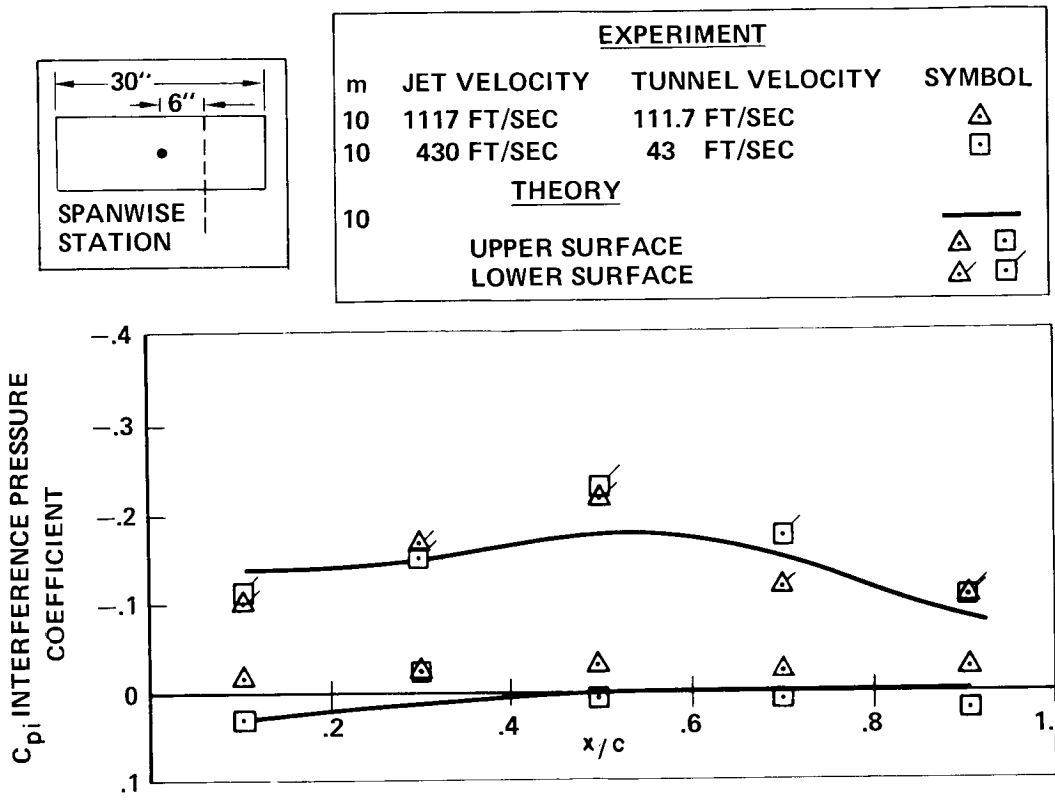

Figure 11.- Interference pressure distribution on wing surface.

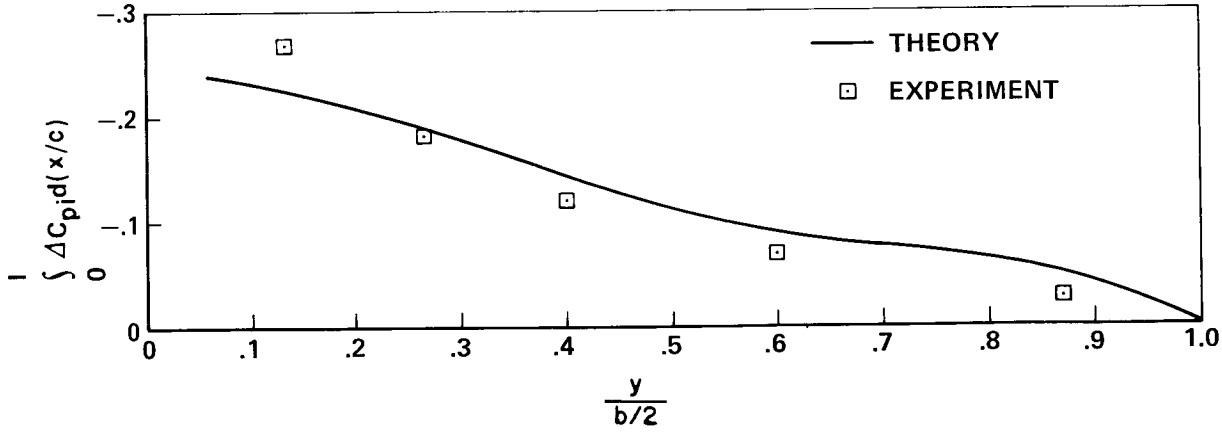

Figure 12.- Theoretical and experimental interference spanwise loading.

NUMERICAL TREATMENT OF LINE SINGULARITIES FOR MODELLING A JET IN A LOW-SPEED CROSS FLOW*

J. G. Skifstad

School of Mechanical Engineering
Purdue University
Lafayette, Indiana

SUMMARY

A simple analytical model for the jet in a low-speed cross flow, comprising two contra-rotating line vortices and a line sink, is described. The numerical formulation of the nonlinear problem and an iterative procedure for its solution are discussed. Means for achieving a more complete analysis by modifying the simple model are considered.

INTRODUCTION

The aerodynamic design of VTOL aircraft would benefit greatly from improved means for determining the aerodynamic influence of the lift jets under widely varying conditions. Reliable theories would offer highly useful means for that purpose and would serve to complement the experimental data. Unfortunately, the theoretical problem is essentially nonlinear. Aside from that inconvenience, the problem cannot be accurately formulated in a strict sense because the turbulent transport properties for three-dimensional free shear layers may only be roughly estimated at best. Experience with semi-empirical theories has shown that reasonable and occasionally accurate results may be obtained with rather rough analytical models of the jet (ref. 1). It may be anticipated, then, that approximate theoretical models of the jet interaction may be sufficiently accurate and reliable for some aerodynamic purposes. The principal concern in this context is the characterization of the aerodynamic effects of the jet rather than the structure of the jet proper.

The object of the study discussed in this paper was to formulate and examine the numerical properties of an analytical model of the jet interaction problem, subject to the conditions:

*This study comprises part of the activity sponsored by the NASA Langley Research Center under Grant No. NGR 15-005-094, initiated in February 1969.

(a) the model should include the principal dynamical aspects of the coupling between the jet and the aerodynamic field,

(b) the initial model should be as simple as possible, but should lend itself to more complete representations without major changes in the basic formulation, and

(c) there should be the capability to extend the analysis to include multiple jets without major changes in the formulation.

As indicated in item (b), the initial model was chosen to be as simple as possible, while retaining the dynamical aspects of the problem judged to be of primary significance. The emphasis was to examine the numerical behavior of nonlinear iterative schemes applied to the solution without the burden of a more sophisticated representation of the jet.

SYMBOLS

A	cross-sectional area of the jet
D	diameter of the jet nozzle
F	force acting on the jet
h	$\lvert\bar{t} \times \bar{r}\rvert$
I_1, I_2	factors in the integrations for the induced velocity
M	local integrated momentum flux of the jet
m	local mass flow rate of the jet
$\bar{n}$	unit vector normal to the jet trajectory
R	radius of curvature of the jet trajectory
$\bar{r}, r$	vector between a field point and a source point and its magnitude, respectively (see Fig. 3)
s	distance along the jet
$\bar{t}$	unit vector tangent to the line singularity
U	free-stream velocity
V	local velocity in the jet
$\bar{v}$	vector velocity at a point on one of the line singularities
x, y, z	Cartesian coordinates of the line singularities

Greek Symbols

β	U/V_o
Γ	circulation of the line vortex
κ	factor in the expression for the flow area of the jet
ρ	mass density of air
σ	strength of the sink singularity per unit length

Subscripts

n	normal to the jet trajectory
o	evaluated at the nozzle exit plane
s	associated with the sink singularity
v	associated with the line vortex
x,y,z	component in the indicated coordinate direction

ANALYTICAL MODEL OF THE JET

The simplified analytical model of a single jet chosen for the initial computations comprised a pair of contra-rotating streamwise line vortices and a line sink positioned midway between the line vortices. Figure 1 illustrates the arrangement of the singularities and the coordinate system for the computations. For a single jet as shown in Fig. 1, the two segments of the curves, $x,y > 0$ for the sink, and $x,y,z > 0$ for the line vortex, are regarded as independent, the other elements of the curves being related to them by symmetry.

The strengths of the line vortices were presumed constant and known. The ratio $\beta = U/V_o$ was also assumed to be given. The positions of the curves in space and the distribution of the sink strength along the central curve were to be determined in the solution.

Continuity within the jet flow was simply treated in this initial model by relating the local flow rate in the jet to an area arbitrarily assumed to be proportional to the square of the spacing between the line vortices. That is, a certain similarity of the cross-sectional shape of the jet at different streamwise positions was assumed (see ref. 2). Thus, if

$$A/A_o = 1 + \kappa(z^2/z_o^2 - 1)$$

then, since

$$m/m_o = \left(\frac{A}{A_o}\,\frac{M}{M_o}\right)^{\frac{1}{2}} = 1 + 16\beta \int_o^{s/D} \frac{\sigma}{DU}\, d(s/D)$$

one has finally

$$\int_o^{s/D} \frac{\sigma}{DU}\, d(s/D) = \frac{1}{16\beta}\left(\left\{\left[1 + \kappa\left(\frac{z^2}{z_o^2} - 1\right)\right]\frac{M}{M_o}\right\}^{\frac{1}{2}} - 1\right) \tag{1}$$

The entrainment of mass per unit length is given by $4\pi\rho\sigma$.

The line vortices were regarded as free streamlines in the tangent plane of the jet; that is, they were considered free to establish equilibrium positions in the z-direction, such that

$$(\bar{v} \times \bar{t})_z = 0 \tag{2}$$

along each curve.

The integrated streamwise momentum flux in the jet was approximately treated by assuming it to be related to the entrainment of mass in the jet according to the expression

$$\frac{dM}{ds} = Ut_x \frac{dm}{ds}$$

The latter may be rewritten in integrated form as

$$\frac{M}{M_o} = 1 + 16\beta^2 \int_o^{s/D} \frac{\sigma}{DU} t_x\, d(s/D) \tag{3}$$

Finally, the force per unit length of the jet acting normal to it was related to the integrated streamwise momentum flux of the jet and its radius of curvature.

$$F_n = \frac{M}{R} \tag{4}$$

The force F_n was evaluated as the sum of the forces per unit length acting on the three line singularities at any given position along the jet. For the sink singularity (ref. 3) one has

$$F_{ns} = 4\pi\rho\sigma\bar{v}\cdot\bar{n} \tag{5}$$

and for the line vortices (ref. 3) the expression is

$$F_{nv} = 2\rho\Gamma(\bar{v} \times \bar{t})\cdot\bar{n} \tag{6}$$

Combining Eqs. (4), (5), and (6), and solving for R/D yields

$$\frac{R}{D} = (M/M_o)\Big/16\beta^2 \left[\frac{-\sigma}{DU}\frac{\bar{v}}{U} + \frac{\Gamma}{2\pi DU}\left(\frac{\bar{v}}{U} \times \bar{t}\right)\right] \cdot \bar{n} \tag{7}$$

The x and y coordinates of the jet trajectory may be expressed (ref. 4) in terms of R as

$$\left.\begin{aligned} x &= \int_0^s \left[\sin \int_0^s ds'/R(s')\right] ds \\ y &= \int_0^s \left[\cos \int_0^s ds'/R(s')\right] ds \end{aligned}\right\} \tag{8}$$

Equations (1), (2), (3), (7), and (8) are to be satisfied by x,y,z, and σ at each position s along the jet. The velocity $\bar{v}$ in Eqs. (2) and (7) may be expressed (ref. 5) in terms of the geometry and σ as

$$\bar{v} = \bar{U} + \frac{\Gamma}{4\pi}\underbrace{\oint \frac{d\bar{s} \times \bar{r}}{r^3}}_{\substack{\text{line}\\ \text{vortices}}} - \underbrace{\oint \frac{\sigma\bar{r}}{r^3} ds}_{\substack{\text{sink}\\ \text{line}}} \tag{9}$$

The analytical model as described above is not considered to be complete in the sense that a number of unnecessary, but expedient approximations are involved. As noted in the introduction, the object of this initial study was to examine the numerical properties of the problem, and the model described did include what were considered to be the principal factors having a bearing on the numerical problem. A more exact representation of the problem may be prepared without introducing significant changes in the numerical scheme. Furthermore, the model could rather simply be extended to include several jets.

The aerodynamic shape of the jet provided even by this simplified model is not unlike that observed. For example, the streamlines in a plane cutting the jet near its origin appear as shown schematically in Fig. 2. The wake of the jet is, of course, entirely neglected by the model in its initial form.

It may be noted that if Γ/DU in Eq. (7) is a constant, as might be anticipated, the formulation of the problem in non-dimensional terms, indicated in the format of the equations, yields solutions with the single parameter β.

NUMERICAL FORMULATION

While the line singularities extend to infinity in the analytical model, the numerical treatment requires approximating the lines by finite line elements, introducing some degree of error. The computational scheme represented each of the two independent curves (the sink and one of the vortices) by 40 points equally spaced along the line. A straight line element tangent to the end of each line was found adequate as an "end correction," compensating for the truncation of the theoretically infinite line. The computational scheme adopted proceeded as follows.

Initial Trajectory of the Jet

A trial set of points representing the two curves was first chosen to start the computations. Each curve was represented by an even number of sequentially numbered points, not counting the point on each curve in the x-y plane. Local interpolation parabolas were determined for sets of 3 points centered at each of the odd-numbered points along a given line singularity. The length of each segment was then computed, the total length of each curve was determined by summing the lengths of the segments, and the increment Δs required for equally spaced points was computed. A new set of points, equally spaced along the initial trial curve, was finally determined as starting data.

Smoothing has been found to be a necessary part of the computational scheme to prevent the development of unstable irregularities in the curves, particularly following an iterative change in the locus of a curve, but also in the initial trial data. A seven-point cubic smoothing routine (ref. 6) was employed to smooth the values. The seven-point cubic routine has been found to work well with the functions considered; higher difference smoothing has been found to be too severe in some circumstances.

Following the smoothing operation, the trial point sets were re-entered as initial data, and the above procedures were repeated, except for the smoothing. In addition, the local length of each curve at all points, together with the components of the tangent and normal vectors, were computed.

A trial distribution for σ (s) was chosen along with the initial coordinate data. Those values were also conditioned and smoothed, as discussed for the point sets.

Computation of the Velocity Induced at Points Along Each Singularity

The velocity induced at a point on one of the line singularities may be determined according to Eq. (9), which involves summing the line integrals over all of the singularities present, including, of course, the images of the curves considered in the initial trial point sets as shown in Fig. 1. For a given "field" point, the integrals were treated numerically by approximating a line element about a "source" point by a straight line segment of length Δs, tangent

to the singularity curve, as illustrated in Fig. 3, and summing over all of the points on the singularities. For a vortex line segment, one has

$$\int_{s-\Delta s/2}^{s+\Delta s/2} \frac{d\bar{s} \times \bar{r}}{r^3} = \frac{\bar{t} \times \bar{r}}{h^2} I_1$$

where $h = |\bar{t} \times \bar{r}|$, and

$$I_1 = \frac{\bar{t}\cdot\bar{r} + \Delta s/2}{[h^2 + (\bar{t}\cdot\bar{r} + \Delta s/2)^2]^{\frac{1}{2}}} - \frac{\bar{t}\cdot\bar{r} - \Delta s/2}{[h^2 + (\bar{t}\cdot\bar{r} - \Delta s/2)^2]^{\frac{1}{2}}}$$

For a sink singularity, the expression is

$$-\sigma \int_{s-\Delta s/2}^{s+\Delta s/2} \bar{r} ds/r^3 = -\frac{\sigma I_1 (\bar{t} \times \bar{r}) \times \bar{t}}{h^2} + \sigma I_2 \bar{t}$$

where $I_2 = \frac{1}{|\bar{t}\cdot\bar{r} + \Delta s/2|} - \frac{1}{|\bar{t}\cdot\bar{r} - \Delta s/2|}$

In the computational arrangement, the contributions of a line segment about a "source" point and those of its images were computed simultaneously employing symmetry relations for the local properties of the curves.

Iteration Procedures for Adjusting the Positions of the Curves and the Sink Strength Distribution

Before proceeding with the iterations, the free-stream velocity, U, was adjusted slightly to ensure that the line vortices at their intersection with the x-z plane remained stationary. That option was chosen for the initial computations over the alternative of changing the initial positions of the vortices at that point. The change required in U was generally rather small and did not tend to affect the iteration procedure adversely. The x-components of all computed velocities were adjusted accordingly.

The first step in the iteration procedure was to allow the line vortices to assume their equilibrium positions in the z-direction, corresponding to the trial coordinates (x,y) of the jet trajectory. That is, the condition given by Eq. (2) was to be satisfied at all points on the line vortex. For rough computations it was found that the approximation obtained by taking the equilibrium separation of a pair of infinite, parallel, rectilinear vortices tangent to the jet at each point was quite reliable. For further refinement, changes in the z-coordinate were taken proportional to $(\bar{v} \times \bar{t})_z$. The predicted corrections were smoothed using the 7-point cubic smoothing routine. Between iterations the adjusted point sets were conditioned as described for the initial data, but without further smoothing.

When the condition (2) was satisfied to within an acceptable error, the variation of the integrated streamwise momentum flux in the jet was determined by numerically integrating Eq. (3). Given those values, the continuity expression for the flow in the jet, Eq. (1), yielded the variation of σ with distance along the jet. A differentiation expression based on five-point Lagrangian interpolation (ref. 6) was employed for the computations.

Following the determination of the new σ values, the entire procedure was repeated until the condition that the vortex lines assume their equilibrium positions was again satisfied, Eq. (2). That normally required no further iteration because their positions in the z-direction were rather insensitive to the sink strength.

Finally, Eq. (7) was employed to compute the distribution of R along the jet. Through Eqs. (8) a projected trajectory for the jet could be determined corresponding to the computed R variation. Unfortunately, no straightforward or reliable iteration scheme for adjusting the position (x,y) of the jet trajectory could be established without some experience with the behavior of the functions involved. The evidence indicated that a conventional Newton-Raphson technique would not be likely to be successful in projecting the coordinate positions. Rather, it was determined that efforts should be concentrated on changing the R(s) variation iteratively. While a completely satisfactory iteration scheme was not established, a refinement of the following scheme appeared likely to be acceptable. The technique adjusted the local radius of curvature proportional to the negative of the difference between the predicted value and the value for the trial curve. That is, if the predicted local radius of curvature was larger than that of the trial curve, the local value was lowered in the succeeding iteration. Sample computations following such a procedure are illustrated in Fig. 4. Figure 4b also shows the variation of σ and the position of the line vortex corresponding to iteration (B) of Fig. 4a. These results merely show the trends in the computations and do not necessarily reflect the final values of the solution. It might be mentioned that trajectories have been computed appearing to agree much more closely with the trial values, but differing more in the local R(s) variation than those shown in Fig. 4.

DISCUSSION

The numerical formulation of the problem adopted appears to be accurate and acceptable. Further alterations of the iteration procedure may be desirable, although the starting curves chosen for the computations were not close to the solution positions, and better initial estimates should improve the performance of the iteration technique.

Extensions of the analysis to yield a more complete description of the problem center on improving the characterization of the jet. Given the aerodynamic field around the jet from the simple model, it is possible to more accurately determine the entrained momentum flux, pressure variations around the surface of the jet, and so forth. The effects of the wake of the jet probably should also be added (ref. 1), accounting for a shedding of streamwise vorticity from the jet and changes in the strengths of the vortices associated with the jet proper.

Further computations should indicate what degree of approximation of the problem is necessary for aerodynamic purposes.

REFERENCES

1. Skifstad, J. G., "Aerodynamics of Jets Pertinent to VTOL Aircraft," AFAPL-TR-69-28, March, 1969.

2. Keffer, J. F., and Baines, W. D., "The Round Turbulent Jet in a Cross-Wind," J. Fluid Mech., Vol. 15, 1963, pp. 481-497.

3. Munk, M. M., "Fluid Mechanics, Part II," Division C, Vol. I of Aerodynamic Theory, ed. by W. F. Durand, Dover Publ., N. Y., 1963, pp. 259 ff.

4. Lass, H., Vector and Tensor Analysis, McGraw-Hill Book Co., N. Y., 1950, Chap. 3.

5. Milne-Thomson, L. M., Theoretical Hydrodynamics, Macmillan Co., 1968, pp. 572-3.

6. Hildebrand, F. B., Introduction to Numerical Analysis, McGraw-Hill Book Co., N. Y., 1956, pp. 296, 82.

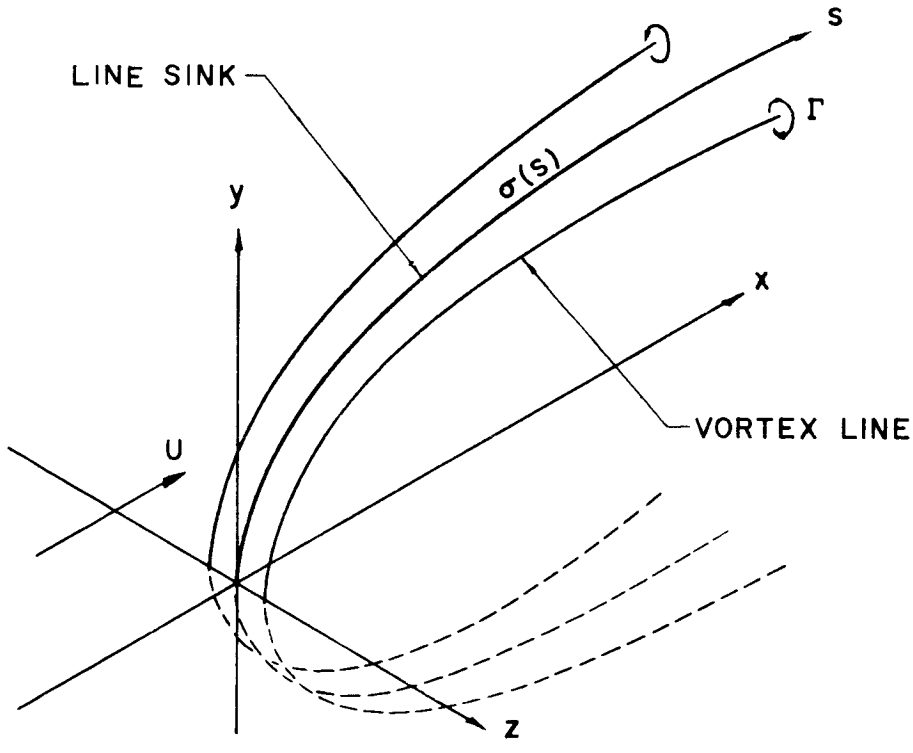

Figure 1.- Arrangement of the line singularities for the model.

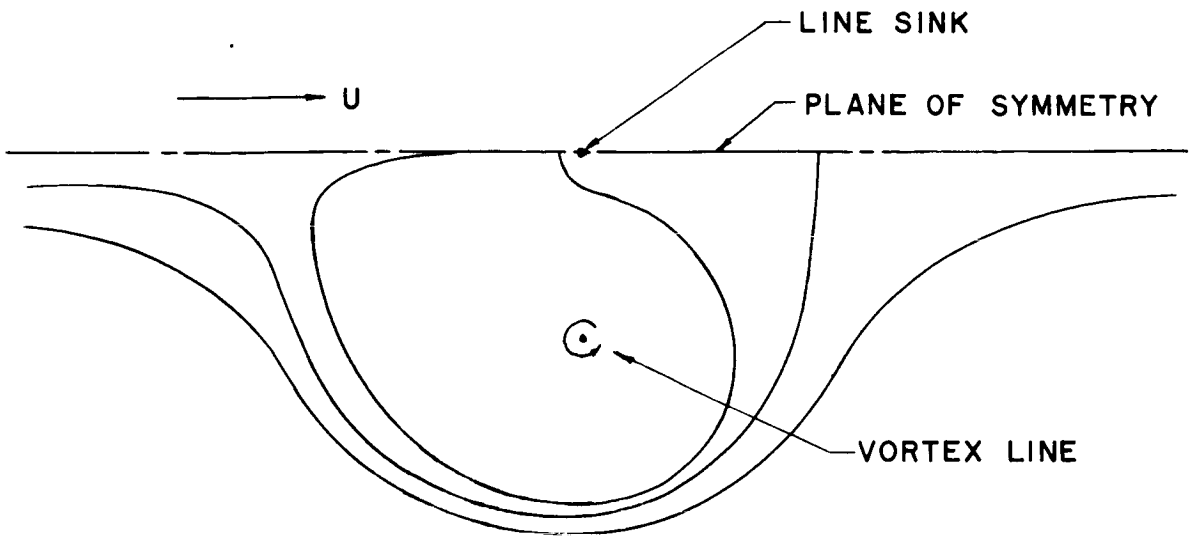

Figure 2.- Schematic diagram of the streamline pattern around the singularities near the origin of the jet.

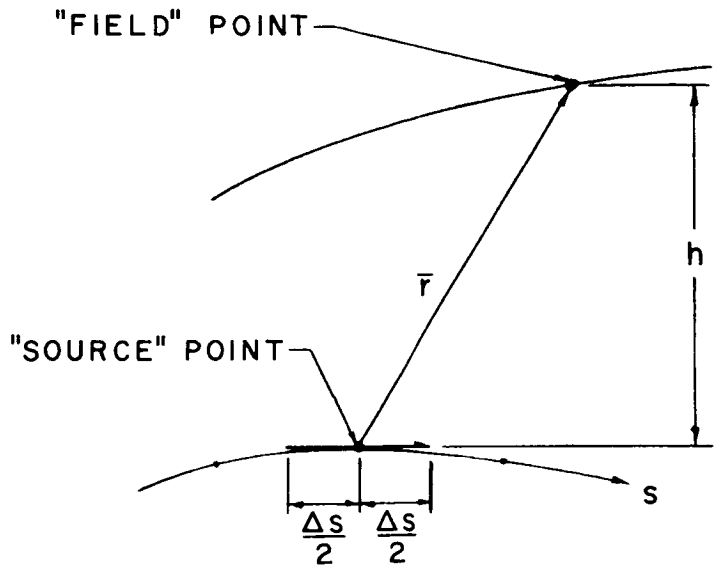

Figure 3.- Nomenclature for the line integration.

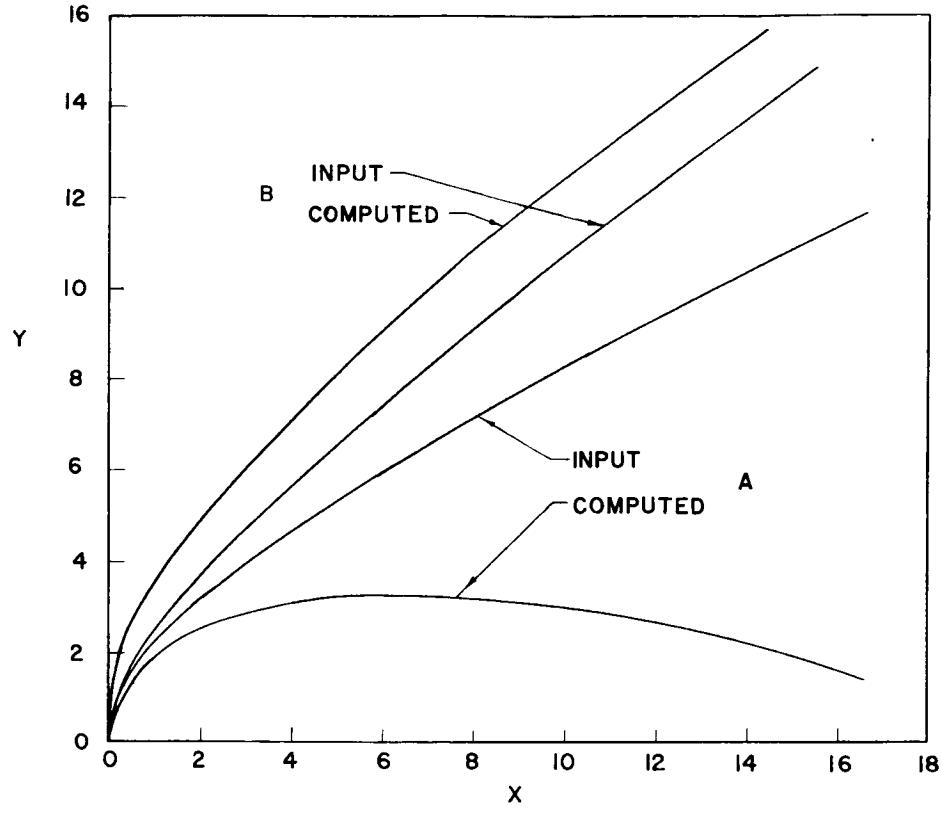

(a) Jet trajectory.

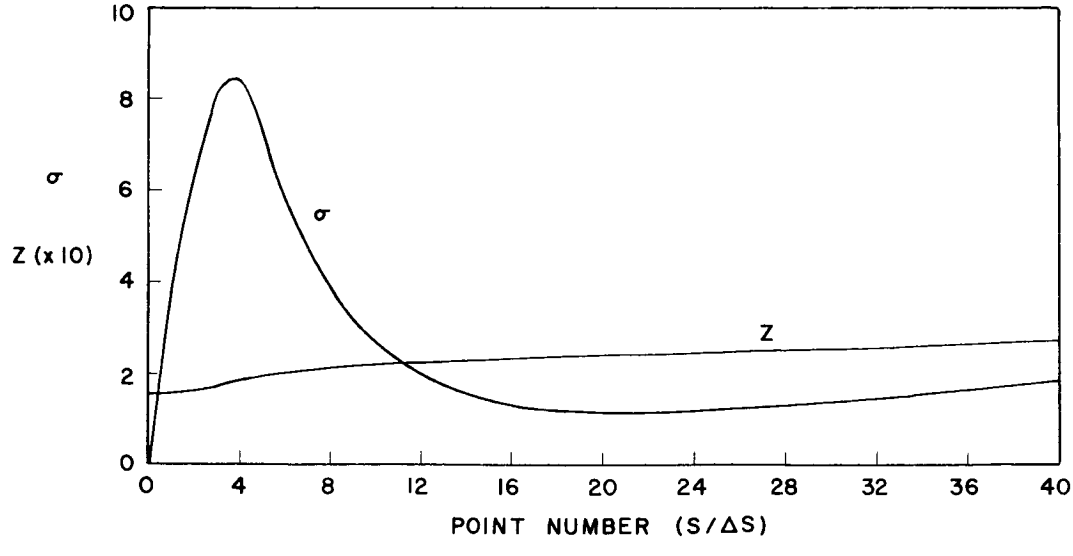

(b) Distribution of sink strength and position of the line vortex for computation (B).

Figure 4.- Samples from preliminary computations.

ANALYTIC DESCRIPTION OF JET-WAKE CROSS SECTIONS FOR A JET NORMAL TO A SUBSONIC FREE STREAM

By Richard J. Margason

NASA Langley Research Center

SUMMARY

An analytic description is given of jet-wake cross sections for a jet exiting normal to the free stream. The results indicate that a reasonable description can be obtained for the cross section. However, a complete description of the jet wake and associated phenomena requires a more complete model of the jet wake than that presented herein.

INTRODUCTION

The analytic description of a jet in a cross flow is difficult because of the complex nature of the flow in the vicinity of the jet. The primary features of the jet are the solid fluid core near the exit, the rollup by the wake into a pair of trailing vortices, and entrainment of free-stream flow into the jet. This entrainment can be considered in two parts: the fluid induced into the wake region by the swirling flow induced by the vortex pair, and the fluid entrained by viscous mixing on the periphery of the jet wake. The jet influences the free-stream flow in several ways. For example, near the jet exit the solid fluid core blocks the free-stream flow and causes a stagnation point ahead of the jet. Beyond the stagnation point, the free stream flows around the jet and separates from the downstream side of the jet efflux and, thus, causes a separated wake region.

SYMBOLS

D	jet diameter
N	number of vortex filaments used to describe a jet cross section
r_j	jet radius
$\vec{s}$	path-element vector
$\vec{V}$	velocity vector
V_j	jet velocity
V_∞	free-stream velocity

V_∞/V_j	effective velocity ratio
X,Y	Cartesian coordinates
z	complex plane coordinate
Γ	circulation strength
Γ_n	circulation strength of the nth vortex filament, where n = 1,2,...N
θ	cylindrical coordinate
ξ	natural jet coordinate along the axis of the jet
Φ	complex velocity potential

CALCULATION OF THE ROLLUP IN THE JET WAKE

Information from reference 1 by Chang-Lu was used in an effort to describe the rollup of the jet wake into a pair of vortices. The cross section of the jet wake at the exit plane is described by filaments of vorticity as shown in figure 1. A discrete number of filaments parallel to the direction of the jet velocity are spaced around the jet exit. The circulation strength of these vortex filaments is defined by the complex potential function which describes flow about a circular cylinder perpendicular to streaming flow:

$$\Phi = V_\infty \left(z + \frac{r_j^2}{z} \right)$$

The total derivative of this complex potential function yields the velocity vector induced by the presence of the cylinder:

$$\vec{V} = \frac{d\Phi}{dz}$$

Then, this derivative is integrated along a path to determine the circulation strength of the discrete vortex filaments, which is given as

$$\Gamma = \oint \vec{v} \cdot d\vec{s}$$

Integration over a sector of the circle gives the circulation strength for a single vortex filament as

$$\Gamma_n = 4V_\infty r_j \sin\frac{\pi}{N} \sin\left[\frac{2\pi}{N}(n - 1)\right]$$

These discrete vortex filaments are used to determine the change in the cross section of the jet as the flow passes downstream. This is done by a series of computations where the cross-section deformation is treated in two dimensions. Each of the vortex filaments is influenced for a small increment of time by the other filaments in the cross section. Since these filaments lie on a free surface, they must move to assume a new position where the net force induced by the other filaments is zero. This process is repeated many times as the flow moves away from the jet exit. As a result, the wake cross section changes shape. This change is indicated in figure 2 for a wake with 12 vortex filaments. The circular cross section in section A flattens on the downstream face to form the cross section labeled section B. Then, farther down the wake at section C, the characteristic kidney shape is formed. In section D and farther downstream, this evolves toward a very tightly wound pair of vortices. To form the surface of the wake boundary, a three-dimensional lattice of vorticity is constructed around the jet path. The jet path has been obtained from an empirical equation (ref. 2). This series of computations represents one feature of the jet, the rollup into a pair of vortices.

The precise form obtained analytically for this deformation is shown in figure 3, where the cross sections are described by 96 vortex filaments. The cross sections are presented at one-diameter increments along the jet axis. They represent the rollup of the wake cross section where the effective velocity ratio is 0.25. Previous attempts at using this procedure to describe the rollup have failed to form the spiral pattern because of truncation error.

The accuracy of this representation is indicated by figure 4. This photograph shows the cross section of a jet wake in a water tunnel at a point approximately 6 nozzle diameters along the jet axis measured downstream from the nozzle exit.

FLOW INDUCED BY THE JET WAKE

The usefulness of this three-dimensional vortex-lattice model of the jet wake will be determined by using it to estimate the pressure distribution induced on a plane flush with the jet exit. A simplified version of this model is represented by potential flow around a solid circular cylinder. (See fig. 5.) Ahead of the jet, there are positive pressures which are a result of the blockage of flow by the clinder; on the sides, there are negative pressures caused by the accelerating flow around the cylinder. Since the potential-flow model does not represent flow separation, there are positive pressures at the rear of the jet exit.

If this circular cylinder is allowed to deform along the jet path and roll up into a pair of vortices as shown earlier, the pressure distribution presented in figure 6 is obtained; there is little change from the pressure distribution shown in figure 5. Poor correlation was obtained between the data of figure 6 and those of figure 7, which are experimental results from reference 3. It should be noted that the present representation describes the rollup of wake caused by the external free stream and the blockage caused by the presence of

the jet. Comparison with experimental results shows the present representation of the jet wake to be incomplete.

CONCLUDING REMARKS

The results presented indicate that a reasonable description of the cross section of a jet wake normal to a free stream can be obtained by an analytic procedure. However, a complete description of the jet wake and associated flow phenomena will require a more complete model of the jet wake than that presented herein.

REFERENCES

1. Chang-Lu, Hsiu-Chen: Aufrollung eines zylindrischen Strahles Durch Querwind (Rollup of a Cylindrical Jet in a Crosswind). Doctorial Dissertation, Univ. of Göttingen, 1942.

2. Margason, Richard J.: The Path of a Jet Directed at Large Angles to a Subsonic Free Stream. NASA TN D-4919, 1968.

3. Bradbury, L. J. S.; and Wood, M. N.: The Static Pressure Distribution Around a Circular Jet Exhausting Normally From a Plane Wall Into an Airstream. C.P. No. 822, Brit. A.R.C., 1965.

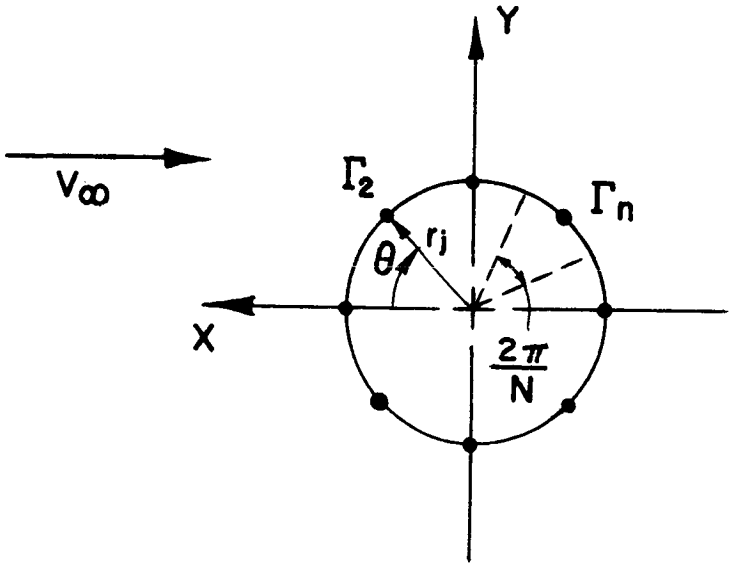

Figure 1.- Cross section of jet wake at exit plane described by filaments of vorticity.

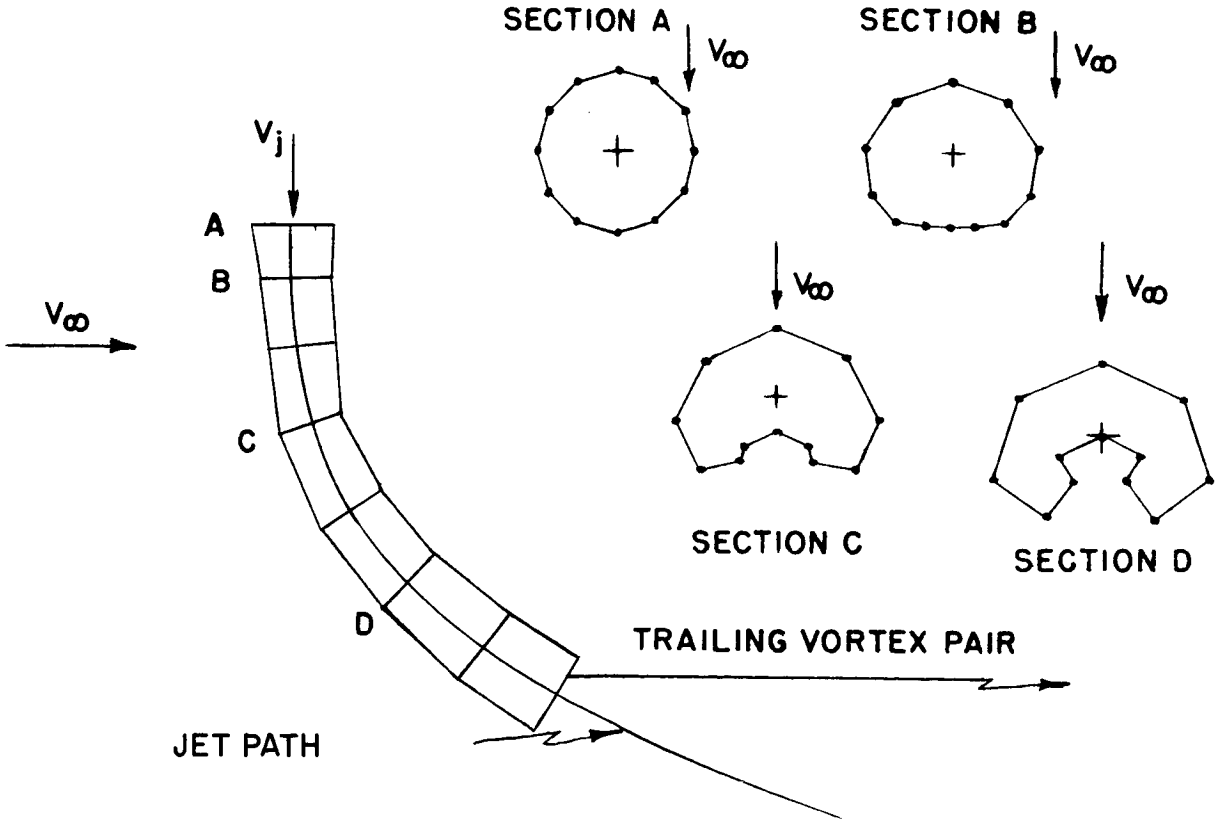

Figure 2.- Representation of a jet wake with a changing cross section.

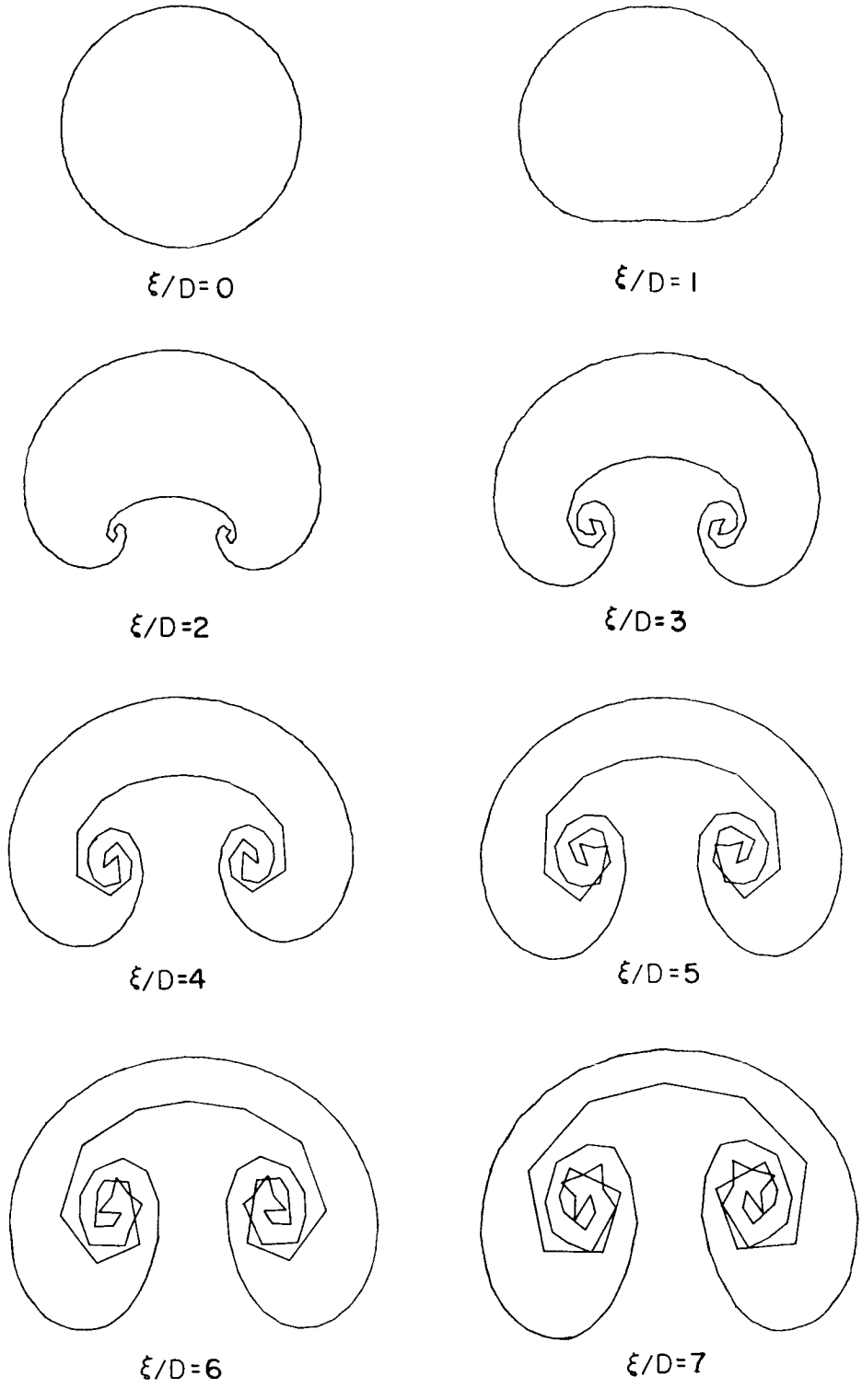

Figure 3.- Wake cross sections showing rollup into a pair of vortices. $V_\infty/V_j = 0.25$.

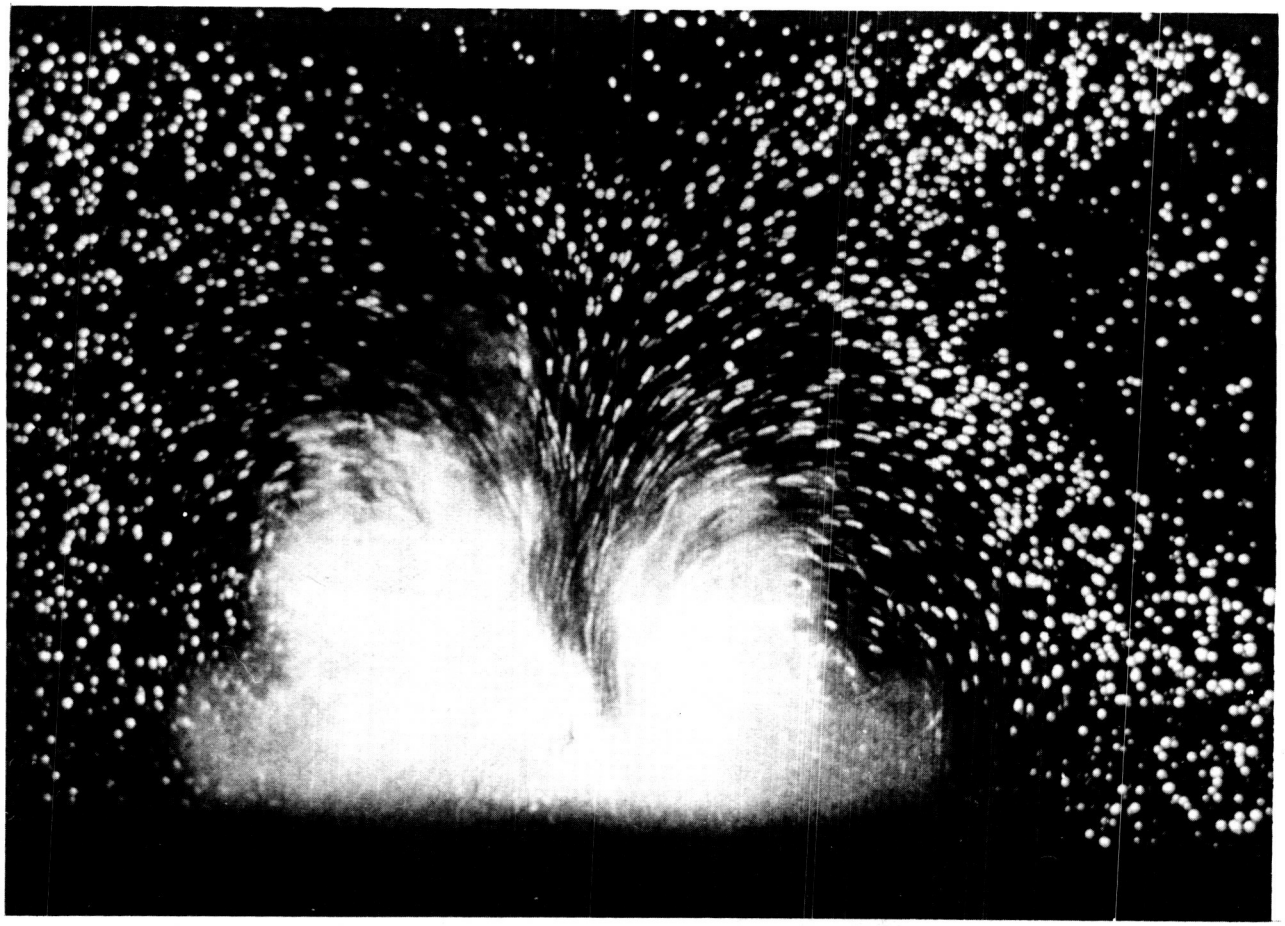

Figure 4.- Photograph of the cross section of a jet wake in a water tunnel exiting perpendicular to the free stream at a point approximately 6 nozzle diameters along the jet axis downstream from the nozzle exit. (Photograph from O.N.E.R.A. Film No. 575 entitled "Flows with Large Velocity Fluctuations.")

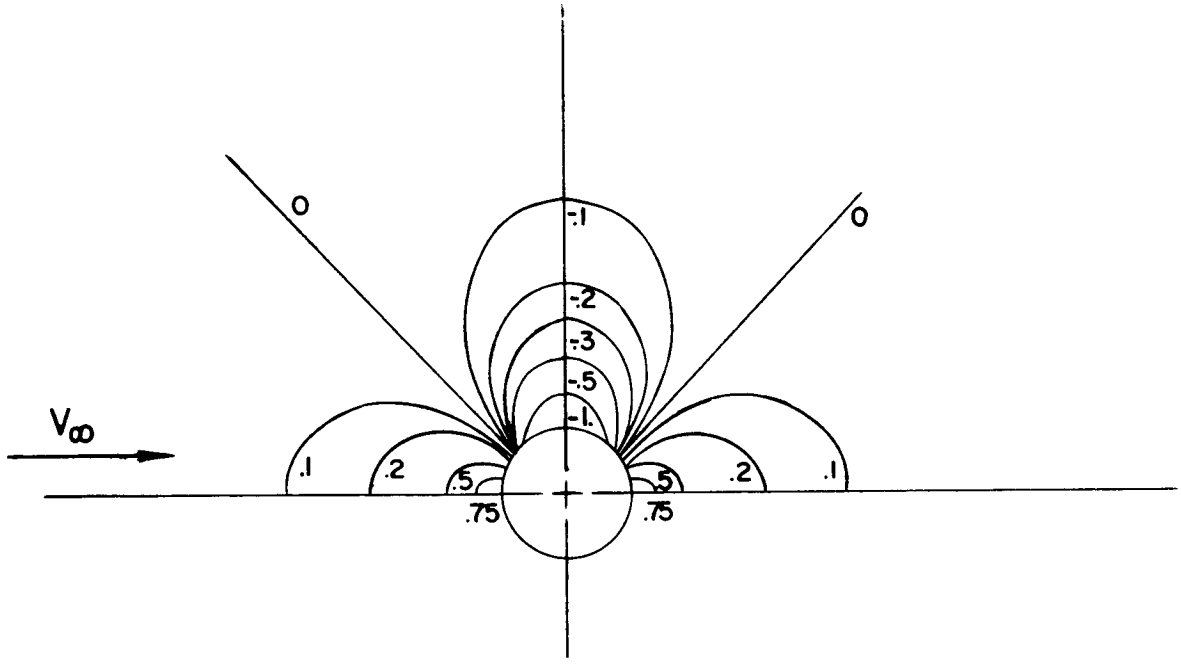

Figure 5.- Pressure distributions around a circular cylinder.

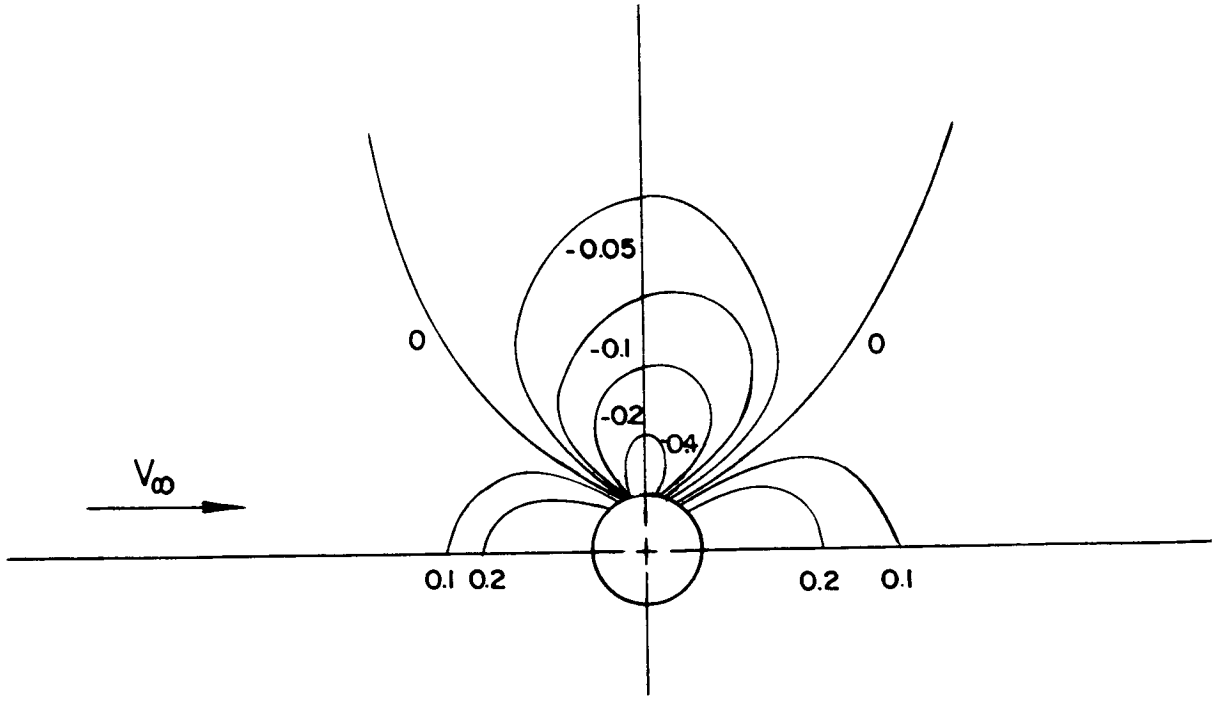

Figure 6.- Pressure distribution induced by a vortex-lattice jet wake with changing cross section.

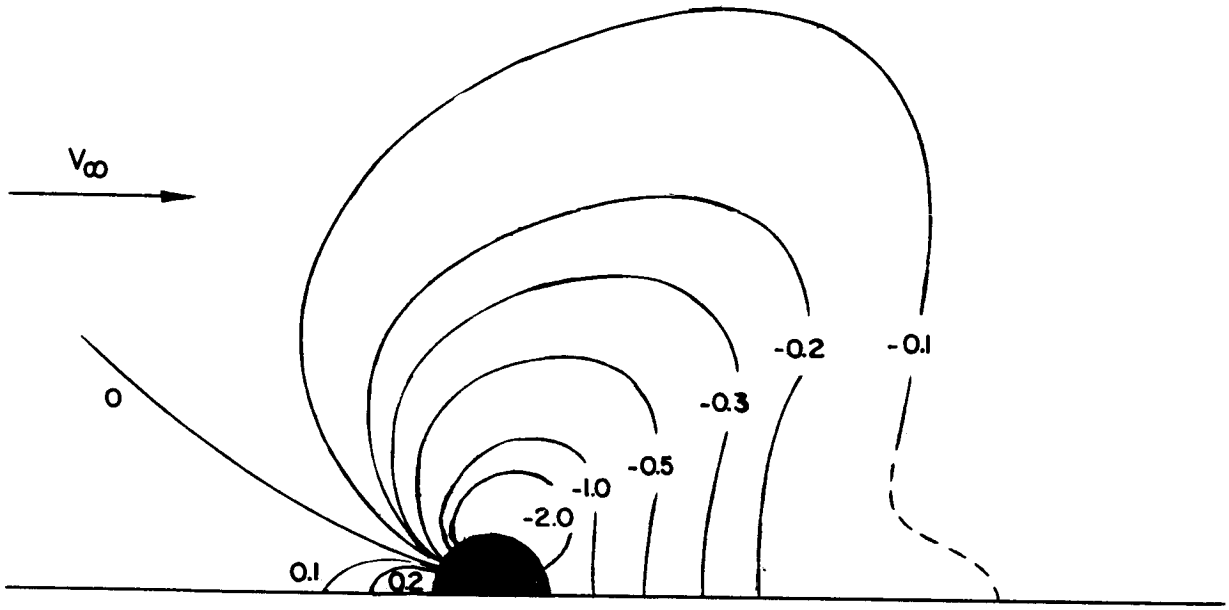

Figure 7.- Pressure distribution around a circular jet. $V_\infty/V_j = 0.25$. (Experimental data from ref. 3.)

CROSS WIND EFFECTS ON TRAJECTORY AND CROSS SECTIONS OF TURBULENT JETS

By Gerhard W. Braun and
Jack D. McAllister

University of Tennessee Space Institute

SUMMARY

Results in two loosely connected research areas concerning jets in cross flow are reported. An analysis of specific mass-momentum flux data showed that the entrained mass flux, Q_e, carries the undisturbed cross flow velocity $\bar{V}_\infty$ into the jet in such a way that it adds the momentum $Q_e\bar{V}_\infty$ to the jet flow. This relation permits a calculation of the jet trajectory, when the mass entrainment is given, or a calculation of the entrainment, when the trajectory is known.

If specific entrainment data are not known, the jet trajectory can be calculated by means of the assumption that the sidewise spreading rate of the jet and the nondimensionalized distribution of the excess velocity are the same as known from submerged jets. Closed form solutions are obtained for simple cases. Measured trajectories are curve fitted by adjusting a free spreading rate parameter.

The second part deals with the roll-up process of a jet in cross flow. Computer results obtained from potential flow calculations are shown for single and double jets with circular or elliptic exit nozzles.

INTRODUCTION

The theory of the submerged turbulent jet of circular cross section, i.e., the jet issuing into still air is, after Tollmien's pioneering work (1), sufficiently well known. The flow pattern of the jet in cross flow, however, is much more complex, and it is unlikely that, in the near future, its theory would be brought up to the level of knowledge on the submerged jet.

On the other hand there exist empirically derived formulae for the jet trajectory in cross flow. Such formulae have been published by Heyson (2), Monical (3), Wooler (4), and others. But these formulae tell too little about the physical reasons for the jet curvature.

More insight is provided by the jet theories which explain the jet bending as the effect of a drag force acting along the jet. Abramovich's (5) formula (12.160) is of this type. If one analyzes what drag coefficients would be needed, then one finds values up to 35 which is about twenty times the value one would expect.

Crowe and Riesebieter (6) recognized this difficulty and tried to eliminate it by prescribing a drag coefficient of 1.5 and making the necessary adjustment by selecting the needed frontal area of the jet. The second author of this paper found (7) that one needs a jet width of up to three times the width one would estimate from experimental observations.

Because of these difficulties it was tried to derive the trajectory equation of a jet in cross flow on the basis of the momentum theorem. The problem was solved by the second author in his thesis (7) to which the bulk of this paper is devoted.

As an appendix some potential flow aspects of the roll-up process of jets are added.

For the sake of clarity it is here mentioned that the following analysis is confined to the similarity region of the jet (Fig. 1), where the unmixed ("potential") core has disappeared and the transition to pure free turbulence has been established. The effects of the jet in front of this similarity region are taken care of by introducing an apparent origin of the jet.

SYMBOLS

a	location of the apparent jet source measured in orifice diameters upstream of the orifice
A_o	jet exit area
A_p	area of the jet projection onto the x-y plane, see figures 7 and 8
d_o	diameter at jet exit
h	width of the jet in y direction
$k_r = \frac{Q_r}{Q_o}$	ratio of jet mass flux at potential core end to value at jet exit
$K(R) = \frac{\partial h}{\partial \xi}$	spread rate of the jet width
M	jet momentum flux
Q	jet mass flux
r	polar coordinate in jet cross plane

$R = \frac{V_j}{V_\infty}$ characteristic ratio for jet in cross flow defined by equation (18)

U local flow velocity

V_c $= \frac{\partial M}{\partial Q}$

x,y,z Cartesian coordinate system, see figure 7

δ $= \sqrt{\frac{8\,K(R)}{\pi \sin \theta_o}}$ see equation (25)

η nondimensional radial distance, $r/r_{\frac{1}{2}}$

θ angle between local jet velocity and free stream velocity

ξ distance along curved center line of jet

ρ density

φ angle of polar coordinates in cross-sectional plane

Subscripts:

¢ value at center line of jet

j pertaining to the jet

n center of jet

o value at jet exit

r reference station at end of "potential core"

x component parallel to x-axis

z component parallel to z-axis

$\frac{1}{2}$ value corresponding to a velocity excess one-half the maximum value

∞ free stream value

MOMENTUM THEORY OF JET TRAJECTORY

Analysis of Mass-Momentum Flux Data

The first goal was to establish assumptions about the jet momentum flux and the mechanism of interaction between the jet and the external flow.

For this purpose mass-momentum flux data published by Keffer and Baines (ref. 8) were analyzed. These values are reproduced in figure 2. They were obtained by integration of measured velocity profiles using as the jet boundary the surface where the velocity excess is one-tenth the maximum value at a given axial distance.

Figure 2 illustrates that the momentum flux increases linearly with mass flux for each jet to free stream velocity ratio. Thus a constant velocity $V_c \equiv \partial M/\partial Q$ characterizes for each velocity ratio the axial momentum per unit mass being entrained into the jet. To obtain quantitative values for this characteristic velocity, V_c, the following assumptions were introduced.

1. The linear relation between mass and momentum fluxes is also valid for the initial mixing region between the orifice and the end of the potential core.

2. The reference mass flux values occurring at the potential core end of a jet in cross flow may be reasonably estimated from data measured for the submerged jet.

3. The velocity is constant over the orifice cross section. (Confirmed by private communication from Professor Keffer.)

4. The jet and external stream have the same density.

The mass-momentum flux data of fig. 2 may be expressed in the form of equation (1) with F representing the experimental slope of the linear relationship.

$$M/M_r = 1.0 + F(Q/Q_r - 1.0). \tag{1}$$

From fig. 2 one reads the values for F:

R	4	6	8
F	.412	.304	.269

Assumption (1) provides a second expression between the mass and momentum fluxes:

$$M = M_o + V_c(Q - Q_o). \tag{2}$$

A relation for the characteristic velocity, V_c, is then obtained by combining equations (1) and (2)

$$V_c = F \frac{M_r}{Q_r} . \tag{3}$$

The desired expression for the characteristic velocity is found in the form of equation (6) after introducing the abbreviations

$$k_r \equiv Q_r/Q_o \tag{4}$$

$$V_j \equiv M_o/Q_o \ , \ V_j \equiv R\, V_\infty \tag{5}$$

$$V_c/V_\infty = \frac{R}{k_r/F - (k_r - 1)} . \tag{6}$$

According to assumption (2) the mass flow ratio, k_r, does not depend upon V_∞ so that for it the value $k_r = 2.2$ based upon measurements for a submerged jet (given by Albertson, et al. (ref. 9)) can be substituted. Equation (6) then gives the values 0.97, 0.99, and 1.14 for the ratio of the characteristic to free stream velocity.

This result suggests that, to the first approximation, mass entrained into the jet brings with it the associated free stream momentum. Further it suggests that deflection of the total jet momentum flux is more adequately treated as an effect of momentum entrainment than as the result of pressure forces normal to the jet.

Fearn took the relation $V_c = V_\infty$ for granted and used it already in early 1968.

Approximate Integral Analysis

In fig. 3 the nondimensional velocity excess above the free stream value published in ref. 8 is plotted versus the nondimensional lateral coordinate. The nondimensionalizing distance $r_{\frac{1}{2}}$ is the radius at which the velocity excess is half the maximum value. The curve is universal, i.e., does not depend on R or ξ. Schlichting's (ref. 10) expression

$$\frac{U - V_\infty}{U_m - V_\infty} \equiv f(\eta) = \frac{1}{[1 + (\sqrt{2} - 1)\,\eta^2]^2} \tag{7}$$

obtained for the submerged axially symmetric jet fits well this curve.

The approximation for the jet axial velocity distribution is completed by using measured values of the decay in center line velocity U_m as published in ref. 8 together with a suitable expression for the angular and axial variations in $r_{\frac{1}{2}}$. The latter was determined by approximating the jet cross section with an ellipse with the eccentricity k and the spread rate α, giving

$$r_{\frac{1}{2}} = \alpha\xi\sqrt{1 - k^2 \cos^2 \varphi}. \tag{8}$$

The factors k and α have to be determined experimentally.

The obtained axial variations in mass and momentum flux are presented as dashed lines in figs. 4 and 5 for velocity ratios of 4 and 8. Note that the mass entrainment is materially increased when the free stream velocity becomes comparable with the jet velocity. The result for the submerged jet was obtained through the limit process of $R \to \infty$ with $k \to 0$ and α taken from submerged jet data of Förthmann (ref. 11). The limit value is in excellent

agreement with the direct measurements of Ricou and Spalding (ref. 12) and data analysis of Albertson (ref. 9), both works indicating $Q/Q_o = 0.32\ \xi/d_o$ for submerged jet.

Applying the same limit process to the momentum flux expression with the conventional assumption of constant momentum flux when the external medium is at rest yields the correct expression for the center line velocity decay even to the numerical constant;

$$G(\xi) \equiv \frac{U_m - V_\infty}{V_j - V_\infty} = \frac{6.3}{\xi/d_o} \quad \text{for submerged jet.} \tag{9}$$

The analysis of the following section will show to what extent the approximate integral analysis is in agreement with the principle that the entrained mass carries its free stream momentum into the jet.

Relation of Jet Trajectory to Mass Flux

The principle of momentum entrainment may also be applied to link the jet center line inclination to the mass flux at a specific axial distance* . The analysis is again based upon three assumptions:

1. The jet trajectory has the direction of the jet momentum flux vector.

2. The momentum flux at a station ξ of the trajectory is the vector sum of the momentum flux through the orifice and the momentum of fluid entrained along the trajectory up to station ξ.

3. The entrained fluid momentum is the product of the undisturbed cross flow velocity and the entrained mass.

Using the coordinate system of fig. 6, the momentum flux has the components:

$$M_x = M_o \sin \theta_o, \tag{10}$$

$$M_z = M_o \cos \theta_o + V_\infty(Q - Q_o). \tag{11}$$

Hence the following relationship exists between the trajectory angle θ and the mass flux:

$$\cot \theta = \frac{M_z}{M_x} = \cot \theta_o + \frac{V_\infty Q_o}{M_o \sin \theta_o}\left(\frac{Q}{Q_o} - 1\right), \tag{12}$$

---

* Fearn also used this principle in ref. 13.

Solving for the mass flux ratio gives

$$Q/Q_o = 1 + R \sin \theta_o \, (\cot \theta - \cot \theta_o), \tag{13}$$

where $R \equiv V_j/V_\infty$.

Mass flux values based upon equation 13 and jet trajectory data of ref. 8 are compared in fig. 4 with the corresponding results of integral analysis. The good agreement not only substantiates the momentum entrainment hypothesis but also suggests that mass entrainment for a jet in cross flow may be readily obtained from center line trajectory data via equation (13).

A simple relationship for the momentum flux may also be obtained by using the fact that the x component is constant

$$M/M_o = \frac{\sin \theta_o}{\sin \theta} . \tag{14}$$

Equation (14) is compared with momentum flux results based upon the integral analysis in fig. 5.

The comparison is satisfactory especially at the more downstream positions where the axial velocity should be quite close to the assumed similarity profile.

Development of the Trajectory Equations

At first thought the back-flow produced by the vortex street, observed in the wake of the jet, seems to eliminate the possibility that the entrained masses carry in the average the full cross flow velocity. Platten and Keffer (ref. 14) developed about simultaneously with the reported work a jet entrainment theory which has the contribution of the shed vortices as a specific feature. The following pages will show that the assumption of a wake with zero velocity can serve the same purpose.

The analysis of a circular jet entering at an angle θ_o to a uniform stream is initiated by considering the balance of momentum flux for the control volume presented in fig. 7. A_3 is part of a rigid wall through which the jet exhausts. The shear force acting on A_3 is assumed to be negligible in comparison to the momentum terms. A_ξ is the surface normal to the jet trajectory at the general axial distance, ξ. The momentum flux in the x and z directions are established under the following conditions:

1. The velocity vectors in each jet cross section are parallel to the jet trajectory.

2. Average pressure differences between corresponding surfaces of the control volume are relatively small and

may be neglected in comparison to the momentum terms.

3. The flow through the plane A_ξ can be divided in three parts:

   a) A jet region, A_j, bounded by the jet-external stream interface.

   b) A wake region in the "shadow of the jet" with essentially zero velocity.

   c) An exterior region comprising the remainder of A_ξ and having the undisturbed free stream velocity.

Using these assumptions the x momentum equation is

$$M_o \sin \theta_o = \sin \theta \int_{A_j} \rho U^2 dA, \tag{15}$$

which is a mathematical statement that the component of jet momentum normal to the free stream is invariant.

The z momentum equation has the form

$$\rho_\infty V_\infty^2 A_1 + M_o \cos \theta_o = \cos \theta \int_{A_j} \rho U^2 dA + (A_1 - A_p)\rho_\infty V_\infty^2 \tag{16}$$

where A_p is the projection of the jet onto the x-y plane, see fig. 7.

This expression is further simplified to equation (17) by using equation (15) and slight rearrangement.

$$\cot \theta = \frac{dz}{dx} = \cot \theta_o + \frac{\rho_\infty V_\infty^2 A_p}{M_o \sin \theta_o} . \tag{17}$$

Equation (17) suggests that the effective velocity ratio be defined in terms of the orifice momentum flux as given by

$$R^2 \equiv \frac{\int_{A_o} \rho_j V_j^2 dA}{A_o \rho_\infty V_\infty^2} = \frac{M_o}{A_o \rho_\infty V_\infty^2} \tag{18}$$

Equation (17) is thus expressible in terms of the jet geometry and the velocity ratio, R:

$$\frac{dz}{dx} = \cot \theta_o + \frac{A_p}{A_o} \frac{1}{R^2 \sin \theta_o} . \tag{19}$$

This trajectory equation may be solved as soon as A_p is expressed in terms of x or z.

By generalizing Vakhlamov's (ref. 15), approach, the projected jet cross section A_p (fig. 8) was built-up of a parabolically flaring out stem of width, h, and a head in form of half an ellipse. The effective jet width is taken to be a linear function of axial distance with an empirical proportionality parameter, K(R) called the spreading factor and a set-back factor, a, which corrects for the fact that the apparent origin is located a orifice diameters upstream of the orifice. This gives

$$h = (2ad_o + \xi)\, K(R) \tag{20}$$

Evaluation of tests gave for a jet entering normal to the free stream

$$\frac{\partial h}{\partial \xi} \equiv K(R) \simeq 1.0, \text{ for } 4 \leq R \leq 8, \tag{21}$$

and

$$\lim_{R\to\infty} \frac{\partial h}{\partial \xi} \simeq 0.32. \tag{22}$$

for a submerged jet.

Solution of the Trajectory Equation

There is no difficulty in solving the trajectory equation (19) on a computer. For basic investigations, however, an analytical solution is desired.

In order to make such solutions easier, the elliptic head of the jet shadow A_p is neglected so that $A_p = \int_0^x h\, dx$. One has then to substitute in equation (19)

$$\frac{A_p}{A_o} = \frac{4}{\pi} \frac{K(R)}{d_o^2} \int_0^x (2ad_o + \xi)\, dx \tag{23}$$

where

$$\xi = \int_0^x \sqrt{1 + \left(\frac{dz}{dx}\right)^2}\, dx \tag{24}$$

Equation (24) causes certain analytical difficulties. However, if one plots the nondimensionalized penetration distance x/d_oR versus the nondimensionalized trajectory arc length ξ/d_oR then one sees that a good approximation of the arc length can be obtained by assuming

$$\xi = x \quad \text{for} \quad \frac{x}{d_oR} \leq 1, \text{ Region A}$$

$$\xi = 2x \quad \text{for} \quad \frac{x}{d_o R} \geq 1 \quad \text{Region B}$$

Integration gives in Region A the trajectory equation

$$Z = X \cot \theta_o + \delta^2 \left[\frac{a}{2R} X^2 + \frac{1}{12} X^3 \right] \tag{25}$$

where $Z = \frac{z}{Rd_o}$; $X = \frac{x}{Rd_o}$; $\delta^2 = \frac{8\ K(R)}{\pi \sin \theta_o}$

For the case a = o and $K = \frac{3\pi}{8}$ equation (25) is identical with Heyson's (ref. 2) empirically found formula

$$Z = X \cot \theta_o + \frac{X^3}{4 \sin \theta_o} \tag{26}$$

For Region B, i.e., $X > X_1$, one finds

$$Z = (Z_1 + \frac{a}{R}) \cosh[\delta(X-X_1)] + \delta^{-1} Z_1' \sinh[\delta(X-X_1)] - a/R \tag{27}$$

Z_1 and Z_1' are the nondimensionalized z-coordinate and its derivative at the matching point of Region A and Region B.

If one would consider a jet issuing perpendicular to the cross flow and if one would expand the validity of (27) down to the jet orifice, i.e., if one would assume $X_1 = Z_1 = Z_1' = 0$, then (27) would be simplified to

$$Z = \frac{a}{R} [\cosh (\delta X) - 1] \tag{28}$$

This formula is similar to an empirical relation given by Wooler in ref. 4.

Correlation of Computed Trajectories with Measurements

The primary substantiation for the simplifying assumptions used in the development of the trajectory equations is the ability to match measured trajectories over a wide range of R using values of K(R) and the apparent origin set-back distance, a that are in agreement with experimental observations. The results of such matchings are presented in this Chapter using previously published data (16), (17), (18), as well as measurements obtained during the present investigation.

It was found that for all trajectories the same value a=0.8 may be used for the apparent origin set-back distance. The

coefficient a/2R in equation (25) provides for the observed change in trajectory shape from quadratic to cube as R increases. Figure 9 illustrates the close degree to which the air jet trajectories of references 16, 17, and 18 may be matched. Values of the spread rate parameter, K(R), used in these computations are plotted in fig. 10. It is important to note the close agreement between the values required to match measured trajectories and the independent experimental values based upon a ten percent velocity excess (equations (21) and (22)). This is a strong substantiation for the assumptions used in developing the trajectory equation.

The original thesis presents also matched water jet trajectories which show the same good agreement. The thesis furthermore investigates the effect of a plate from which the jet issues.

Finally, the effect of having the jet enter at angles other than normal to the external stream was investigated. Trajectories measured for entry about thirty degrees each way from the normal are shown in fig. 11.

The numerical predictions of fig. 11 were accomplished with the K(R) and a used to match for the normal jet entry. Note that, as θ_o decreases, the jet turns more slowly toward the free stream indicating decreased mixing and hence the desirability of a smaller value for K(R). However, for θ_o between sixty and one hundred twenty degrees the predictions presented are considered to be quite satisfactory.

INVESTIGATION OF JET ROLL-UP DUE TO CROSS FLOW

A typical and very conspicuous phenomenon of the jet in cross flow is the formation of the already mentioned vortex system. This system consists of two types of vortices. One type stays within the jet and causes it to roll-up into two vortices; the other vortex system separates from the jet and forms a type of von Karman vortex street.

Chang (ref. 19) has investigated the roll-up process on the basis of two-dimensional potential flow theory. She represents the deformation which takes place on a jet slice while it moves down the jet by assuming that it would be identical with the deformation a cylindrical jet would undergo in two-dimensional cross flow while time goes on. Mrs. Chang's investigations are based on potential flow theory, but her results show such a striking similarity to the actual phenomenon that it was decided to continue her investigation. This was done by Mr. Stephen M. Soukup (ref. 20), who included in his analysis also jets with elliptical outlets and added investigations on couples of jets

in side by side and tandem arrangements.

The analytical approach is as follows: The two-dimensional flow around the jet outlet configuration is established by distributing a vortex sheet of such strength around the openings that it would become a stream line. For computation purposes the continuous vortex sheet is replaced by 32 discrete vortices, and the velocity components, v_x and v_y, imparted to each vortex by the rest of the vortices, are calculated. Selecting a time interval Δt and permitting the vortices to move freely, the displacement of each vortex in the direction of the two coordinate axes is given by $\Delta x = \Delta t \cdot v_x$ and $\Delta y = \Delta t \cdot v_y$. The vortex displacements are different for the different vortices and represent the deformation of the jet cross section. Two examples of cross section deformations are shown in fig. 12. The upper row is for a circular exit nozzle and the lower row for an elliptical exit nozzle with the numerical eccentricity E = 0.80 and the same area as the circle.

The calculations for single jets cover elliptical nozzles with the numerical eccentricities of 0.0, 0.2, 0.4, 0.6, 0.8, and 0.95. For a more compressed presentation the deformed cross sections were stacked as it is shown in figs. 13 and 14. The side by side configurations consisted of elliptical jets with the following eccentricities, e:

right jet	e = 0.00	0.0	0.95
left jet	e = 0.00	0.95	0.95

Circle and ellipse have the same outlet cross section area of $A_o = \pi$. The distance between the centers of the two cross sections was in all cases 3 units.

Finally the following two configurations of jets in tandem arrangement were investigated:

Front jet	circle	circle
Rear jet	circle	ellipse e = 0.95

The results of the first case are shown in fig. 14.

The calculations reveal that the jets of elliptic cross section roll-up slower than the circular jets. For side by side configurations the cross section deformation is much larger on the inside than on the outside of the jets. In tandem arrangement the rear jet is pulled into the front jet.

Unfortunately no relation between the time sequence of the deformation of the hypothetical two-dimensional jets and the deformation of the actual jets in space has been found. It is obvious that the potential flow theory cannot describe the mixing phenomenon of the jet. However, it is hoped, that Soukup's

calculations may help in finding the effect of the cross flow on the enlargement of the jet surface which obviously is important for the entrainment process.

CONCLUDING REMARKS

The presented studies lead to the following conclusions:

1. The deflection of a turbulent jet in cross flow is primarily due to a mixing process which entrains free stream momentum into the jet. This process permits determination of the jet mass flux from the more easily measured trajectory angle.

2. Momentum mixing considerations allow jet trajectory predictions over a wide range of velocity ratios, R, and jet entry angles, θ_o.

3. These favorable results should not raise the hope that refinements of this approach, like a more careful representation of the jet shadow area, A_p, could produce an essential improvement of the accuracy of the results.

4. The momentum theory is confined to cases where flow restrictions are of minor importance. If one wants to include ground or wall effects one would have to introduce new features like vortices which have a far-field effect and are subject to a feedback from flow obstructions.

5. A challenging extension is seen in including the vortex system especially the shed vortices in the mathematical model of the jet in cross flow.

REFERENCES

1. Tollmien, W., "Berechnung turbulenter Ausbreitungs-vorgänge," Zeitschrift für Angewandte Mathematic und Mechanik, 6:1, 1926.

2. Heyson, H. H., "Wind Tunnel Wall Effects at Extreme Force Coefficients," International Congress of Subsonic Aero-dynamics, New York, April 3-6, 1967.

3. Monical, Richard E., "A Method for Representing Fan-Wing Combinations for Three-Dimensional Potential Flow Solutions," IAAS Paper No. 65-85, Presented at IAS

Meeting, New York, New York, June 25-27, 1965.

4. Wooler, P. T., "On the Flow Past a Circular Jet Exhausting at Right Angles from a Flat Plate or Wing," Journal of the Royal Aeronautical Society, 71:216, 1967.

5. Abramovich, G. N., "The Theory of Turbulent Jets," Cambridge: Massachusetts Institute of Technology Press, 1963.

6. Crowe, C. T. and H. Riesebieter, "An Analytical and Experimental Study of Jet Deflection in a Cross Flow," Fluid Dynamics of Rotor and Fan Supported Aircraft at Subsonic Speed, Paris: Advisory Group for Aerospace Research and Development Preprint, 1967.

7. McAllister, Jack Donald, "A Momentum Theory for the Effects of Cross Flow on Incompressible Turbulent Jets," Ph.D. Dissertation, University of Tennessee, Tullahoma, Aug. 1968.

8. Keffer, J. F. and W. D. Baines, "The Round Turbulent Jet in a Cross-Wind," Journal of Fluid Mechanics, 15:481, 1963.

9. Albertson, L. M., Y.B. Dai, R. A. Jensen and H. Rouse, "Diffusion of Submerged Jets," Transactions of the American Society of Civil Engineers, 115:639, 1950.

10. Schlichting, H., "Boundary Layer Theory," New York: McGraw-Hill, 1960.

11. Förthmann, E., "Über turbulente Strahlausbreitung," Ingenieur-Archiv, 5:1, 1934.

12. Ricou, F. P. and D. B. Spalding, "Measurements of Entrainment by Axisymmetrical Turbulent Jets," Journal of Fluid Mechanics, 11:21, 1961.

13. Fearn, Richard L., "Mass Entrainment of a Circular Jet in a Cross Flow," paper no. 15 of this compilation.

14. Platten, J. L. and J. F. Keffer, "Entrainment in Deflected Axisymmetric Jets at Various Angles to the Stream," University of Toronto, Department of Mechanical Engineering, UTME-TP 6808, June 1968.

15. Vakhlamov, S. V., "Computation of the Trajectory of a Jet in a Drifting Flow," Inzhenerno- Fizicheskiy Zhurnal, 7:112, 1964.

16. Shandorov, G. S., "Flow from a Channel into Stationary and Moving Media," Zhurnal Technicheskoi Fiziki, 27:1, 1957.

17. Jordinson, R., "Flow in a Jet Directed Normal to the Wind," Aeronautical Research Council Reports and Memoranda Number 3074, London, 1958.

18. Pratte, B. D. and W. D. Baines, "Profiles of the Round Turbulent Jet in a Cross Flow," Journal of the Hydraulics Division, American Society of Civil Engineers, 93:53, 1967.

19. Chang, H., "Aufrollung eines Zylindrischen Strahles durch Querwind," Doctoral Dissertation, Göttingen, 1942.

20. Soukup, Stephen M., "Potential Flow Aspects of the Cross-Sectional Deformation of Jet Configurations in Cross-Flow," Master of Science Thesis of the University of Tennessee Space Institute, December 1968.

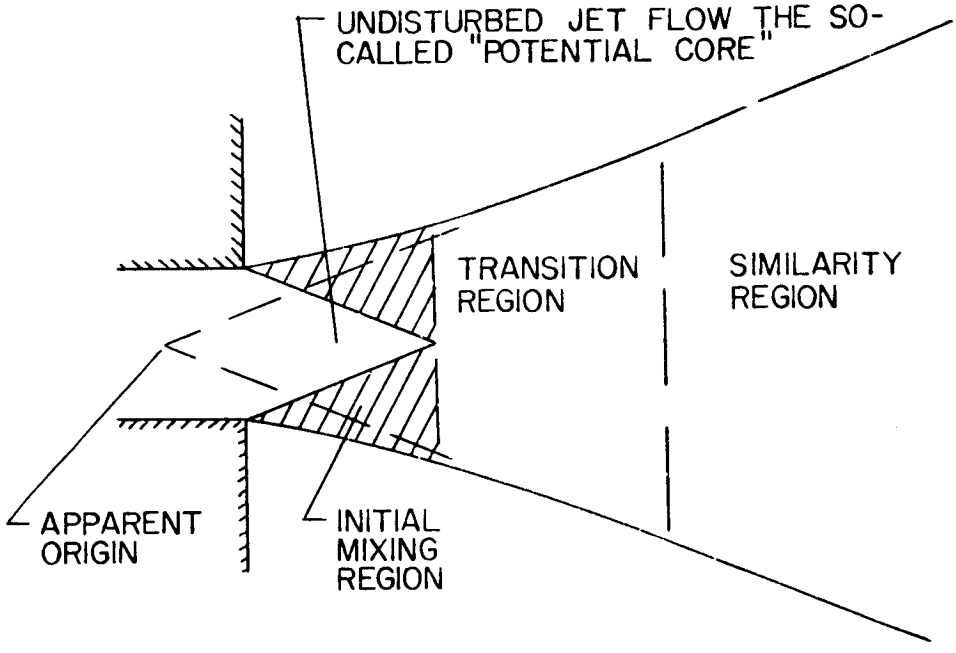

Figure 1.- Schematic representation of the flow near a jet nozzle.

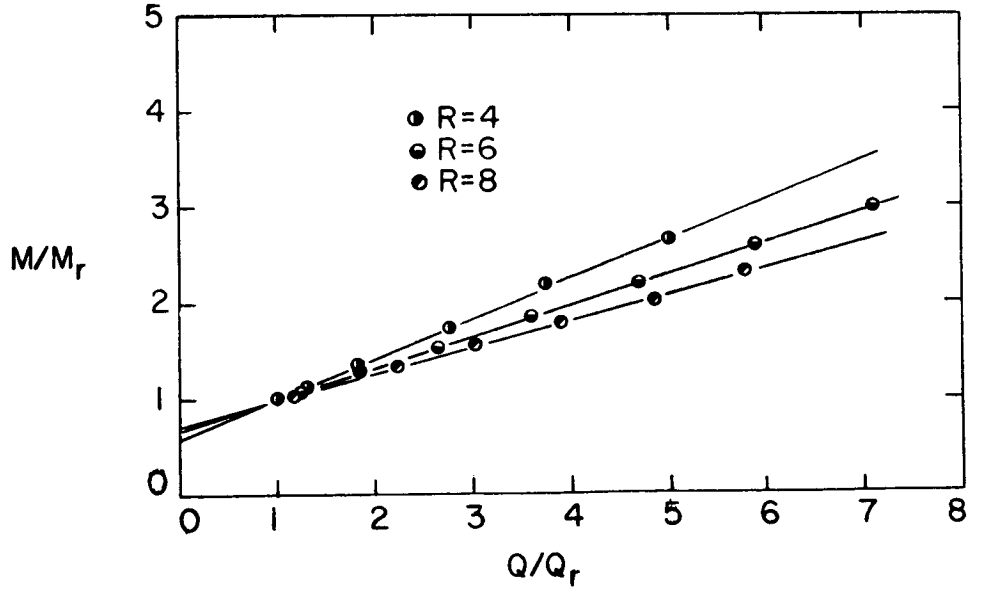

Figure 2.- Mass-momentum flux data.

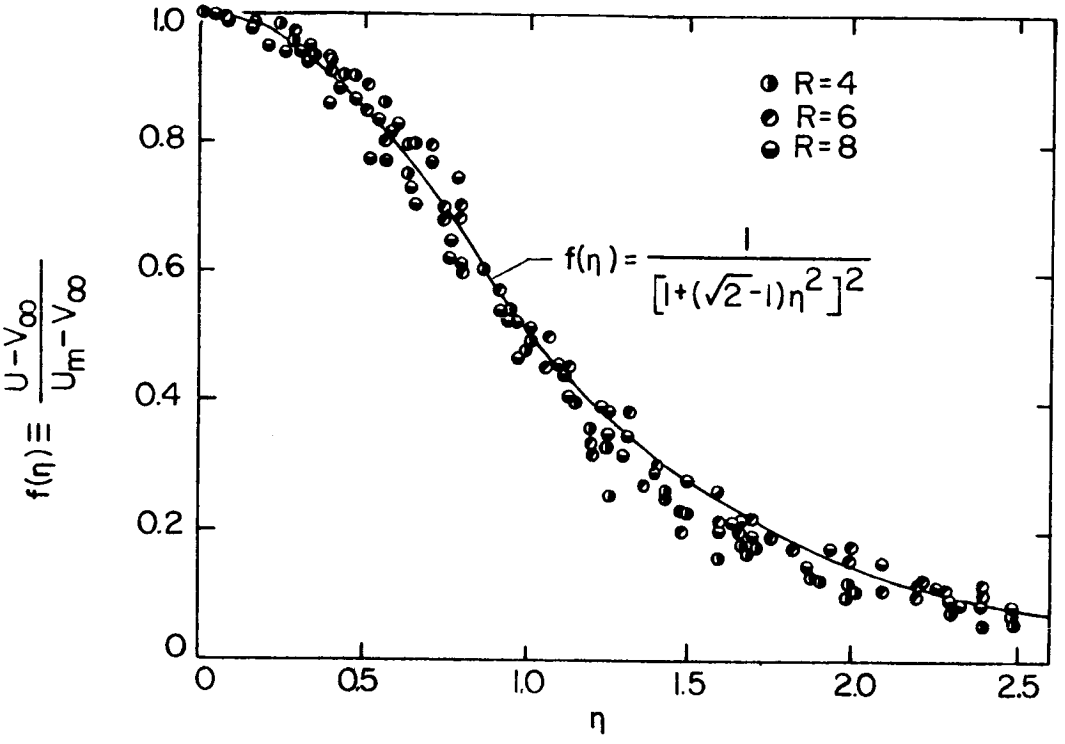

Figure 3.- Lateral distribution of jet velocity.

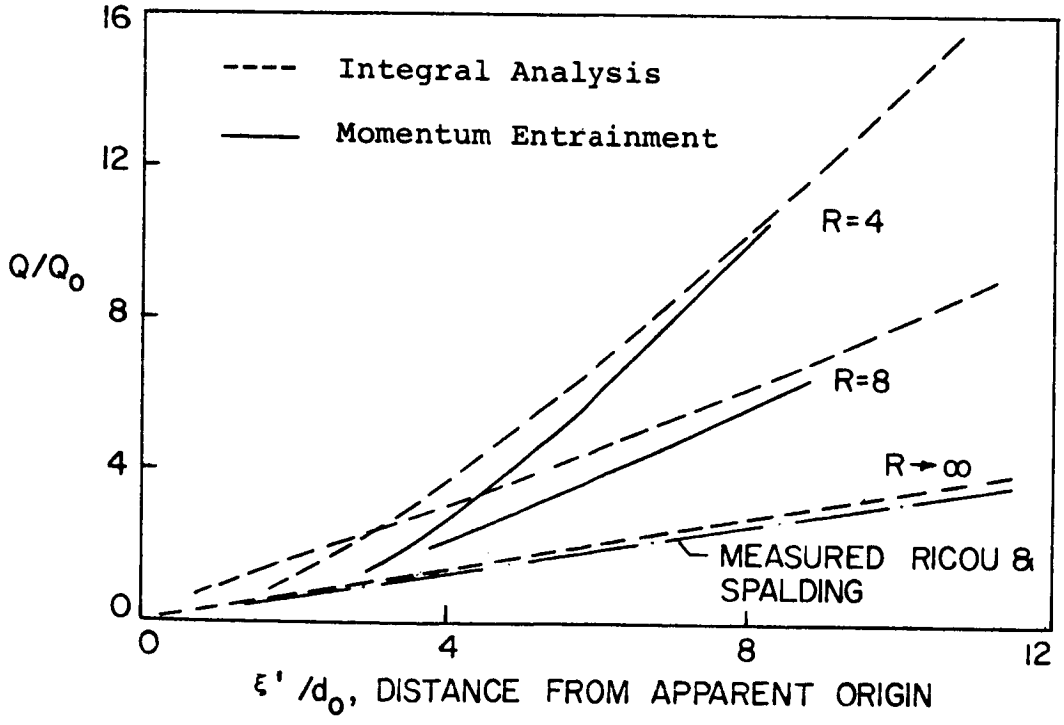

Figure 4.- Comparison of mass flux calculations.

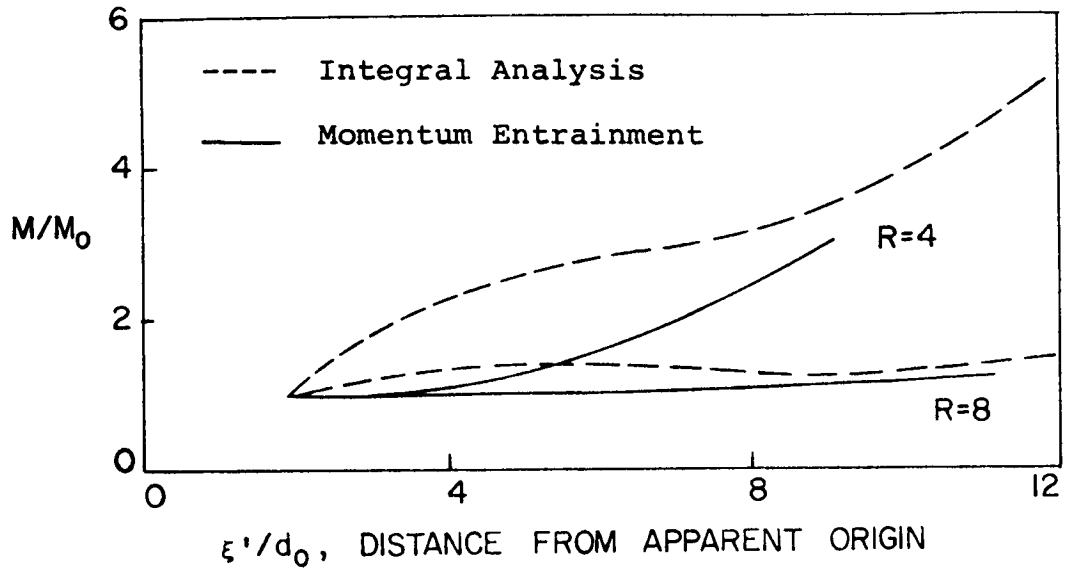

Figure 5.- Comparison of momentum flux calculations.

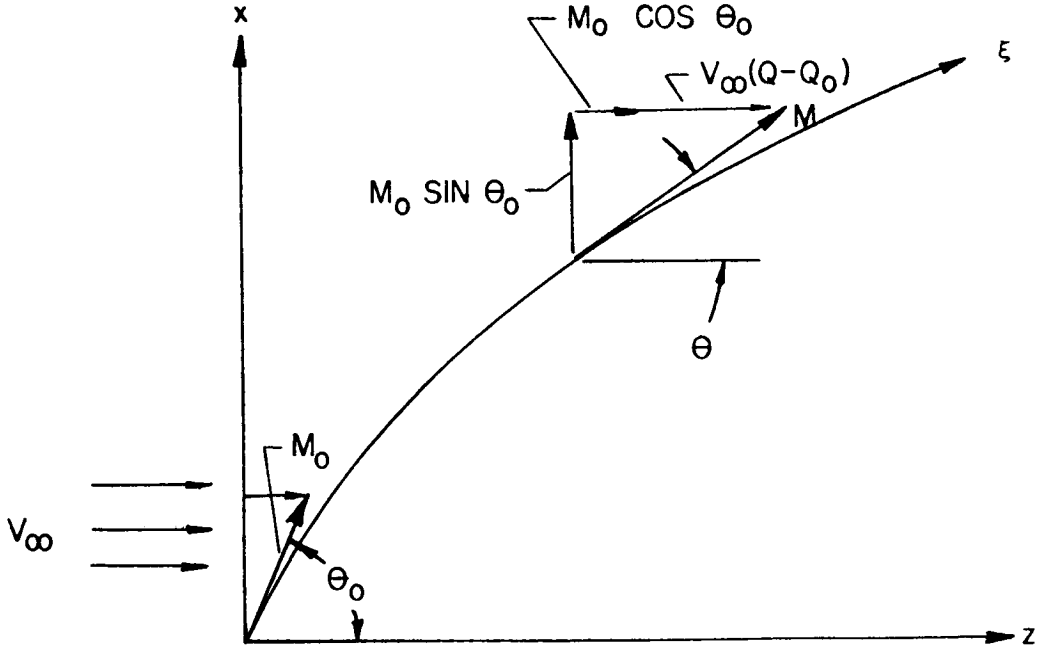

Figure 6.- Coordinate system for relating jet trajectory to momentum flux.

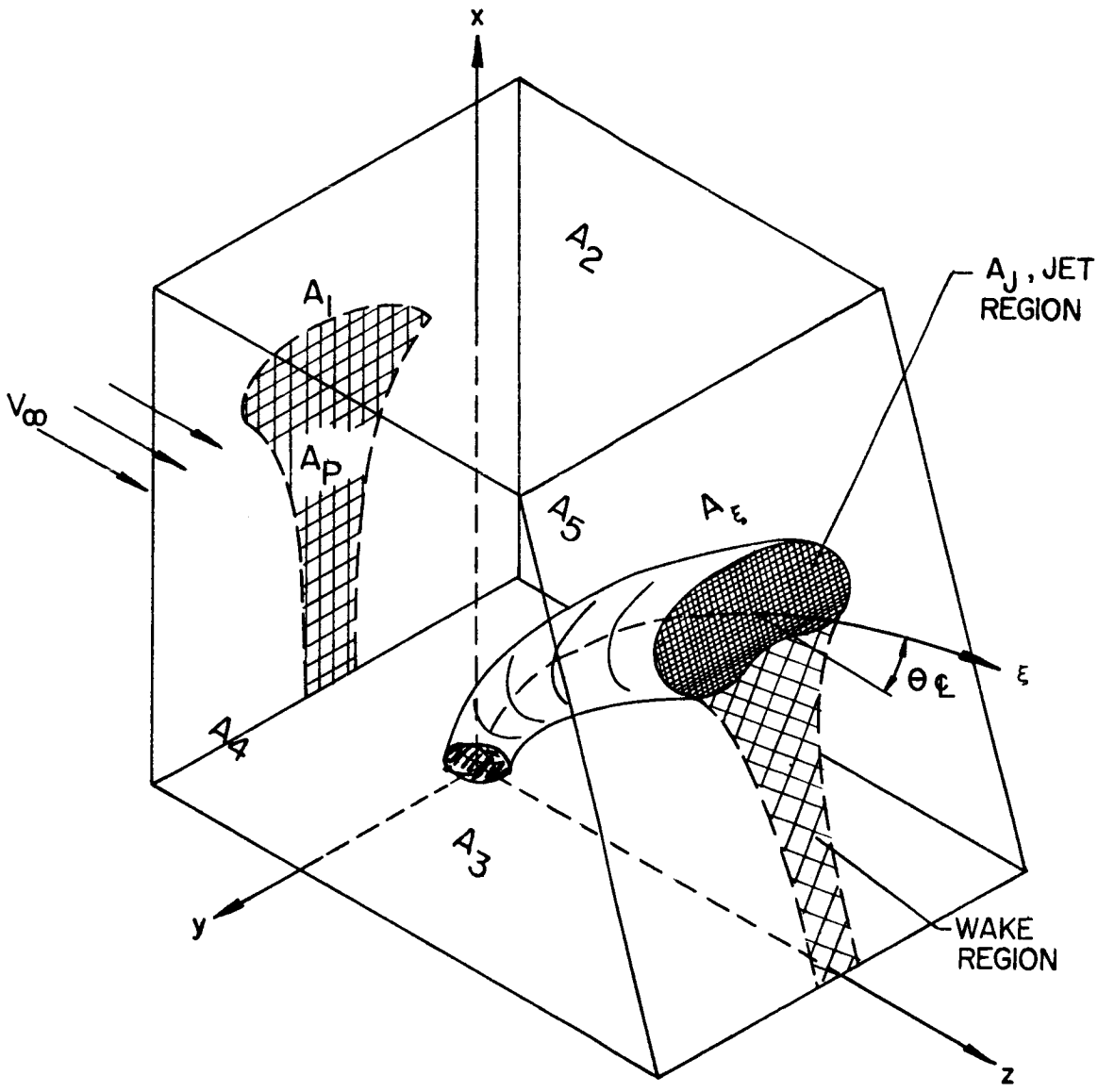

Figure 7.- Coordinates and control surfaces for trajectory analysis.

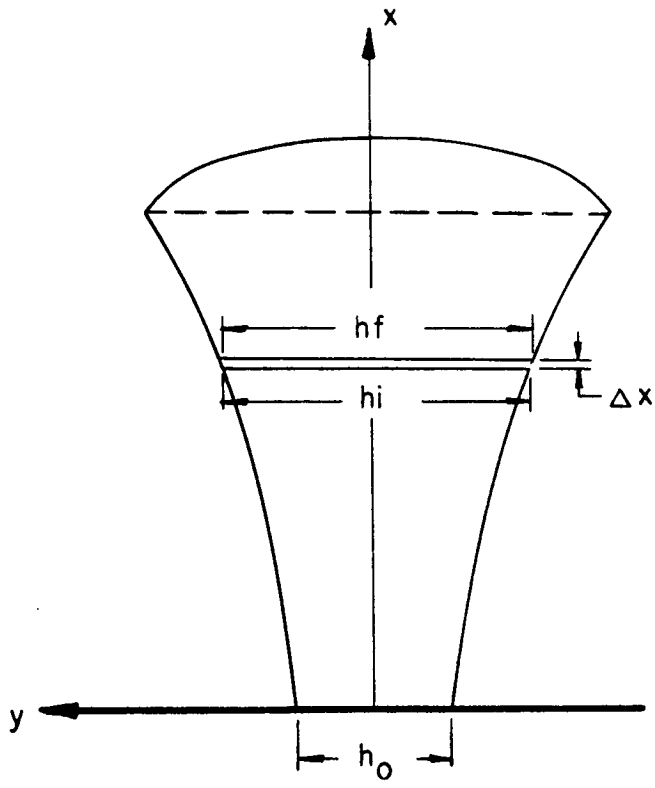

Figure 8.- Schematic representation of projected jet cross section, A_p.

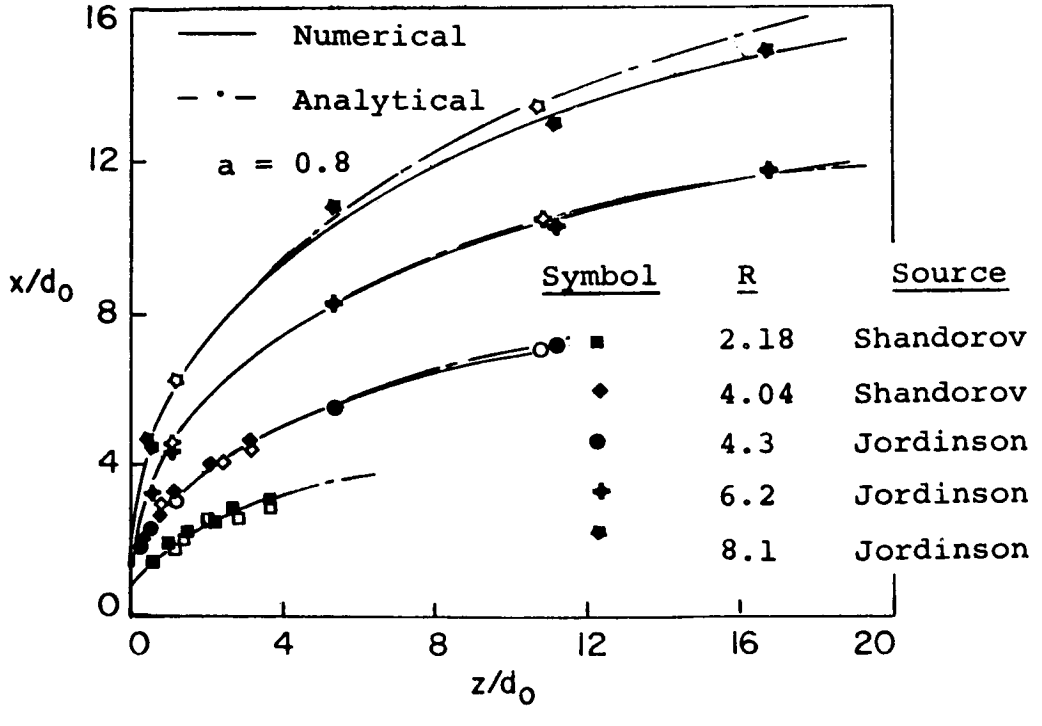

Figure 9.- Matching of published air jet trajectories.

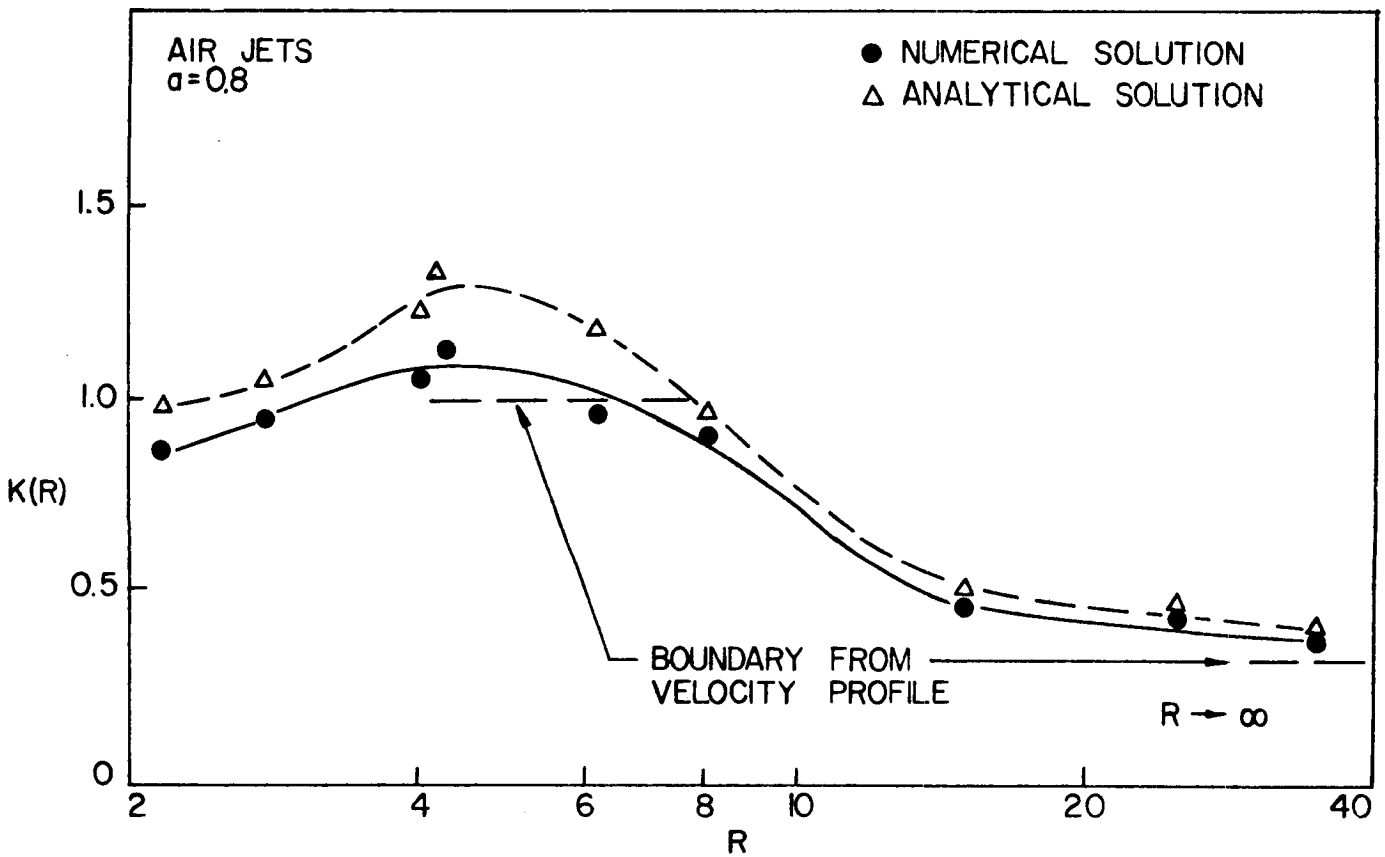

Figure 10.- Spread rate parameters, based on published air jet data.

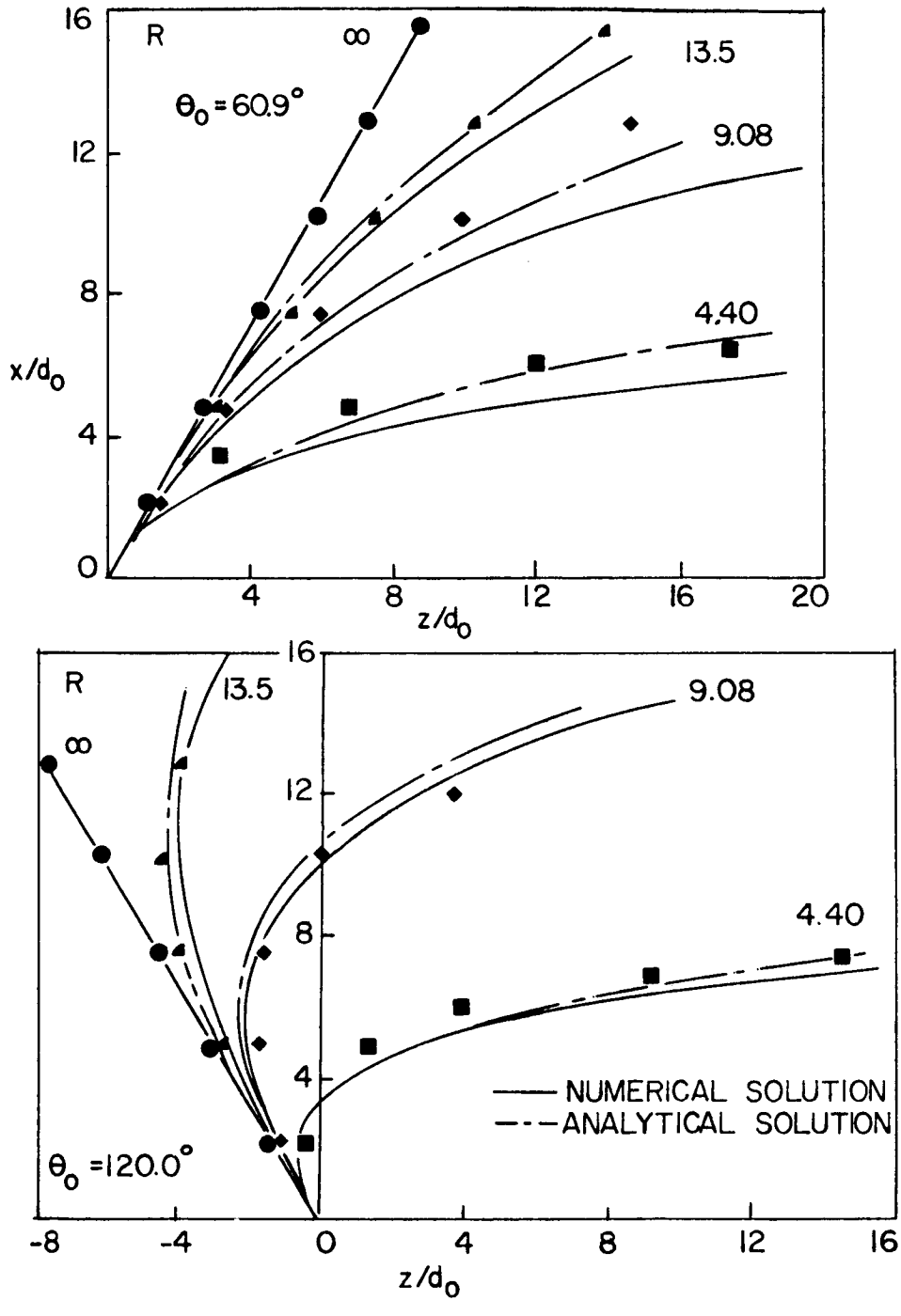

Figure 11.- Matching of trajectories with oblique entry.

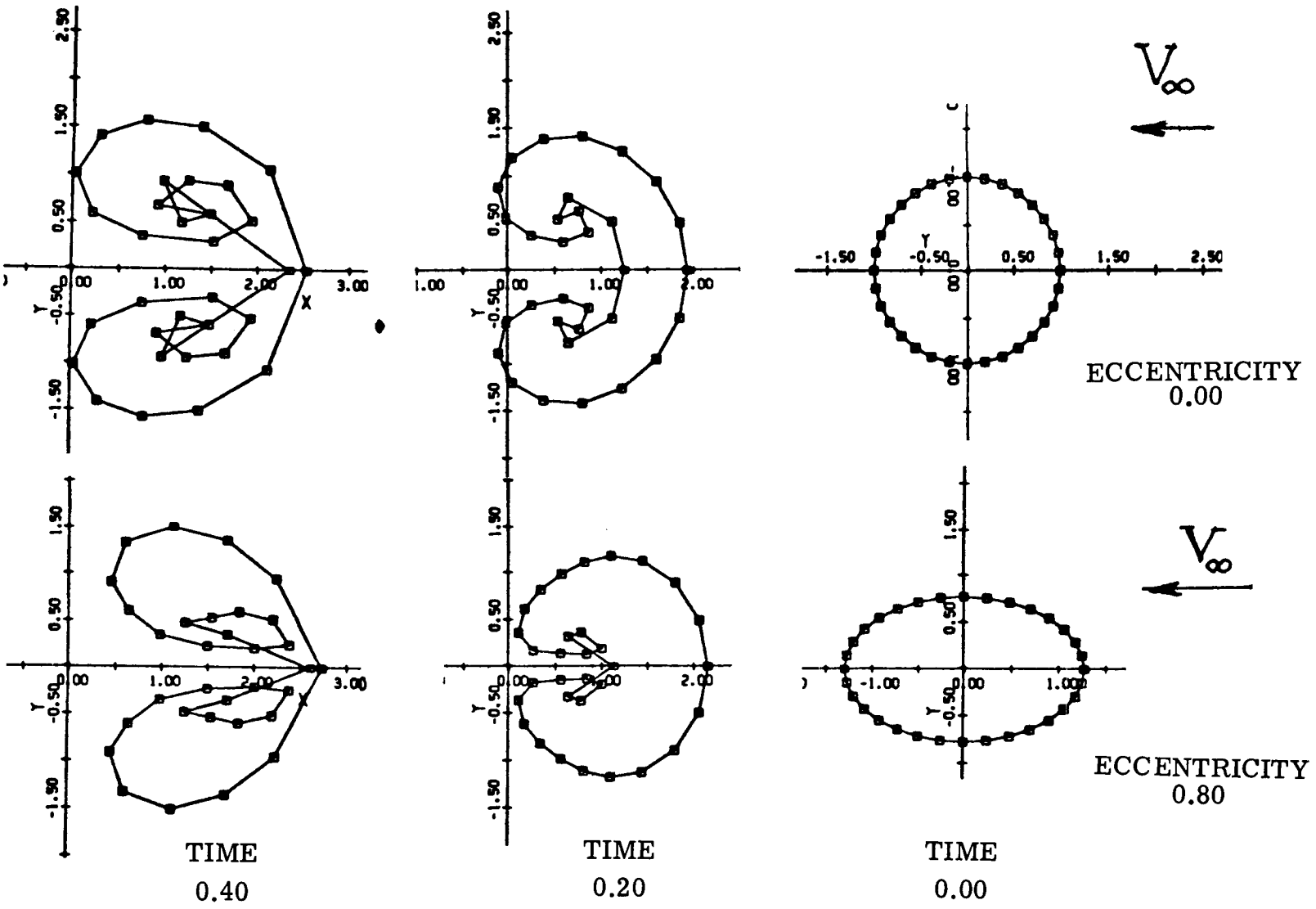

Figure 12.- Rolling-up of two jet cross sections, one with circular, the other with elliptic exit nozzle.

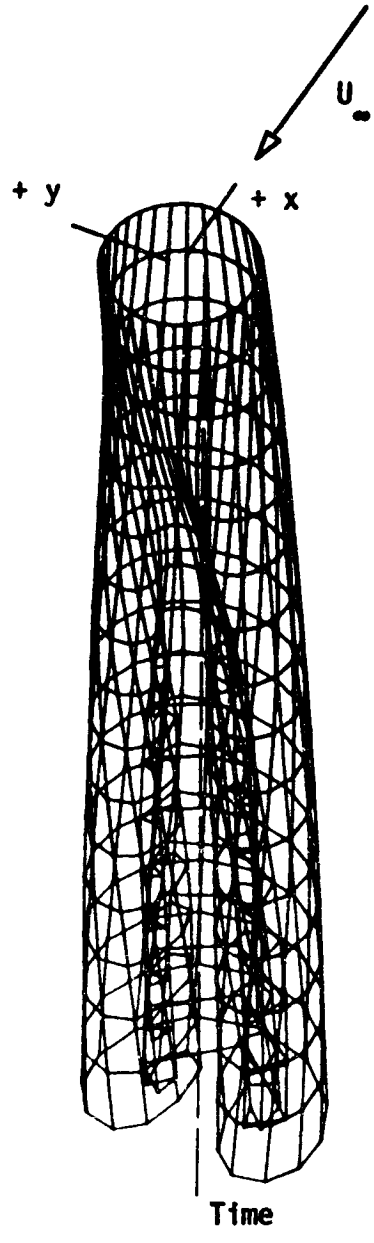

Figure 13.- Stacked cross sections of a circular jet.

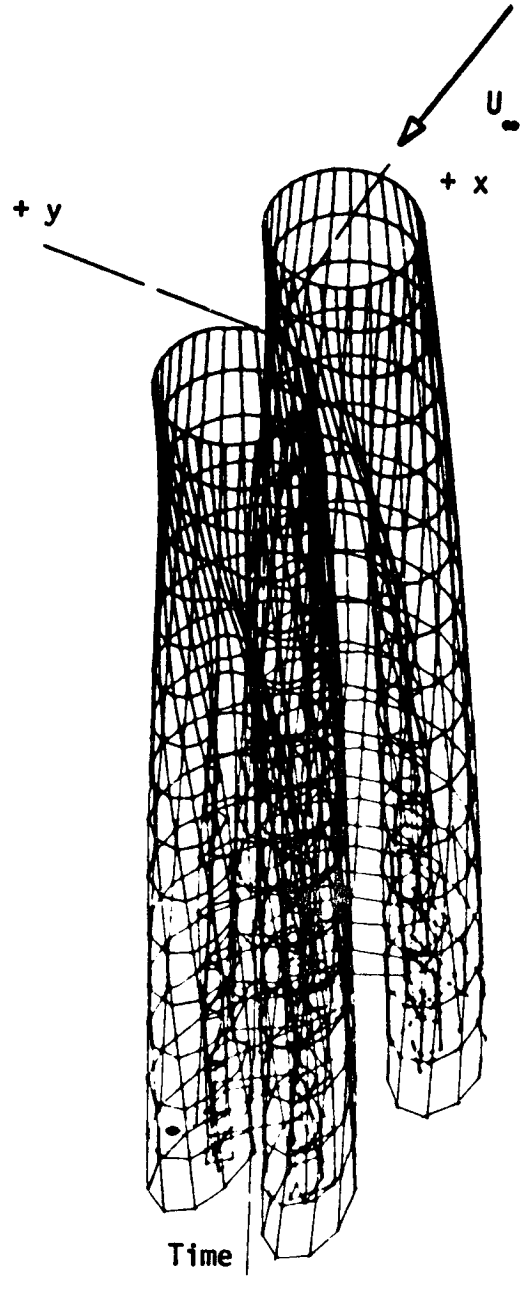

Figure 14.- Stacked cross sections of two circular jets in tandem arrangement.

A GENERAL JET EFFLUX SIMULATION MODEL

By Fred L. Heltsley and Richard A. Kroeger

ARO, Inc.

SUMMARY

The complex flow fields induced by V/STOL aircraft in transition flight give rise to an interest in the problem of a jet issuing into a crossflowing stream. The greatest contributor to the induced flow is the roll up and ensuing vorticity of the viscous jet as it penetrates the free stream. This paper describes recent work done both to understand the forces of interaction of the jet and the field and to present a satisfactory mathematical modeling technique which will be useful in aircraft engineering. The results suggest a need for extensive experimental and analytical studies of the jet in a cross flow.

INTRODUCTION

Classical air vehicles produce an exhaust jet efflux which is oriented nearly parallel to the vehicle flight path. The literature contains many approaches to the solution of the flow resulting from the interaction of the jet and the surrounding field. For analytical simplicity, the flow may be considered in three parts:

1. The internal jet flow
2. The flow external to the jet
3. The boundary of interaction of these fields

Regions one and three require viscous modeling; however, upon application of suitable boundary conditions region two may be effectively represented by singular solutions to Laplace's equation.

V/STOL lift systems in transition flight offer an additional complication in analytical modeling. This is known as the "jet in a crosswind" problem. The three regions of interest are shown in figure 1. The purpose of this paper is to introduce a semiempirical method for providing solutions to region number two, which is of importance in the performance, stability and control of the air vehicle. Special emphasis is placed on generality and engineering simplicity.

SYMBOLS

A	area
b	span of vortex element
d	jet diameter

du/dn	rate of change of velocity with respect to a surface normal
e	entrainment per diameter
$\bar{F}$	force acting on jet
$\bar{M}$	momentum flux
s	distance along jet trajectory
V	velocity
X,Y,Z	jet coordinates in diameters
$\bar{I}$	unit vector
μ	viscosity
ρ	density
τ	shearing stress
ψ	angle between vortex element and impinging velocity
Γ	vortex filament strength

Subscripts:

e	exit conditions
i	entry conditions
j	referring to jet
n	normal component
p	referring to potential solution
t	axial component
∞	referring to remote stream
o	initial condition
$1,2,3,4,5$	order of shed vorticity

PHYSICS OF THE JET

The high degree of complexity of the flow created by a jet issuing normal to a free stream has led to a search for suitable variables for describing its

performance. For example, variables such as jet temperature, exhaust distortion, turbulence and total pressure distribution, Mach number and Reynolds number may be used. On the other hand, these variables may be implied in an empirical set such as entrainment, wake separation, trailing sheet roll up, trajectory and cross-section geometry. Once a sufficient amount of empirical evidence has been compiled, these characteristics may further be condensed to the following set:

1. Jet to free-stream velocity ratio

2. Geometric distortion due to
   Vehicle interference
   Ground interference
   Multiple jet interaction.

Some variables not expressed in this arrangement have disappeared as a result of compromise for simplicity or are implicit in the mathematical formulation.

As a starting point, the simple free jet in a cross flow was studied. The trajectory (ref. 1) was approximated by

$$X = \frac{1}{4}\left(\frac{V_\infty}{V_j}\right)^2 (Z)^3 \qquad (1)$$

where X,Z are the jet coordinates nondimensionalized by diameter from figure 1 and V_∞/V_j is the ratio of the free stream to jet velocity ratio. The jet entrainment was found by integration of experimental data from reference 1 to be

$$e = 0.19 \text{ per diameter} \qquad (2)$$

which is the decimal rate of mass flow increase along a specified jet surface per exit diameter. Due to the lack of experimental data, the accuracy or variation of this parameter with V_∞/V_j was not known.

Figure 2 shows the distortion of the total pressure profile along the path of the jet. Two major counterrotating vortices appear to be formed which increase in strength as the jet grows. These have been observed in many experimental studies and are of great importance to the flow.

This has been a cursory description of the jet in light of its extreme complexity. It remains to be shown that such naive observations can be useful in defining the flow region external to the jet.

VORTEX SINGULARITY MODELING

A good approximation to the flow in the region where viscous effects are small may be made by the potential theory. This was applied by direct superposition of singular solution to Laplace's equation with the appropriate boundary

conditions. Vortex singularities are very useful for three-dimensional lifting bodies. Other types of singularities including doublets, bicirculation, sources and sinks may be more appropriate for particular applications. Though some compromise in numerical simplicity was paid, vortex singularities were used for the modeling for total system simplicity.

Figure 3 shows the application of the vortex lattice method to a simple fan-in-wing configuration. Vortex singularities were used throughout with the following boundary conditions:

1. V_∞ = uniform
2. The flow component normal to the wing surface vanishes
3. The flow into the inlet = V_j
4. The flow normal to the jet efflux simulation tube surface must compensate for entrainment.

Figure 4 shows an isometric view of the simulation of a propeller with its axis normal to the free stream. Some calculated streamlines are shown. The flow asymmetry at the prop inlet was induced by variation of the inlet flow between the individual boundary control points.

Figure 5 shows how the jet roll-up was simulated by the trailing vortex elements. Two cross sections are shown for comparison of the model flexibility. Note that the downstream cross section (B-B) has grown in size and the number of trailing vortices used in its composition have increased. Figure 6 shows how these vortices were dispatched. The similarity with the low aspect ratio lifting surface analogy was noted. As the jet axis is traversed away from the exhaust nozzle, the number of trailing elements may be seen to continuously increase.

INTERACTION BETWEEN THE JET AND THE SURROUNDING FLUID

As the jet issues into the crossflowing stream, forces of action and reaction develop. The jet is deflected and distorted by the stream with a set of forces whose reaction causes an influence to be felt over the entire field. Figures 1 and 2 show the two primary results of these forces. It seems reasonable that if the surrounding fluid acts to form such distortions, and if that field may also be represented by singular solutions to Laplace's equation, then vortex elements may be employed to simulate the forcing elements in that field.

In the model described here vortices were used for simulating wake blockage, entrainment and the trailing sheet. The latter was shown to be the greatest contributor to the flow distortion behind the jet. As in the case of wing theory, the strength of the trailing sheet was calculated by application of the correct boundary conditions. However, the presence of the viscous jet made the corresponding boundary difficult to define.

The objective of this section is to present an analytical model for the jet which will provide a solution to the field away from the jet. In effect, this is the inverse of the jet trajectory problem as the kinematics of the jet are a priori empirically specified. The vortex model described in the previous section was applied to the jet in a cross-wind problem. The trailing system was arranged as in figure 6. The results are shown in figure 7. Though the trailing system was very roughly approximated by the straight vortex lines, the experimental data shown in the plane of symmetry were matched quite nicely. The importance of the trailing system can be seen by comparison with figure 8 wherein the same jet was simulated by entrainment and blockage only.

The boundary condition sought in the modeling of the trailing vortex system was that no flow could cross the defined sheet. A one pass semiempirical computer solution was found which simultaneously solved all the vortex strengths as a consequence of the geometry and the boundary conditions. The strengths of the individual vortices in the trailing system were distributed along the jet axis as shown in figure 9. A cut was taken across the sheet, normal to the filaments, and the total wake vorticity on one side of the jet was obtained. This strength reflects the forces acting on the fluid field. A plot of the trailing element strength is shown in figure 10.

It must be pointed out that the vortex strengths calculated in this exercise are effective strengths and would correspond to the viscous case only if the latter were 100 percent effective. It would be expected that if the actual vorticity could be experimentally measured it would appear higher than those which the mathematics requires in the simulation model. This argument must preclude the existence of a complex wake system with additional counterrotating filaments.

As a means of further understanding the meaning of the results of the analytical modeling, a more in-depth look was taken at the development of the trailing system. This approach required a detailed experimental knowledge of the internal jet flow. Since such data were nonexistent, a particular jet boundary was defined and information was extrapolated from the experiments of Shandorov. The goal was to compute, for comparison, the circulation strength from the calculated induced forces of reaction between the jet and the surrounding fluid.

Figure 11 shows the jet induced force $\overline{F}$ which was to be found. The component $\overline{F}_n$ is normal to the jet axis while $\overline{F}_t$ is tangential. The momentum flux rate along the jet is

$$\overline{M} = \int \rho V^2 dA\overline{l} \tag{3}$$

where ρ is the fluid density, A is the jet cross-sectional area, V is the local jet velocity component and $\overline{l}$ is a unit vector in the direction of local flow. If the momentum flux was known along the jet, the interaction force could be easily calculated. In finite element form, the force acting on a jet control volume element is given by

$$-\bar{F} = \int \rho V_e^2 \, dA_e \bar{l}_e - \int \rho V_i^2 dA_i \bar{l}_i \tag{4}$$

The subscripts i and e denote entry and exit, respectively. The control volume was defined as an axial element of the jet whose extremes are planes normal to the jet axis. The peripheral surface coincided with the locus of the velocity profile where the shear stresses become sufficiently small to divide the jet from the field which was called potential. This roughly matched the outer boundary of the profiles shown in figure 2. The need becomes apparent for the definition of a maximum allowable shearing stress

$$\tau_p = \mu \frac{du}{dn} \tag{5}$$

which would not invalidate a potential solution. The derivative in equation (5) is the rate of change of velocity with respect to a surface normal.

The next step was to calculate the strength of the bound vortices which would produce the force described in equation (4). From elementary three-dimensional lifting theory the force on a bound vortex is given by

$$\bar{F} = \rho \bar{V} \times \bar{\Gamma} b \tag{6}$$

where $\bar{\Gamma}$ is the strength and b is the span of the lifting element. Next, the force on the jet was assumed equal to that induced by a group of distributed bound vortices, each with a pair of trailing elements. This arrangement is shown in figure 9. Their strengths were found by equating equations (4) and (6). Thus,

$$\bar{\Gamma} = \frac{F}{\rho V b \sin \psi} \bar{l} \tag{7}$$

Since the jet velocity vector imposed on $\bar{\Gamma}$ was normal to the bound element, sin ψ was taken as unity and the scalar magnitude of vorticity written

$$\Gamma = \frac{F}{\rho V b} \tag{8}$$

The rationale for using the jet velocity in this equation was that the bound element was assumed to span the jet. In the potential model, the average internal jet flow velocity could be matched with that in the real jet. As each vortex strength was determined by the induced velocity over the bound filament, the jet velocity fulfilled the requirement.

Upon breaking the jet into longitudinal control volumes, equation (8) was calculated and integrated along the trajectory s for the total sheet strength.

The propeller model introduced earlier was used as an example of the application of this technique. This example was chosen at the risk of making the foregoing developments appear somewhat precocious in light of the experimental data at hand.

First, the jet characteristics were calculated using the data from reference 2. Some guess work was necessary to arrive at the integrals of the flow. Figure 12 shows the axial momentum distribution. It is interesting to note that the momentum starts to decrease quite rapidly upon exit to the free stream and then begins to increase. Though the validity of the data application was somewhat in question, it is felt that the resulting flux could be reasonable. The mechanism for such distortions was felt to be the trailing sheet rapidly rolling up at the knee of the trajectory causing some of the axial momentum to be changed to rotational momentum. Later, the rotational component is apparently reintroduced in the axial direction as the vortices are bent.

By applying equation (4) to this data, figure 13 was obtained. The force vectors shown are the negative of those forces which act on the fluid field. Figure 14 shows the strength of the trailing sheet calculated from the forces on the fluid field. The width of the jet was taken from figure 2 to be the span of the bound vortex filament.

The forces of interaction between the jet and the free stream have been defined and a method of semiempirically evaluating the resulting remote potential flow field described. The interesting comparison between figures 10 and 14 shows the existence of a method for imposing vorticity in the trailing jet wake either by direct potential calculations or by derivatives of experimental data.

CONCLUSIONS AND RECOMMENDATIONS

A semiempirical solution of the flow field induced by a jet in a crossflow has been presented. It is yet somewhat premature to speculate on the quantitative effectiveness of the technique even though figure 7 is very well matched in the plane of symmetry.

The comparative trends of figures 10 and 14 show the logic of the simulation to be in order. The shortcoming in the proof is in the limitation of applications due to the availability of adequate experimental information. Experiments should be conducted which define the jet boundary and momentum flux so that the induced forces may be computed accurately. Flow-field information away from the jet should be compiled to complete the verification of the semiempirical model. Finally, computer experimentation should be conducted to define the boundary conditions which provide adequate analytical representation.

REFERENCES

1. Margason, Richard J.: The Path of a Jet Directed at Large Angles to a Subsonic Free Stream. NASA TN D-4919, 1968.

2. Abramovich, G. N.: The Theory of Turbulent Jets. M.I.T. Press, c.1963.

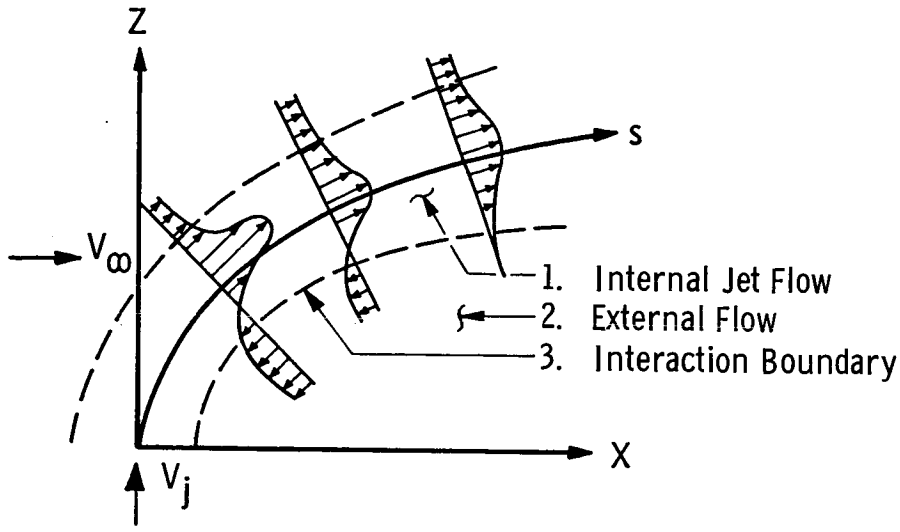

Figure 1.- Areas of interest.

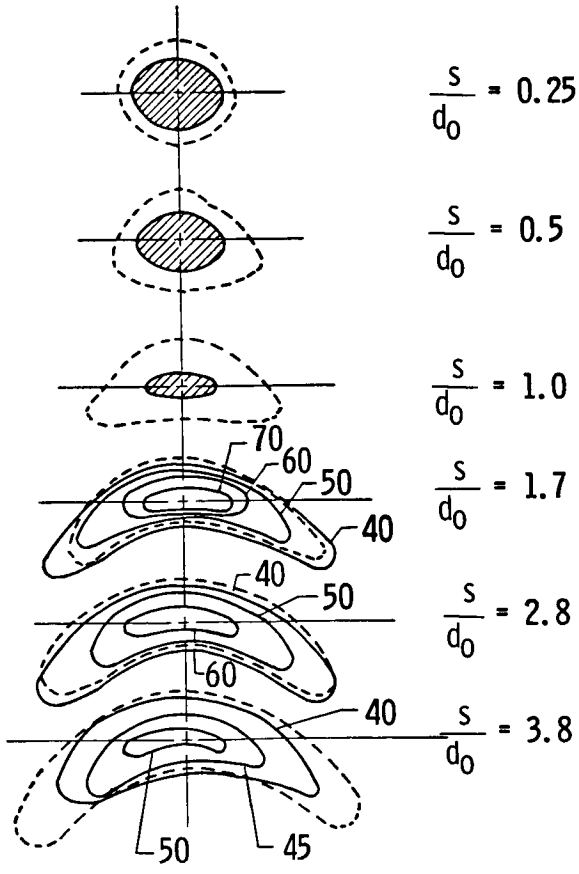

Figure 2.- Total pressure per cross section.

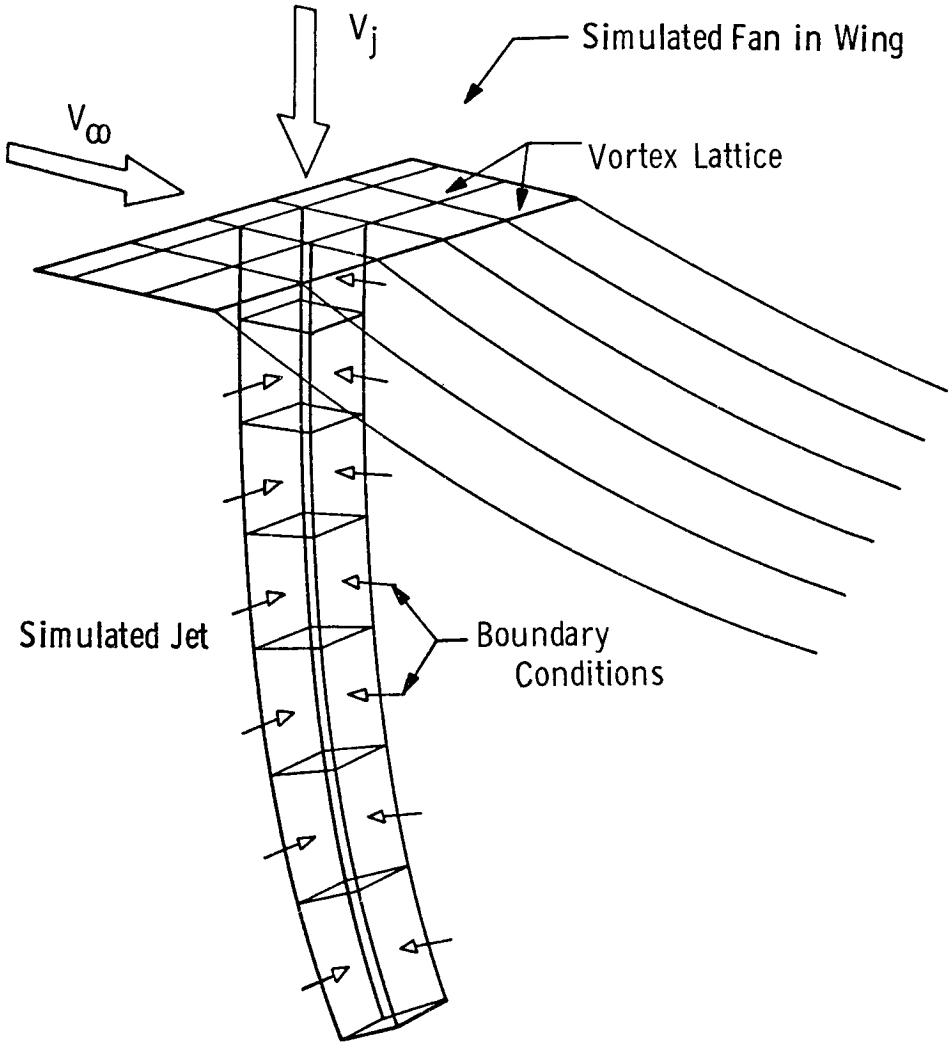

Figure 3.- Vortex lattice model.

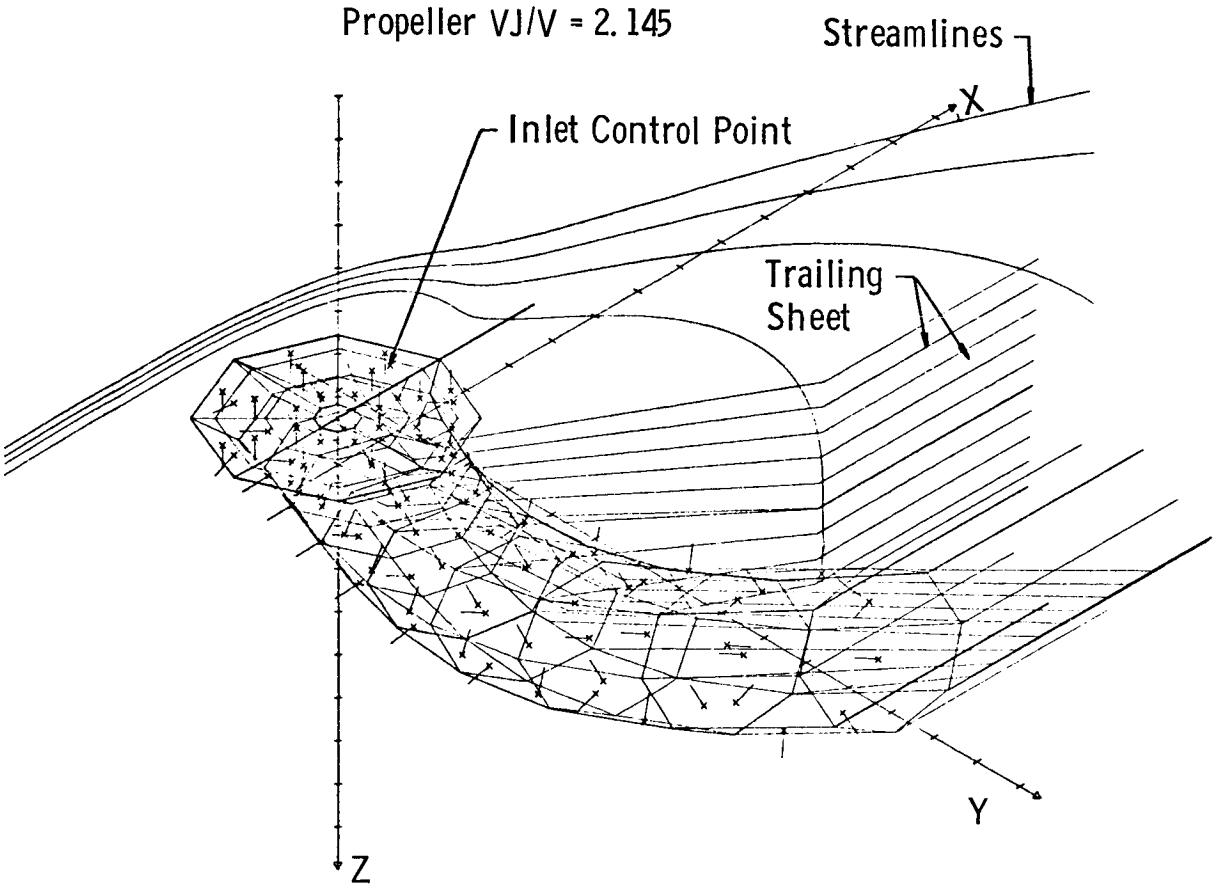

Figure 4.- Propeller representation.

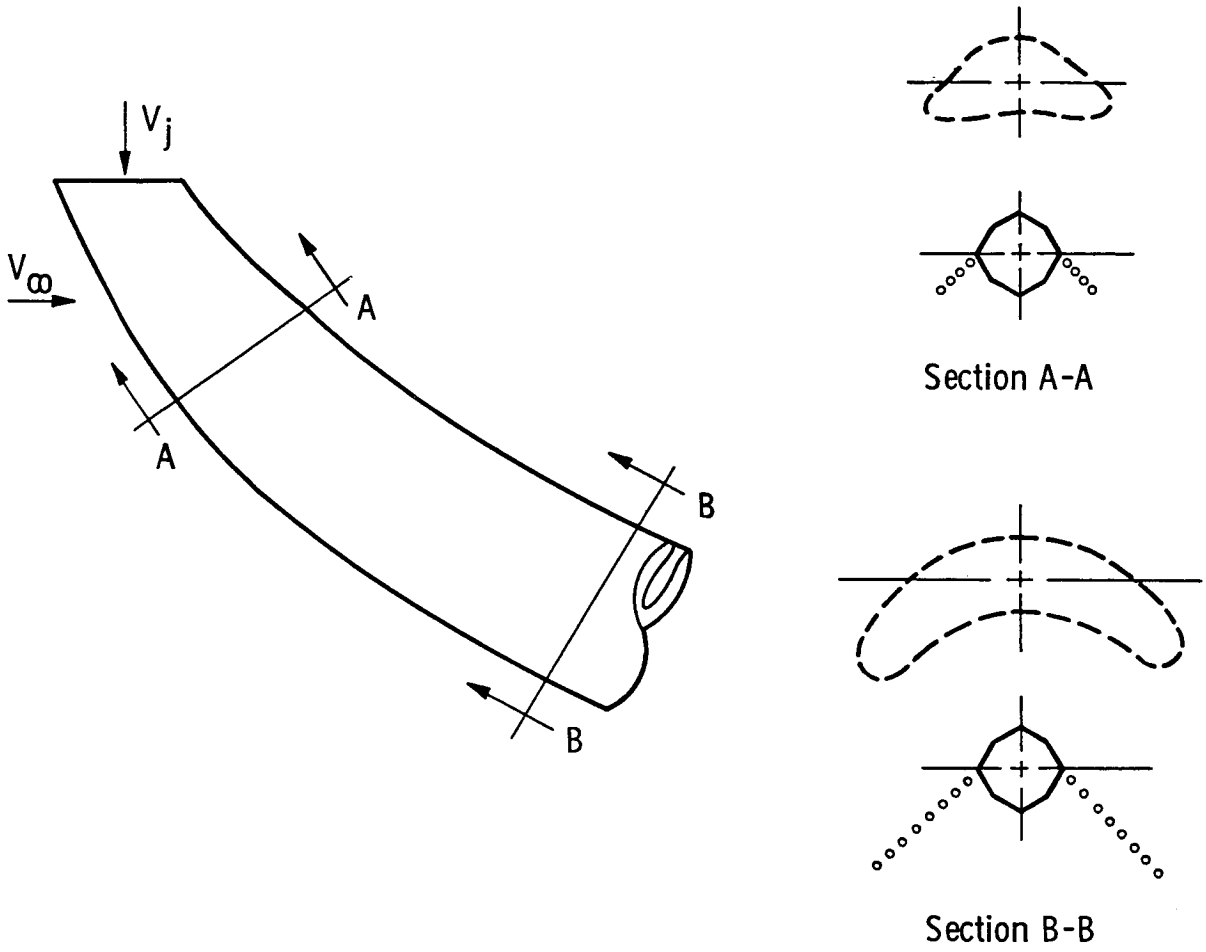

Figure 5.- Specification of trailing vortex element position.

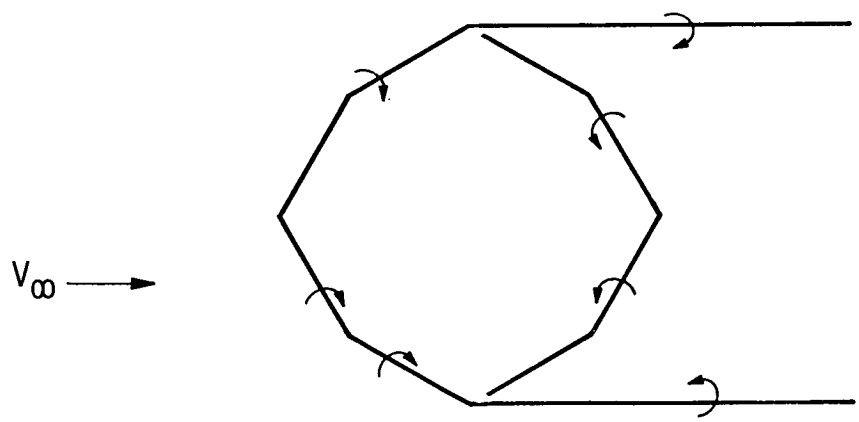

Figure 6.- Bound vortex positions.

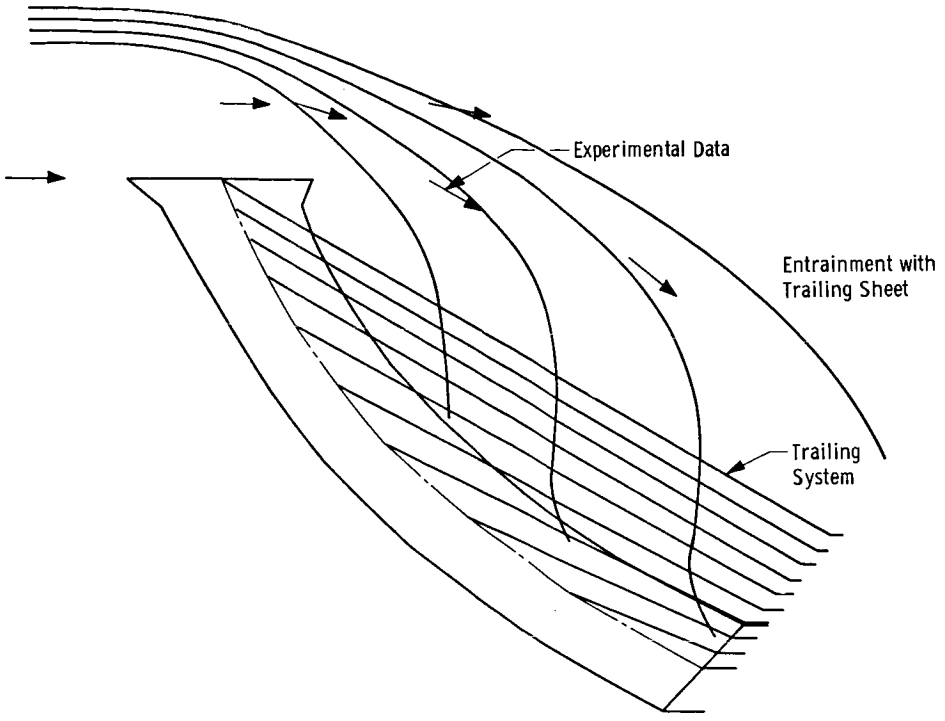

Figure 7.- Comparison of analytical and experimental results.

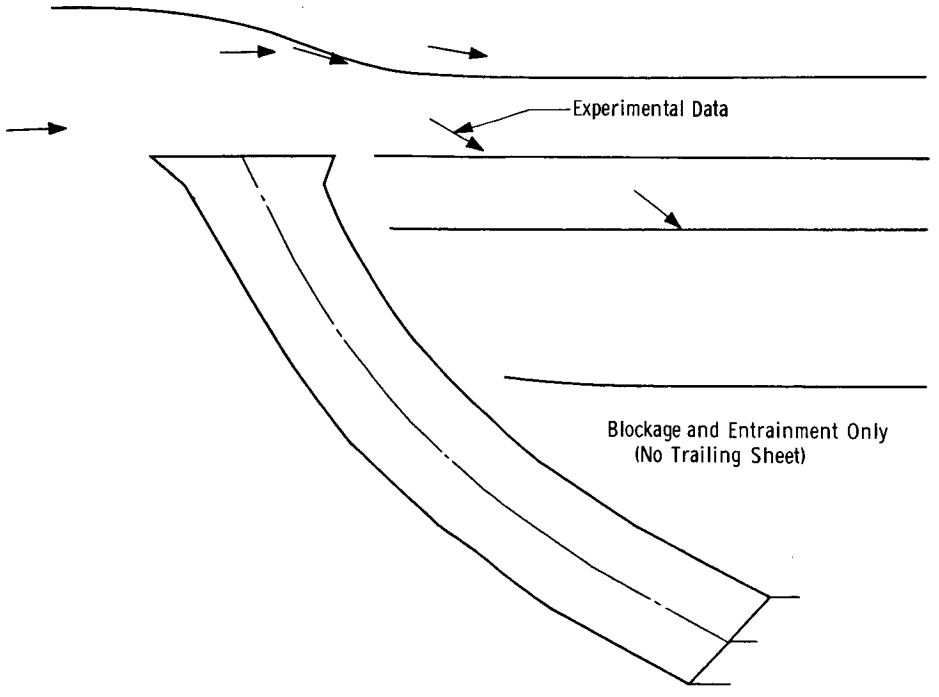

Figure 8.- Comparison of analytical and experimental results with only blockage and entrainment encountered for.

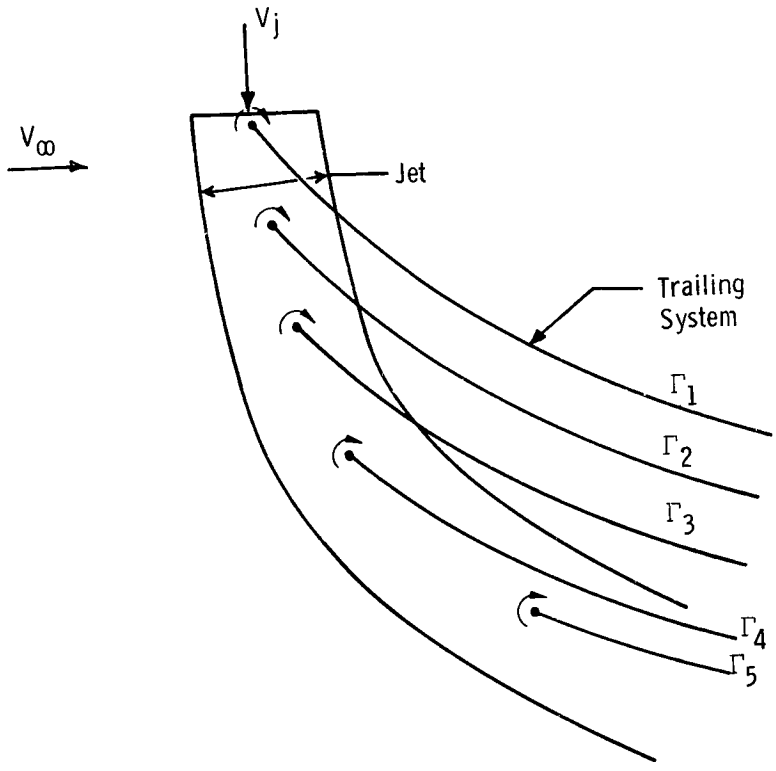

Figure 9.- Trailing vortex nomenclature.

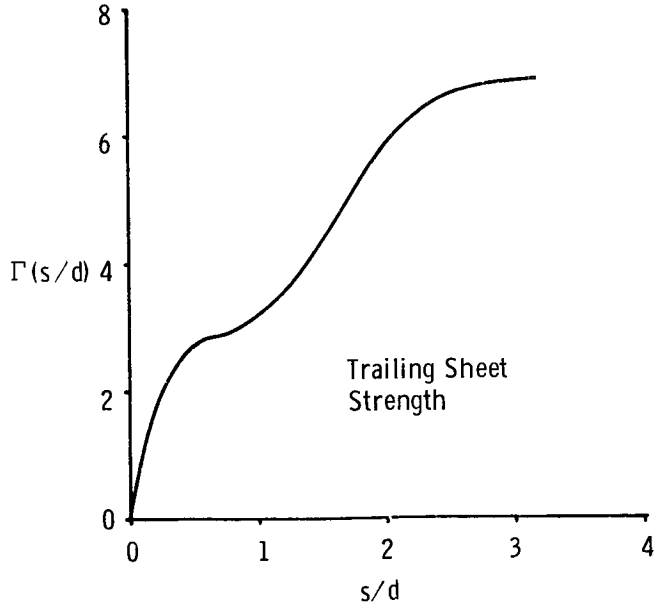

Figure 10.- Analytical distribution of shed vorticity.

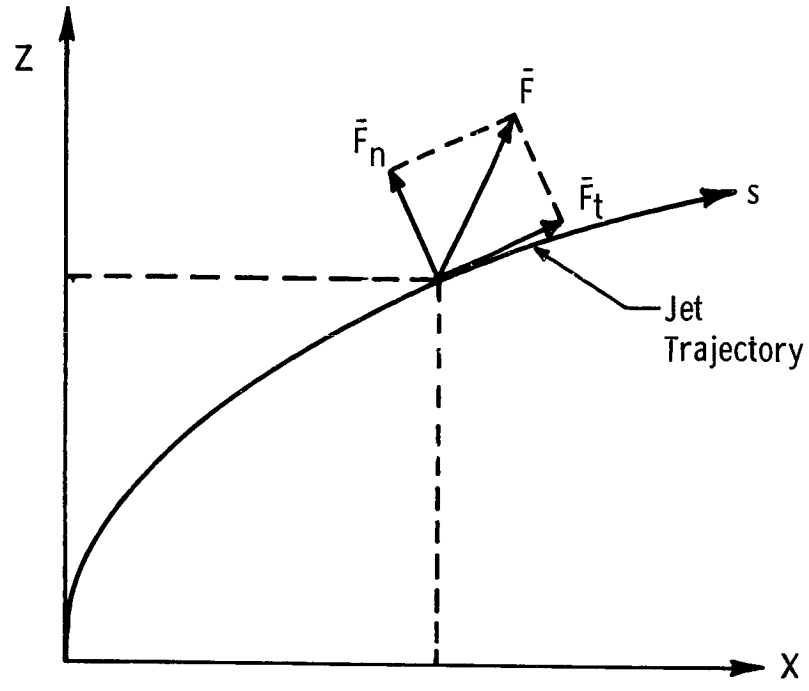

Figure 11.- Definition of force acting on jet.

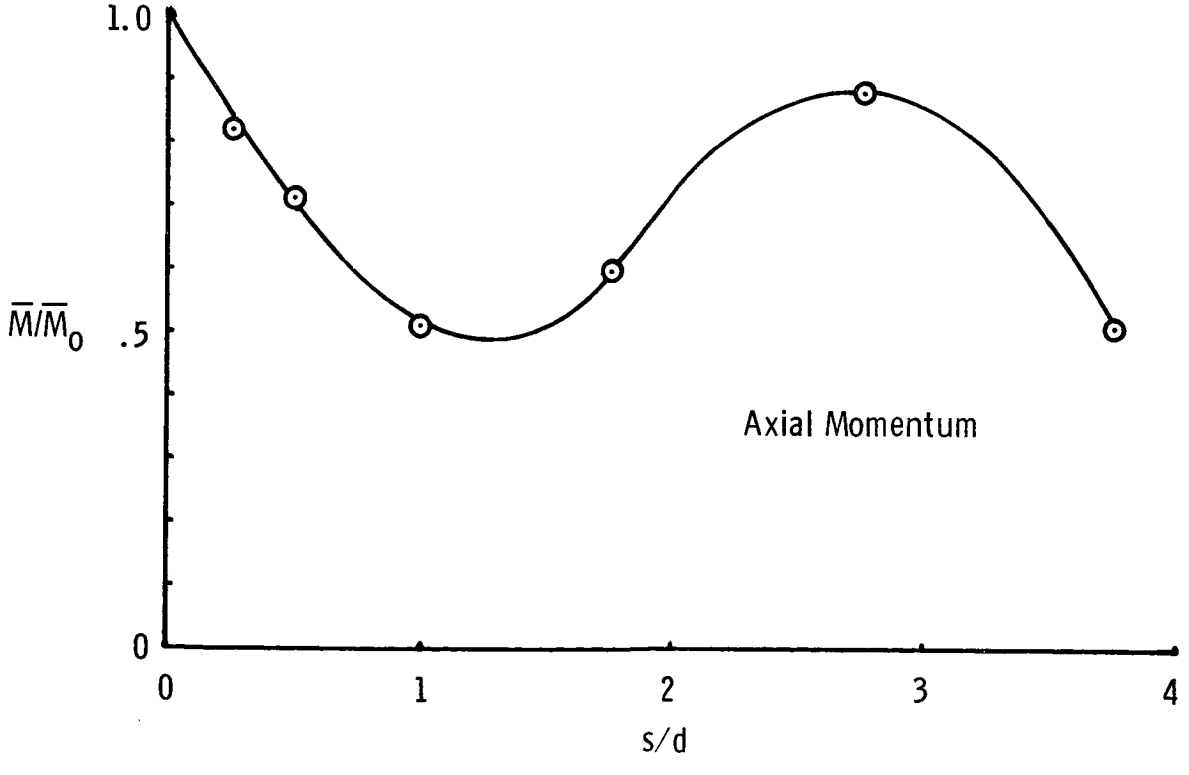

Figure 12.- Empirical distribution of axial momentum.

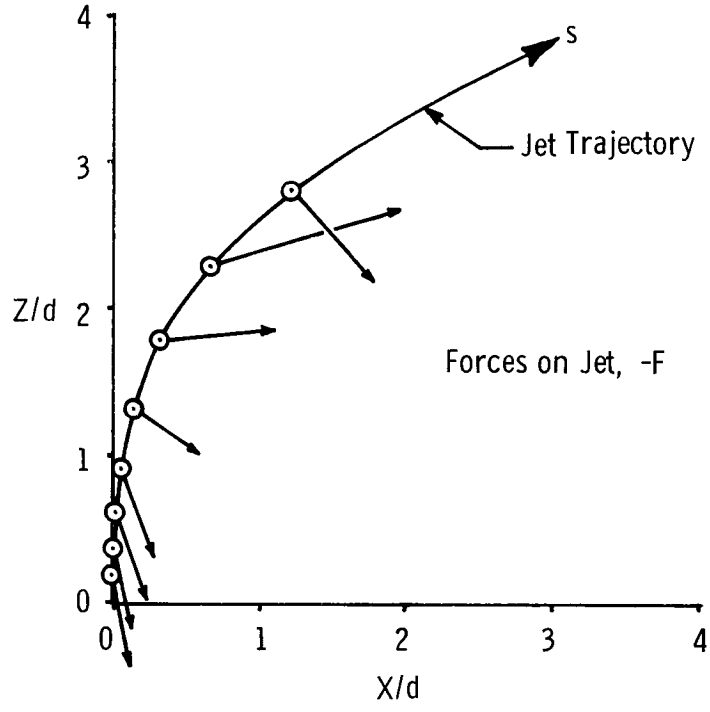

Figure 13.- Forces acting on jet.

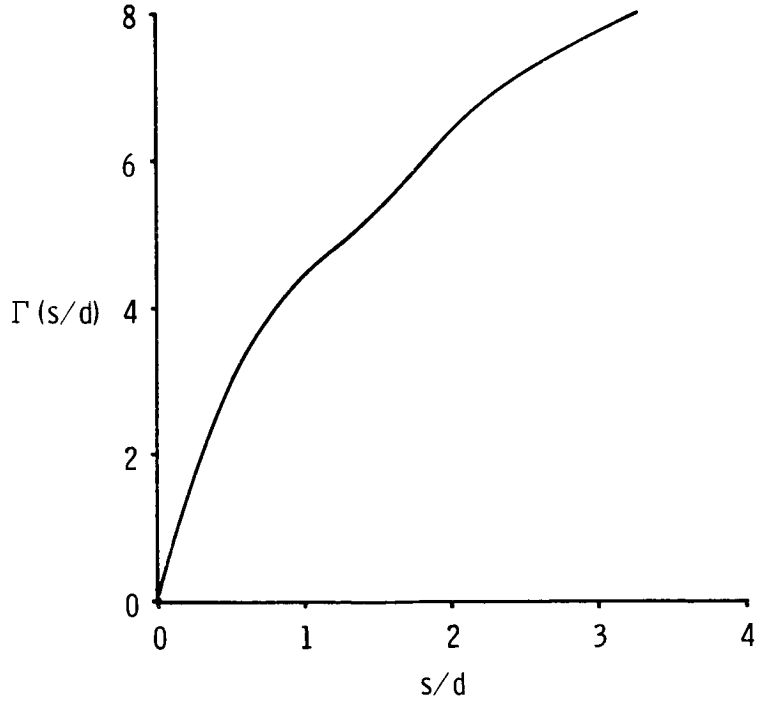

Figure 14.- Empirical distribution of shed vorticity.

CALCULATION OF JET INTERFERENCE EFFECTS ON V/STOL AIRCRAFT BY A NONPLANAR POTENTIAL FLOW METHOD

By Paul E. Rubbert

The Boeing Company

SUMMARY

A method of calculating the flow field about V/STOL aircraft with a potential flow model is reviewed with emphasis on the flow modeling requirements. Comparisons with experimental data are used to demonstrate the importance of proper jet simulation. The dominant flow features associated with a jet are reviewed and a theoretical model is proposed which recognizes these features. An experimental program is suggested as a means for determining various parameters appearing in the jet model.

INTRODUCTION

The calculation of jet interference effects on V/STOL aircraft is considerably more complex than the classical treatment of interference in the context of linearized lifting line or lifting surface theory based on small disturbance concepts. Within the linearized small disturbance framework, interference effects are interpreted in terms of superimposed downwash fields which are akin to camber and angle-of-attack changes, and buoyancy effects associated with the longitudinal interference velocity field. Such concepts are based on the requirement that all disturbance velocities are small compared with the freestream speed, and that the rate of variation of the interference velocity components within the confines of the airplane dimension remain small. Such is not the case for V/STOL aircraft, which typically operate with high inlet inflow velocities, are subject to interference effects from jet entrainment that vary widely over distances comparable to the aircraft dimensions, and can operate at low forward speeds.

Thus, one is led to abandon the simplified small disturbance concepts and adopt a less approximate scheme. The present paper describes such a scheme (refs. 1 and 2) and focuses attention on its limitations and on the particular problems associated with the efflux jet.

SYMBOLS

a_n	entrainment coefficient (n = 0, 1, . . .)
C_D	drag coefficient
C_L	lift coefficient
C_m	pitching moment coefficient
C_p	pressure coefficient
c	chord
m	source strength
n	distance normal to a surface
$\vec{p}$	unit vector normal to centerline in plane of trajectory curve
$\vec{q}$	velocity
r	distance
s	distance along the jet centerline
S	boundary in a potential flow model
S_1	portion of S consisting of the body surface
S_2	portion of S encompassing the jet
V_∞	freestream speed
V_{INFLOW}/V_∞	jet velocity ratio
x,y,z	Cartesian coordinates
α	angle of attack
η	span fraction
θ	angle around the jet
μ	doublet strength
σ_j	singularity strength on panel with index j
φ	velocity potential

POTENTIAL FLOW CALCULATION METHOD

Modeling the Real Flow

The present scheme is based upon a capability for solving Laplace's equation (irrotational incompressible flow) numerically in three dimensions subject to arbitrary but properly posed boundary conditions; namely, Neumann, Dirichlet or mixed boundary conditions, or variants thereof, on closed boundaries whose spacial orientation is known. The initial task, when applying this method to a V/STOL problem, is to formulate a theoretical model of the real flow that meets the above requirements while yet retaining the essential features of the flow.

Figure 1 shows such a theoretical model that was developed (refs. 1 and 2) for a fan-in-wing aircraft. The assumptions inherent in its formulation are as follows:

1. The outer flow is assumed to be incompressible and irrotational.

2. Boundary layer displacement effects are ignored.

3. Regions of separated flow are not simulated.

4. The spacial orientation of the trailing vortex sheet is prescribed on the basis of a priori knowledge or experience.

5. The inflow distribution at the fan face must be prescribed.

6. The trajectory and distribution of entrainment on surfaces encompassing the efflux jets must be prescribed. For this model the entrainment was assumed to be zero.

7. The fuselage has been deleted for computational economy.

These assumptions serve to reduce the problem to manageable form. They also impose certain limitations on the usefulness and domain of applicability of the present calculation procedure as discussed in refs. 1 and 2.

Numerical Procedure

The numerical solution procedure is based on the concept of source and doublet (or vortex) distributions on the boundary surfaces. Distributions of these singularities are approximated numerically by networks of small quadrilateral panels with the singularity strength of each panel set equal to an arbitrary constant value, say σ_j . Figure 2 shows the paneling used for the model of Fig. 1. Certain portions have been omitted for clarity. This numerical panel approximation reduces the problem to the determination of a finite number of discrete singularity strengths, one for each panel.

One point in each panel, the "boundary point", is selected as the point where the boundary conditions are to be satisfied. The requirement that the boundary conditions be satisfied at all boundary points produces a system of linear algebraic equations whose solution yields the desired values of σ_j. From these the entire velocity and pressure field are calculated. References 1 and 2 contain a more detailed description of the procedure.

Experience has shown that one of the key points in using the method is the selection of the singularity type (either source or doublet) to represent the various surfaces. There are an infinite number of possible choices, and the user must be careful to select a combination of source and doublet panels that guarantees a unique solution. The basic concepts contained in Chapter III of Lamb (ref. 3) are invaluable for providing the proper insight. Another guideline for the choice of singularity distributions is that the panel approximation is limited accuracy-wise in a manner related to the change in singularity strength from panel to panel (refs. 1 and 2). This limitation imposes restrictions on both panel size and spacing and on the initial selection of singularity types. Experience with the numerical method together with a firm understanding of the fundamentals of potential flow theory serve to minimize the importance of these restrictions. These words of caution are offered to prevent the uninitiated from becoming overly enamored at the outset by the apparent simplicity and power of the method. Successful application of this method to new and different problems is strongly dependent on the user's ability to model the real flow properly and to select the appropriate singularity and panel arrangements.

Initial Results and Problem Areas Uncovered

The present method, when properly used, provides a finely detailed solution of the inviscid model problem. The solution provides surface and flow field pressures and velocities, and forces and moments obtained from integrated surface pressures. Figure 3, which has been reproduced from ref. 2, shows a comparison between the measured and calculated forces on the fan-in-wing model described in Fig. 1. These were obtained with a moderate inlet velocity ratio of $V_{INFLOW}/V_\infty = 1.667$ and with the efflux jet vectored aft by 20°. No entrainment was assumed on the periphery of the jet boundary. The various theoretical curves denote different assumed inflow distributions at the fan face and demonstrate the sensitivity of the calculated forces to this parameter. The differences between the curves arise primarily from the computed internal force on the fan assembly calculated by a momentum balance across the fan. This force is added to the integrated pressure force on the external surfaces to give the total force acting on the configuration. The calculated drag levels are lower than the measured values, which is to be expected since the profile drag is not included in the calculated values. The variation between the pitching moment curves can be attributed to the absence of the fuselage on the theoretical model and to boundary layer displacement and local separation effects.

A comparison of the calculated surface pressures with experiment often shows a variation between them which increases with inlet velocity ratio. Figure 4, taken from ref. 2, shows an example with an inlet velocity ratio of 3.636. Large differences are apparent, particularly in the vicinity of the fan and flap regions. Gross deviations of upper surface pressures near the fan are probably caused by inaccuracies in the assumed inflow distribution. Large deviations on the lower surface near the fan exit can be attributed to jet entrainment effects which were not simulated theoretically. The discrepancies in the flap pressures, which are greatest at the station directly aft of the jet, may also be due in part to the strong influence of the entraining jet as well as to viscous effects which are important in this region. This example serves to illuminate the importance of both inflow distribution and proper jet representation in the theoretical treatment of V/STOL problems. Lesser discrepancies that exist in regions more remote from the fan must also be due partly to these effects, because experience with the method applied to conventional airplanes has demonstrated an order of magnitude improvement in detailed surface pressure comparisons when lift fans are not present.

Thus it appears of utmost importance for V/STOL applications to improve our capability to treat these effects properly. The question of what is the proper inflow distribution can be answered partly by further experimental measurements and correlation with the basic parameters, and involves no change in the basic theoretical or numerical representation. The representation of the jet efflux, however, poses a more difficult problem.

REPRESENTATION OF A JET IN A POTENTIAL FLOW

Let us examine the jet representation in some detail and attempt to identify those parameters which can have the most significant effects on the calculated flow near the surfaces of the airplane.

Basic Concept

The representation of a viscous, turbulent jet by means of a potential flow model is based on the following concept. Consider the example of a jet emerging from a body into a flow field. The flow external to the jet is considered to be inviscid and irrotational. This allows the definition of a velocity potential φ associated with the inviscid external flow. Let us define a closed boundary S consisting of two parts; one part S_1 being the body surface and the other part S_2 being any arbitrary surface encompassing the turbulent jet flow, Fig. 5. Green's theorem applied to the exterior potential flow field (ref. 3) leads to the following expression for the potential φ .

$$\varphi(x,y,z) = \underbrace{-\frac{1}{4\pi}\iint_S \frac{m(s)}{r}\,ds}_{\text{SOURCE DISTRIBUTION}} + \underbrace{\frac{1}{4\pi}\iint_S \mu(s)\,\frac{\partial}{\partial n}\left(\frac{1}{r}\right)ds}_{\text{DOUBLET DISTRIBUTION}} \qquad (1)$$

where

$m(s)$ = source strength on S

$\mu(s)$ = doublet strength on S

r = distance from S to a field point (x,y,z)

n denotes the direction normal to S

The terms on the right-hand side of Eqn. (1) can be interpreted as distributions of source and doublet singularities on the boundary surfaces. The singularity strengths, $m(s)$ and $\mu(s)$, can be obtained as the solution of the boundary value problem obtained by letting the field point (x,y,z) in Eqn. (1) approach the boundary surface and differentiating the entire equation with respect to the surface normal, giving

$$\frac{\partial\varphi}{\partial n}(S) = -\frac{1}{4\pi}\vec{n}\cdot\nabla\iint\frac{m(s)}{r}ds + \frac{1}{4\pi}\vec{n}\cdot\nabla\iint\mu(s)\,\frac{\partial}{\partial n}\left(\frac{1}{r}\right)ds \qquad (2)$$

The numerical method previously described furnishes solutions for $m(s)$ and $\mu(s)$ as a function of the normal velocity component $\frac{\partial\varphi}{\partial n}(S)$ on the boundary surfaces. Thus the entire flow field described by $\varphi(x,y,z)$ is ultimately dependent upon a knowledge of the normal velocity component $\frac{\partial\varphi}{\partial n}(S)$ on the boundary surfaces.

In the usual problem, $\frac{\partial\varphi}{\partial n}$ is known on the body surface S_1, which includes the external surface of the airplane through which no flow can pass, plus the portion of S_1 across an inlet on which the value of $\frac{\partial\varphi}{\partial n}$, which provides the inflow distribution, must be specified. If $\frac{\partial\varphi}{\partial n}$ were known on S_2 as well, then the influence of the jet on the external flow would be accurately established. However, this is not the case, and so our ability to simulate the effect of a jet on the external flow ultimately reduces to a need for estimating the distribution of the normal velocity component $\frac{\partial\varphi}{\partial n}(S_2)$ on any arbitrary boundary surrounding the turbulent jet.

This needed information must be obtained from experimental observation. The recent literature (ref. 4) indicates that experimentalists are acquiring greater insight into this problem. Ultimately, it is hoped that their work will lead to a set of empirical relationships which provide the information necessary for an accurate jet representation with a potential flow model.

Important Features of a Jet

These experimental efforts lead one to try and identify the most important characteristics of the theoretical jet model in order to reduce the task from one of predicting the detailed $\frac{\partial \varphi}{\partial n}$ distribution on an arbitrary boundary surrounding the jet to that of establishing those gross features of the jet which produce the greatest influence on the flow near the configuration surfaces. Let us consider first the jet trajectory. There is no need to place S_2 exactly at the jet boundary, but it is necessary to estimate the approximate path of the jet. Its initial path is usually known from the nozzle orientation and so the problem reduces to the establishment of the trajectory some distance downstream from the exit where the jet is turning in response to its interaction with the cross flow. The required accuracy of the trajectory estimation is strongly dependent on the proximity of the jet to any of the configuration components (wing, tail, etc.). If the jet passes close to any parts of the configuration, its path must be known with greater accuracy than if it is directed away from the configuration, because the error in the velocity at the configuration surface caused by an error Δr in the location of a segment of the jet located a distance r from the configuration surface behaves as $\frac{\Delta r}{r^3}$.

Experimental observations of a single jet emerging into a uniform cross flow have led to the formulation of a well-known empirical trajectory equation by R. J. Margason (ref. 4). This equation is adequate for those configurations where the jet does not pass near any of the configuration components. In cases where the jet does pass in proximity to the configuration, it may be necessary to take into consideration the effect of the local airplane-induced flow field on the jet, and also perhaps the detailed properties of the jet flow which govern to some extent the rate of entrainment and the subsequent turning force applied to the jet by the outer flow. These effects greatly complicate the problem, and it thus appears that in the near future the application of potential flow methods will be restricted to configurations having jets directed away from any configuration components.

Having determined the trajectory of the jet centerline, the remaining problems involve the determination of an appropriate approximation for the location of the surface S_2 with respect to the jet centerline, and the specification of the velocity component $\frac{\partial \varphi}{\partial n}$ on S_2. Consider first the limited portion of the jet immediately adjacent to the nozzle exit and extending down the jet perhaps one or two nozzle diameters, as shown in Fig. 6. The jet boundary in this limited region must retain quite closely the known cross-sectional shape of the jet nozzle and expands in a manner that could be approximated by known relationships governing the rate of spreading of axisymmetric turbulent jets. Such an approximation could easily be checked and possibly improved by means of flow visualization experiments. Actually, it is probably not necessary to attempt that degree of sophistication in order to locate S_2. A simple approximation consisting of a nonexpanding jet cross section retaining the shape of the jet exit, Fig. 6, may be adequate as discussed below. Referring to Fig. 6, the normal velocity components on the

actual jet boundary can be analytically continued by Taylor series expansion to the proposed surface S_2 by an equation of the form

$$\frac{\partial \varphi}{\partial n}(r+\Delta r) = \frac{\partial \varphi}{\partial n}(r) + \Delta r \frac{\partial^2 \varphi(r)}{\partial n \partial r} + O(\Delta r^2) \qquad (3)$$

where

$\frac{\partial \varphi}{\partial n}(r+\Delta r)$ = normal velocity component on the actual jet boundary

$\frac{\partial \varphi}{\partial n}(r)$ = normal velocity component at a corresponding point on the surface S_2

r = radial distance from the jet boundary to the surface S_2

If $\Delta r \ll r$, which is the case in this limited region near the jet exit, then $\frac{\partial \varphi}{\partial n}(r+\Delta r)$ may be replaced by $\frac{\partial \varphi}{\partial n}(r)$. Or, one could seek to refine the value of $\frac{\partial \varphi}{\partial n}(r)$ specified on S_2 by including the second term on the right-hand side of Eqn. (3). Actually, as will become apparent, it is probably as easy to establish the value of $\frac{\partial \varphi}{\partial n}$ on S_2 needed to produce the correct jet influence as to establish the correct normal velocity on the jet boundary. If that is true, there is no need for a jet boundary representation in this region that is more sophisticated than the simple one proposed above.

Let us continue our examination of this limited portion of the jet and turn to the property most important and most difficult to determine; namely, the value of $\frac{\partial \varphi}{\partial n}$ on S_2. Figure 7, taken from ref. 4, shows the pressure distribution measured on the surface of a plate which has a jet exhausting normal to the plate in the presence of a freestream. The pressure pattern displays fore and aft asymmetry, which strongly indicates that the flow around the jet is not similar to attached flow about a cylinder. Reference 4 also shows oil flow patterns on the plate which display the features sketched in Fig. 8. The gross features indicate that the flow is deflected about the jet as with a cylinder. However, the details show flow into the jet along the sides, a stagnation point on the plate aft of the jet with upstream flow ahead of the stagnation point into the jet, and a well-defined oil accumulation line streaming aft of the jet. There is obviously entrainment of exterior flow into the jet, both on the sides and into the aft portion. Thus we are faced with the prospect of having to determine the strength and distribution of this inflow around the jet. In a potential flow model this inflow, which appears as the value of $\frac{\partial \varphi}{\partial n}$ to be specified on the boundary S_2, is the quantity which most strongly controls the detailed features of the flow near the jet exit.

Let us now consider the downstream portions of the jet. Flow visualization studies have revealed that in the presence of a cross flow, the jet progressively rolls up into a vortex pair, such as sketched in Fig. 9. Photographs of the cross section of a jet wake such as given in Fig. 21 of ref. 4 reveal a strong induced inflow into the aft portion of the jet (see Fig. 9).

Thus it appears that the downstream portions of the jet can be characterized as a vortex pair that is continuously entraining fluid from the outer inviscid flow into the viscous jet.

The main objective in attempting to model this jet flow is to reproduce the proper induced effects in the vicinity of the configuration surfaces. The detailed features of the flow in the immediate vicinity of the jet wake itself do not matter as long as its long-range effects are correct. This is true in so far as the distance of the jet from the configuration components is large compared with the mean jet radius. Hence let us attempt to identify those features of the jet wake which dominate its long-range influence.

One can speak of the influence of a jet in terms of the velocities induced by a distribution of singularities on a surface S_2 surrounding the viscous jet. This representation is exact provided the singularity strengths are known. Alternately, the surface distribution of singularities can be replaced by a multipole expansion on the jet centerline, which will be of the form

$$\varphi(x,y,z) = -\frac{1}{4\pi}\int \frac{m(s)}{r}\,ds + \frac{1}{4\pi}\int \frac{\mu(s)(\vec{r}\cdot\vec{p})}{r^3}\,ds + O\left(\frac{1}{r^3}\right) \qquad (4)$$

where

r = distance from jet centerline to the point (x,y,z)

$\vec{p}$ = unit vector normal to the centerline in the plane of the trajectory curve, Fig. 10

The first term on the right hand side contains the long range effect of the entrainment, or inflow into the jet. It represents a distribution of sinks along the jet centerline, with their net strength per length Δs approximately equal to the integral of the inflow velocity $-\frac{\partial \varphi}{\partial n}$ around a strip of width Δs encompassing the viscous jet, as sketched in Fig. 10. At very large distances from the jet, this term alone will produce the primary effect, because all other terms die off more rapidly with increasing r.

At intermediate distances, the second term may also be important. It represents a distribution of doublets with axes normal to the jet centerline in the plane of the paper, Fig. 10, and produces the major long range effect due to the distribution of entrainment or inflow around the jet circumference. Furthermore, its effect at large distances will be the same as that due to a vortex pair oriented in the manner of Fig. 9. This latter feature can be

derived by expanding the potential of a two-dimensional vortex pair spaced a distance 2d apart in powers of d/r . The result is

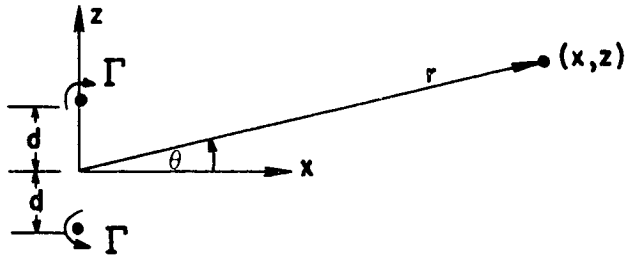

$$\varphi(x,z) = \frac{\Gamma}{2\pi}\left[\tan^{-1}\frac{z+d}{x} - \tan^{-1}\frac{z-d}{x}\right] \approx \frac{\Gamma d}{2\pi}\left[\frac{2\cos\theta}{r} + O\left(\frac{d^2}{r^2}\right)\right] \qquad (5)$$

The first term on the right represents a two-dimensional doublet located at the origin. The difference between the influence of the doublet and the vortex pair at distances larger than the jet radius ($r_{jet} \approx d$) is $O(d^2/r^2)$.

Thus one is able to associate with a sink and doublet distribution along the jet axis the major features of the jet that have yet been identified by flow visualization; namely, a net entrainment into the jet with the distribution of entrainment around the circumference dominated by the vortex pair flow pattern. Figure 11 shows a two-dimensional velocity pattern about a superimposed sink and doublet which clearly displays these characteristics. It should be noted that an actual distribution of sinks and doublets on the axis is not necessary to produce these effects. The jet can be represented by any convenient surface cross section having boundary conditions producing the sink and doublet effects. As an example, a circular cross section of radius R with boundary conditions of the form

$$\frac{\partial\varphi(R,\theta)}{\partial n} = \frac{C_1}{2\pi R} + \frac{C_2\cdot\cos\theta}{2\pi R^2} \qquad (6)$$

will produce the same effect as a sink and doublet at the circle center having strength C_1 and C_2 respectively.

For configurations where the jet does not pass in close proximity to any aircraft component it is unlikely that the finer details contained in the higher order multipoles will have a significant effect because of their rapid attenuation with distance. In any event, the estimation of the jet trajectory itself with sufficient accuracy becomes very difficult with close proximity jets, as previously noted, so it appears that, for the present, the use of potential flow methods shall be restricted to configurations with remote jets for which the sink-doublet representation is applicable.

In summary, the most important properties of the jet representation are the following:

1. Trajectory. At present there exists an empirical trajectory equation which is adequate for jets not in close proximity to the configuration.

2. Near the jet exit, a surface S_2 is required. It can have the cross-sectional shape of the jet exit and need not be tapered to correspond to the expansion of the jet.

3. A detailed distribution of $\frac{\partial \varphi}{\partial n}$ on S_2 near the jet exit is required. This probably has the greatest influence of any of the jet properties. Our present knowledge concerning the distribution of $\frac{\partial \varphi}{\partial n}$ on S_2 is only qualitative.

4. The influence of the downstream portions of the jet must contain sink and doublet effects. The magnitude of these effects is presently unknown.

PROPOSED POTENTIAL FLOW MODEL OF A JET

In view of these properties, I propose the model shown in Fig. 12 as suitable and convenient for use with the potential flow calculation procedure described herein. The cross-sectional shape of the jet exit is retained all along the jet as a matter of convenience. The trajectory is established by Margason's equation (ref. 4). The remaining quantity to be established is the distribution of $\frac{\partial \varphi}{\partial n}$ on the surface, and this must come from experimental observation. Ideally, one would like to express the $\frac{\partial \varphi}{\partial n}$ distribution in terms of a few parameters and attempt to establish a correlation between these parameters and the jet deflection angle and velocity ratio. One possible parametric representation is the expression

$$\frac{\partial \varphi}{\partial n}(s,\theta) = \sum_{n} a_n(s) \cos n\theta \qquad (7)$$

The first term, $a_0(s)$, provides the longitudinal distribution of the total inflow or entrainment along the jet. The second coefficient, $a_1(s)$ gives the longitudinal variation of the doublet or vortex pair effect. Higher order terms, if needed, will be important only near the jet exit. Their influence on the configuration rapidly disappears with increasing s, and their presence or absence for large s will not affect the flow in the vicinity of the configuration surfaces. This latter behavior suggests that the variation of a_n with s for $n \geq 2$ can possibly be neglected, leaving only constants corresponding to the value of $a_n(0)$. This possibility should certainly be explored.

SUGGESTED EXPERIMENTAL PROGRAM FOR THE DETERMINATION OF THE JET PARAMETERS

With this type of representation, one is faced with the necessity of determining, as a minimum, the functions $a_0(s)$ and $a_1(s)$ plus perhaps some constants for the next few a_n's. These will have to be established from experimental observation, but how?

One possible approach would be to examine the results of an experiment conducted with a jet emerging into a cross flow at various angles from a large flat plate as sketched in Fig. 13a. The plate must be large enough to avoid boundary layer separation at the edges due to jet induction effects and should contain a detailed static pressure survey. The basic idea is to adjust the a_n's in a theoretical solution of this problem, Fig. 13b, to reproduce the measured pressure distributions on the plate. The final result would be a number of curves or fitted equations describing the variation of the a_n's with jet velocity ratio, thrust vector angle, and a jet dynamic pressure decay parameter (see ref. 4). An attractive feature of the scheme is that theoretical solutions for several different distributions of $a_n(s)$ can be obtained nearly as economically as for one, since the influence coefficient matrix in the numerical solution procedure is independent of the a_n's. Or, one could attempt to mechanize the process by expressing $a_0(s)$ and $a_1(s)$ as power series in s and calculating, with a potential flow model, the separate influence of each term in the series. This could also be done economically due to the constancy of the influence coefficient matrix. These individual solutions, or flows, would serve as basic building blocks which could be linearly superimposed to produce any desired flow pattern. Armed with these, an investigator could readily construct all possible theoretical flows.

A point to note in attempting to match theoretical and experimental plate pressures is that the pressures away from the jet exit are governed mainly by $a_0(s)$ and $a_1(s)$, whereas the pressures adjacent to the exit are strongly influenced by the higher order a_n's .

CONCLUDING REMARKS

The results of previous potential flow calculations for V/STOL applications have demonstrated a need for improved modeling of the jet flow. With this objective in mind, a theoretical model for a jet has been proposed which is based on the observed major features of real jet flows. An experimental program is suggested as a means of obtaining a correlation relating the jet boundary conditions in the theoretical model to the jet parameters.

REFERENCES

1. Rubbert, P. E., et al., "A General Method for Determining the Aerodynamic Characteristics of Fan-in-Wing Configurations", Vol. 1 - Theory and Application. USAAVLABS Technical Report 67-61A, 1967.

2. Rubbert, P. E. and Saaris, G. R., "A General Three-Dimensional Potential-Flow Method Applied to V/STOL Aerodynamics". Presented at the SAE Air Transport Meeting, New York, April-May, 1968.

3. Lamb, H., "Hydrodynamics". New York; Dover Publishing Company, 1945.

4. Margason, R. J., "A Discussion of V/STOL Propulsion Induced Effects on the Aircraft's Aerodynamics". Notes for Lecture Presented at the University of Tennessee Space Institute Short Course on V/STOL, November 1968.

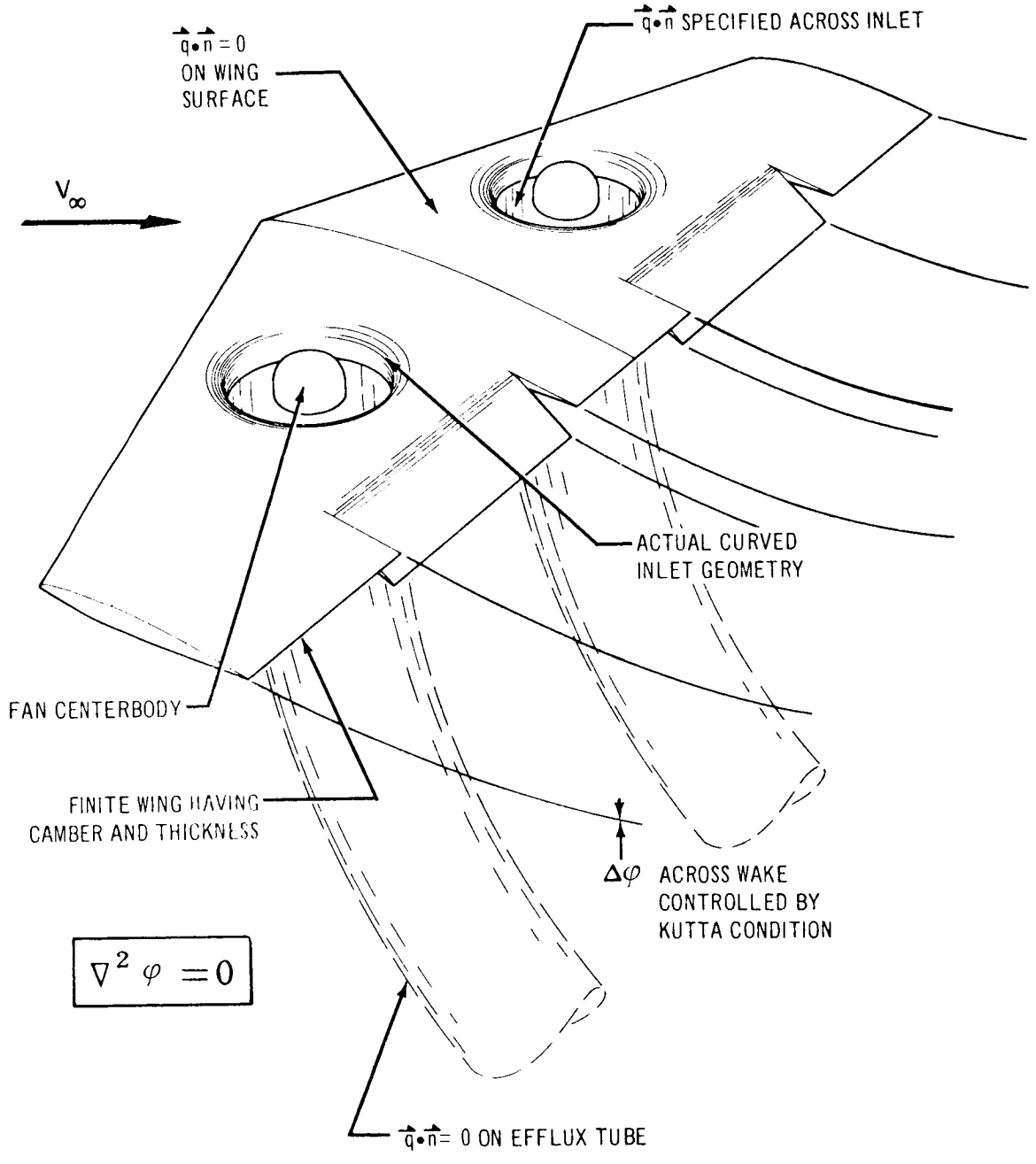

Figure 1.- Theoretical model of fan-in-wing configuration.

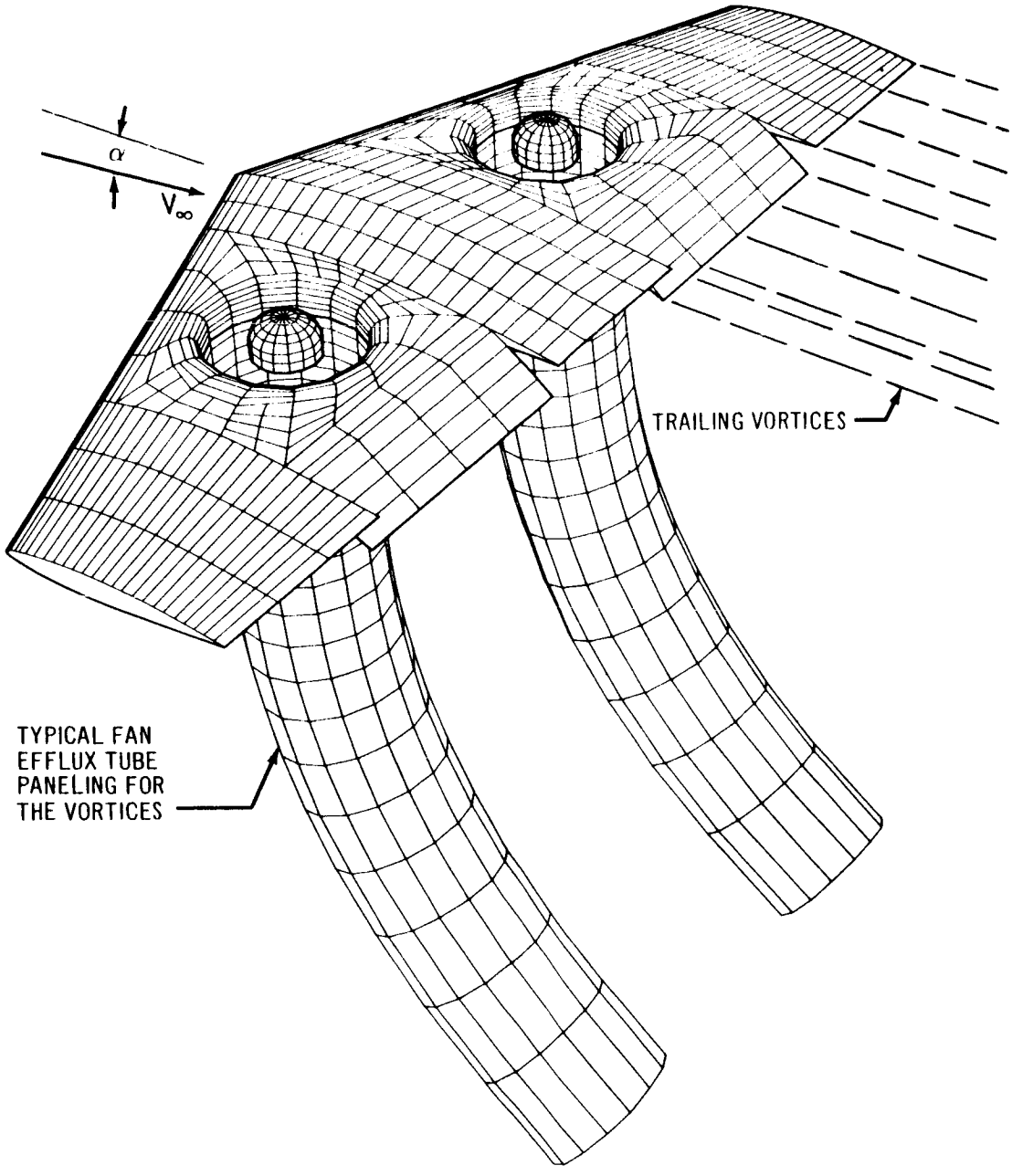

- Arbitrary planform, thickness, camber, inlet geometry, and fan inflow distribution
- Source panels on wing and centerbody surfaces
- Vortices on efflux tube and trailing sheet
- Internal and fan face vortices omitted for clarity

Figure 2.- Panel arrangement on fan-in-wing configuration.

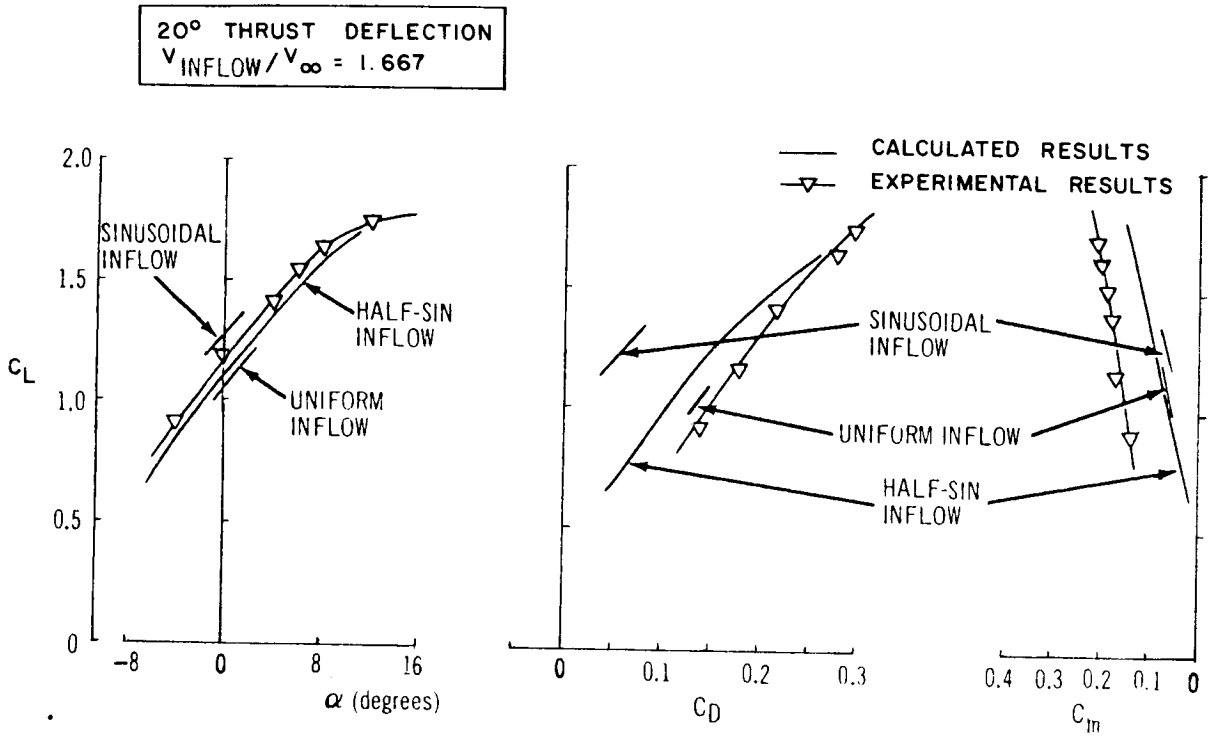

Figure 3.- Force and moment comparison on fan-in-wing configuration.

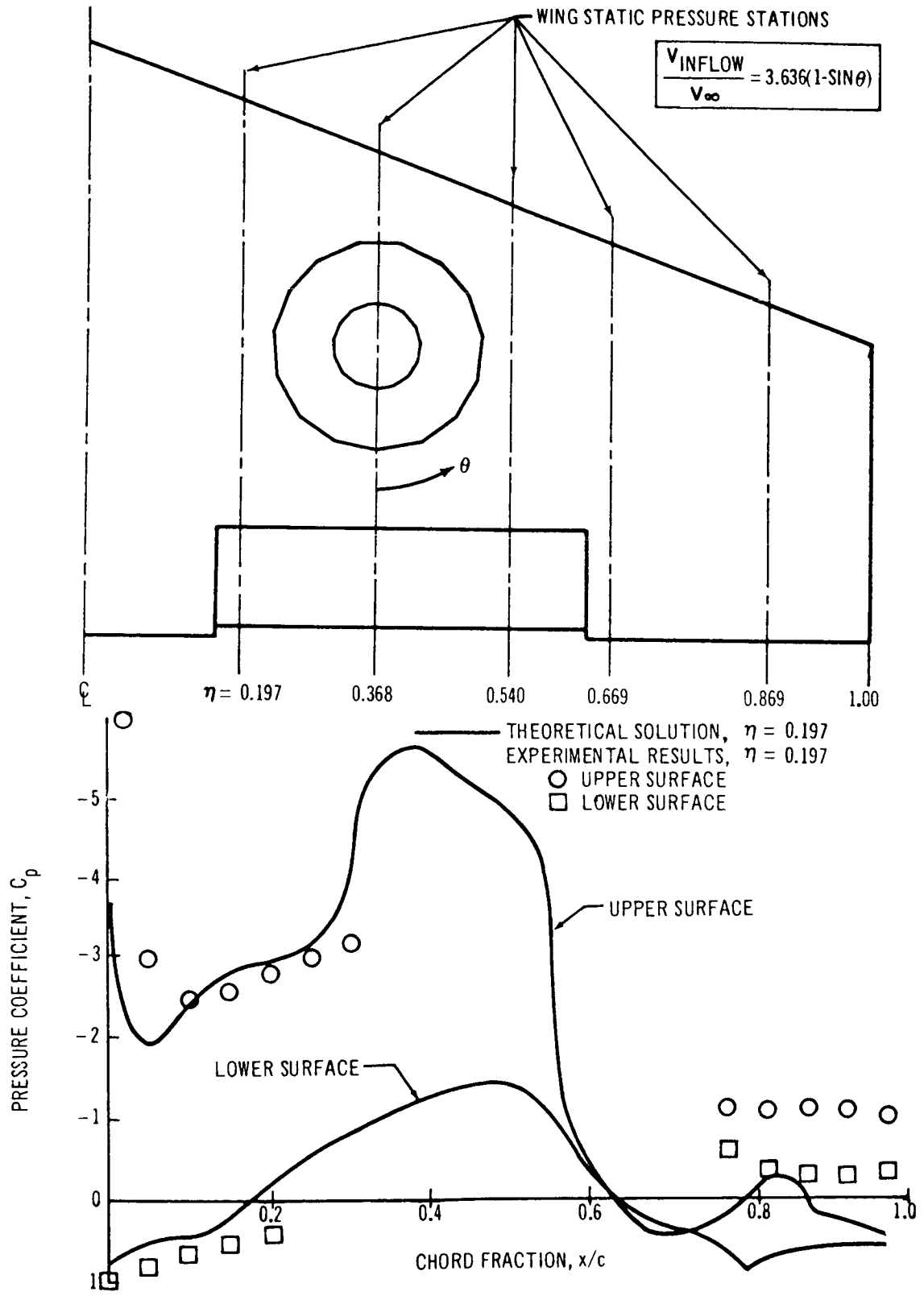

Figure 4.- Surface pressure comparison on fan-in-wing configuration.

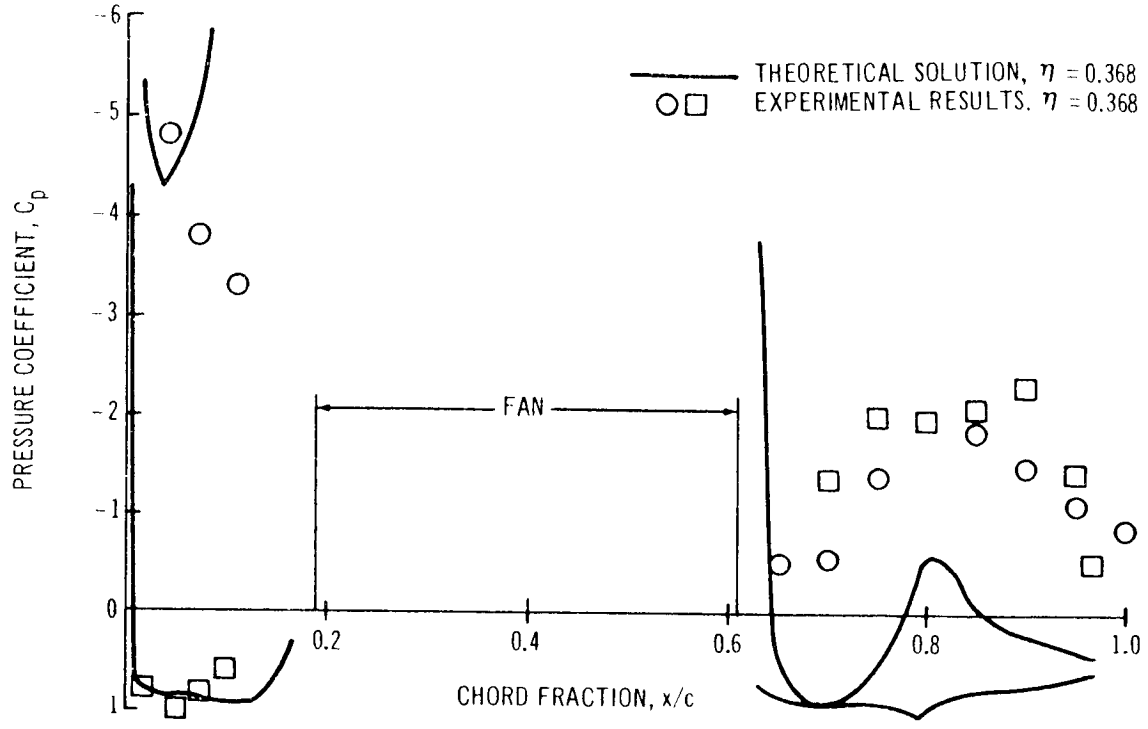

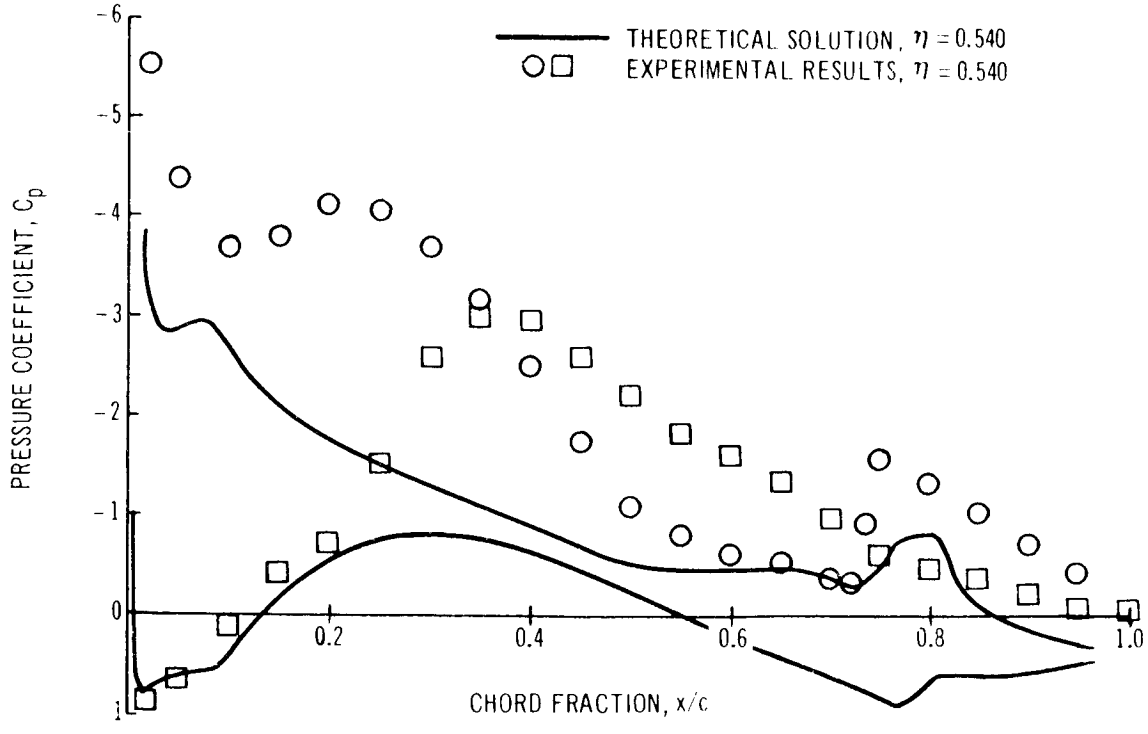

Figure 4.- Continued.

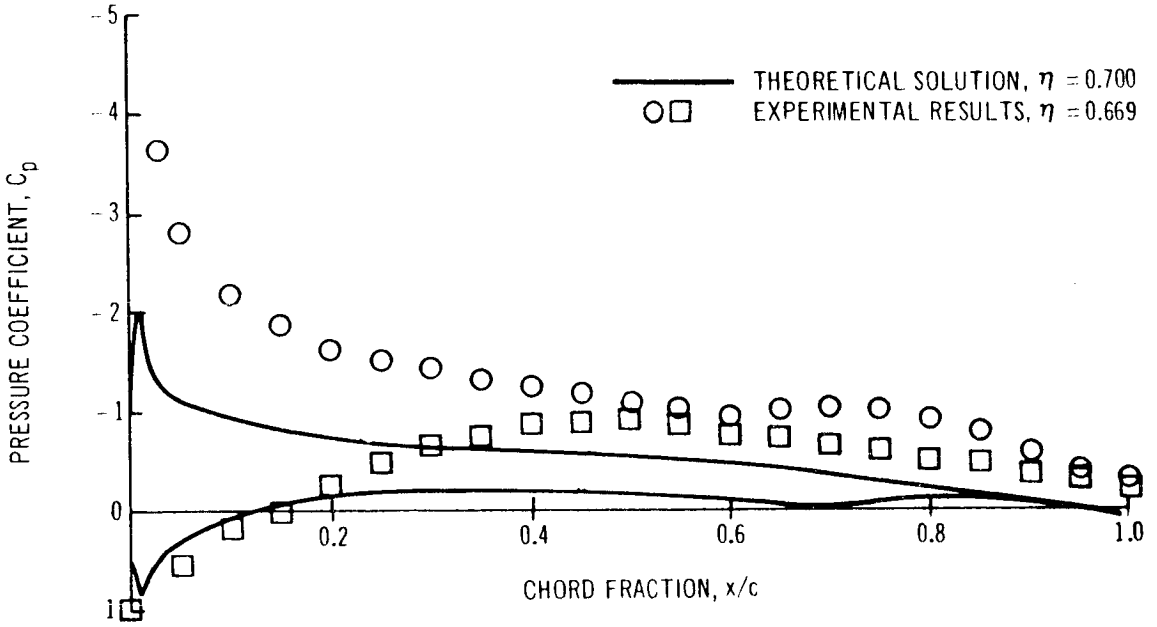

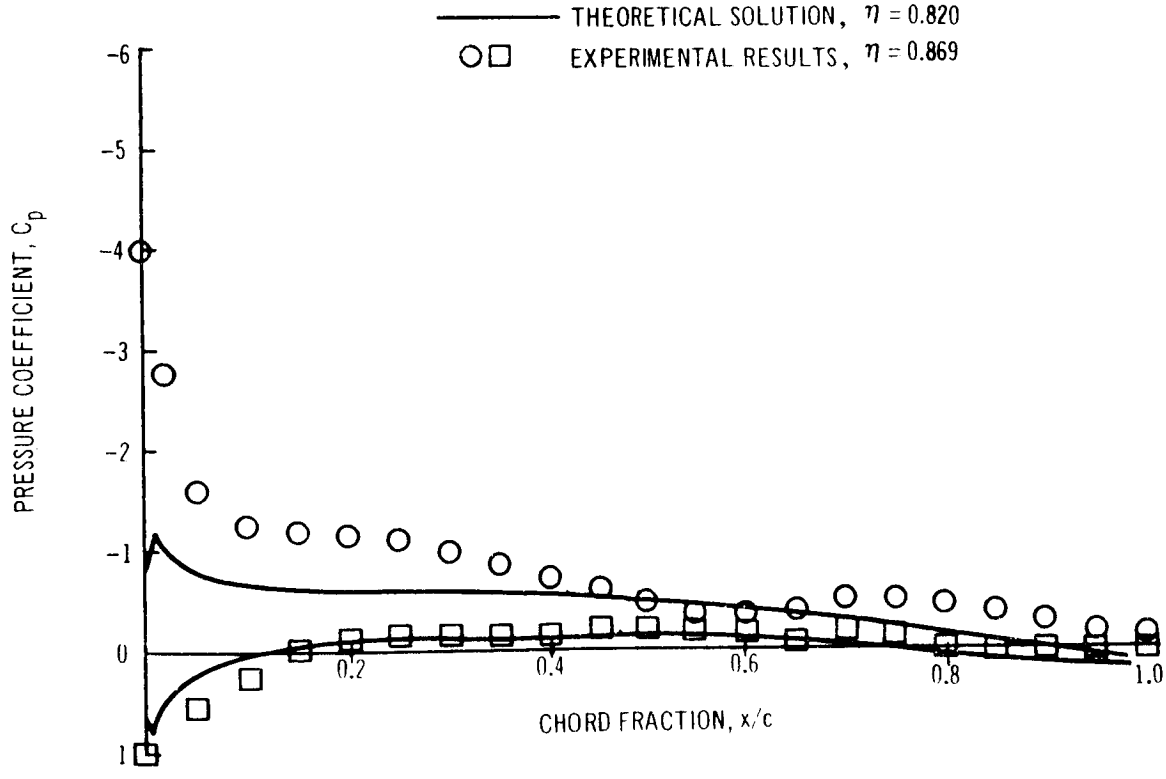

Figure 4.- Concluded.

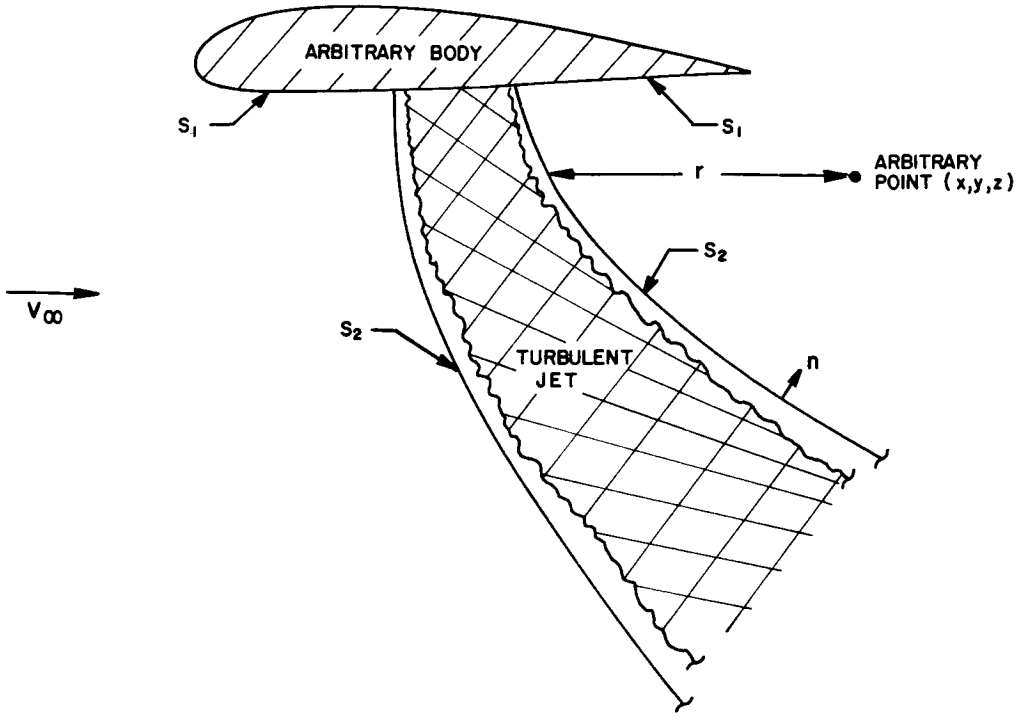

Figure 5.- Potential flow boundaries.

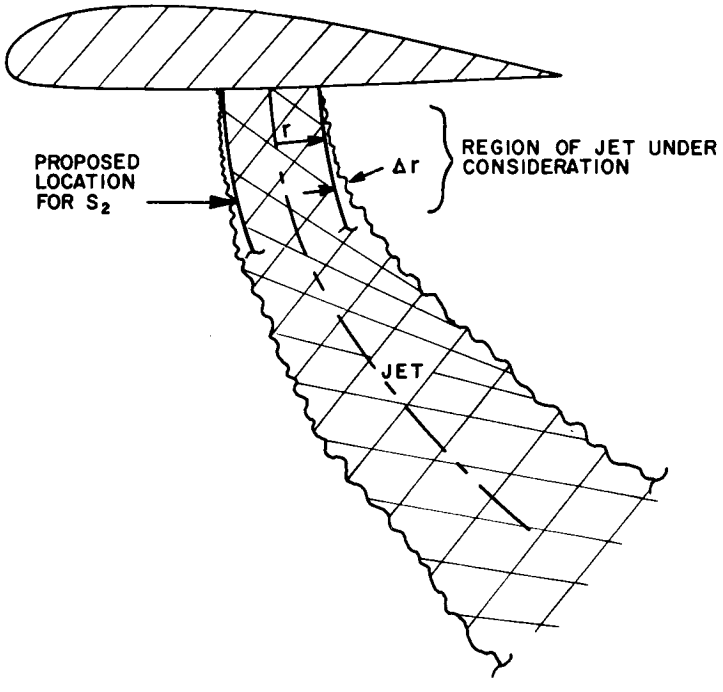

Figure 6.- Initial portion of jet.

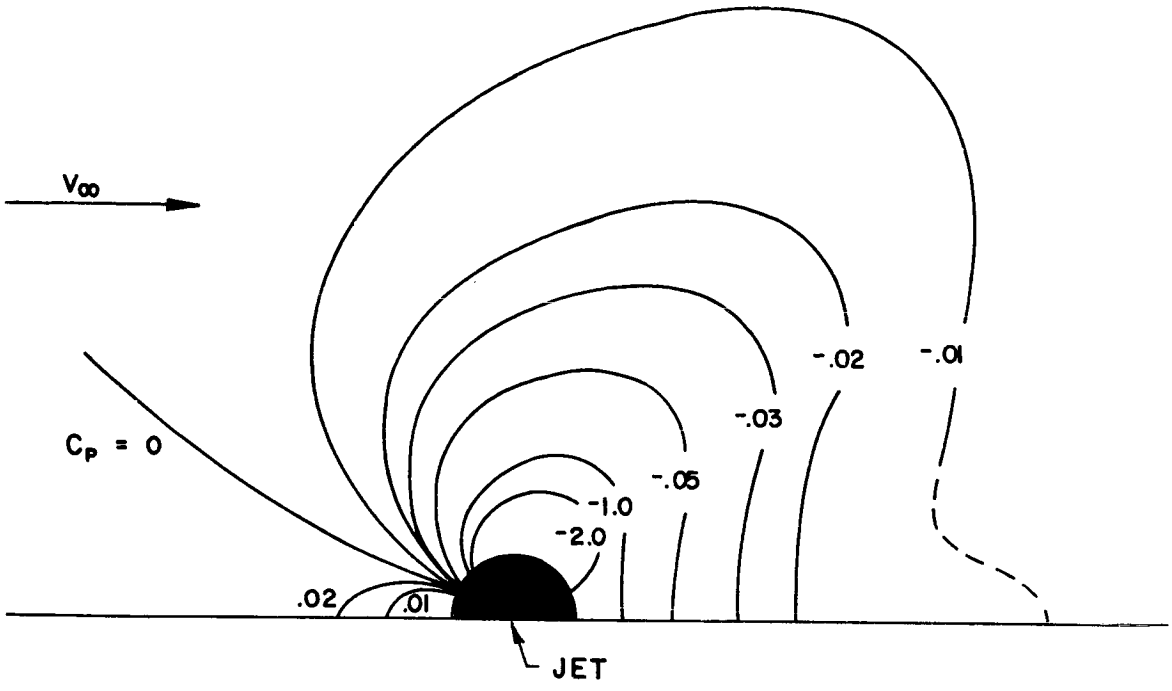

Figure 7.- Pressure distribution on plate with jet exhausting into a cross flow.

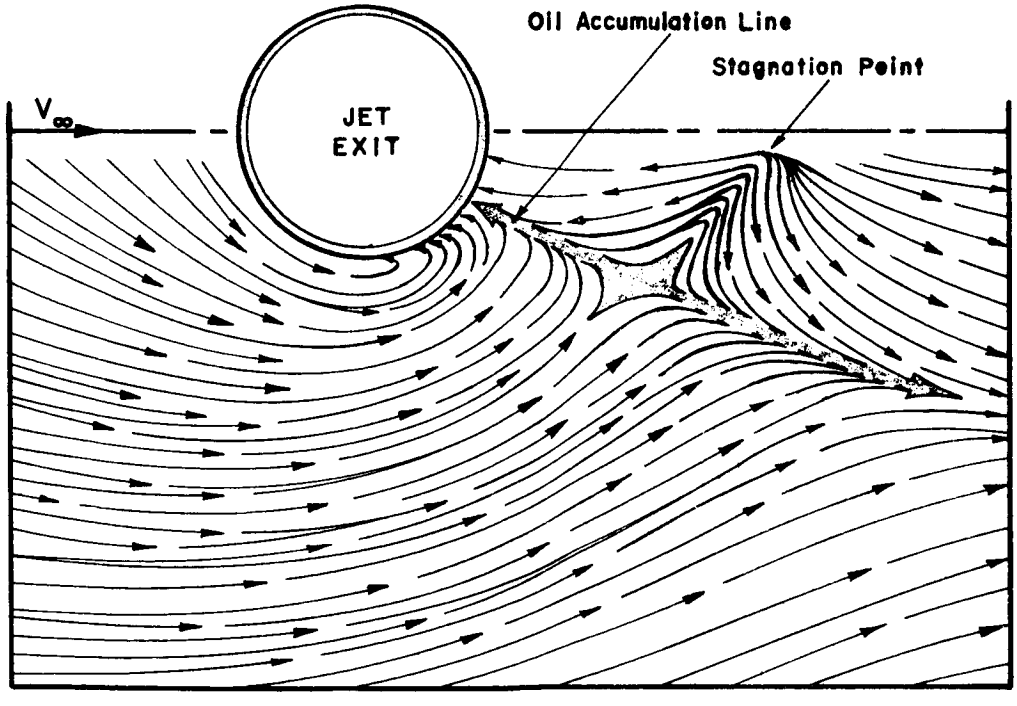

Figure 8.- Oil flow pattern on plate with jet exhausting into a cross flow.

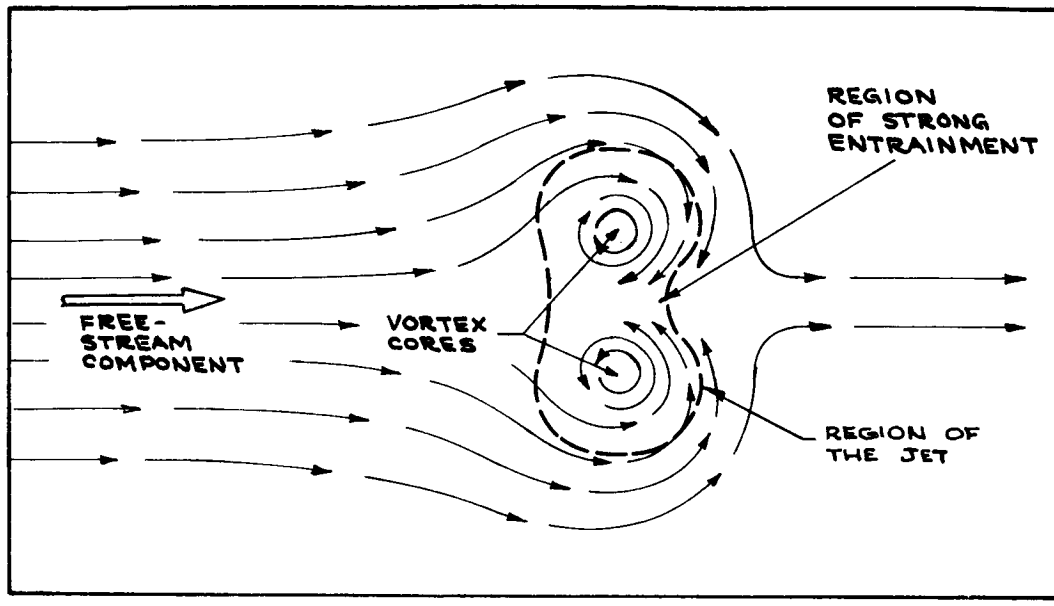

Figure 9.- Cross-sectional flow pattern in the jet wake several diameters downstream of the nozzle.

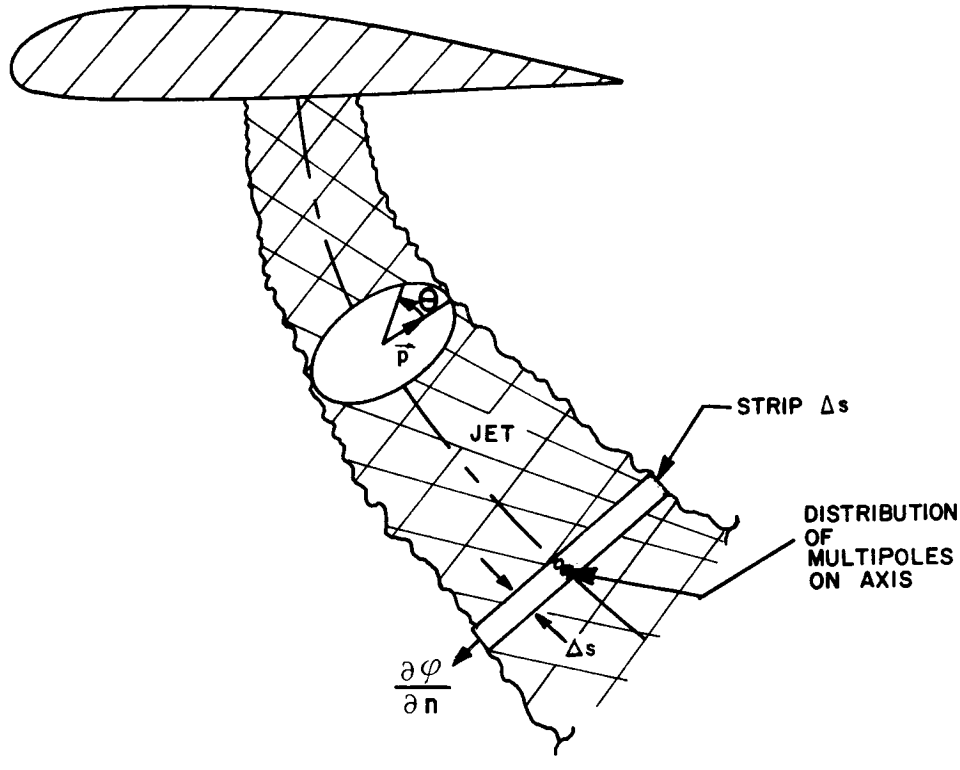

Figure 10.- Multipole distribution on axis of jet.

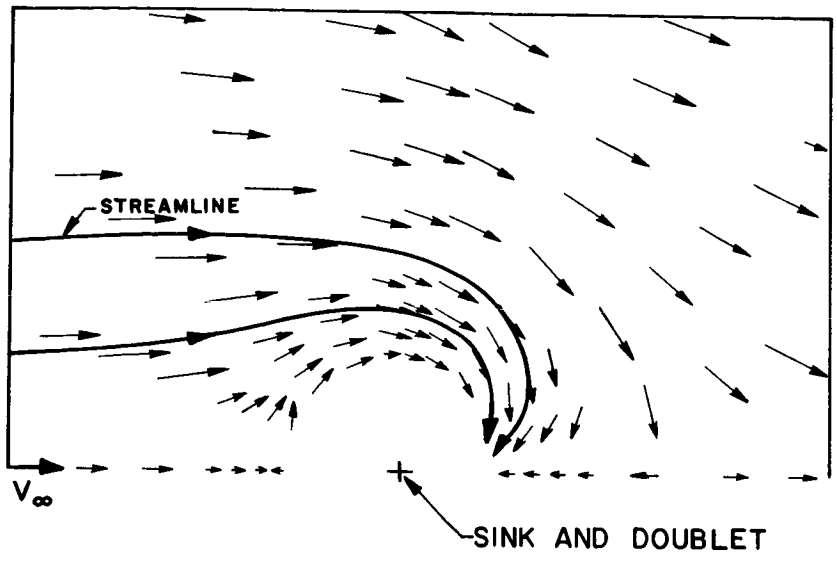

Figure 11.- Velocity pattern about a superimposed sink and doublet in a uniform stream.

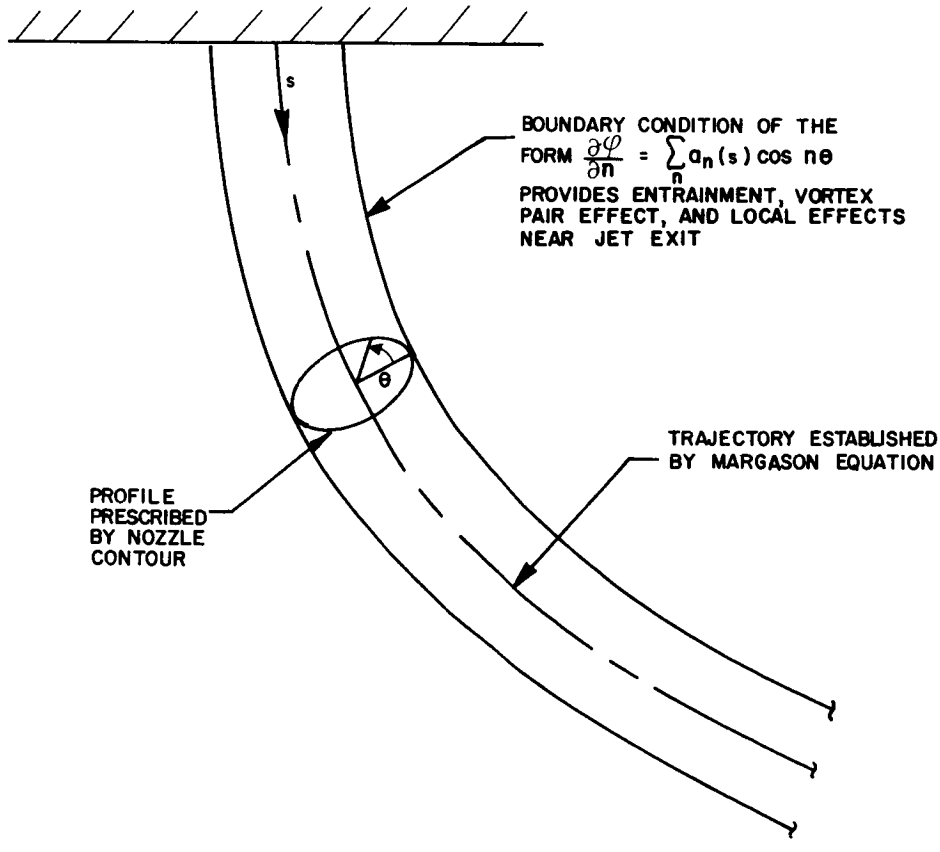

Figure 12.- Proposed model of jet.

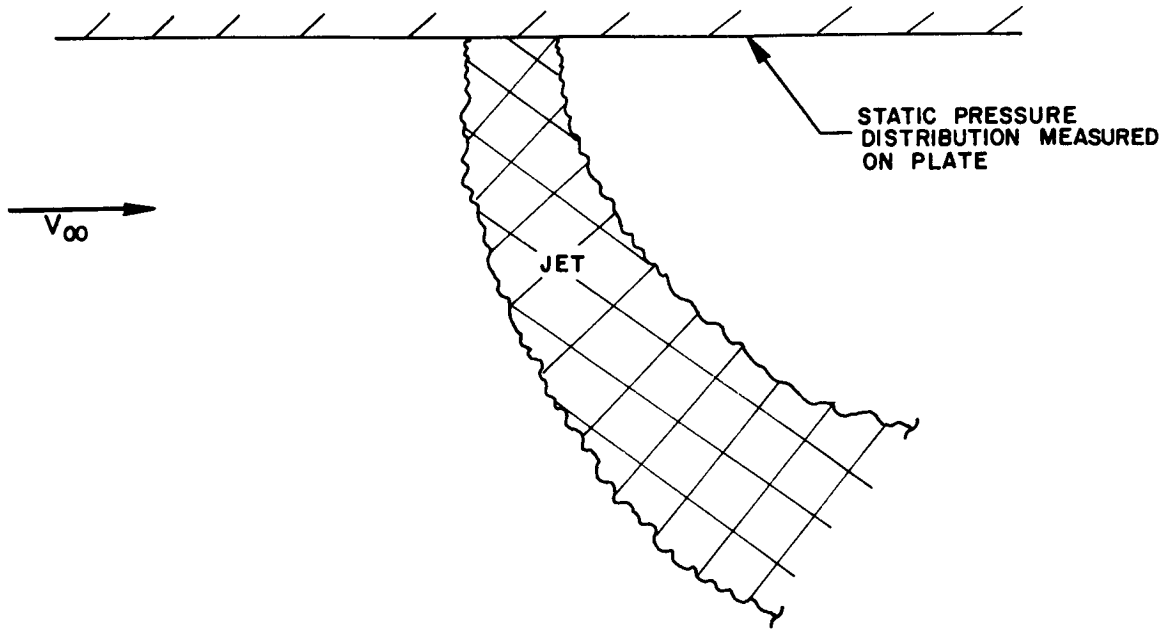

(a) Experimental setup.

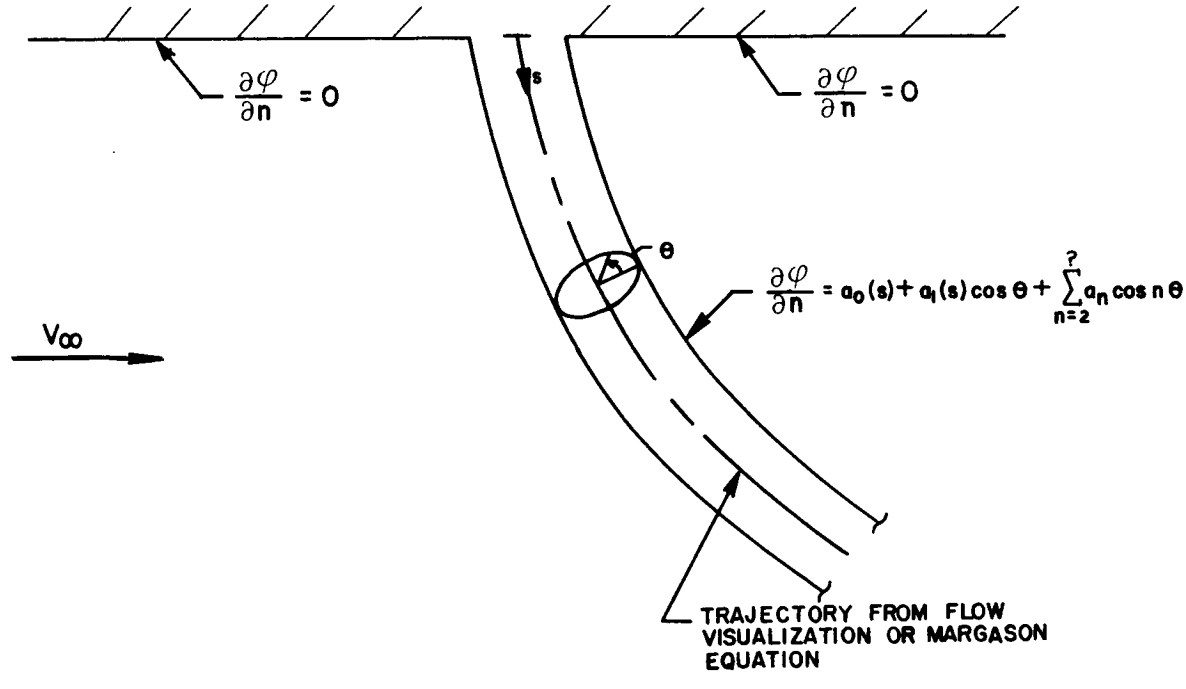

(b) Theoretical model.

Figure 13.- Test setup for evaluation of jet entrainment characteristics.

INVISCID MODELS FOR THE PRESSURE INDUCED BY A JET TRANSVERSE TO A SUBSONIC STREAM*

By Robert Rosen, Norbert A. Durando, and Louis A. Cassel

McDonnell Douglas Astronautics Company--Western Division

SUMMARY

Methods are presented for approximately predicting the pressure distribution on a flat plate in the vicinity of a transverse jet exhausting into a subsonic uniform stream. A method is formulated for empirically fitting the available data to enable interpolation and extrapolation. In addition, several inviscid flow models are postulated, based on incompressible potential flow theory. Some models were found reasonably successful while others were not. This paper presents the formulation of the empirical fit, analysis of the models, and comparison of results from the models with experimental data.

The first subject discussed is the formulation of an empirical technique for fitting the data. Following this, results of two approaches to potential modeling of the flow are presented. In the first approach, all of the known significant phenomena, such as entrainment and blockage, are included in an approximate way. Singularities are distributed to account for these effects but their strengths are left arbitrary. A pressure-matching scheme is employed to quantitatively determine the strengths. The potential flow methods used in the second approach are more direct for the purpose of the study. They consist of postulating a flow field which will give the proper qualitative pressure distribution and adjusting constants to fit this distribution as closely as possible.

INTRODUCTION

Interaction of a highly underexpanded sonic or supersonic jet with a subsonic transverse flow represents a jet interaction (JI) problem encountered in the design of many reaction-controlled atmospheric flight vehicles. Consequently, an effort is being made to develop analytical methods for predicting the pressure distribution, and therefore the forces and moments produced by the jet, and the interaction flow field for various flow conditions and vehicle geometries. Some results of such an effort, being conducted by the McDonnell Douglas Astronautics Company--Western Division under the sponsorship of the U. S. Army Missile Command, are described in this paper. The work discussed here is limited to an analysis of the pressure on a flat plate in the vicinity of a jet exhausting transverse to the plate. Both empirical methods and incompressible potential flow modeling will be described.

*This research supported by the Advanced Systems Laboratory, U. S. Army Missile Command under Contract number DAAH01-68-C-19-19.

Detailed descriptions of the flow surrounding a subsonic jet exhausting transverse to a subsonic uniform stream, based on the results of careful experiments, are available in references 1 and 2. Similar detailed experiments for sonic or supersonic underexpanded jets do not exist. In the opinion of the authors, however, adding a sonic or supersonic jet only complicates the flow field further. In both cases, the complexity of the flow field is such that an exact analytical description of it is beyond current developments in fluid mechanics. Consequently, empirical methods and potential flow analogies to the fluid mechanics, as known from available experimental data, have been employed in the initial efforts to predict pressure distributions. The objectives of effort described in this paper are to devise techniques for approximately predicting the forces and moments on bodies from which the jet exhausts and not necessarily to derive detailed analytical descriptions of the flow. The direct problem of interest initially has, therefore, been taken to be the analytical modeling of the pressure distribution on a flat plate in the plane of the jet exit.

In the analysis that follows, it will be assumed that the fluid behaves as if it were incompressible and irrotational. Viscosity, if taken into account at all, will be introduced through its bulk effects, such as entrainment, and will not enter any of the equations. Thus, a potential exists for this flow and solution will be sought based on incompressible potential flow theory. Some other authors (refs. 3 through 6) have also used inviscid flow theory to describe the problem but with limited success.

Although some flat-plate pressure data do exist for an underexpanded jet exhausting into a subsonic stream (refs. 7 and 8), they are rather incomplete. Recent experiments have been carried out by the U.S. Army Missile Command which are quite comprehensive, but data from these tests are not yet available. For lack of data more appropriate to the present study, the subsonic jet data of Vogler (ref. 9) will be used. It is felt that theoretical and empirical models which can be made to agree with these data can also be made to agree with sonic and supersonic jet data.

The coordinate system used in the analysis of the pressure distribution on a flat plate is shown in figure 1. The polar coordinate, θ, is measured counterclockwise from the mainstream velocity. The radial coordinate, indicated as r^* when dimensional, is measured from the jet center. When nondimensionalized by the jet diameter, the radial coordinate is indicated as r.

SYMBOLS

a_n	singularity strengths, where $n = 0, 1, \ldots$
C_p	pressure coefficient
c_n	Fourier coefficients, where $n = 0, 1, \ldots$
d_j	jet nozzle diameter

F	force
k	scale factor
M	moment
p	pressure
q	dynamic pressure
r	radial distance normalized by jet diameter
r^*	dimensional radial coordinate
U	velocity
w	complex potential
x^*,y^*,z^*	dimensional Cartesian coordinate
z	complex variable normalized by d_j
θ	azimuthal angle measured positive in the counterclockwise direction from the leeward ray
ρ	density

Subscripts:

j	jet
o	vortex position
∞	free stream

A bar over a symbol denotes a complex conjugate.

DISCUSSION

Empirical Data Fit

A typical plot of pressure coefficient, C_p, versus θ at a given value of r is shown in figure 2 based on the data of Vogler. Because of the smoothness of these data for $\theta > 30^\circ$ and the fact that the data are even, it appears that the data can be approximated quite well at a given radius by the first few terms in a Fourier cosine series.

$$C_p = \sum_{n=0}^{m} c_n(r) \cos(n\theta) \tag{1}$$

where the coefficients c_n are given by their usual integral definitions. Figures 3 and 4 show comparisons of two- and a three-term series to the data at two values of r. It can be seen that the truncated Fourier series does indeed provide a good representation of the θ dependence of the data. The same

results have also been found to hold true at other values of r and other velocity ratios (U_∞/U_j).

To complete the empirical fit, the radial dependence of the coefficients c_n must be found for the various values of the velocity ratio. This dependence is shown empirically in figures 5 and 6. It can be seen that the variations of c_0 and c_1 as functions of r and the velocity ratio are well behaved. It would be a simple matter to obtain functional relations for this dependence to completely determine the empirical fit. However, a better way has been found to use this information through potential flow models.

Phenomenological Models

Two models will be considered under this heading. The first, called the doublet model, consists of the superposition of a free stream, a source (or sink), and a doublet. The second flow model, called the doublet-vortex model, is the same as the first except that two counterrotating vortices are added downstream of the origin. A sketch of this model is shown in figure 7. Both of these models are two dimensional, in that it is assumed that there are no variations in flow properties in the direction normal to the plate.

The complex potentials of these simple models are well known. The only quantities to determine are the strengths of the singularities and locations of the vortices for the doublet-vortex model. In the present analysis, the complex potential for the flow field is written in terms of the unknown singularity strengths. From this complex potential, an expression for the pressure coefficient in terms of cosine functions is obtained and put in the form of equation (1). By setting each coefficient in the derived pressure-coefficient expression equal to the corresponding one in the Fourier series obtained from the data at a given value of r, the strengths of the source, doublet, etc., are found. This is done for several values of the velocity ratio, and curves of the source strength, etc., are obtained as a function of the velocity ratio. The benefits of this technique are twofold: First, with its use a limited amount of data can be greatly extended; second, and perhaps more important, by seeing which singularities are strongest, the dominant factors in the flow field can be inferred. This information could be important in trying to relate the results obtained for a flat plate to an axisymmetric body.

The model will yield results that are accurate at one value of r, the one where the data and model were matched. The accuracy of results at other values will depend upon how closely the r dependence of the model depicts the actual situation. There is an assumption implicit in the above analysis which must be satisfied to obtain reasonable results. The quantity which will ultimately have to agree with experiments is the expression for the complete pressure coefficient, not just the first few terms in its Fourier series representation. In order for theoretical and experimental pressure distributions to agree, the first few terms in the series derived from the complex potential must be the dominant ones. Terms which appear later in the series and are not used in determining the strength of the singularities, must be small. For the models considered, this has been the case.

There is one distinct advantage to this truncated Fourier series technique. The force or moment on the plate due to the interaction can be calculated from the formula,

$$F \text{ or } M = \int_0^{\infty}\int_0^{2\pi} q_{\infty} r^{(1+n)} C_p \cos(n\theta) dr d\theta$$

where the force is obtained if n = 0 and the moment results if n = 1. If the pressure coefficient is written in the form of equation (1), the integral becomes

$$\int_0^{\infty}\int_0^{2\pi} q_{\infty} r^{(1+n)} \cos(n\theta) \left[\sum_{m=0}^{k} c_m \cos(m\theta)\right] dr d\theta$$

or

$$\sum_{m=1}^{k} \int_0^{\infty}\int_0^{2\pi} q_{\infty} r^{(1+n)} c_m \cos(n\theta) \cos(m\theta) dr d\theta$$

Due to the orthogonality of the cosine, this now becomes

$$F = \int_0^{\infty}\int_0^{2\pi} q_{\infty} c_0 r dr d\theta$$

and

$$M = \int_0^{\infty}\int_0^{2\pi} q_{\infty} c_1 \cos\theta \, r^2 dr d\theta$$

Thus, the total contribution to the force comes from the first term of the Fourier series (truncated or complete), and the total contribution to the moment comes from the second.

Matching the first couple of terms of a Fourier series takes on more significance in the light of these results. If models could be found that would

have very close agreement in these terms for all values of r, then the two quantities of specific interest could be predicted quite well.

Although comparison of forces and moments between the theoretical models and experimental data will not be made, an approximate indication of how the forces compare can be obtained from the following. Consider equation (1) at $\theta = \pi/2$,

$$C_p(\pi/2) = c_0 - c_2 + c_4 + \ldots$$

If

$$c_0 \gg c_2 \gg c_4$$

which is true in at least some cases, then

$$C_p(\pi/2) \cong c_0$$

Thus, since the force is equal to the area under the $c_0(r)$ curve, weighted by r, the force will also be equal to the area under the $C_p(\pi/2)$ curve, again weighted by r. In this case if the model predicts accurate pressure coefficients along the ray $\theta = \pi/2$, then the force predicted will also be accurate. Therefore by just comparing pressures at $\theta = \pi/2$, a good indication of the quality of force prediction of the model can be obtained.

The best way to illustrate the above ideas is through an example. The complex potential for the doublet model is

$$w(z) = a_0 z + a_1 \log(z) + \frac{a_2}{z} \qquad (2)$$

where z is normalized by d_j. Usually a_0 is chosen equal to U_∞ and the pressure coefficient defined

$$C_p = \frac{p - p_\infty}{(1/2)\rho U_\infty^2}$$

is given by

$$C_p = 1 - \frac{1}{U_\infty^2}\left(\frac{dw}{dz}\right)\left(\overline{\frac{dw}{dz}}\right)$$

However, this leaves only two arbitrary constants in the analytical expression for the pressure coefficient which can be matched to only the first two terms of the Fourier series representation. Since three terms in the series are considered necessary to approximate the wake-like distribution for $\theta \leq 30°$, a third constant is required in the analytical expression. To provide this third constant, a_0 is chosen equal to U'_∞ / U_∞, and the pressure coefficient is defined as

$$C_p = \frac{p' - p_\infty}{(1/2)\rho U_\infty^2}$$

where the primed quantities are for the two-dimensional model and are not necessarily equal to the unprimed, or actual quantities. With these definitions, the pressure coefficient becomes

$$C_p = a_0^2 - \left(\frac{dw}{dz}\right)\left(\overline{\frac{dw}{dz}}\right) \tag{3}$$

These relations can be obtained by considering the static pressure at infinity in the model to equal the actual static pressure, while the total pressure (and therefore free-stream velocity) of the actual flow differs from that of the model. These manipulations leave a_0 free to be used in the pressure matching.

Substituting equation (2) into equation (3) gives

$$C_p = -\frac{a_1^2}{z\bar{z}} - \frac{a_2^2}{z^2\bar{z}^2} - a_0 a_1 \frac{z + \bar{z}}{z\bar{z}} + a_0 a_2 \frac{z^2 + \bar{z}^2}{z^2\bar{z}^2} + a_1 a_2 \frac{z + \bar{z}}{z^2\bar{z}^2} \tag{4}$$

Equation (4) is now to be expressed in the form of equation (1). This can be done directly for the present example by the substitution

$$z = re^{i\theta}, \quad \bar{z} = re^{-i\theta}$$

or for more complex models by the integral definitions of the coefficients $c_n(r)$,

$$c_0(r) = \frac{1}{\pi} \int_0^{\pi} C_p(r, \theta) d\theta$$

$$c_n(r) = \frac{2}{\pi} \int_0^{\pi} C_p(r, \theta) \cos(n\theta) d\theta$$

After some algebraic reduction the constants for the present example are found to be

$$\left.\begin{aligned} c_0(r) &= -\frac{a_1^2}{r^2} - \frac{a_2^2}{r^4} \\ c_1(r) &= -2\frac{a_1}{r}\left(a_0 - \frac{a_2}{r^2}\right) \\ c_2(r) &= \frac{2}{r^2} a_0 a_2 \end{aligned}\right\} \qquad (5)$$

These expressions for the coefficients c_n are to be set equal to experimentally determined values at a fixed value of r. The location chosen was the circle r = 1, a choice which is somewhat arbitrary. For a velocity ratio (U_∞ / U_j) of 0.4, the values of the coefficients c_n are

$$c_0(1) = -0.619$$

$$c_1(1) = -0.843$$

$$c_2(1) = +0.287$$

Numerical solution of equations (5) then gives

$$\left.\begin{aligned} a_0 &= 0.745 \\ a_1 &= 0.762 \\ a_2 &= 0.192 \end{aligned}\right\} \tag{6}$$

These results indicate that for the proper behavior, the source is indeed a source and not a sink. Further, the blockage effect of the doublet, which opposes the free stream, is considerably smaller than the effect of the source.

Expressing equation (4) in the form of equation (1) gives a summation which contains just three terms. Thus, the constants given by equations (6) will reproduce the three-term cosine series exactly at r = 1. An idea of the accuracy possible through use of this doublet model can be obtained from figure 3 in which results from a three-term series are compared to the data at r = 1. It can be seen that the agreement of the doublet model with the data is quite good for most values of θ. The real test of the model, however, is the agreement at other values of r. Comparison of the model with Vogler's data for five rays, θ = const, is shown in figures 8 through 12. Examination of these figures shows considerable disagreement around the upstream and downstream rays and fairly good agreement near the ray $\theta = \pi/2$.

The accuracy of other results obtained from this model at different velocity ratios is similar to that described above. Thus, it can be concluded that this choice of singularities will not yield pressure distributions sufficiently accurate to be of practical use.

The other phenomenological model employed in this study is shown in figure 7, as mentioned previously. In addition to the source (or sink), doublet, and free stream, there are two vortices of equal strength (but opposite sign) located downstream of the origin. These are included to represent the vortex motion that actually exists in the flow. It was at first expected that by taking the reverse flow downstream of the jet into account, increased accuracy would result.

The complex potential for this flow is

$$w(z) = z + a_1 \log(z) + \frac{a_2}{z} + ia_3 \log\left(\frac{z - z_o}{z - \bar{z}_o}\right) \tag{7}$$

Here z is, again, normalized by d_j, and w is normalized by U_∞. Since the free-stream velocity in this model is U_∞, the usual definition for the pressure coefficient is chosen in the form

$$C_p = \frac{p - p_\infty}{q_\infty} = 1 - \left(\frac{dw}{dz}\right)\left(\frac{\overline{dw}}{dz}\right)$$

Calculating C_p from the above expression results in

$$C_p = \frac{a_2}{z^2} + \frac{a_2}{\bar{z}^2} - a_1\left(1 - \frac{a_2}{z\bar{z}}\right)\left(\frac{z + \bar{z}}{z\bar{z}}\right) - \frac{a_1^2}{z\bar{z}} - \frac{a_2^2}{z^2\bar{z}^2}$$

$$+ a_3(z_o - \bar{z}_o)\left\{\frac{z^2\bar{z}^2 + a_1 z^2\bar{z} - a_1 z^2}{z^2\bar{z}^2(z - z_o)(z - \bar{z}_o)} + \frac{1}{z_o\bar{z}_o}\frac{z^2 + a_1 z - a_2}{\left(z - \frac{z\bar{z}}{z_o}\right)\left(z - \frac{z\bar{z}}{\bar{z}_o}\right)}\right\}$$

$$+ a_3^2\frac{(z_o - \bar{z}_o)^2}{z_o\bar{z}_o}\left\{\frac{z^2}{(z - z_o)(z - \bar{z}_o)\left(z - \frac{z\bar{z}}{z_o}\right)\left(z - \frac{z\bar{z}}{\bar{z}_o}\right)}\right\} \qquad (8)$$

This expression contains five unknowns, a_1, a_2, a_3, r_o, and θ_o, where the last two are the coordinates of the location of the vortices. These unknowns can be determined in several ways. One is to express the pressure coefficient in a five-term cosine series and equate the coefficients to a five-term series of the data. Another is to write a three-term series and equate the coefficients at two values of r (i.e., equate three coefficients at one location and two at the other). A third option is to use physical considerations to determine two unknowns, and use the three-term series to determine the other three. This third option was chosen as the one to use, although it is obviously an arbitrary choice. The physical consideration is the so-called vortex equilibrium criterion; namely, the velocity at the location of each vortex due to all of the other singularities is zero. This criterion insures that there is no force tending to convect the vortices downstream (ref. 10). It yields the two relations,

$$\frac{\cos\theta_o}{r_o} = \frac{a_1}{2a_2}$$

and

$$\tan^3\theta_o - \frac{a_3}{a_1}\tan^2\theta_o + \left(\frac{4a_2}{a_1^2} + 1\right)\tan\theta_o - \frac{a_3}{a_1} = 0$$

After some algebraic reduction, equation (8) can be written in the form of equation (1) and the coefficients c_n set equal to those determined from the data. The expressions are rather lengthy and will not be presented here. Solutions of these three equations along with the two stability equations have been obtained numerically for a velocity ratio of 0.4. Since the equations are nonlinear, several extraneous roots appear. However, there is little doubt as to which ones are physically realistic. The results are

$$a_1 = -0.121$$

$$a_2 = -0.048$$

$$a_3 = 0.668$$

$$\theta_o = 36.3°$$

$$r_o = 0.64$$

These again show that the doublet is considerably weaker than the source but in this case, the source is really a sink. Physically, this result seems more realistic than the result of the doublet model since the sink represents entrainment. Also, the vortices have the sense of rotation expected physically.

The value of the pressure coefficient determined from these results as a function of r for various values of θ, compared with the data of reference 9, is again shown in figures 8 through 12. Evidently, the agreement is unsatisfactory. For much of the surface of the plate, the agreement is worse than that obtained with the simpler doublet model without vortices.

The failure of the doublet-vortex model to correctly predict pressure distributions on the leeward side points to a fundamental difficulty of all inviscid models which attempt to simulate the observed velocities near the plate surface. It is known from experiment (ref. 11) that immediately behind the jet the fluid velocity is inward toward the orifice. (The presence of vortices in the doublet-vortex model was supposed to account for this fact.) Considering figure 7, it is evident that because of symmetry and the condition of no flow through the plate, the velocity vector along the $\theta = 0$ ray must be aligned with that ray. Consequently, if far downstream perturbations are to decay and the velocity along the $\theta = 0$ ray is to become equal to U_∞, the flow

must reverse direction and have a stagnation point in between. If no account is taken of viscous dissipation, the pressure at this stagnation point will recover to free-stream stagnation pressure, and the value of the pressure coefficient will be unity. Apparently, this difficulty will be encountered with any inviscid model that attempts to reproduce the inward velocity observed experimentally, no matter how complicated.

Pressure Models

For these models the point of view is taken that since the pressure distribution is known qualitatively, a flow can be constructed that will yield approximately this pressure distribution. At this point, free parameters (if there are any) are adjusted to obtain the best agreement with the data.

With this viewpoint, it is clear that the results obtained from the model should have a high-pressure region on the windward side of the jet and a low-pressure region on the leeward side. These both asymptotically decay to free-stream pressure at infinity. The nature of potential flow is such that to obtain this sort of pressure distribution, the velocity of the fluid due to whatever represents the jet must be in the same direction as the free stream on the leeward side of the jet and opposing the free stream on the windward side. Further, the singularities making up the disturbance to the free stream must be restricted to the neighborhood of the origin.

The simplest model which will meet those criteria is a source in a free stream. A source, doublet and free-stream model is more general and was tried above. However, by considering the $\theta = 90°$ ray and the fact that the sign of the doublet is positive it can be seen that agreement will improve if the doublet was removed. Another model was tried which consisted of the superposition of the axisymmetric flow out of an orifice in a flat plate and a uniform free stream. Both the source model and this orifice model will be described in this section.

The complex potential for the source model is well known. It is

$$w(z) = a_0 z + a_1 \log z \tag{9}$$

Calculating a_0 and a_1 by using the method described above for the doublet model yields the pressure coefficient

$$C_p = \frac{a_1^2}{z\bar{z}} - a_0 a_1 \frac{z + \bar{z}}{z\bar{z}} \tag{10}$$

which can be written as

$$C_p = -\frac{a_1^2}{r^2} - 2a_0 a_1 \frac{\cos\theta}{r} \tag{11}$$

The coefficients of the $\cos(n\theta)$ terms are now equated to the c_n determined from experimental data. Since these Fourier coefficients are independent of each other, c_0 and c_1 for a velocity ratio of 0.4 should have the same value as given above. However, for these last two models an adjustment has been made in the data of Vogler. At large distances from the orifice, the pressure coefficient should approach zero but the data do not show this. To correct this, the simplest approach was taken. A constant was added to the value of the pressure coefficient, C_p, on each ray so that it approached zero as r grew large. Of course, a different constant was used for each value of θ.

With this, the values of c_0 and c_1 become

$$c_0 = -0.725$$

$$c_1 = -0.823$$

where the matching is again at r = 1. Solving for a_0 and a_1 yields

$$a_0 = 0.483$$

$$a_1 = 0.851$$

Comparison of this model with experimental data is shown in figures 13 through 17. Like figures 8 through 12, these are plots of the pressure coefficient as a function of the radial distance from the center of the nozzle for several values of θ. As can be seen, this model gives quite good agreement in the vicinity of $\theta = 90°$, but the agreement around $\theta = 0°$ and $\theta = 180°$ is not as good. This is typical of the results obtained for other velocity ratios. It can therefore be expected that while this model will not predict pressure distributions accurately for all θ, it will be good for θ near 90° and will give good results for forces on plates.

The discrepancy between the data point at r = 1 in figures 10 and 15 is due to difficulties in reading Vogler's data at these values for r and θ.

Curves of the values of a_0 and a_1 for this model as functions of the velocity ratio are shown in figure 18.

The final model to be discussed has been mentioned before. It is composed of the superposition of two simpler flows, but this time one is axisymmetric and the other is added to it in such a way that the result is fully three dimensional. The axisymmetric portion is the flow out of a circular orifice in a flat plate. Reference 12 has a discussion of this solution. The other flow is a uniform free stream aligned so that its velocity vector is tangent to the plate. Carrying out the analysis and obtaining an expression for the pressure coefficient on the plate gives

$$C_p = -\frac{U_j/U_\infty \cos\theta}{\left(\frac{r}{k}\right)\sqrt{\left(\frac{r}{k}\right)^2 - 1}} - \frac{1}{4}\frac{(U_j/U_\infty)^2}{\left(\frac{r}{k}\right)^2\left[\left(\frac{r}{k}\right)^2 - 1\right]} \tag{12}$$

where the pressure coefficient retains its usual definition and k is a function of the velocity ratio, which is used to adjust the accuracy of the results. A curve of k as a function of the velocity ratio is shown in figure 18, along with the dependence of a_0 and a_1 on U_∞/U_j.

Comparison of the results of equation (12) with data is shown in figures 13 through 17. It can be seen that there is good agreement except near $\theta = 90^\circ$. Since the model is inaccurate near $\theta = 90^\circ$, it cannot be expected to give good results for forces (the singularity in the model is excluded from the integration), but its accuracy along the $\theta = 0$ and 180° rays indicates that the moments derived from it should agree closely with experiment.

CONCLUSIONS

A summary of the conclusions which have been reached in this paper are given below

1. By using a truncated Fourier series, a relatively simple empirical fit of the data is possible. While it is clear that an exact fit, in the mean, is always possible using an infinite series for a fixed r, it is shown that good results are possible by using only two or three terms.

2. Reasonable results for pressure distributions can be obtained using inviscid models. However, good agreement is usually restricted to a particular range of θ. For instance, the source model gives good results around $\theta = \pi/2$, while the orifice model is best near $\theta = 0$ and $\theta = \pi$.

3. As a corollary to conclusion 2, it is possible to obtain forces accurately from an inviscid model, and it is possible to obtain moments accurately from an inviscid model. At the present time, it does not seem to be possible to obtain both from the same model.

4. Adding greater complexity to the phenomenological models does not appear to improve their results. This is due to the stagnation point occurring along the axis.

5. Effects of viscosity must be included in any analysis which is intended to predict the flow properly, especially downstream of the jet.

REFERENCES

1. Keffer, J. F.; and Baines, W. D.: The Round Turbulent Jet in a Crosswind. J. of Fluid Mech., vol. 15, 1963, pp. 481-496.

2. Pratte, B. D.; and Baines, W. D.: Profiles of the Round Turbulent Jet in a Crossflow. Journal of the Hydraulics Division, Proceedings of the ASCE, November 1967.

3. Cassel, L. A.; Davis, J. G.; and Engh, D. P.: Lateral Jet Control Effectiveness Prediction for Axisymmetric Missile Configurations. U.S. Army Missile Command, Report No. RD-TR-68-5, Redstone Arsenal, Ala., June 1968.

4. Wooler, P. T.; Burghart, G. H.; and Gallagher, J. T.: Pressure Distribution on a Rectangular Wing with a Jet Exhausting Normally into an Airstream. Journal of Aircraft, vol. 4, no. 6, November-December 1967.

5. Kuiper, R. A.: Control Jet Effectiveness in the Subsonic and Transonic Flight Regimes. Philco, Aeronutronic Division Publication No. U-2932, December 1964.

6. Bradbury, L. J. S.; and Wood, M. N.: The Static Pressure Distribution Around a Circular Jet Exhausting Normally from A Plane Wall into an Airstream. Gt. Brit. Aero. Research Council, CP No. 822, 1965.

7. Reichenau, D. E. A.: Interference Effects Produced by a Cold Jet Issuing Normal to the Airstream from a Flat Plate at Transonic Mach Numbers. AEDC-TR-67-220. Arnold Air Force Station, Tenn., October 1967.

8. Spring, D. J.; Street, T. A.; and Amick, J. L.: Transverse Jet Experiments and Theories--A Survey of the Literature, Part I. U.S. Army Missile Command, Redstone Arsenal, Report RD-TR-67-4, June 1967.

9. Vogler, R. D.: Surface Pressure Distribution Induced on a Flat Plate by a Cold Air Jet Issuing Perpendicularly from the Plate and Normal to a Low Speed Free-stream Flow. NASA TN D-1629, March 1963.

10. Milne-Thompson, L. M.: Theoretical Hydrodynamics. Third Edition, The MacMillian Co., New York, 1955.

11. Jordinson, R.: Flow in a Jet Directed Normal to the Wind. Gt. Brit. Aero. Res. Council RM No. 3074, 1958.

12. Lamb, Sir H.: Hydrodynamics. Sixth Edition, Dover Publications, New York, N.Y.

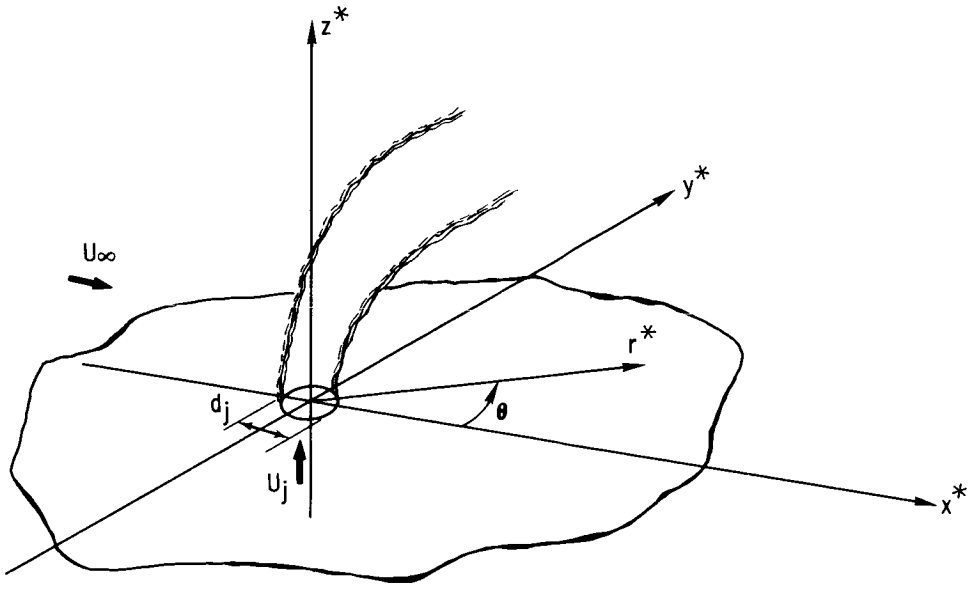

M71745

Figure 1.- Coordinate system for describing interference pressure distribution on a flat plate.

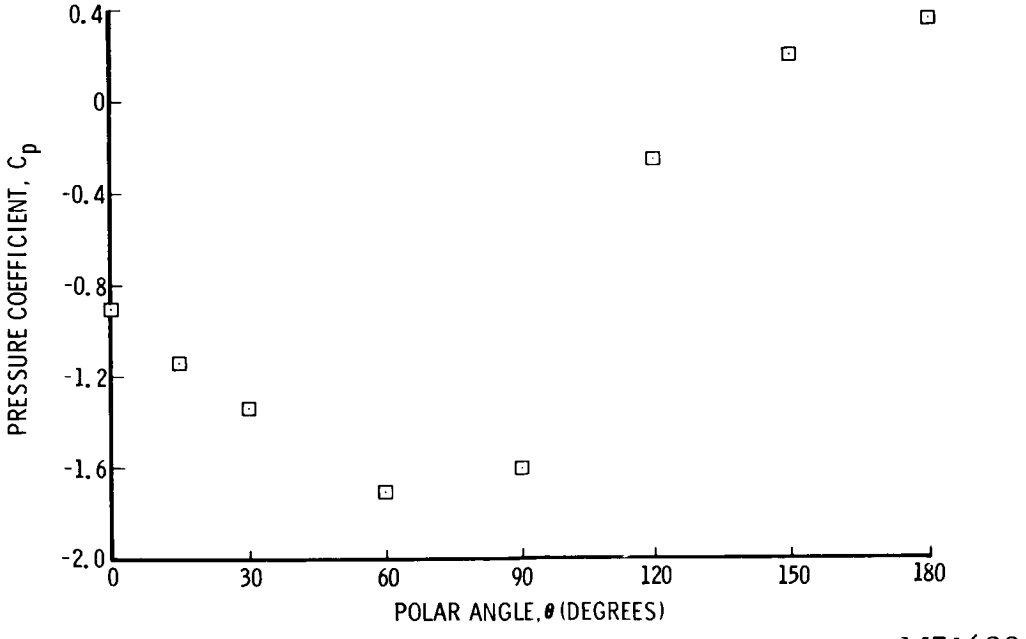

M71622

Figure 2. - Example of data of reference 9 for $U_\infty / U_j = 0.4$ and $r = 1.0$.

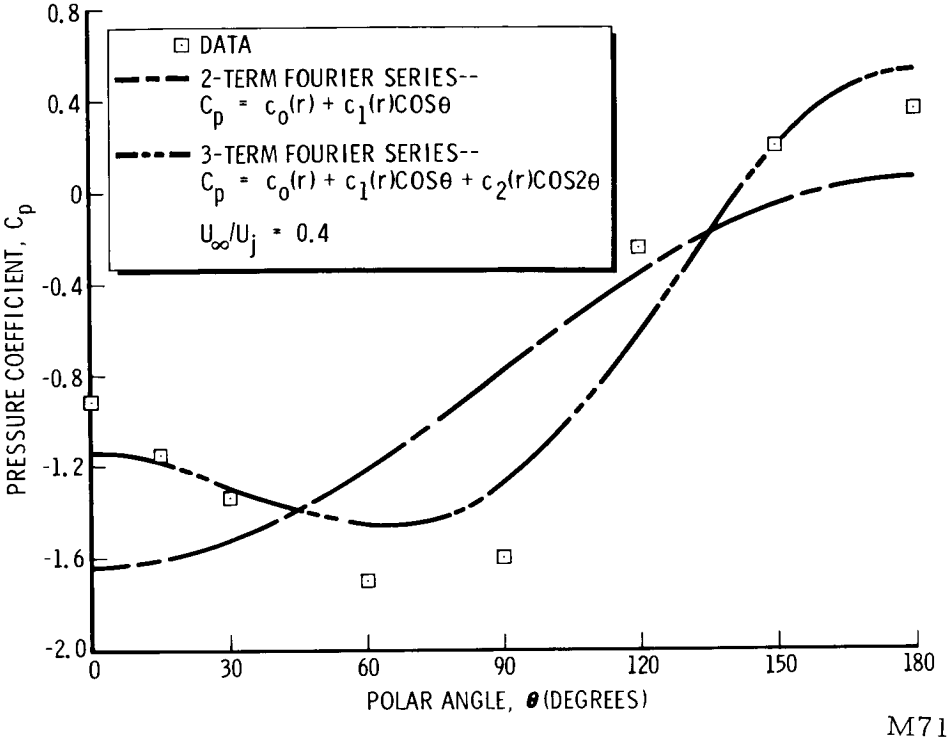

Figure 3.- Comparison of two- and three-term series with data from reference 9 at r = 1.

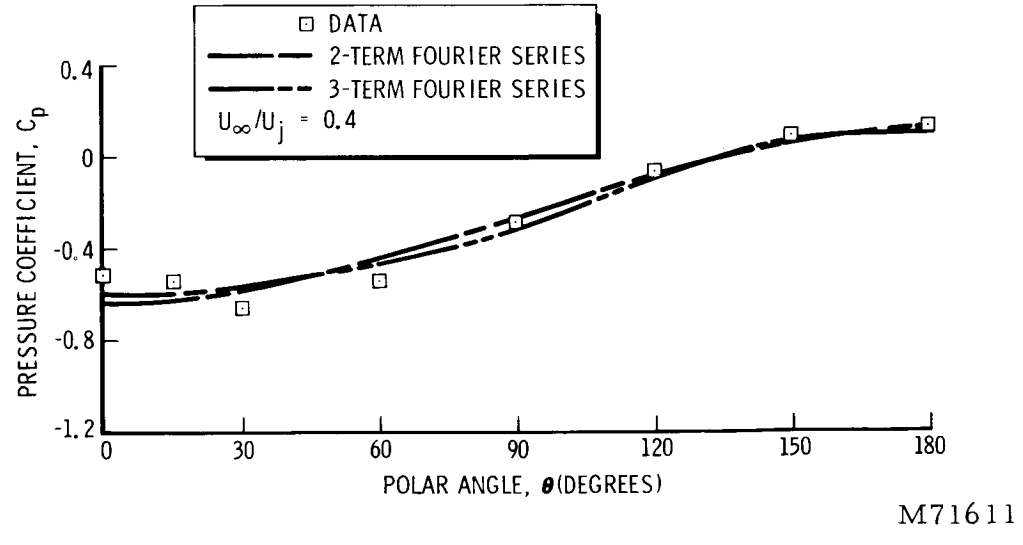

Figure 4.- Comparison of two- and three-term series with data from reference 9 at r = 2.

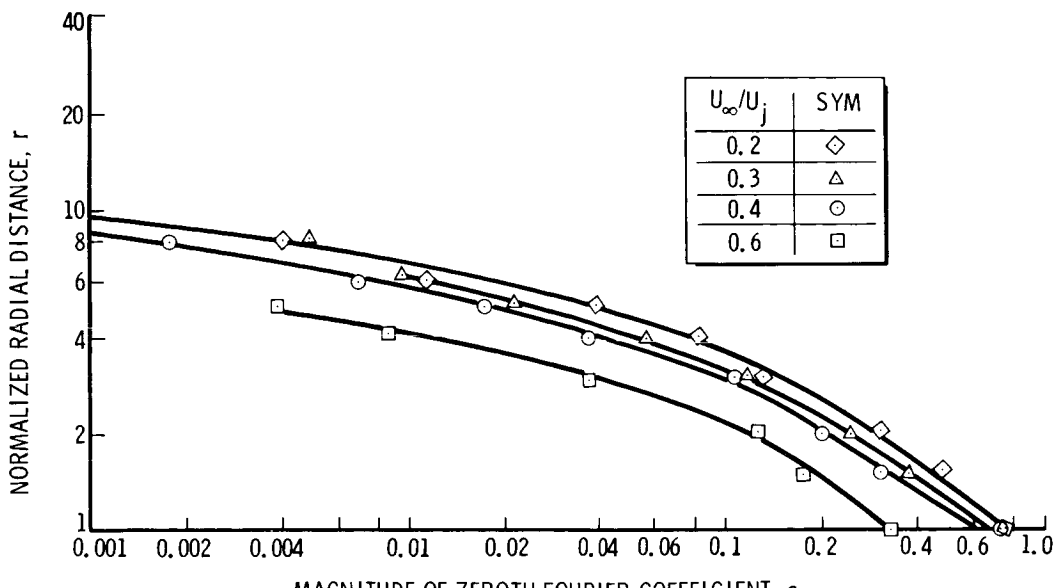

Figure 5.- Variation of zeroth Fourier coefficient with normalized distance from the nozzle and velocity ratio.

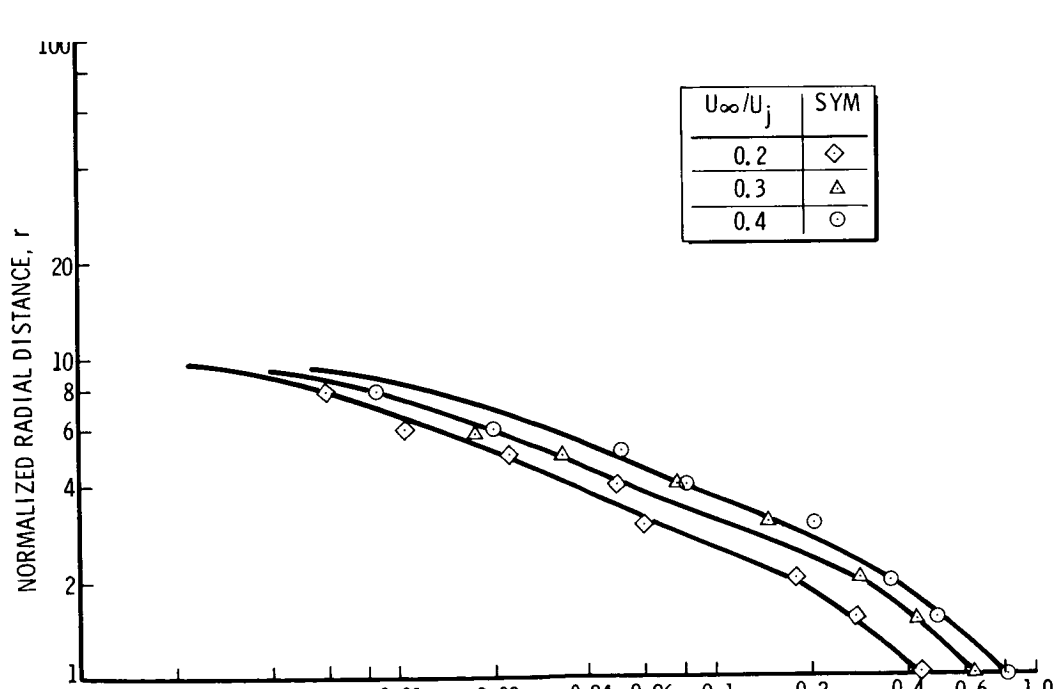

M71627

Figure 6.- Variation of first Fourier coefficient with normalized distance from the nozzle and velocity ratio.

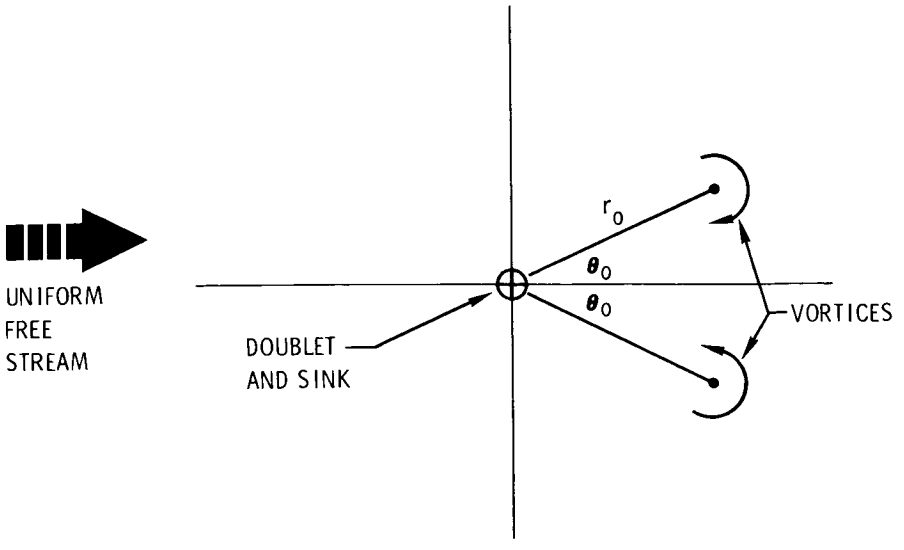

M71624

Figure 7. - Sketch of doublet—vortex model.

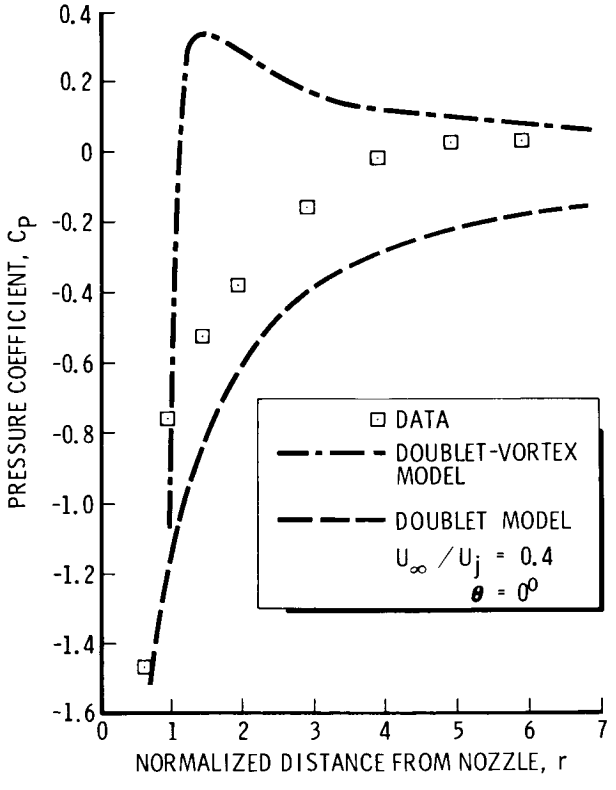

M71617

Figure 8.- Results of doublet-vortex and doublet models compared with data from reference 9. $\theta = 0^{\circ}$.

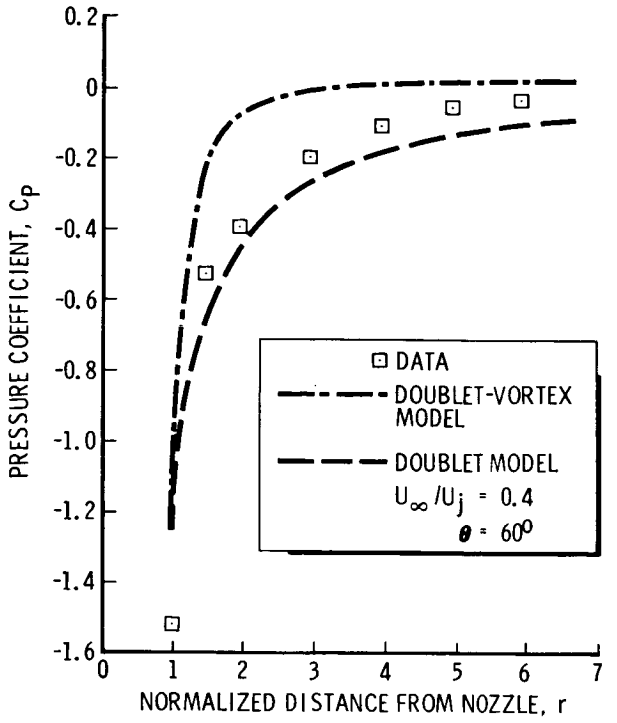

M71618

Figure 9.- Results of doublet-vortex and doublet models compared with data from reference 9. $\theta = 60^\circ$.

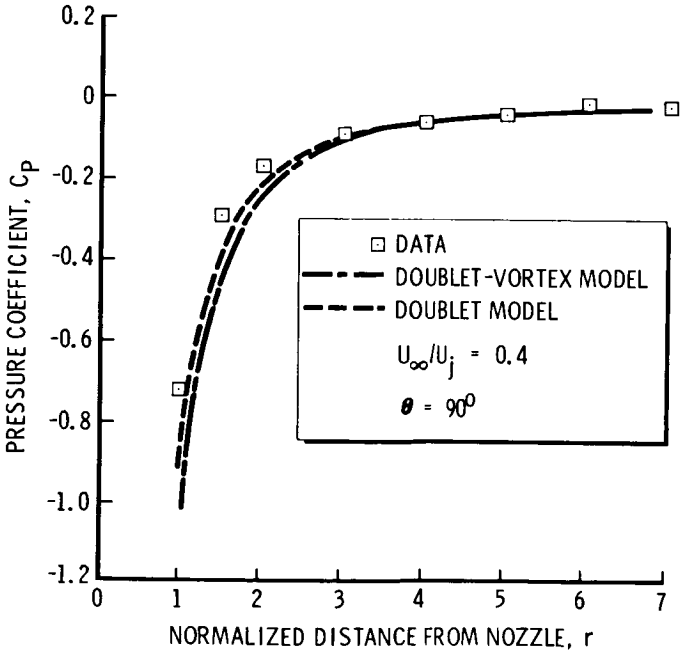

M71619

Figure 10.- Results of doublet-vortex and doublet models compared with data from reference 9. $\theta = 90^\circ$.

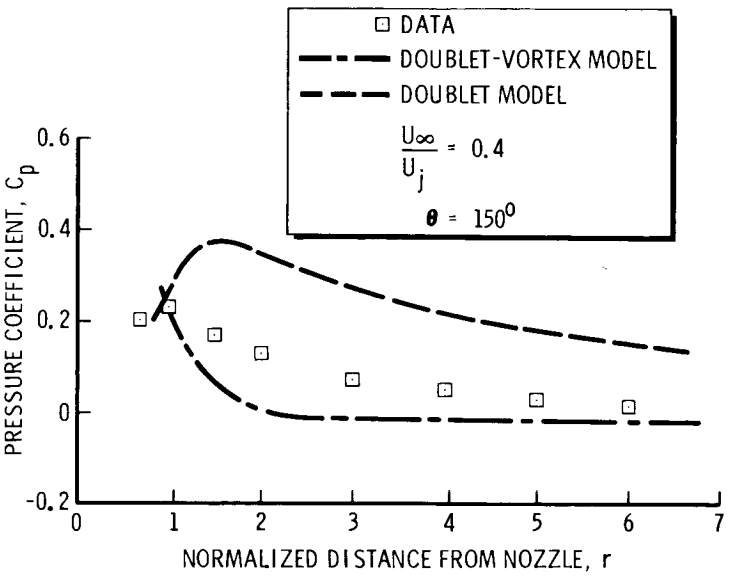

M71620

Figure 11.- Results of doublet-vortex and doublet models compared with data from reference 9. θ = 150°.

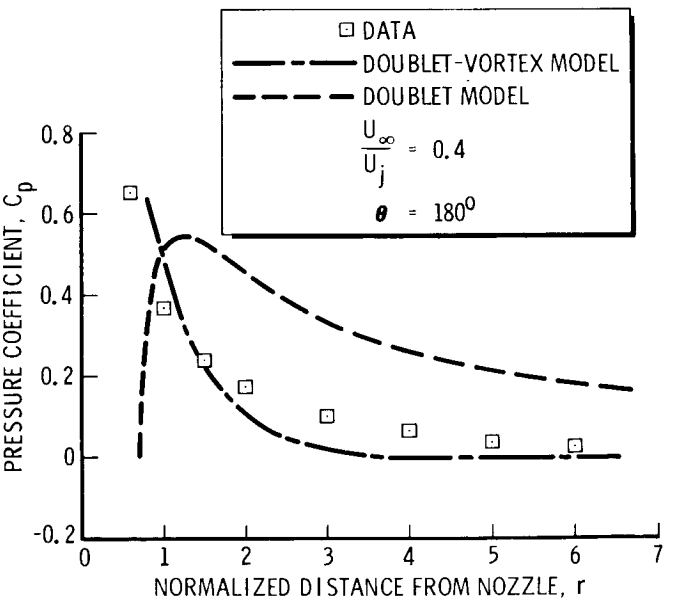

M71621

Figure 12.- Results of doublet-vortex and doublet models compared with data from reference 9. θ = 180°.

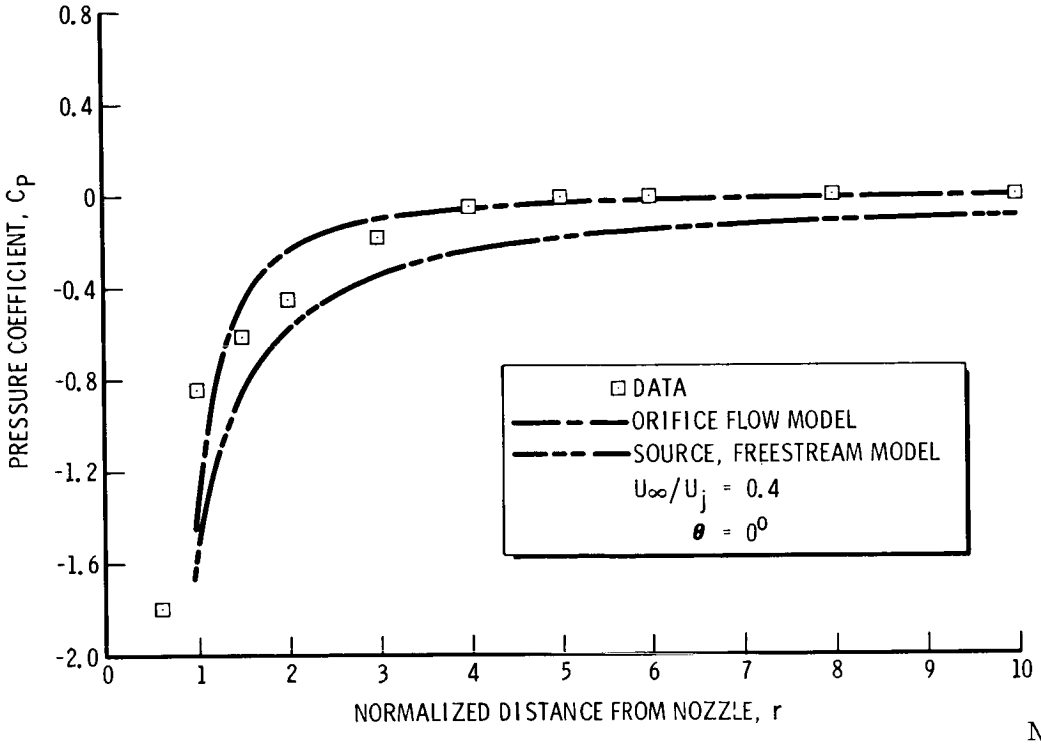

Figure 13.- Results of source and orifice models compared with data from reference 9. $\theta = 0^{\circ}$.

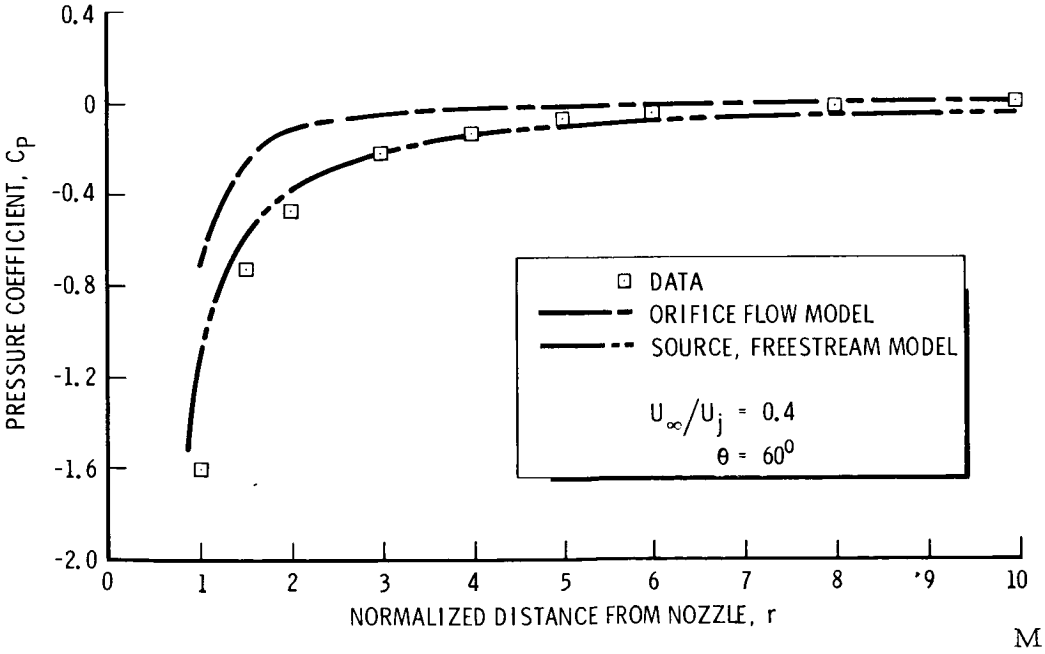

Figure 14.- Results of source and orifice models compared with data from reference 9. $\theta = 60^{\circ}$.

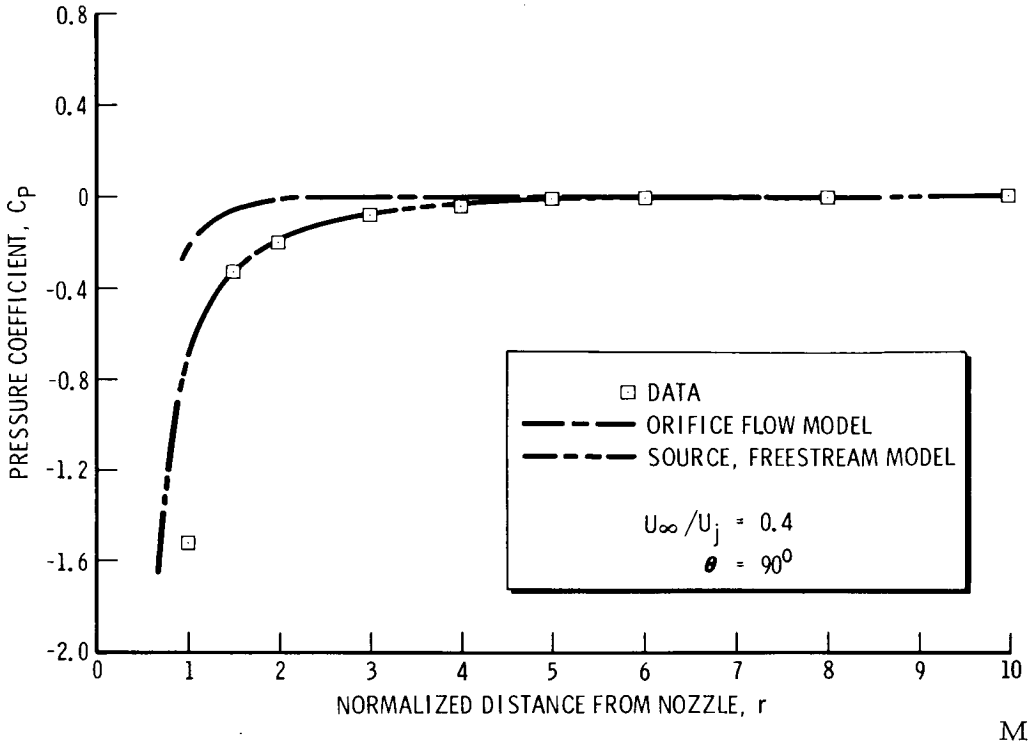

M71613

Figure 15.- Results of source and orifice models compared with data from reference 9. $\theta = 90^\circ$.

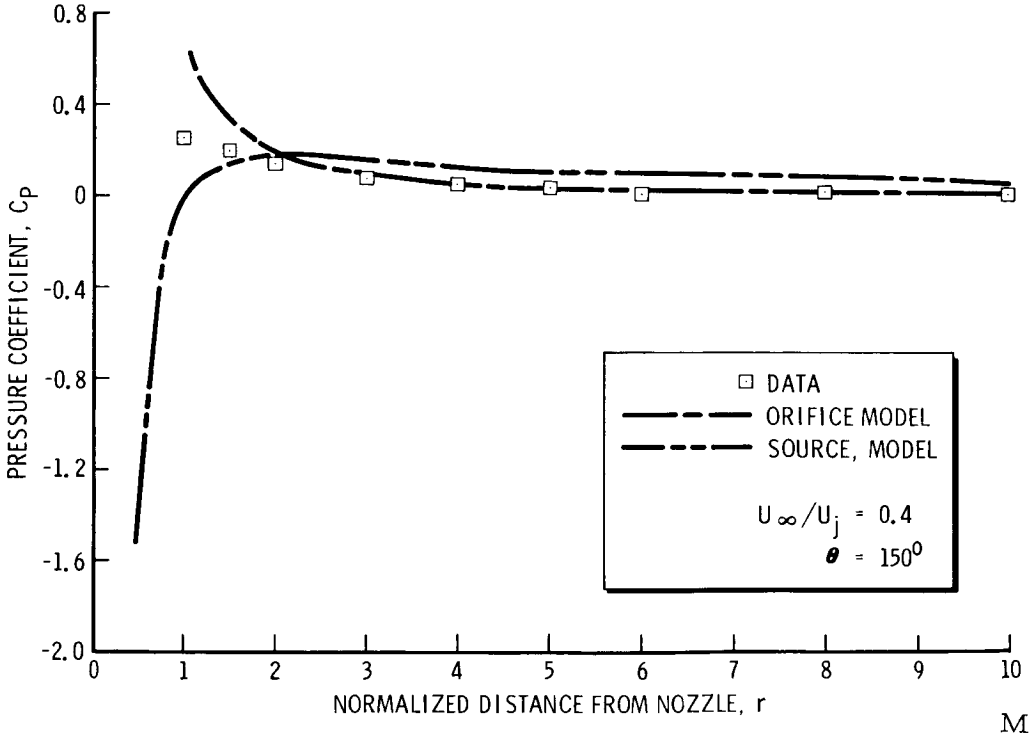

M71614

Figure 16.- Results of source and orifice models compared with data from reference 9. $\theta = 150^\circ$.

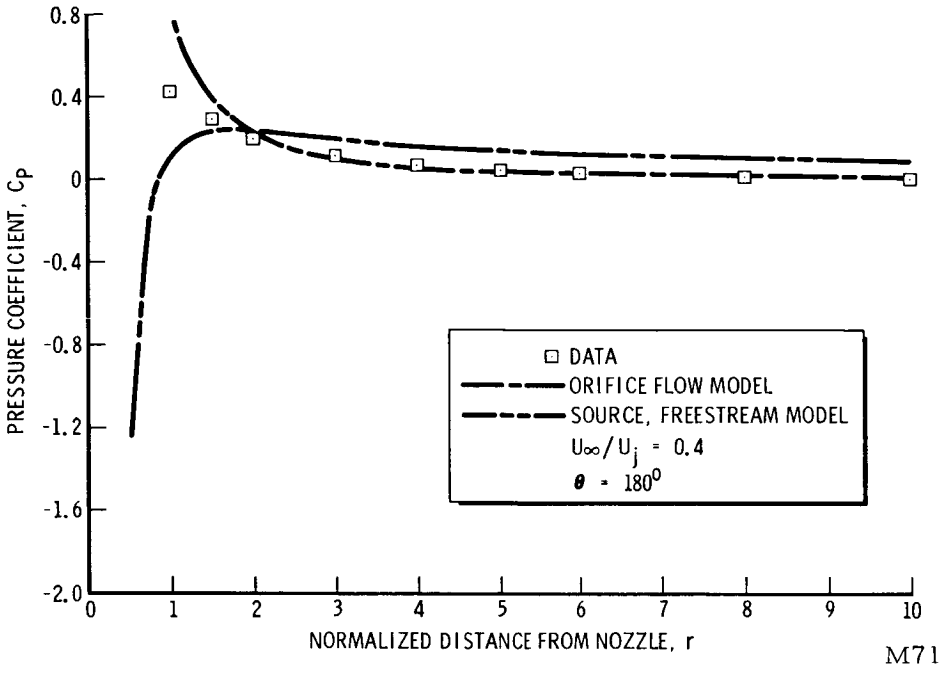

Figure 17.- Results of source orifice models compared with data from reference 9. $\theta = 180^\circ$.

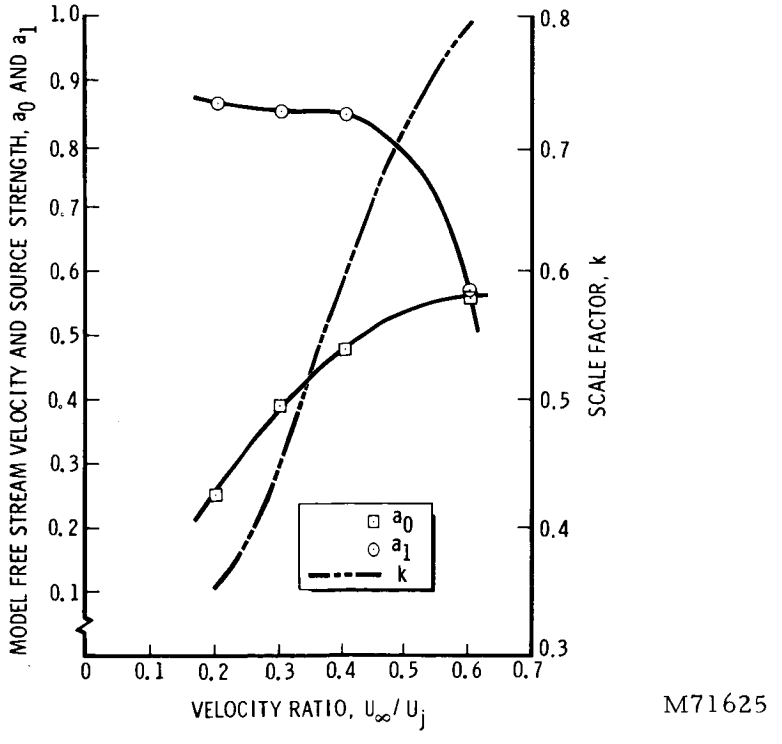

Figure 18.- a_o, a_1, and k as functions of the velocity ratio.

THE USE OF MATCHED ASYMPTOTIC EXPANSIONS AS AN APPROACH TO THE PROBLEM OF THE JET IN A CROSSFLOW

By Jack E. Werner

New York University

SUMMARY

The method of matched asymptotic expansions is proposed as an approach to the problem of a circular jet issuing from a plane surface into a crossflow. "Inner" and "outer" expansions are written in powers of the parameter r_o/R. Introduction of these expansions into Laplace's eq. for the velocity potential results in a series of quasi two-dimensional equations for the terms of the inner expansion. The matching principle is illustrated and the manner in which different models of the flow may be introduced into the theory and compared is discussed.

SYMBOLS

r_o	characteristic "diameter" of jet cross section
R	radius of curvature of jet trajectory
U	undisturbed upstream flow velocity
x_1	coordinate in downstream direction
y_1	coordinate perpendicular to x_1 and jet axis
z_1	coordinate perpendicular to plane of jet orifice
φ	velocity potential
φ^o	outer expansion for velocity potential
φ^i	inner expansion for velocity potential
ζ	complex variable $x + iy$
$\bar{\zeta}$	complex variable $X + iY$
$\mathrm{Re}\{f(\zeta)\}$	real part of $f(\zeta)$

INTRODUCTION

One of the important objectives of an analytical treatment of the jet in a crossflow is the determination of the induced flow particularly near the aerodynamic surfaces of jet VTOL craft. Unfortunately the phenomenon is too complex to admit of a complete theoretical treatment. The effects of viscosity and turbulence in the jet present formidable enough obstacles but to this must be added the difficulties of solving the free-boundary problem of the three-dimensional flow around the jet to arrive at the induced flow field. Among the initial efforts in this field were investigations of the jet itself and its trajectory, refs. [1] to [4]. More recently the results of these investigations have been used to infer the shape of the trajectory at the outset and thus reduce the induced flow problem to a fixed rather than free-boundary problem. Such a treatment has been carried out by Wooler, ref. [5] and by Rubbert and Saaris, ref. [6], to evaluate the flow field near lifting surfaces.

Presently the state of development is such that we must accept admittedly crude models of the physical situation in order to make analytical headway. This being the case it is still worthwhile to propose and compare different analytical models in an effort to arrive at one or a combination of useful ones. It is the purpose of this paper to propose a theoretical framework in which various analytical models may be explored and compared. Basically the method centers about the use of matched asymptotic expansions, Van Dyke ref. [7].

FORMULATION OF THE PROBLEM

We consider the problem of a jet issuing into a crossflow from an orifice in a flat plate. Outside the jet we seek solutions to the inviscid flow governed by the Laplace eq. for the potential. Far from the jet, in the so-called "outer" region, we expect the flow to be undisturbed away from the wake. On the jet itself the flow is to be tangential to the jet surface and for small values of the parameter r_o/R we may expect this flow to be almost two dimensional but not completely so.

To accomodate these last considerations the "inner" and "outer" expansions of the potential are introduced in the form:

$$\varphi^{o}(x,y,z) = \sum_{o}^{\infty} \left(\frac{r_o}{R}\right)^{m} \varphi_m^{o}\ (x,y,z)$$

$$\varphi^{i}(X,Y,Z) = \sum_{o}^{\infty} \left(\frac{r_o}{R}\right)^{m} \varphi_m^{i}\ (X,Y,Z)$$

where x, y, z are nondimensional outer variables

$$x = x_1/R \quad , \quad y = y_1/R \quad , \quad z = z_1/R$$

and X, Y, Z are the dimensionless inner variables

$$X = \frac{x}{r_o/R} \quad , \quad Y = \frac{y}{r_o/R} \quad , \quad Z = z$$

φ^o is a solution to the Laplace eq. satisfying the boundary conditions far from the jet. φ^i is a solution to the Laplace eq. satisfying boundary conditions on the jet surface. Each of these solutions requires another condition to determine them uniquely. The remaining condition is the requirement that the two expansions match asymptotically over a region intermediate to the inner and outer regions. By this we mean that over the matching region the Nth partial sums of φ^o and φ^i exhibit the same functional behavior and agree within an order of $(r_o/R)^N$. Thus the condition supplying the intermediate boundary condition is for each value of N

$$\lim_{(r_o/R)\to 0} \frac{\left[\sum_{o}^{N} \left(\frac{r_o}{R}\right)^m \varphi_m^i\right]_o - \left[\sum_{o}^{N} \left(\frac{r_o}{R}\right)^m \varphi_m^o\right]_i}{(r_o/R)^N} = 0$$

Where $[\quad]_o$ represents the behavior of the inner solution near the outer bound of the matching region, i.e., as $X,Y \to \infty$ with x,y finite this limiting process is equivalent to letting r_o/R approach zero with x,y finite. Similarly $[\quad]_i$ represents the behavior of the outer solution near the inner bound of the matching region and is found by allowing r_o/R to approach zero with X,Y finite, i.e., letting x,y tend to zero.

EVALUATION OF φ_m^o , φ_m^i

The governing eqs. for the functions φ_m^o and φ_m^i are obtained by substitution of the expansions into the Laplace eq. and setting the coefficient of powers of (r_o/R) equal to zero. Thus the complete eqs. governing φ^o and φ^i are

$$\frac{\partial^2 \varphi^o}{\partial x^2} + \frac{\partial^2 \varphi^o}{\partial y^2} + \frac{\partial^2 \varphi^o}{\partial z^2} = 0$$

$$\frac{\partial^2 \varphi^i}{\partial X^2} + \frac{\partial^2 \varphi^i}{\partial Y^2} + \left(\frac{r_o}{R}\right)^2 \frac{\partial^2 \varphi^i}{\partial Z^2} = 0$$

Substituting the inner expansion into the second of these yields

$$\frac{\partial^2 \varphi_o^i}{\partial X^2} + \frac{\partial^2 \varphi_o^i}{\partial Y^2} = 0$$

$$\frac{\partial^2 \varphi_1^i}{\partial X^2} + \frac{\partial^2 \varphi_i^i}{\partial Y^2} = 0$$

$$\frac{\partial^2 \varphi_m^i}{\partial X^2} + \frac{\partial^2 \varphi_m^i}{\partial Y^2} = - \frac{\partial^2 \varphi_{m-2}^i}{\partial Z^2} \qquad m \geq 2$$

The terms of the outer solution all obey

$$\frac{\partial^2 \varphi_m^o}{\partial x^2} + \frac{\partial^2 \varphi_m^o}{\partial y^2} + \frac{\partial^2 \varphi_m^o}{\partial z^2} = 0 \qquad m \geq 0$$

Thus φ_o^o is a solution of the Laplace eq. satisfying the outer boundary condition of uniform flow at infinity. A solution for φ_o^o will therefore be

$$\varphi_o^o = Ux$$

From the matching condition with N = 0

$$\lim_{(r_o/R)\to 0} \left\{ \left[\varphi_o^i \right]_o - \left[\varphi_o^o \right]_i \right\} = 0$$

Where $\left[\varphi_o^o \right]_i = \lim_{\substack{(r_o/R)\to 0 \\ X \text{ finite}}} [Ux] = \lim_{\substack{(r_o/R)\to 0 \\ X \text{ finite}}} \left[U \frac{r_o}{R} X \right] = 0$

Therefore we have $\left[\varphi_o^i \right]_o = 0$ which together with the governing eq. for φ_o^i and the inner boundary condition yields

$$\varphi_o^i = 0$$

This result, although very simple, serves to illustrate the rudiments of the matching technique. Turning to the next order φ_1^i satisfies the two dimensional Laplace eq. together with the condition that its derivative normal to the jet surface is zero to within terms of order (r_o/R). A general solution satisfying these conditions will be assumed in the form

$$\varphi_1^i = \mathrm{Re}\left\{ \sum_1^\infty {}^nC\, \bar{\zeta}^n + \sum \frac{C_n}{\bar{\zeta}^n} \right\}$$

This form assumes a general two-dimensional symmetrical flow about a closed streamline enclosing the origin $\bar{\zeta} = 0$. The closed streamline may be completely on the jet surface, i.e.: fully attached flow, or may follow the upstream portion of the jet surface but then separate from it to enclose a wake region and then close at some point downstream. It is at this point that we may introduce any one of a number of possible models for the flow around the jet.

Applying the matching condition with N = 0 we arrive at the conditions

$$^1C = U$$

$$^nC = 0 \qquad n \geq 2$$

$$\left[\varphi_1^o\right]_i = 0$$

Thus we shall have $\varphi_1^o = 0$ and

$$\varphi_1^i = \mathrm{Re}\left\{ U\bar{\zeta} + \sum_o^\infty \frac{C_n}{\bar{\zeta}^n} \right\}$$

in which the constants C_n are determined by the requirement that φ_1^i represent the potential for a uniform flow about the closed streamline (tangential to jet and wake surfaces) at the station z. In other words, the third dimension z enters by means of the coefficients C_n determined by the boundary condition at the station z.

Continuing the process to N = 2 yields the result

$$\varphi_2^i = \mathrm{Re}\left\{ \sum_1^\infty D_n/\bar{\zeta}^n \right\}$$

$$\left[\varphi_2^o\right]_i = -\,\mathrm{Re}\left\{ C_1/\zeta \right\}$$

The interpretation placed on the latter result is that to within the order of $(r_o/R)^2$ the outer solution consists of a uniform flow plus a distribution of doublets along the jet axis. The origin of the doublet flow is found in the "blockage" of the jet and the presence of sheets of vorticity occurring symmetrically over the jet and wake surfaces. Since the strength of these vortex sheets are determined by the jet cross section at a given station z along the jet axis, the vorticity will vary with z. To maintain the balance of vorticity according to the laws of Helmholtz we must have a trailing vortex system breaking away symmetrically from the sides of the jet and wake surfaces. Far from the jet these trailing vortices appear as a distribution of vortex doublets inducing a downwash behind the jet.

CONCLUDING REMARKS

The above considerations represent a rough sketch of the more important features of the proposed method as they are discernible at this stage. Principal among these is the quasi two-dimensional nature of the equations for φ_1^i, φ_2^i and at least the homogeneous parts of the subsequent terms φ_n^i. This makes available to us the growing body of knowledge regarding two-dimensional wake flows. The method also contains a built-in system of "accounting" in the matter of obtaining solutions which are valid to within a given order of magnitude. Thus, in obtaining say the first two terms of φ^i it is only necessary to satisfy an approximate boundary condition to within an order of $(r_o/R)^2$ rather than inconsistently posing an exact boundary condition for an approximate formulation of the solution.

REFERENCES

1. Keffer, J. F.; and Baines, W. D.: The Round Turbulent Jet in a Cross-Wind. J. Fluid Mech., vol. 15, pt. 4, Apr. 1963, pp. 481-496.

2. Margason, Richard J.: The Path of a Jet Directed at Large Angles to a Subsonic Free Stream. NASA TN D-4919, 1968.

3. Abramovich, G. N.: The Theory of Turbulent Jets. M.I.T. Press, c.1963, pp. 541-552.

4. Wooler, P. T.: Flow of a Circular Jet Into a Cross Flow. J. Aircraft (Eng. Notes), vol. 6, no. 3, May-June 1969, pp. 283-284.

5. Wooler, P. T.; Burghart, G. H.; and Gallagher, J. T.: Pressure Distribution on a Rectangular Wing With a Jet Exhausting Normally Into an Airstream. J. Aircraft, vol. 4, no. 6, Nov.-Dec. 1967, pp. 537-543.

6. Rubbert, P. E.; Saaris, G. R.; Scholey, M. B.; Standen, N. M.; and Wallace, R. E.: A General Method for Determining the Aerodynamic Characteristics of Fan-in-Wing Configurations. Vol. 1 - Theory and Application. USAAVLABS Tech. Rep. 67-61A, U.S. Army, Dec. 1967.

7. Van Dyke, Milton: Perturbation Methods in Fluid Mechanics. Academic Press, 1964.

MASS ENTRAINMENT OF A CIRCULAR JET IN A CROSS FLOW

By R. L. Fearn

University of Florida
Gainesville, Florida

SUMMARY

By use of conservation of mass and momentum, an equation is derived relating the mass entrainment of a round turbulent jet exhausting into a cross flow to the equation for the jet axis. If an empirical equation for the jet axis is used, one finds that the mass entrainment approximates a linear dependence on distance along the jet axis. If, on the other hand, a linear entrainment of undetermined slope is assumed, a differential equation is obtained for the jet axis which can be solved analytically. Several members of the resulting family of one-parameter curves are fitted to empirically determined jet axes to obtain the entrainment as a function of the ratio of free-stream velocity to jet velocity.

15

INTRODUCTION

An approximate technique to determine numerically the aerodynamic characteristics of a wing in subsonic flow is to use lifting-surface theory. This method is a generalization of Prandtl's lifting-line theory in which the wing is represented by a superposition of singular solutions to Laplace's equation. Boundary conditions that the flow be tangent to the surface of the wing and that the Kutta condition be satisfied are imposed at appropriate points. This method has also been used in an attempt to calculate the aerodynamic characteristics of the fan-in-wing configuration which is one design approach to VTOL aircraft (ref. 1). The slipstream from the wing fan constitutes a round turbulent jet exhausting into a cross flow. Since this is a boundary-layer phenomenon, one would expect the singularity method to be applicable in the region exterior to the wing and jet. However, knowledge of the jet in a cross flow is required to establish the boundary conditions for the potential flow problem. The lack of such knowledge is illustrated by the work of Rubbert and associates who found that the only usable information available to them about the jet in a cross flow was an empirical equation for the jet axis. In the absence of any other information, they used a constant-cross-section jet with no entrainment. (See ref. 1.)

Despite this lack of information, considerable effort has been expended to describe this phenomenon both experimentally and theoretically. Experimental studies have established the location of the jet center line for various conditions at the jet orifice and have provided some information about velocity and pressure distributions. (See refs. 2 and 3.) Because of the complexity of the theoretical problem, however, little more has been attempted than to describe the location of the jet center line. One theoretical approach has been to

assume that the interaction of the jet with the free stream could be represented by an appropriate drag coefficient for the jet (refs. 4 to 6) which presupposes that a pressure distribution is a mechanism for jet deflection. This is possibly significant in the vicinity of the jet orifice, but it is probably negligible compared with the momentum mixing of the jet with the free stream for distances along the jet axis greater than a few jet diameters.

SYMBOLS

a	parameter, M_Z/mV_∞, feet
C_1	constant, $a\sqrt{1 + (x_o')^2} - x_o$, dimensionless
E	entrainment coefficient, $\frac{1}{Q_o}\frac{dQ}{ds}$, dimensionless
$\hat{e}_s$	unit vector tangent to jet axis
$\hat{i},\hat{k}$	Cartesian unit vectors
$\vec{M}$	momentum flux across jet cross section, slug-feet/second^2
M_Z	component of jet momentum flux perpendicular to free-stream velocity, slug-feet/second^2
$\Delta\vec{M}_E$	momentum flux entrained across increment of jet boundary, slug-feet/second^2
m	slope of curve of mass entrainment as a function of distance along jet axis, constant, slugs/foot-second
Q	mass flux across jet cross section, slugs/second
Q_o	mass flow across jet orifice
ΔQ_E	mass flux entrained across increment of jet boundary, slugs/second
s	distance along jet axis, measured in jet diameters, dimensionless
V_j	initial jet velocity, feet/second
V_∞	free-stream velocity, feet/second
$x,z;$ x_o,z_o	Cartesian coordinates of jet axis, measured in jet diameters, dimensionless
x'	derivative of x with respect to z, dimensionless

z', z'' first and second derivatives of z with respect to x, dimensionless

α angle between jet axis and free-stream velocity, degrees

Arrow over symbol indicates vector.

MASS ENTRAINMENT AND THE EQUATION FOR THE JET AXIS

The purpose of this paper is to investigate the possibility of obtaining some information about the jet axis and entrainment of a circular turbulent jet exhausting into a cross flow by considering conservation of mass and momentum. Simply stated, the approach is to assume that the mechanism for deflecting the jet is an inelastic collision of the entrained mass with the mass of the jet,[1] that is, the pressure field as a mechanism for deflecting the jet is neglected. Additionally, the mass entrained by the jet is assumed to have a velocity approximately equal to the free-stream velocity V_∞.

To formulate this assumption quantitatively, consider the conservation of mass and momentum for a small control volume defined by two cross sections of the jet, located at s and $s + \Delta s$ from the jet orifice along the jet center line, and by the jet boundary. The conservation equations for the control volume may be written as

$$Q(s+\Delta s) = Q(s) + \Delta Q_E(s) \tag{1}$$

$$\vec{M}(s+\Delta s) = \vec{M}(s) + \Delta \vec{M}_E(s) \tag{2}$$

where $Q(s)$ and $\vec{M}(s)$ are the mass and momentum flux across the jet cross section at s, and $\Delta Q_E(s)$ and $\Delta \vec{M}_E(s)$ are the mass and momentum flux entrained across the jet boundary between the cross section at s and $s + \Delta s$. Assume that the momentum entrained across the jet boundary is the entrained mass with a velocity equal to the free-stream velocity V_∞, that is,

$$\Delta \vec{M}_E(s) = \Delta Q_E(s)\, \vec{V}_\infty \tag{3}$$

The change in the momentum of the jet with respect to distance along the jet axis may thus be written

$$\frac{d\vec{M}}{ds} = \frac{dQ}{ds} \vec{V}_\infty \tag{4}$$

---

[1]This approach was first brought to the author's attention by Dr. Gerhard Braun in December 1967.

If $\vec{dM}/ds$ is related to the equation for the jet axis, then equation (4) can be used to obtain a relation between mass entrainment and the equation for the jet axis. Define the jet axis as the curve passing through the center of the jet orifice with the direction at every point on the curve tangent to the momentum flux at that point. If the momentum flux is written as

$$\vec{M}(s) = M(s)\,\hat{e}_s$$

and the unit vector $\hat{e}_s$ is written in terms of the Cartesian unit vectors, then

$$\frac{\vec{dM}}{ds} = \left[\frac{1}{z'}\frac{dM_z}{ds} - \frac{z''M_z}{z'^2\left(1 + z'^2\right)^{1/2}}\right]\hat{i} + \frac{dM_z}{ds}\,\hat{k} \tag{5}$$

where $\hat{i}$ and $\hat{k}$ are the unit vectors parallel and normal to the free stream, respectively, $z(x)$ defines the equation for the jet axis, and M_z is the component of the jet momentum flux perpendicular to the free-stream velocity. Equating equations (4) and (5) gives the desired relation

$$\frac{dQ}{ds}\,V_\infty = -\frac{z''M_z}{z'^2\left(1 + z'^2\right)^{1/2}} \tag{6}$$

where M_z is constant.

Using an empirical equation for the jet axis to calculate the mass entrainment as a function of s, one finds that the dependence is approximately linear except in the vicinity of the jet orifice (fig. 1).

A SEMIEMPIRICAL EQUATION FOR THE JET AXIS

If the mass entrainment is assumed to vary linearly with distance along the jet axis in the region of established flow, that is,

$$dQ/ds = m$$

where m is a constant, then the jet axis is described by the differential equation

$$mV_\infty = \frac{z''M_z}{z'^2\left(1 + z'^2\right)^{1/2}} \tag{7}$$

Letting $a = M_z/(mV_\infty)$ and integrating equation (7) results in a semiempirical equation for the jet axis

$$z = z_o + a \ln \left\{ \frac{\left[(x + C_1)^2 - a^2\right]^{1/2} + x + C_1}{\left[(x_o + C_1)^2 - a^2\right]^{1/2} + x_o + C_1} \right\} \tag{8}$$

where $C_1 = a\left[1 + (x_o')^2\right]^{1/2} - x_o$ and the parameter a must be determined experimentally. The position (x_o, z_o) and the slope x_o' of the jet axis at one point in the region of established flow must be specified as initial conditions.

For a jet exhausting normally into a cross flow,

$$M_z = Q_o V_j$$

where Q_o is the mass flux across the jet orifice. One may define an entrainment coefficient as

$$E = \frac{1}{Q_o} \frac{dQ}{ds}$$

which in terms of the parameter a is

$$E = \frac{V_j}{aV_\infty}$$

The parameter a, or equivalently E, may be varied to obtain a best fit to experimentally determined jet axes for various velocity ratios V_∞/V_j.

The entrainment coefficient for a number of velocity ratios was obtained by fitting equation (8) to the following empirical equation for the jet axis developed by Ivanov (ref. 4, p. 544):

$$x = \left(\frac{V_\infty}{V_j}\right)^{2.6} z^3 + z \cot \alpha \tag{9}$$

where α is the initial angle that the jet axis makes with the free-stream velocity. Margason confirms that this equation provides a good fit to experimental results (ref. 7). It was found that a good fit between the semiempirical equation (8) and the empirical equation (9) could be obtained by assuming that the jet does not deflect from the Z-axis until it reaches a particular distance from the jet orifice. The point at which deflection begins is referred to as the effective source of the jet, and the distance from the jet orifice to the effective source varies with velocity ratio. This probably marks the point

where the potential core has disappeared and where the region of established flow begins. Under these assumptions, the semiempirical equation simplifies to

$$z = z_o + \frac{1}{ER} \ln \left[1 + ER\left(x + \sqrt{x^2 + \frac{2x}{ER}} \right) \right] \tag{10}$$

where z_o locates the effective source, and R is the velocity ratio V_∞/V_j.

The entrainment coefficient E as a function of velocity ratio V_∞/V_j is shown in figure 2. This entrainment coefficient is relatively insensitive to the matching point, that is, to whether equation (10) or equation (8) is used. The entrainment for the submerged jet (ref. 8) has been included for comparison. The location of the effective source z_o, which is obtained in addition to the entrainment coefficient when equation (10) is fitted to the empirical curve, is shown for several velocity ratios in figure 3. An example of the fit between the semiempirical and empirical equations for the jet axis is presented in figure 4.

From consideration of the integral equations for the conservation of mass and momentum, it becomes apparent that equation (4) is an oversimplification. By assuming that the velocity on the jet boundary does not differ appreciably from the free-stream velocity, it can be shown that the entrainment presented in figure 2 may be too large by as much as a factor of 2.

CONCLUDING REMARKS

It has been shown that the observed jet axis can be accounted for by considering momentum mixing to be the only mechanism for jet deflection. Recourse has not been made to a drag coefficient which in the region of established flow has the disturbing connotation of flow over a solid body. The values predicted for the mass entrainment necessary to account for the observed jet deflection are physically reasonable and should be considered as upper limits.

REFERENCES

1. Rubbert, P. E.; Saaris, G. R.; et al.: A General Method for Determining the Aerodynamic Characteristics of Fan-In-Wing Configurations. Vol. I - Theory and Application. USAAVLABS Tech. Rep. 67-61A, U.S. Army, Dec. 1967.

2. Keffer, J. F.; and Baines, W. D.: The Round Turbulent Jet in a Cross-Wind. J. Fluid Mech., vol. 15, pt. 4, Apr. 1963, pp. 481-497.

3. Jordinson, R.: Flow in a Jet Directed Normal to the Wind. R. & M. No. 3074, Brit. A.R.C., 1958.

4. Abramovich, G. N.: The Theory of Turbulent Jets. M.I.T. Press, c.1963.

5. Wooler, P. T.; Burghart, G. H.; and Gallagher, J. T.: Pressure Distribution on a Rectangular Wing With a Jet Exhausting Normally Into an Airstream. J. Aircraft, vol. 4, no. 6. Nov.-Dec. 1967, pp. 537-543.

6. Wu, J. C.; McMahon, H. M.; Mosher, D. K.; and Wright, M. A.: Experimental and Analytical Investigations of Jets Exhausting Into a Deflecting Stream. AIAA Paper No. 69-223, Feb. 1969.

7. Margason, Richard J.: The Path of a Jet Directed at Large Angles to a Subsonic Free Stream. NASA TN D-4919, 1968.

8. Albertson, M. L.; Dai, Y. B.; Jensen, R. A.; and Rouse, Hunter: Diffusion of Submerged Jets. Paper No. 2409, Trans. Amer. Soc., Civil Eng., vol. 115, 1950, pp. 639-664.

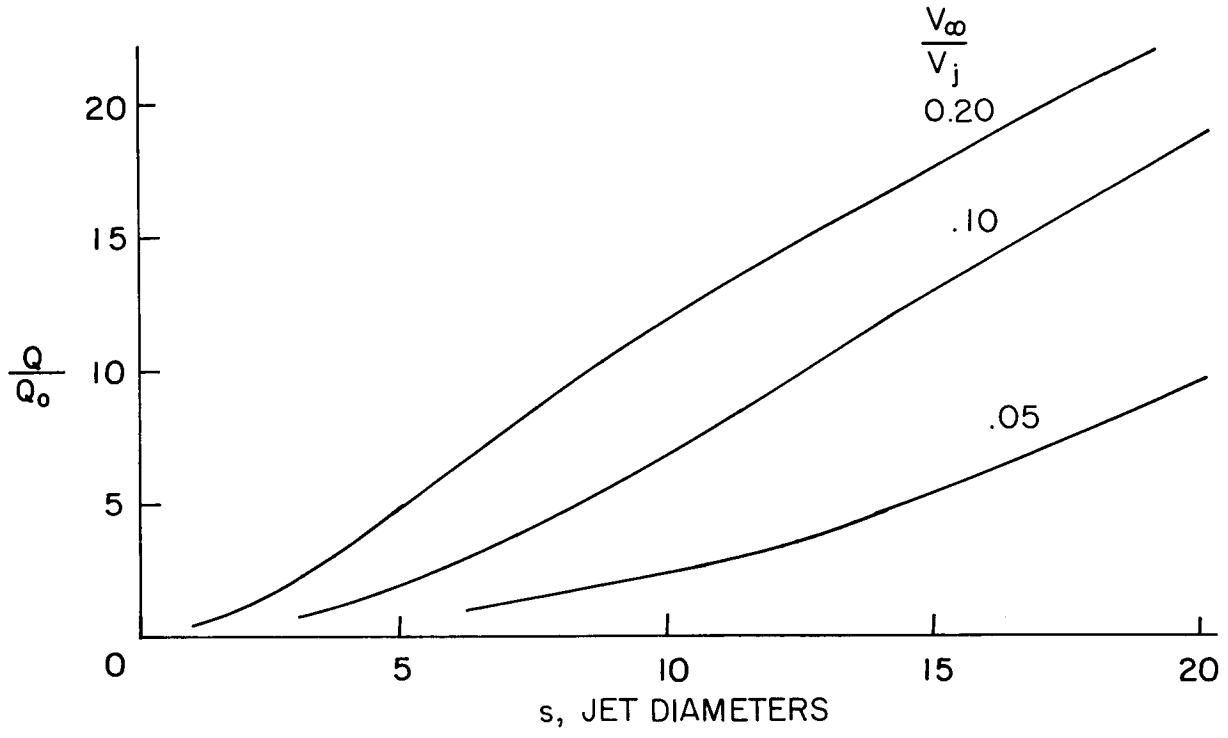

Figure 1.- Mass entrainment obtained by using an empirical equation for the jet axis.

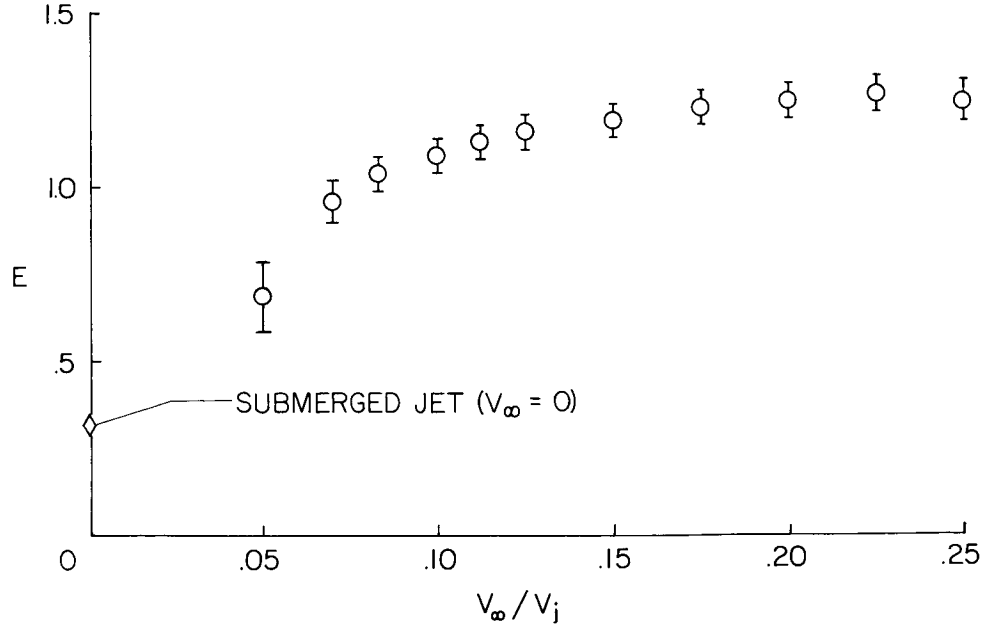

Figure 2.- Variation of entrainment coefficient with velocity ratio.

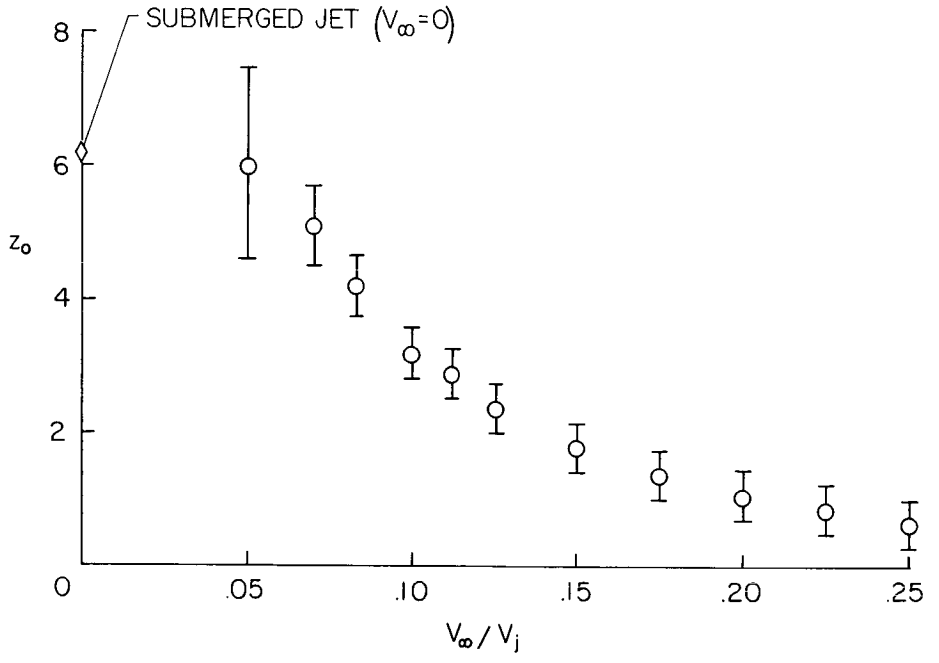

Figure 3.- Effective source location.

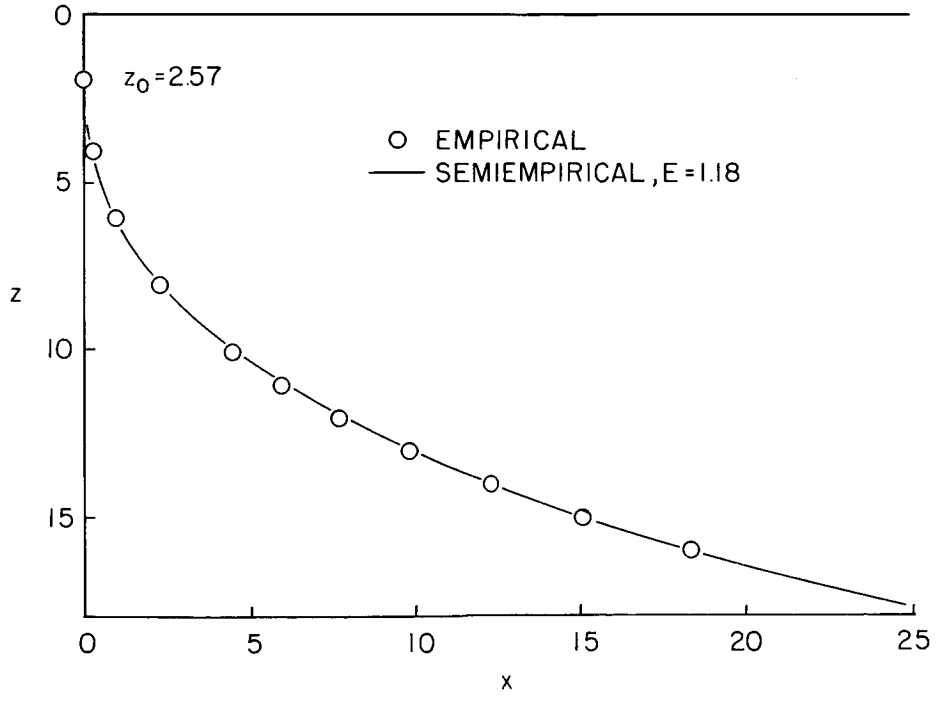

Figure 4.- Comparison of empirical and semiempirical jet axes. $\frac{V_\infty}{V_j} = 0.125$.

LIST OF ATTENDEES

Boswinkle, Robert W., Jr.	NASA Langley Research Center
Braun, Gerhard W.	University of Tennessee Space Institute
Capone, Francis J.	NASA Langley Research Center
Carr, Lawrence W.	U.S. Army Aeronautical Research Laboratory, Ames Research Center
Corsiglia, Victor	NASA Ames Research Center
Durando, Norbert A.	McDonnell-Douglas Astronautics Company - Western Division
Fox, Charles H., Jr.	NASA Langley Research Center
Hammond, Alexander D.	NASA Langley Research Center
Heltsley, Fred L.	ARO, Inc.
Henderson, Robert L.	NASA Langley Research Center
Judd, Michael	University of Southampton
Keffer, J. F.	University of Toronto
Kuhn, Richard E.	NASA Langley Research Center
Lopez, Michael L.	McDonnell-Douglas Astronautics Company - Western Division
Margason, Richard J.	NASA Langley Research Center
McKinney, Marion O.	NASA Langley Research Center
McLemore, H. Clyde	NASA Langley Research Center
McMahon, Howard M.	Georgia Institute of Technology
Miller, Ron	Lockheed-Georgia Aerospace Research Laboratory
Morris, Charles E.	NASA Langley Research Center
Nielsen, Jack N.	Nielsen Engineering & Research, Inc.
Osborn, Russell F.	U.S. Air Force Flight Dynamics Laboratory, Wright-Patterson AFB
Ousterhout, Don S.	St. Louis University
Putnam, Lawrence E.	NASA Langley Research Center
Quinn, Brian P.	Aerospace Research Laboratories, Wright-Patterson AFB
Re, Richard J.	NASA Langley Research Center
Rubbert, Paul E.	The Boeing Company
Runckel, Jack F.	NASA Langley Research Center
Russell, Horace	Purdue University
Skifstad, J. G.	Purdue University
Smith, Charles C., Jr.	NASA Langley Research Center
Stolberg, Carl	Purdue University
Street, Troy A.	Advanced Systems Laboratory of the U.S. Army Missile Command
Vretakis, Nicholas G.	U.S. Air Force Scientific and Technical Liaison Office, Langley
Werner, Jack	New York University
Wright, Ray H.	NASA Langley Research Center
Wooler, Peter T.	Northrop Corporation, Aircraft Division
Wu, J. C.	Georgia Institute of Technology

NASA-Langley, 1969 —— 2